MODELING MULTIPLE PRINTED ANTENNAS EMBEDDED IN STRATIFIED UNIAXIAL ANISOTROPIC DIELECTRICS

A Dissertation
Submitted to the Graduate Faculty
of the
North Dakota State University
of Agriculture and Applied Science

By

Benjamin Davis Braaten

In Partial Fulfillment of the Requirements
for the Degree of
DOCTOR OF PHILOSOPHY

Major Department:
Electrical and Computer Engineering

February 2009

Fargo, North Dakota

ABSTRACT

Braaten, Benjamin Davis, Ph.D., Department of Electrical and Computer Engineering, College of Engineering and Architecture, North Dakota State University, February 2009. Modeling Multiple Printed Antennas Embedded in Stratified Uniaxial Anisotropic Dielectrics. Co-Major Professors: Dr. Robert M. Nelson and Dr. David A. Rogers.

New spectral domain immittance functions based on Hertz vector potentials were derived to study the resonant frequency, input impedance and mutual coupling of printed dipoles in the presence of stratified uniaxially anisotropic dielectrics. In this study the current on each dipole was not assumed but was solved for using the moment method. This differs from all of the previous printed dipole research associated with anisotropic dielectrics because in previous work the printed dipoles were assumed to be Hertzian (i.e., constant current) or had an assumed sinusoidal current distribution. Original results show that the mutual coupling usually can be reduced by placing an anisotropic layer above both printed dipoles. In particular, it is determined that the permittivity in the direction of the optical axis below the dipoles could be used to design a specific resonant frequency of a given dipole while the permittivity orthogonal to the optical axis in the layer above the dipoles could be used to control mutual coupling. This is very important knowledge to have as a designer, especially for array applications. Computed results are compared to measurements, published literature and commercial software and are shown to have good agreement in all cases.

ACKNOWLEDGMENTS

I am very grateful to take this opportunity to thank Dr. Robert M. Nelson, Dr. David A. Rogers, Dr. David C. Farden, Dr. Doğan Çömez and Dr. Orven F. Swenson for serving on my graduate committee. Dr. Robert M. Nelson was with North Dakota State University for 23 years and is now a Professor at the University of Wisconsin - Stout. During his time at North Dakota State University he was my Master's and Ph.D. advisor in electromagnetics. I cannot thank him enough for the guidance, encouragement and wisdom he gave me during my graduate studies. He has shown me the joys of teaching, rewards of research and importance of life, and for this I thank him. I would like to thank Dr. David A. Rogers for his willingness to move into the role of my advisor after the departure of Dr. Robert M. Nelson. He has been an invaluable part of my research and teaching during my graduate studies at North Dakota State University.

I would like to thank Dr. David C. Farden and Dr. Doğan Çömez for serving on my graduate committee. I have always enjoyed discussing many aspects of engineering and mathematics with these two gentlemen and look forward to future discussions.

I would especially like to thank Dr. Orven F. Swenson for serving on my graduate committee. I appreciate the comments and help you have provided as well as the willingness to serve on my committee with such short notice.

I would also like to thank Dr. Adaildo D'Assunção for his collaboration and input on various aspects of this reseach.

Finally, I would like to thank my family for their support and understanding that I had to leave my hometown to pursue this work.

DEDICATION

To my family.

TABLE OF CONTENTS

LIST OF TABLES

LIST OF FIGURES

LIST OF SYMBOLS

a ..... Radius of a wire

$a_{m,n}$ ..... Impedance matrix coefficient

$\hat{a}_x$ ..... Unit vector in the x-direction defined on a rectangular coordinate system

$\hat{a}_y$ ..... Unit vector in the y-direction defined on a rectangular coordinate system

$\hat{a}_z$ ..... Unit vector in the z-direction defined on a rectangular coordinate system

α ..... Fourier variable with respect to x

α_n ..... Unknown magnitudes

A, B, C, D, A_j, A'_j, B_j, B'_j ..... Constants

$\bar{A}$ ..... Magnetic vector potential

β ..... Fourier variable with respect to z

$\bar{B}$ ..... Magnetic flux density

∇ ..... Gradient

$\nabla\cdot$ ..... Divergence

$\nabla\times$ ..... Curl

d ..... Thickness of a single layer

d_N ..... Thickness of the N^{th} layer

d_{1N} ..... Distance from the ground plane to the top of the N^{th} layer

$\delta(x)$ ..... Spatially impulsive source

Δx, Δz ..... Segment size

$\bar{D}$ ..... Electric flux density

$\widetilde{D}$ ..... Electric flux density in the transform domain

ε, ε_r, ε_i ..... Isotropic relative permittivity

ε_0 ..... Permittivity of free-space

ε_{j2}, ε_x ..... Anisotropic relative permittivity of the j^{th} region in the x-direction

ε_{j1}, ε_y ..... Anisotropic relative permittivity of the j^{th} region in the y-direction

ε_z ..... Anisotropic relative permittivity in the z-direction

$[\varepsilon]$ ..... Anisotropic permittivity

$[\varepsilon_i]$ ..... Anisotropic permittivity of the i^{th} region

$\bar{E}$, $\bar{E}_a$, $\bar{E}_b$ ..... Electric field intensity

E_x ..... x-component of the electric field

E_y ..... y-component of the electric field

E_z ..... z-component of the electric field

$\widetilde{E}_x$ ..... x-component of the electric field in the transform domain

$\widetilde{E}_y$ ..... y-component of the electric field in the transform domain

$\widetilde{E}_z$ ..... z-component of the electric field in the transform domain

$\bar{E}^i_{\tan}$ ..... Tangential component of the incident field

$\bar{E}^s_{\tan}$ ..... Tangential component of the scattered field

f ..... Source frequency in Hertz

g ..... Forcing function

γ_0 ..... Free-space propagation constant

γ_{ej}, γ_{hj} ..... Propagation constants in the j^{th} region

G ..... Dipole separation along the x-axis

$G(x, x')$ ..... Green's function

$\widetilde{G}(x, x')$ ..... Green's function in the transform domain

$\bar{H}$, $\bar{H}_a$, $\bar{H}_b$ ..... Magnetic field intensity

H_x ..... x-component of the magnetic field

H_y ..... y-component of the magnetic field

H_z ..... z-component of the magnetic field

$\widetilde{H}_x$ ..... x-component of the magnetic field in the transform domain

$\widetilde{H}_y$ ..... y-component of the magnetic field in the transform domain

$\widetilde{H}_z$ ..... z-component of the magnetic field in the transform domain

I, $\bar{I}$, I_a, I_b ..... Line current

I_n ..... Current supplied by the n^{th} terminal

I_{xn} ..... Unknown current in the x-direction

I_{zn} ..... Unknown current in the z-direction

$\bar{J}_a$, $\bar{J}_b$, $\bar{J}_s$ ..... Surface current density

$\widetilde{\bar{J}}_k$ ..... Surface current density on the k^{th} layer in the transform domain

$\widetilde{J}_x$ ..... x-component of the surface current density in the transform domain

$\widetilde{J}_z$ ..... z-component of the surface current density in the transform domain

k_0 ..... Free-space wavenumber

λ_0 ..... Free-space wavelength

λ_d ..... Dielectric wavelength

L ..... Conductor length

L(f) ..... Linear operator on f

μ_0 ..... Permeability of free-space

μ_r ..... Relative permeability

M_i, N_i, P_i ..... Constants

$\bar{M}_a$, $\bar{M}_b$ ..... Magnetic current

n ..... Anisotropy ratio

N ..... Number of segments

ω ..... Source frequency in radians

ϕ_e, ϕ_h ..... Scalar functions

ϕ_n ..... Expansion functions

$\widetilde{\phi}_n$ ..... Expansion functions in the transform domain

Φ ..... Potential

$\widetilde{\Phi}$ ..... Fourier transform of the function Φ

$\bar{\Pi}_e$ ..... Electric Hertz potential

Π_{ex} ..... x-component of the electric Hertz potential

Π_{ey} ..... y-component of the electric Hertz potential

Π_{ez} ..... z-component of the electric Hertz potential

$\widetilde{\Pi}_{ej}$ ..... Electric Hertz potential in the j^{th} region in the transform domain

$\bar{\Pi}_{h}$ ..... Magnetic Hertz potential

Π_{hx} ..... x-component of the magnetic Hertz potential

Π_{hy} ..... y-component of the magnetic Hertz potential

Π_{hz} ..... z-component of the magnetic Hertz potential

$\widetilde{\Pi}_{hj}$ ..... Magnetic Hertz potential in the j^{th} region in the transform domain

$\frac{\partial}{\partial x}$, $\frac{\partial}{\partial z}$ ..... Partial derivatives

r_{xn} ..... x-component of the expansion function

r_{zn} ..... z-component of the expansion function

$\widetilde{r}_{xn}$ ..... x-component of the expansion function in the transform domain

$\widetilde{r}_{zn}$ ..... z-component of the expansion function in the transform domain

ρ_{n} ..... Unknown total surface charge density (charge pulse)

ρ_{v} ..... Volume charge

$\tilde{R}$ ..... Residual

σ ..... Conductivity

S ..... Dipole separation along the z-axis

V_{m} ..... Voltage at the m^{th} terminal

V_{a}^{oc}, V_{b}^{oc} ..... Open circuit voltage

w_{m}, W_{m} ..... Weighting functions

w_{xm} ..... x-component of the weighting function

w_{zm} ..... z-component of the weighting function

$\widetilde{w}_{m}$ ..... Weighting functions in the transform domain

$\widetilde{w}_{xm}$ ..... x-component of the weighting function in the transform domain

$\widetilde{w}_{zm}$ ..... z-component of the weighting function in the transform domain

W ..... Conductor width

x, y ..... Field (observation) points

x', y' ..... Source points

Z_A, Z_{in}, Z_{aa}, Z_{bb} ..... Input impedance

Z_{ab}, Z_{ba}, Z_{mn} ..... Mutual impedance

$\widetilde{Z}_{xx}$, $\widetilde{Z}_{xz}$, $\widetilde{Z}_{zx}$, $\widetilde{Z}_{zz}$ ..... Immittance functions

CHAPTER 1. INTRODUCTION

1.1. A Brief History of the Development of Maxwell's Equations

The field of electrical science has a rich and very interesting history. The ancient Greek's were among the first people to observe and study electrostatics but it was Coulomb (1736-1806) who first understood and quantified electrostatics [1]. During this time many other people were working to understand the field of electrical science. Volta (1745-1827) was the first to discover continuous current [1] and this lead to the ground-breaking observation by Oersted (1777-1851) who discovered electromagnetism [1]. This resulted in his significant paper entitled "Experiments on the effect of an electric current on the magnetic needle," July 21, 1820. This paper related the electric current of a wire to the magnetic field around the wire for the very first time. This relation has been called one of the greatest announcements in electrical science. After Oersted's ground-breaking paper Ampere (1775-1836), the French pioneer of electrodynamics, discovered that conductors of various sizes and shapes carrying current interact through forces and that these forces were related to the polarity and magnitude of the current [1]. Meanwhile, in England, Faraday (1791-1867) was studying the relation between light and magnetism [2], [3]. Faraday's 40-year career had many significant breakthroughs that included the very first electromagnetic generator [1]. During this time in America, Henry (1797-1878) showed that electricity could travel through space and more importantly, how to control this electricity in space. Gauss (1777-1855) and Weber (1804-1891) worked on establishing the mathematics and electrical measurement systems that would later be used as a universal language in the field of electrical science [1]. In a period of approximately 100 short years the field of electrical science went from an understanding of the existence of static charge to the foundations of electrodynamics. What makes these breakthroughs more remarkable is that they happened in a time of

great political change. In the late 1700s the United States was forming a new nation and the French revolution was underway. The 1800s saw the reign of Napoleon and an American civil war. But through all this change, these remarkable researchers were able to establish the foundations of the entire field of electrical engineering.

1.2. One Hundred and Thirty-Six Years of Maxwell's Equations

James Clerk Maxwell (1831-1879) is known as a giant of 19th-century physics. Maxwell's most significant contributions were the laws of electrodynamics [1]. This work was based on Faraday's ground-breaking discoveries on light and magnetism and culminated in a textbook entitled "A Treatise on Electricity and Magnetism" first published in 1873 and later by Dover Publications, Inc. in 1954 [4]. The following equations, often denoted as Maxwell's equations, are given in this book as:

$$\nabla \times \bar{E} = -\frac{\partial \bar{B}}{\partial t} \tag{1.1}$$

$$\nabla \times \bar{H} = \bar{J}_s + \frac{\partial \bar{D}}{\partial t} \tag{1.2}$$

$$\nabla \cdot \bar{D} = \rho_v \tag{1.3}$$

$$\nabla \cdot \bar{B} = 0 \tag{1.4}$$

where $\bar{E}$ is the electric field intensity, $\bar{H}$ is the magnetic field intensity, $\bar{D}$ is the electric flux density, $\bar{B}$ is the magnetic flux density, $\bar{J}_s$ represents a source current in the region and ρ_v represents a charge source in the region. Equations (1.1)-(1.4) are very significant and lay the foundation for the laws of electrodynamics. For the first time, researchers in the area of electrical science had a general relation between all types of sources and the fields associated with these sources. Equations (1.1) and (1.2) involve a curl operation. In fact, the curl is a vortex source finder (i.e., fields form closed paths). For example, (1.1) states that the time-varying magnetic fields are vortex sources of electric fields and (1.2) states that sources of magnetic fields

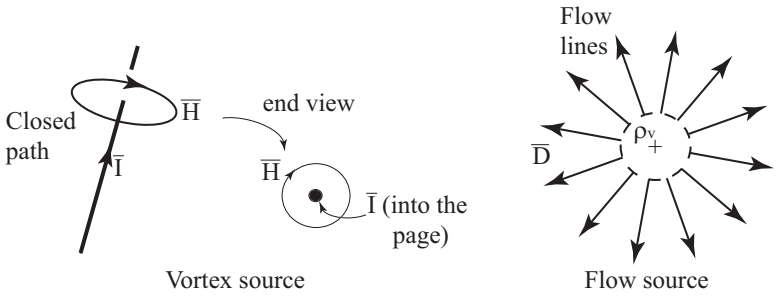

Figure 1. Vortex and flow sources.

are current or time varying electric fields. An example of a vortex source in shown in Figure 1. Equations (1.3) and (1.4) involve a divergence operation. In this case, the divergence is a flow source finder (i.e., fields start and stop at specific points). For example, (1.3) states that charge is a flow source of electric fields or that electric fields "flow" from a source charge and (1.4) states that magnetic fields do not have any flow sources. An example of a flow source in also shown in Figure 1.

Maxwell's results led to the work by Hertz (1857-1894). Hertz was responsible for many breakthroughs such as: experiments in electrical oscillations, observing resonance, reporting on the periodicity of the emissions from an oscillator and writing a book on electromagnetic waves called "Electric Waves" [1], [5], [6]. "Electric Waves" outlines a number of experiments with dipoles, loops and reflectors made by Hertz. Hertz was a student of Helmholtz and Kirchhoff at the University of Berlin. By the year 1888 Hertz established the existence of radio waves by generating and receiving electromagnetic waves. Hertz's most important contribution was the experimental confirmation of Maxwell's equations. Later the work by Maxwell and the contributions from Hertz led to the first transatlantic radio communication by Marconi (1874-1937) [7], [8]. Marconi sent Morse code via radio waves from Poldhu, Cornwall, England to St. John's, Newfoundland on December 12, 1901 at 12:30 p.m. In many ways this was a significant step in wireless communications and a result of

many different efforts in the area of electrical science.

The 1900's saw a tremendous amount of research in the area of electrical science, in particular, wireless communications. Researchers such as Stratton (1901-1994) [9], King (1905-2005) [10] and Kraus [6] were writing books in a manner that allowed the subject of electromagnetics and antennas to be taught in universities all over the world. Researchers of this era investigated many different aspects of wireless communications such as antennas, transmission lines, transmitters, receivers, etc. In the meantime societies such as Union Radio Scientifique Internationale (URSI) and The Institute of Electrical and Electronics Engineers (IEEE) were formed to provide a place for research and ideas to be shared in the interest of radio science.

Naturally, new research has benefited significantly from previous work. Areas such as dual-frequency antennas, ultra-wide band (UWB) networks, metamaterials and radio frequency identification (RFID) have grown at incredible rates over the past 10 years. As expected, operating frequencies have also increased substantially during this time. This has lead to an effort to be able to model the materials associated with manufacturing antennas with much more accuracy.

CHAPTER 2. AN INTRODUCTION TO PRINTED ANTENNAS AND THE PROPOSED RESEARCH

2.1. Background and Literature Search

Not long after the field of electrical science was written about by authors such as R.W.B. King and Julius Stratton, Deschamps formally introduced the first microstrip antenna in 1953 [11]. At this point an entire new area of research involving printed antennas was born. And for good reason. It is well known that printed antennas are very light, occupy a small volume, are useful at high frequencies and provide a wide range of patterns [12]; making them very useful in many applications. Thus, it is no surprise that this is a very rich field of research.

Many different areas of research are involved with the study of printed antennas. These include resonant type antennas, dual frequency antennas, dipoles, monopoles, microstrip patches, electrically small antennas, wide-band antennas, ultra wide-band antennas, fractal antennas, space-filling antennas, printed arrays, and, more recently, integrated circuit (IC) antennas (i.e., printed antennas directly embedded in an IC) and metamaterial-based antennas. Among all these areas there exists different methods of printing an antenna. One popular method is the microstrip antenna. This involves printing the antenna above a grounded dielectric substrate. An example of a rectangular microstrip antenna is shown in Figure 2. Other types of printed antennas may be located above or in a dielectric without a conducting plane. These antennas are usually referred to as dipole or space-filling antennas. Examples of these may be radio frequency identification (RFID) [13]-[21] antennas and wireless sensors. The different types of dielectrics that may be associated with printed antennas may also be studied. These include isotropic, anisotropic and lossy dielectrics.

Before the problem of interest is defined, a brief introduction to the behavior of microstrip antennas and material properties is presented. First, the types of structures

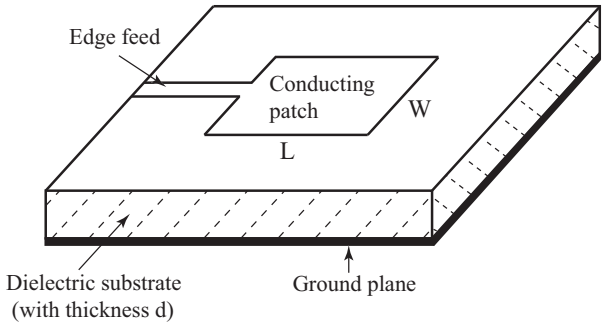

Figure 2. The rectangular microstrip antenna.

under investigation will be defined; then the fields above and around the conducting surfaces will be illustrated. Next, an expression for resonant length is given and the significance of this expression is discussed. After this, the idea of mutual coupling is presented and illustrated with a two-port antenna network. Then, a brief literature review is presented followed by a discussion on anisotropy. Discussing these topics will lay the foundation for the research presented in this document.

2.1.1. The microstrip antenna and mutual coupling

A microstrip device has two planar conducting layers separated by a thin dielectric material [22]. The top conducting layer is usually driven by a source and the lower conducting layer acts as a ground plane. The microstrip device in Figure 2 has a conducting patch separated from the ground plane by a material denoted as the dielectric substrate with thickness d. This type of microstrip device is called a rectangular microstrip patch antenna. Usually the length L of the conducting patch in Figure 2 is an appreciable fraction of the source wavelength. Because of this the microstrip patch antenna belongs to the class of resonant antennas [22]. The resonant nature of the antenna inherently results in a narrow bandwidth and very large dimensions at frequencies below 1 GHz. Thus microstrip antennas are typically used at frequencies of 1 GHz to 100 GHz [22].

The region between the conducting patch and the ground plane acts as the

region between a transmission line and a ground plane with both ends open. This leads to a standing wave in the dielectric. The fields associated with the standing wave between the conducting patch and ground plane are shown in Figure 3. The fringing fields at each end of the conducting patch are 180° out of phase and equal in magnitude. It is these fringing fields exposed to the region above the conducting patch that are responsible for the radiation.

The top view of the fields is shown in Figure 4. The arrows at each end of the conducting patch are illustrating the electric field component in the same plane of the conducting patch. The fields are in phase and this leads to a broadside radiation pattern.

The resonant length and input impedance at resonance can be approximated for the antenna in Figure 2 which is edge fed with a microstrip transmission line. The length L and width W of the patch are chosen to give a real input impedance on and near the operating frequencies. It has been shown that for a substrate thickness much less than the source wavelength the resonant length L is approximately [22]:

$$L \approx 0.49\lambda_d = 0.49\frac{\lambda_0}{\sqrt{\varepsilon_r}} \tag{2.1}$$

where ε_r is the permittivity of the dielectric substrate, λ_0 is the free space wavelength and λ_d is the wavelength in the dielectric substrate. Just like a dipole the resonant length L is approximately $0.5\lambda_0$, but the fringing fields in Figure 4 act to extend the effective length of the patch. Thus the patch length needs to be a bit shorter than a half-wavelength to achieve resonance. Equation (2.1) clearly shows that the patch length cannot vary much otherwise an input reactance begins to appear at the feed location. Also, the input impedance at resonance can be approximated as [22]

$$Z_A = 90\frac{\varepsilon_r^2}{\varepsilon_r - 1}\left(\frac{L}{W}\right)^2 \Omega. \tag{2.2}$$

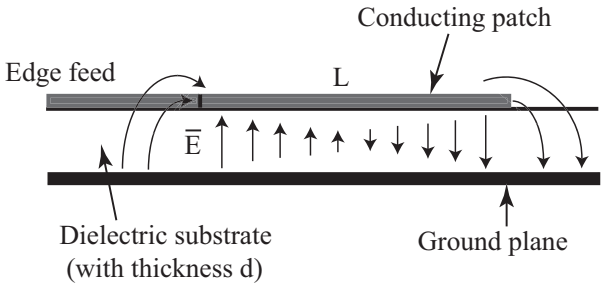

Figure 3. Side-view of the rectangular microstrip antenna.

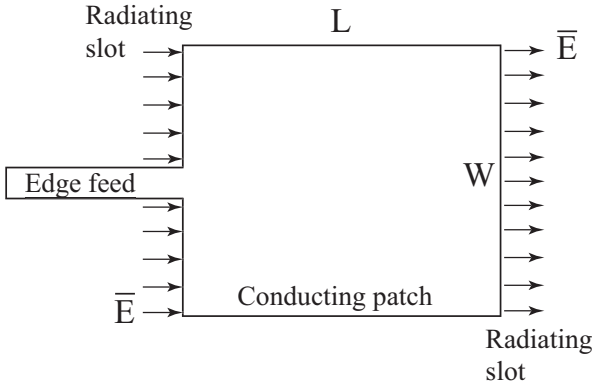

Figure 4. Top-view of the rectangular microstrip antenna.

Equations (2.1) and (2.2) assume that the antenna in Figure 2 is not located near any source in the region or other conducting bodies; otherwise, the expressions are not valid.

When driving an isolated printed antenna with an ideal source, the input impedance of the antenna is dependent on the voltage at the terminal and the current induced on the antenna by the source. When another conducting element is brought into the region where the antenna is radiating, this other conducting element can affect the current distribution on the radiating antenna. This effect on the current distribution is called mutual coupling. In an antenna array, mutual coupling can be caused by other array elements, feed networks and nearby conducting objects

(enclosure, mounts, etc.) [22]. In particular, the mutual impedance Z_{mn} between two terminal pairs of antennas m and n is the open circuit voltage (V_{oc}) at the m^{th} terminal divided by the current supplied by the n^{th} terminal. This then gives

$$Z_{mn} = \frac{V_m}{I_n}. \tag{2.3}$$

The result in (2.3) can be derived from a reciprocity point of view. The sources $\bar{J}_a$ and $\bar{M}_a$ in Figure 5 are in volume V_a and sources $\bar{J}_b$ and $\bar{M}_b$ are in volume V_b. Using the Lorentz reciprocity theorem [22], the fields from $\bar{J}_a$ and $\bar{M}_a$ are denoted as $\bar{E}_a$ and $\bar{H}_a$, respectively, and the fields from $\bar{J}_b$ and $\bar{M}_b$ are denoted as $\bar{E}_b$ and $\bar{H}_b$, respectively. If the frequency for all sources is assumed to be the same then the Lorentz reciprocity theorem states that

$$\int\int_{V_a}\int (\bar{E}_b \cdot \bar{J}_a - \bar{H}_b \cdot \bar{M}_a)dv' = \int\int_{V_b}\int (\bar{E}_a \cdot \bar{J}_b - \bar{H}_a \cdot \bar{M}_b)dv'. \tag{2.4}$$

The left side of (2.4) is the reaction of the fields from the sources in V_b on the sources in V_a (a measure of coupling), and the right side is the reaction of the fields from the sources in V_a on the sources in V_b. The second reciprocity theorem can be derived from the Lorentz reciprocity theorem. Suppose that the sources are antennas excited with an ideal current I_a and I_b, respectively. This then implies $M_a = M_b = 0$. Thus,

$$\int\int_{V_a}\int \bar{E}_b \cdot \bar{J}_a dv' = \int\int_{V_b}\int \bar{E}_a \cdot \bar{J}_b dv'. \tag{2.5}$$

The tangential components of the $\bar{E}$-field are zero on the surface of the antennas. If the current is constant at the terminals, then (2.5) reduces to the following line integral:

$$I_a \int_{l_a} \bar{E}_b \cdot d\bar{l}' = I_b \int_{l_b} \bar{E}_a \cdot d\bar{l}' \tag{2.6}$$

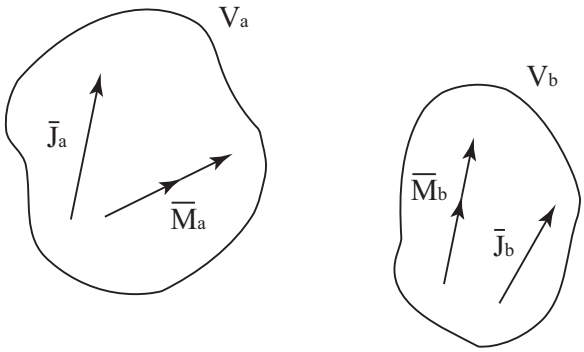

Figure 5. Radiating problem from a reciprocity point of view.

where I_a and I_b are the constant currents at terminals a and b, respectively. Then using $V = -\int \bar{E} \cdot d\bar{l}$, (2.6) becomes

$$V_a^{oc} I_a = V_b^{oc} I_b \tag{2.7}$$

where V_a^{oc} is the open circuit voltage of antenna a due to the field $\bar{E}_b$ generated by antenna b. Also V_b^{oc} is the open circuit voltage of antenna b due to the field $\bar{E}_a$ generated by antenna a. This then gives

$$\frac{V_a^{oc}}{I_b} = \frac{V_b^{oc}}{I_a} \tag{2.8}$$

which is the reciprocity theorem in circuit form. Superposition then gives $V_a = Z_{aa} I_a + Z_{ab} I_b$ and $V_b = Z_{ba} I_a + Z_{bb} I_b$ where Z_{ba} and Z_{ab} are the mutual impedances between antennas a and b, and V_a, I_a, V_b and I_b are the terminal voltages and currents on antenna a and b, respectively [23]. If $I_b = 0$ then $V_b = Z_{ba} I_a$. This means that if antenna b is an open circuit, then the open circuit voltage at antenna b due to the current driving antenna a is $Z_{ba} I_a$. Solving for Z_{ba} gives $Z_{ba} = V_b / I_a$. Similarly $Z_{ab} = V_a / I_b$ for $I_a = 0$. Next, consider the two antennas in Figure 6. If an ideal

Figure 6. Two port antenna problem.

current source I excites antenna a then $V_b = IZ_{ba}$ where $I_b = 0$. If the same current I excites antenna b then $V_a = IZ_{ab}$ where $I_a = 0$. But $Z_{ab} = Z_{ba}$ implying $V_a = V_b = V$. Thus I will generate the same terminal voltage regardless of the terminal it is exciting. Reciprocity states that the source and receiver can be interchanged without changing the system response.

The concept of mutual coupling and how to calculate the mutual impedances Z_{ab} and Z_{ba} was discussed above. The antenna system in Figure 6 can take on many different forms. One of the forms that it can take on is that of multiple anisotropic layers with multiple microstrip antennas.

2.1.2. Previous work on a microstrip antenna

Some of the initial work on microstrip antennas was in 1974 by Munson [24]. This work focused on microstrip antennas conformed to cylindrical antennas. Part of this work was based on work in 1969 by Campbell [25] dealing with omnidirectional antenna arrays. A year later Howell [26] presented design guidelines for a large class of coaxial and edge-fed microstrip antennas. This work included both linearly and circularly polarized antennas and treated the antenna as a radiating resonator.

In 1979 a significant step was taken by Uzunoglu *et al.* [27] who for the first time analyzed the radiation properties of the microstrip dipole shown in Figure 7. This work is based on obtaining the Green's function for a horizontal Hertzian dipole

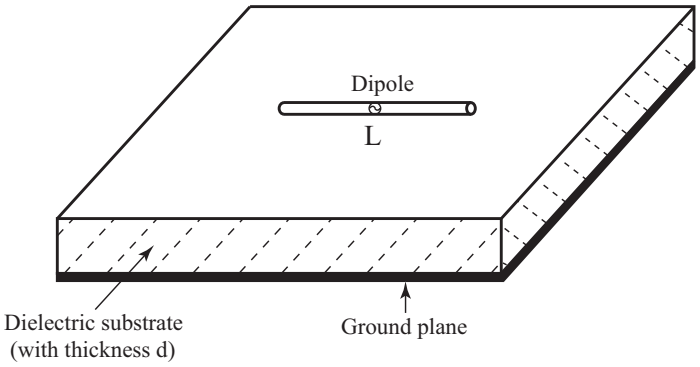

Figure 7. The "cylindrical" printed dipole on a single dielectric substrate.

printed on a grounded isotropic dielectric substrate. Working from that base, Rana and Alexopoulos [28] presented work in 1981 on the current distribution and input impedance of printed dipoles. The above work with Green's functions in the spectral form laid the foundation for future work by Pozar [29] and others to analyze properties of various other microstrip antennas.

In parallel with the development by Alexopoulos and his colleagues, in 1980 and 1981 Itoh and Menzel [30]-[31] developed a spectral domain immittance approach to study microstrip antennas of the type shown in Figure 2. The method was based on an equivalent circuit concept for dispersion characteristics of printed transmission lines. This work included a spectral domain version of the Green's function and was applied to problems similar to the one shown in Figure 8 with multiple isotropic dielectric layers surrounded by a shield where the top and bottom dielectric layer was air. The spectral domain immittance approach used a full-wave analysis technique to overcome previous quasi-static analysis techniques of microstrip structures. This allowed structures comparable to the source wavelength to be analyzed. Then in 1982 Bahl *et al.* [32] presented work on the design of microstrip antennas covered with an isotropic dielectric layer. The resonant frequency, loss and bandwidth of various antennas were studied by using a variational technique.

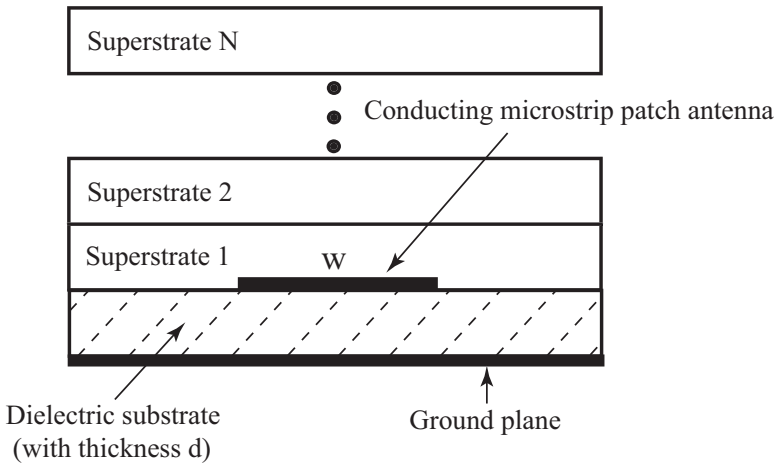

Figure 8. A single microstrip antenna in layered anisotropic material.

In 1982 Lee and Tripathi [33] extended the work by Itoh and others to include microstrip structures with planar anisotropic substrates. This work was based on the Hertz vector potential function and not on the equivalent circuit concept by Itoh and Menzel [31]. It was later shown by Nelson *et al.* [34] that the immittance functions in both the methods presented by Lee and Tripathi [33] and Itoh and Menzel [31] were similar except for a difference in sign. Then in 1984 Krowne [35] derived the spectral domain Green's function solution of an anisotropic layered structure in terms of Maxwell's equations. The anisotropic material could be biaxial or uniaxial. Later in 1986 Krowne [36] applies this technique to radiators and resonators in layered anisotropic structures. In 1987 Pozar [37] presented the radiation and scattering properties of a microstrip patch antenna on an uniaxial substrate. Pozar's results were developed using the spectral domain version of the Green's function found in previous work by Alexopoulos. Then in 1990 Nelson *et al.* [34] extended the problem in Figure 8 and investigated the effects of multiple anisotropic uniaxial dielectric layers on the resonant frequency of a rectangular microstrip antenna. This work used the full-wave immittance matrix technique. This was followed in 1996 by Oliveira

and D'Assunção's work [38] which investigated for the first time the input impedance of microstrip patch antennas on multiple anisotropic dielectric substrates.

The research outlined above is just a summary of work over the past 34 years that has focused on the input impedance, efficiency, gain and radiation patterns of printed antennas in layered anisotropic and isotropic structures. Many other areas that involve different feed techniques, patch configurations, frequency selective structures and arrays on infinitely extended substrates exist and are not discussed here.

2.1.3. Previous work on mutual coupling

Some of the initial computations for mutual coupling between printed dipoles was done by Baker and LaGrone [39] in 1962 and then later by Alexopoulos and Rana [40] in 1981. Baker and LaGrone assumed a current distribution with a dielectric substrate permittivity of unity. Alexopoulos and Rana relaxed the current distribution assumption and used the Green's function in the spectral form in terms of the Sommerfeld type of integrals [9] to solve for the mutual impedance between two printed dipoles over a grounded isotropic dielectric substrate. The printed dipoles are shown in Figure 9 with a specific separation. Alexopoulos and Rana presented the mutual impedance of two dipoles in broadside, collinear and echelon forms. This work is significant because it shows for the first time that a spectral domain method can be used to compute mutual impedance between two printed antennas on a grounded dielectric substrate. Also in 1981 Jedlicka *et al.* [41] presented a method for measuring coupling between microstrip antennas. This method involves attaching the ground plane of the two elements to a large rigid aluminum ground plane (Figure 10). Then spacers are inserted between the two antennas to act as a continuous dielectric substrate between the two antennas under test. As the antenna spacing increases, dielectric spacers are inserted. The antennas are then driven by a network

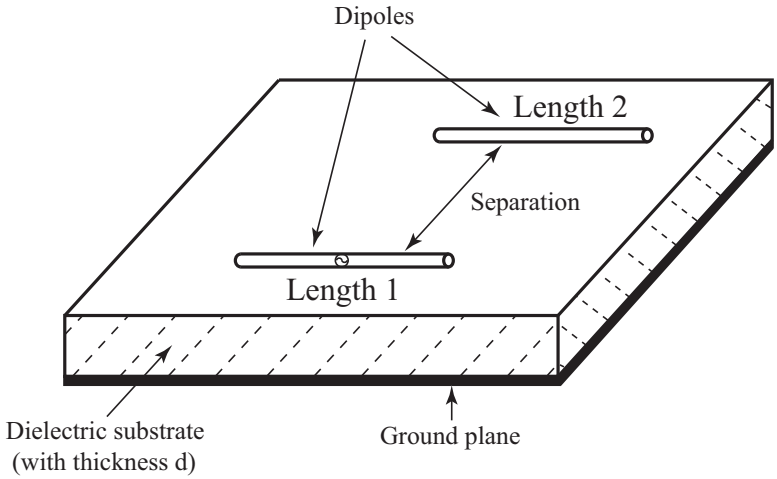

Figure 9. Printed dipoles on a single dielectric substrate.

analyzer with a coax through the aluminum ground plane, and it is shown that this provides accurate measurements of S_{12}.

The next step in the area of research involving mutual coupling was taken in 1982 by Pozar [29]. Pozar investigated the input impedance and mutual coupling between rectangular microstrip antennas. This was done by evaluating the exact Green's function for an isotropic grounded dielectric substrate with the moment method, thus accounting for surface waves and coupling to nearby antennas. Pozar then presented numerical and measured results for the input impedance and mutual coupling of various rectangular microstrip antenna configurations. Then in 1983 Newman *et al.* [42] directly solved for the mutual impedance between two rectangular microstrip antennas similar to the structures in Pozar's work [29]. This was done by using the moment method to directly solve the reaction integral equation [42]

$$-\int_S \int \bar{J}_s \cdot \bar{E}_T ds = \int_L \bar{J}_i \cdot \bar{E}_T dl \tag{2.9}$$

where the surface integral is evaluated over the surface of the conducting patches, the line integral is evaluated over the electric field in the presence of the dielectric

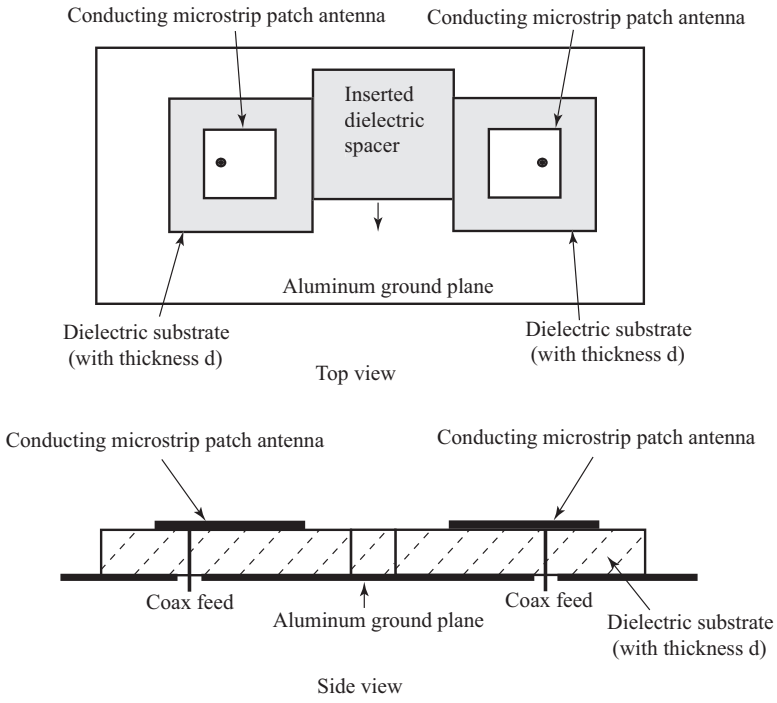

Figure 10. Test setup for measuring mutual impedance.

slab and $\bar{J}_T$ is an arbitrary test current on the surface S. Equation (2.9) can then be solved directly for $\bar{J}_S$.

In 1984 a transmission line model for mutual coupling between microstrip antennas was presented by Lil and De Capelle [43]. This model was presented assuming that the surface waves could be neglected and each rectangular resonator was approximated by two equivalent radiating slots. Again, in this case the author assumes that conducting patches were on the same isotropic grounded dielectric substrate. Then in 1986 Hansen and Patzold [44] presented the input and mutual impedance of a rectangular microstrip antenna with a dielectric superstrate for the first time. This was developed in the spectral domain from Richmond's reaction theorem. The dielectric substrates and superstrates were assumed to be isotropic and the conducting patches were on the same dielectric substrate. The input impedance and mutual coupling was presented for various conducting patch configurations.

In 1989 two papers were presented on mutual coupling between elements in microstrip antenna arrays. First, a paper by Katehi [45] computed the mutual coupling between microstrip dipoles in multielement arrays. The dipoles were excited by an electromagnetically coupled transmission line in the isotropic substrates below the printed dipoles. The mutual impedance between various array configurations was then calculated using the dyadic Green's function. The second paper presented on mutual coupling in 1989 was by Mohammadian *et al.* [46]. This work was on a theoretical and experimental study of mutual coupling in microstrip arrays. This was done by replacing each element of the array by an equivalent magnetic current source and using the reaction theorem to calculate the mutual impedance between two printed antennas on a grounded isotropic dielectric substrate. S_{12} was presented for both the $\bar{E}$ and $\bar{H}$ planes.

The 1990's saw a lot of work on mutual coupling between antennas. During this time many other problems were looked at and, naturally, this work was based on the work from the 1980's. In 1990 Benalla and Gupta [47] looked at the mutual coupling between rectangular microstrip antennas with an isotropic substrate and superstrate. In this work the antennas were edge fed and on the same dielectric layer. The mutual coupling was calculated by replacing the edge aperture field by an equivalent magnetic line source. The $\bar{H}$-plane coupling was presented with respect to the antenna spacing. Numerical and theoretical results showed good agreement. In 1991 Terret *et al.* [48] presented a paper on mutual coupling in stacked microstrip antennas. They used the reciprocity theorem and the spectral domain Green's function used by Pozar [29]. The mutual impedance was calculated using

$$Z_{21}^{p} = \frac{-\int_{V_2} \bar{E}^{(1)T} \cdot \bar{J}_{V_2}}{|I_{V_1}| \cdot |I_{V_2}|} \tag{2.10}$$

where Z_{21}^{p} is the transfer impedance between ports 1 and 2, $\bar{E}^{(1)T}$ is the total electric

field at port 2 from the current at port 1, $\bar{J}_{V_i}$ is the current density at port i and I_{V_i} is the terminal current at the port i. In 1992 Pan and Wolff [49] presented work on computing the mutual coupling between slot-coupled microstrip patches in a finite array. This was done by using the spectral domain Green's function for an isotropic dielectric substrate. In this case the excitation source for each patch was taken into account by defining an equivalent N-port network. This allowed the coupling mechanism to be modeled in the mutual coupling computations. The next step in mutual coupling computations between rectangular patch antennas was taken by Wahid and Voor [50]. In this case the microstrip patches were on the same isotropic dielectric substrate except this time the patches were skewed, the $\bar{E}$ and $\bar{H}$ planes were not parallel. These computations were done by applying the exact Green's function [51]. Theoretical and measurement results compared well. Then in 1995 Tam *et al.* [52] presented work on mutual coupling between rectangular microstrip antennas on a cylindrical surface. With this work the authors studied the effect of curvature and separation on the mutual coupling between the printed antennas. The spectral domain Green's function was used to compute the mutual coupling and good comparison with measurements was shown.

It should be noted that all the problems mentioned above were solved using the method of moments. The work by Terret *et al.* [48] is the closest to the work presented here. Their work seems to be the first time mutual coupling is considered between two printed antennas on different isotropic layers.

2.2. Current Work on Microstrip Antennas and Arrays

More recently, printed antennas on multiple anisotropic materials have been revisited. In 2001 Verma and Nasimuddin [53] investigated the input impedance of rectangular microstrip antennas on multiple anisotropic layers. In this work it was assumed that the entire problem was above a ground plane and the top most

anisotropic superstrate was capped by a conducting shield. This differs from the work by Oliveira and D'Assunção [38]. In 2002 Wang [54] studied the characteristics of a printed dipole embedded in biaxial anisotropic dielectrics. This was done by assuming a current distribution on the dipole and defining a perfectly conducting sheet below the bottom layer and above the top layer. In 2003 Costa *et al.* [55] investigated the input impedance of an electromagnetically coupled microstrip antenna in multiple anisotropic layers. This was done by using a full-wave spectral domain technique and solved using the method of moments. Also, recently printed antennas have been developed [56]-[60] to provide a small surface area and wide-band characteristics. In 1998 Waterhouse *et al.* [56] discussed the design and performance of using shorting posts on a microstrip patch antenna on an isotropic substrate. It is shown in Figure 11 that a shorting post is a conducting material connected between the conducting patch and ground plane. By using shorting posts a smaller patch area and a higher bandwidth was achieved. Waterhouse *et al.* showed the predicted and measured input impedance and far-field patterns for an antenna similar to the one in Figure 11. Later in 2002 Li *et al.* [60] presented an antenna similar to Waterhouse *et al.* for communication systems such as Bluetooth ISM. In 2001 Shackelford *et al.* [58] presented the small-sized wide-band U-slot and L-probe fed microstrip antenna with shorting walls shown in Figure 12. It is shown that the printed antenna is on two isotropic layers. The printed antenna is on the second isotropic layer and the L-probe is on the first isotropic layer. Depending on the configuration, a bandwidth (BW) of 45.1 percent was achieved. Later in 2004 two other broadband patch antennas were presented. Li *et al.* [59] presented a triangular patch antenna with a folded shorting wall and air as the dielectric substrate. They determined the patterns, reflection coefficient S_{11} and that the antenna has a BW of 36.2 percent. Chiu *et al.* [57] also presented a broadband antenna with double shorting walls and a dielectric substrate

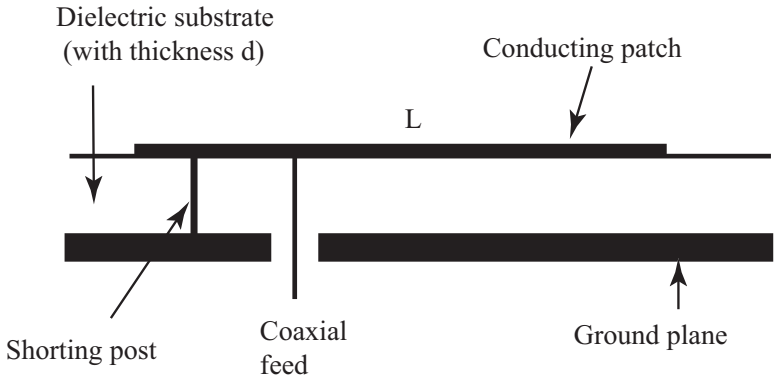

Figure 11. Microstrip antenna with a shorting post.

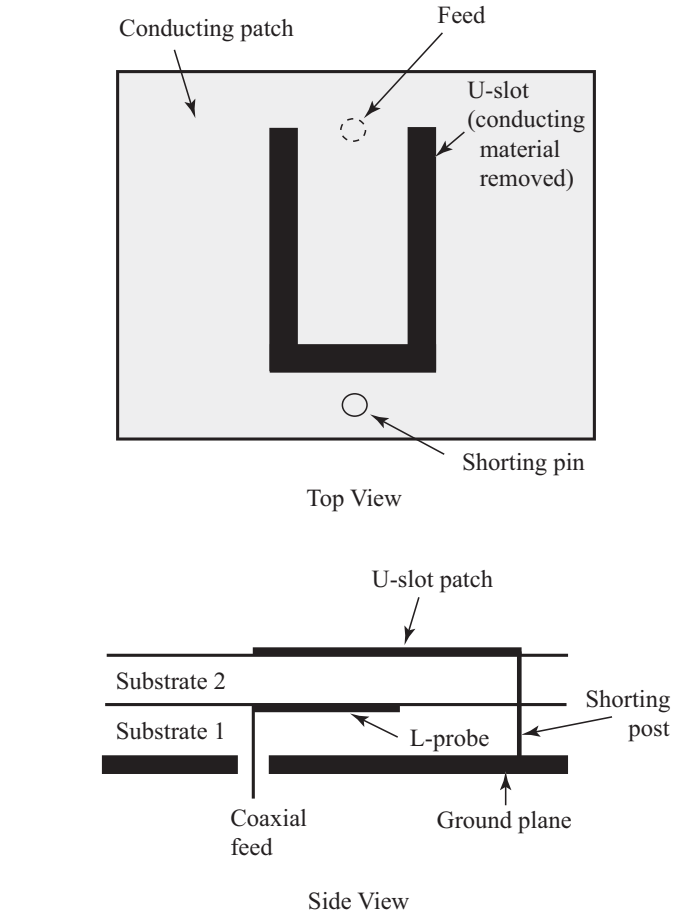

Figure 12. U-slot microstrip antenna.

of air. They determined the VSWR from 3.5 GHz to 9.5 GHz and observed a BW of 71.7 percent. This antenna is very useful for wide-band communications.

Dual-band capabilities is another emerging field in antenna research. In 2006 Sheta *et al.* [61] presented a dual-band microstrip antenna. They showed that by designing two antennas for different center frequencies and combining them appropriately, the resulting antenna can operate near or at the two original center frequencies. They presented S_{11} and various far-field radiation patterns.

New properties on metamaterials [62]-[66] has also grown tremendously in the past several years. In 2003 Balmain *et al.* [66] presented a type of metamaterial that can be used as a superstrate to direct the field of a single antenna in a conical form through the material. These conical regions were called resonance cones. The authors showed that the fields calculated by the moment method are in good agreement with measurements. In 2005 Baccaralli *et al.* [63] investigated the modal properties of surface waves of grounded metamaterial for planar antennas. Preliminary results for the far-field patterns of a dipole source above grounded metamaterial were presented. In 2007 Markley and Eleftheriades [62] presented a negative-refractive-index metamaterial for incident plane waves of an arbitrary polarization. This was achieved by metalization patterns above and below an isotropic dielectric slab.

Significant research on mutual coupling has also been performed in the past few years. In 2003 Yang and Rahmatt-Sammi [67] presented a low mutual coupling design of an array of electromagnetic band gap structures. This structure was analyzed using the finite difference time domain (FDTD) method and used printed antennas on a single isotropic dielectric substrate. In 2005 Chair *et al.* [68] presented work on the mutual coupling between a two-element array of circular patch antennas on an isotropic dielectric substrate. The computations were performed using the commercially available software IE3D [69], and S_{11} was shown versus frequency for

various patch configurations. Then in 2007 Buell *et al.* [64] used metamaterial to suppress the mutual coupling between elements in a densely packed array. This was achieved by using metamaterial as the isolation walls between the elements.

In this summary it was shown that significant research is still being conducted on microstrip antennas and arrays. It also was shown that much more work has yet to be done.

Several properties of dielectric material along with anisotropy are defined in the next section. This is done before the section on the proposed research to establish an understanding about the material properties of this work.

2.3. Anisotropy

The material around the printed antennas in this research is assumed to be a dielectric. In dielectrics, the constitutive parameters (ε, μ and σ) determine how the dielectric material will react when subjected to an electromagnetic field [23], [70]. Dielectrics with constitutive parameters that are not functions of the applied electromagnetic field are called *linear*; otherwise they are called *nonlinear* dielectrics. Similarly, if the constitutive parameters of a dielectric are not a function of position, then the dielectric is called *homogeneous*. If the constitutive parameters are a function of position then the dielectric is *inhomogeneous* or *nonhomogeneous*. Many dielectrics are almost linear within a certain frequency range [23] and are assumed to be linear in this work. Similarly, many dielectrics are slightly nonhomogeneous [23], but in practice this nonhomogeneous characteristic is so small that it can be neglected. If the constitutive parameters are a function of frequency, the material is called *dispersive*; otherwise the material is called a *nondispersive* material [23]. The dielectric material in this research is assumed to be *nondispersive*. If the constitutive parameters are a function of the direction of the applied field then the material is called *anisotropic*; otherwise the material is called *isotropic* [23]. This work assumes that the material

is anisotropic. In anisotropic dielectrics the permittivity ε cannot be represented as a single value. Therefore the permittivity in the anisotropic dielectric is represented as a 3x3 tensor [23], [71]

$$[\varepsilon] = \begin{bmatrix} \varepsilon_{11} & \varepsilon_{12} & \varepsilon_{13} \\ \varepsilon_{21} & \varepsilon_{22} & \varepsilon_{23} \\ \varepsilon_{31} & \varepsilon_{32} & \varepsilon_{33} \end{bmatrix}. \tag{2.11}$$

It is well known that many dielectric materials exhibit some dielectric anisotropy. This may occur naturally or during the manufacturing process [72]. In fact, the following symmetry $\varepsilon_{ij} = \varepsilon_{ji}$ [71], [72] is assumed for the lossless case. Alexopoulus [72] mentions that the matrix (2.11) for this lossless case can be transformed to the following diagonal matrix:

$$[\varepsilon] = \begin{bmatrix} \varepsilon_r & 0 & 0 \\ 0 & \varepsilon_s & 0 \\ 0 & 0 & \varepsilon_t \end{bmatrix} \tag{2.12}$$

where ε_r, ε_s and ε_t are the eigenvalues of $[\varepsilon]$. If the anisotropic dielectric is *biaxial* then ε_r, ε_s and ε_t have distinct values. But if ε_r=ε_t then the anisotropic dielectric is called *uniaxial*. For this work it is assumed that the anisotropic dielectric material is lossless and uniaxial. Thus, (2.12) simplifies down to the following case:

$$[\varepsilon] = \begin{bmatrix} \varepsilon_r & 0 & 0 \\ 0 & \varepsilon_s & 0 \\ 0 & 0 & \varepsilon_r \end{bmatrix}. \tag{2.13}$$

The directions of ε_r, ε_s and ε_t in (2.12) define the principal axes of the anisotropic dielectrics as shown in Figure 13. As mentioned above, for this work the anisotropic dielectrics are assumed to be uniaxial and are characterized by a single axis of symmetry (optical axis). This symmetry leads to a parallel y-axis and optical axis

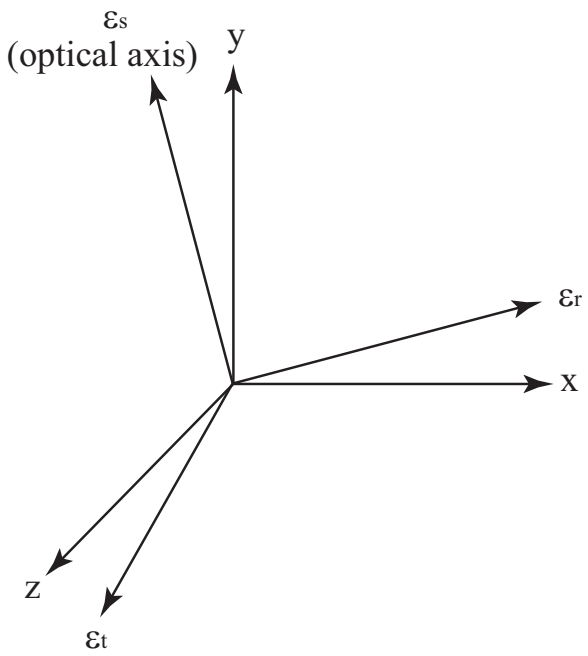

Figure 13. Physical and optical axis relation
for biaxial anisotropic dielectrics.

as well as the definition of $[\varepsilon]$ in (2.13). Thus, the optical axis will be normal to any printed conductors. Therefore, the permittivity in the j^{th} region will be given as:

$$[\varepsilon_j] = \begin{bmatrix} \varepsilon_{j2} & 0 & 0 \\ 0 & \varepsilon_{j1} & 0 \\ 0 & 0 & \varepsilon_{j2} \end{bmatrix} \tag{2.14}$$

where ε_{j2} is the permittivity in the direction along the axis orthogonal to the optical axis and ε_{j1} is the permittivity in the direction along the optical axis (i.e., y-direction).

2.4. Proposed Research

The study of microstrip antennas has many different areas and properties of interest. These include input impedance, resonant frequency, resonant dimensions, bandwidth, gain, efficiency, far-field patterns, near-field patterns and different feed techniques. If the antenna is in the presence of another conductor, then in addition

to all the properties just mentioned, mutual coupling is also of interest. The previous summary shows that more recent research involves printed antennas in complex structures such as layered anisotropic material [53], metamaterial [63] and structures with complex shorting walls [57]. But throughout all this research many fundamental questions have not been answered about the interaction between conducting elements in these types of environments.

In the proposed research the generalized layered structure in Figure 14 will be considered. Each layer of material is a uniaxial anisotropic dielectric layer extending infinitely in the x- and z-directions. Each layer has a permittivity of

$$[\varepsilon_j] = \begin{bmatrix} \varepsilon_{j2} & 0 & 0 \\ 0 & \varepsilon_{j1} & 0 \\ 0 & 0 & \varepsilon_{j2} \end{bmatrix} \varepsilon_0, \tag{2.15}$$

$\mu_r = \mu_0$ and $\sigma = 0$. Each layer can have a microstrip antenna defined on it; except below layer 1 because of the ground plane. This structure will allow any number of conducting patches to be driven and any number to be parasitic elements. Note that the conducting patches can be printed dipoles, rectangular microstrip patches, circular patches, broadband triangular patches or any array configuration.

It can be seen that if any element is driven in the structure, other printed conductors will have a significant impact on the properties listed above. Nelson *et al.* [34] studied the resonant frequency of an isolated rectangular microstrip antenna in a structure similar to the one defined in Figure 14, and Oliveira and D'Assunção [38] presented the input impedance of an isolated rectangular microstrip patch above layer 1 and with two anisotropic superstrates. Further work on a number of other properties such as bandwidth, gain, efficiency, field patterns and feed techniques could be done next. But with the presence of other conducting patches and other anisotropic layers,

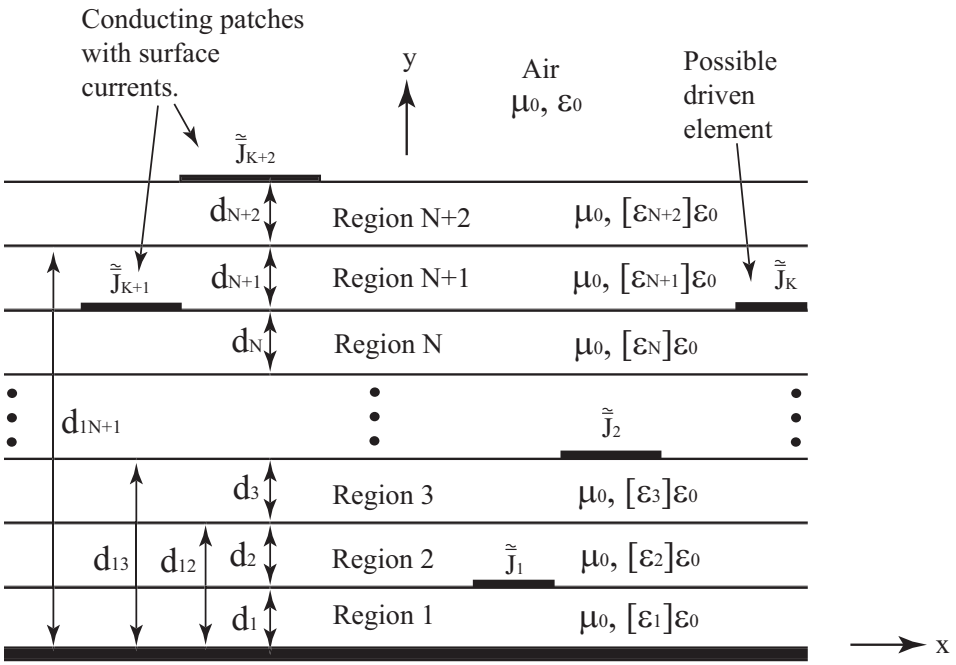

Figure 14. Printed conductors in layered anisotropic dielectrics.

the input impedance and mutual impedance may be of interest.

This work consists of numerical techniques and experimental measurements of problems defined on the arbitrary structure in Figure 14. In particular, the input impedance and mutual coupling between printed dipoles embedded in the anisotropic structure in Figure 14 will be studied.

Studying the input impedance and mutual coupling of these antennas in the stratified structure has a significant interest in many fields. One very large area is microstrip antenna arrays [12], [73]-[75]. Mutual coupling between elements of an array and the feed can have a significant impact on the design and ultimately the performance. Another area of interest is the study of frequency selective structures [76]-[78]. Some of these structures contain many printed conductors and mutual coupling is present. Radio frequency identification (RFID) [13]-[21] is another very fast growing area. The application of many different ultra high-frequency (UHF)

RFID tags in close proximity is an environment of extensive mutual coupling. A generalized version of the proposed research could study this effect on power harvesting capabilities and read ranges.

2.5. Numerical Techniques

Many different numerical methods could possibly be used to evaluate the structure in Figure 14. These include the exact Green's functions method, the equivalent magnetic source method, the transmission line method and a cavity model [29], [47]. But many of these methods have not been generalized to evaluate problems with multiple printed conductors or layered anisotropic dielectrics. This led to the choice of using the spectral domain immittance method [33]-[34] to evaluate these general problems. It has been shown by others that problems with multiple printed conductors in layered anisotropic material can be evaluated with accuracy using this method [38], [76]-[78].

The spectral domain immittance functions for one-, two- and three-layer anisotropic structures are derived in terms of the Hertz vector potentials in the next chapter. These expressions will then be used to solve for the unknown currents on the printed conductors.

CHAPTER 3. DERIVATION OF THE IMMITTANCE FUNCTIONS USING HERTZ VECTOR POTENTIALS

3.1. Introduction

In this chapter the electric field in each layer of anisotropic material will be written in terms of the Hertz vector potentials [79]. These fields will then be applied to problems with printed conductors in one, two and three layers of uniaxial anisotropic material. Then the Moment Method [80]-[81] will be used to determine the resonant frequency, input impedance and mutual coupling for various printed dipole configurations.

3.2. Field Derivation Using the Hertz Vector Potentials

Consider the problem in Figure 15 of an arbitrary conducting patch on an anisotropic substrate extending infinitely in the x- and z-directions. Assume that the substrate has an optical axis in the y-direction and is uniaxially anisotropic with permittivity

$$[\varepsilon_j] = \begin{bmatrix} \varepsilon_{j2} & 0 & 0 \\ 0 & \varepsilon_{j1} & 0 \\ 0 & 0 & \varepsilon_{j2} \end{bmatrix} \varepsilon_0. \tag{3.1}$$

The following Hertz vector potentials are introduced to solve for the fields in the anisotropic substrate and the region above the conducting patch [34], [79]:

$$\bar{\Pi}_e = \Pi_{ex}\hat{a}_x + \Pi_{ey}\hat{a}_y + \Pi_{ez}\hat{a}_z \tag{3.2}$$

and

$$\bar{\Pi}_h = \Pi_{hx}\hat{a}_x + \Pi_{hy}\hat{a}_y + \Pi_{hz}\hat{a}_z \tag{3.3}$$

where $\bar{\Pi}_e$ is denoted as the electric Hertz potential and $\bar{\Pi}_h$ is denoted as the magnetic

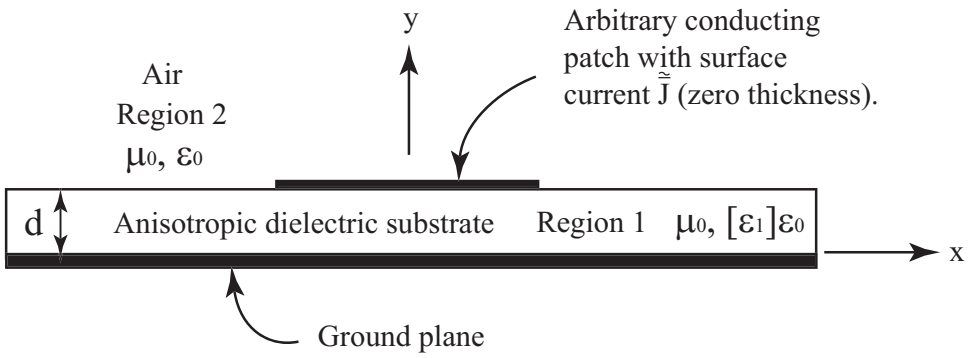

Figure 15. Arbitrary conducting patch on a single grounded anisotropic substrate.

Hertz potential. Other common vector potential functions used to solve many electromagnetics problems are the magnetic vector potential $\bar{A}$ and the electric vector potential $\bar{F}$ [23]. The electric Hertz potential is similar to $\bar{A}$ and the magnetic Hertz potential is similar to $\bar{F}$. The lowest-order mode in an electromagnetics problem is the Transverse Electromagnetic (TEM) mode. The TEM mode has electric and magnetic field components transverse to the direction of propagation. The higher order modes are referred to as the Transverse Electric (TE) and Transverse Magnetic (TM) modes and contain a magnetic and electric field component, respectively, in the direction of propagation. In many radiation problems a low-order TEM mode will satisfy the boundary conditions (BC) but, in a problem that contains dielectric waveguides, it is impossible for a TEM mode to satisfy all the BC in the problem. This results in a restriction of using higher order TE and TM modes as a solution to the problem [79]. First, a definition for the TM and TE mode to a given direction is needed. Since the optical axis is chosen to be in the y-direction and the tangential components are in the x-z plane, the y-components of (3.2) and (3.3) will be used to yield a TE and TM

mode with respect to the optical axis [33]-[34]. This then gives [33]-[34]

$$\bar{\Pi}_e = \Pi_e \hat{a}_y \tag{3.4}$$

and

$$\bar{\Pi}_h = \Pi_h \hat{a}_y. \tag{3.5}$$

In (3.4) and (3.5) the simplified terms Π_e and Π_h are used to represent the y-component of the electric and magnetic Hertz potentials, respectively, instead of Π_{ey} and Π_{hy}. The electric Hertz potential will result in a TM-to-y solution and the magnetic Hertz potential will result in a TE-to-y solution [34]. Then, the total solution in each region will be the sum of the TM and TE solutions [79]. Next, the fields for all regions in Figure 15 will be written in terms of the Hertz vector potentials defined in (3.4) and (3.5). Using (3.4) the following expression for the magnetic field $\bar{H}$ is defined:

$$\bar{H} = j\omega\varepsilon_0 \nabla \times \bar{\Pi}_e. \tag{3.6}$$

Substituting (3.6) into Maxwell's equation,

$$\nabla \times \bar{E} = -j\omega\mu_0 \bar{H}, \tag{3.7}$$

results in

$$\begin{aligned} \nabla \times \bar{E} &= -j\omega\mu_0 (j\omega\varepsilon \nabla \times \bar{\Pi}_e) \\ &= \omega^2 \mu_0 \varepsilon_0 (\nabla \times \bar{\Pi}_e). \end{aligned} \tag{3.8}$$

By grouping the expressions in (3.8) on the left side and noting that the curl of the

gradient of a scalar function ϕ_e is always zero [9] results in:

$$\begin{aligned}\nabla \times \bar{E} - \omega^2 \mu_0 \varepsilon_0 \nabla \times \bar{\Pi}_e &= \nabla \times (\bar{E} - \omega^2 \mu_0 \varepsilon_0 \bar{\Pi}_e) \\ &= \nabla \times \nabla \phi_e \\ &= 0.\end{aligned}$$

Solving for $\bar{E}$ gives

$$\bar{E} = \omega^2 \mu_0 \varepsilon_0 \bar{\Pi}_e + \nabla \phi_e. \tag{3.9}$$

Next, using Maxwell's equation of $\nabla \times \bar{H} = j\omega[\varepsilon_j]\bar{E}$ gives

$$\begin{aligned}\nabla \times \bar{H} &= j\omega \bar{D} \\ &= j\omega[\varepsilon_j]\bar{E}\varepsilon_0 \\ &= j\omega[\varepsilon_{j2}\varepsilon_0 E_x \hat{a}_x + \varepsilon_{j1}\varepsilon_0 E_y \hat{a}_y + \varepsilon_{j2}\varepsilon_0 E_z \hat{a}_z] \\ &= j\omega[\varepsilon_{j2}\varepsilon_0 E_x \hat{a}_x + \varepsilon_{j1}\varepsilon_0 E_y \hat{a}_y + \varepsilon_{j2}\varepsilon_0 E_z \hat{a}_z + \varepsilon_{j2}\varepsilon_0 E_y \hat{a}_y - \varepsilon_{j2}\varepsilon_0 E_y \hat{a}_y] \\ &= j\omega\varepsilon_0[\varepsilon_{j2}\bar{E} + (\varepsilon_{j1} - \varepsilon_{j2})E_y \hat{a}_y] \\ &= j\omega\varepsilon_0\varepsilon_{j2}[\bar{E} + \frac{\varepsilon_{j1} - \varepsilon_{j2}}{\varepsilon_{j2}} E_y \hat{a}_y] \qquad (3.10)\end{aligned}$$

where $\bar{E} = E_x \hat{a}_x + E_y \hat{a}_y + E_z \hat{a}_z$. Then taking the curl of both sides of (3.6) and substituting in (3.10) results in

$$\varepsilon_{j2}[\bar{E} + \frac{\varepsilon_{j1} - \varepsilon_{j2}}{\varepsilon_{j2}} E_y \hat{a}_y] = \nabla \times \nabla \times \bar{\Pi}_e. \tag{3.11}$$

Next, substituting (3.9) in (3.11) yields

$$\varepsilon_{j2}\left[\omega^2 \mu_0 \varepsilon_0 \bar{\Pi}_e + \nabla \phi_e + \frac{\varepsilon_{j1} - \varepsilon_{j2}}{\varepsilon_{j2}}(\omega^2 \mu_0 \varepsilon_0 \bar{\Pi}_e + \frac{\partial \phi_e}{\partial y}\hat{a}_y)\right] = \nabla \times \nabla \times \bar{\Pi}_e. \tag{3.12}$$

Then, using the identity $\nabla \times \nabla \times \bar{\Pi} = \nabla\nabla \cdot \bar{\Pi} - \nabla^2\bar{\Pi}$ gives

$$\omega^2\mu_0\varepsilon_0\varepsilon_{j2}\bar{\Pi}_e+\varepsilon_{j2}\nabla\phi_e+(\varepsilon_{j1}-\varepsilon_{j2})\omega^2\mu_0\varepsilon_0\bar{\Pi}_e+(\varepsilon_{j1}-\varepsilon_{j2})\frac{\partial\phi_e}{\partial y}\hat{a}_y = \nabla\nabla\cdot\bar{\Pi}_e-\nabla^2\bar{\Pi}_e. \quad (3.13)$$

This implies

$$\nabla(\nabla \cdot \bar{\Pi}_e - \varepsilon_{j2}\phi_e) = \nabla^2\bar{\Pi}_e + \omega^2\mu_0\varepsilon_0\varepsilon_{j1}\bar{\Pi}_e + (\varepsilon_{j1} - \varepsilon_{j2})\frac{\partial\phi_e}{\partial y}\hat{a}_y. \quad (3.14)$$

Since ϕ_e and $\nabla \cdot \bar{\Pi}_e$ are arbitrary, the following condition is chosen

$$\nabla \cdot \bar{\Pi}_e = \varepsilon_{j2}\phi_e. \quad (3.15)$$

This implies

$$\frac{\partial\phi_e}{\partial y}\hat{a}_y = \frac{1}{\varepsilon_{j2}}\frac{\partial^2\bar{\Pi}_e}{\partial y^2}\hat{a}_y \quad (3.16)$$

and

$$\nabla\phi_e = \frac{1}{\varepsilon_{j2}}\nabla\nabla \cdot \bar{\Pi}_e. \quad (3.17)$$

Substituting (3.15)-(3.17) into (3.14) results in

$$\nabla^2\bar{\Pi}_e + \omega^2\mu_0\varepsilon_0\varepsilon_{j1}\bar{\Pi}_e + (\varepsilon_{j1} - \varepsilon_{j2})\frac{1}{\varepsilon_{j2}}\frac{\partial^2\bar{\Pi}_e}{\partial y^2} = 0. \quad (3.18)$$

Also, substituting (3.17) into (3.9) gives

$$\bar{E} = \omega^2\mu_0\varepsilon_0\bar{\Pi}_e + \frac{1}{\varepsilon_{j2}}\nabla\nabla \cdot \bar{\Pi}_e. \quad (3.19)$$

Equations (3.6), (3.18) and (3.19) are all in terms of one unknown, $\bar{\Pi}_e$. These expressions represent the extraordinary wave [34],[79].

The next step is to derive similar expressions to (3.6), (3.18) and (3.19) in terms

of the magnetic Hertz potential $\bar{\Pi}_h$. To do this the following relation is defined:

$$\bar{E} = -j\omega\mu_0 \nabla \times \bar{\Pi}_h \tag{3.20}$$

where $\bar{\Pi}_h$ is defined in (3.5). Then, substituting (3.20) into Maxwell's equation of $\nabla \times \bar{E} = -j\omega\mu_0 \bar{H}$ gives

$$-j\omega\mu_0(\nabla \times \nabla \times \bar{\Pi}_h) = -j\omega\mu_0 \bar{H}. \tag{3.21}$$

Then using the identity $\nabla \times \nabla \times \bar{\Pi} = \nabla\nabla \cdot \bar{\Pi} - \nabla^2\bar{\Pi}$ gives

$$\bar{H} = \nabla\nabla \cdot \bar{\Pi}_h - \nabla^2\bar{\Pi}_h. \tag{3.22}$$

Next, using (3.20), $\nabla \times \bar{H} = j\omega[\varepsilon_j]\bar{E}$ can be written in the follower manner:

$$\begin{aligned}
\nabla \times \bar{H} &= j\omega\varepsilon_0[\varepsilon_j]\bar{E} \\
&= j\omega\varepsilon_0[\varepsilon_{j2}E_x\hat{a}_x + \varepsilon_{j2}E_z\hat{a}_z] \\
&= j\omega\varepsilon_0\varepsilon_{j2}\bar{E} \\
&= j\omega\varepsilon_0\varepsilon_{j2}(-j\omega\mu_0\nabla \times \bar{\Pi}_h) \\
&= \omega^2\mu_0\varepsilon_0\varepsilon_{j2}\nabla \times \bar{\Pi}_h.
\end{aligned} \tag{3.23}$$

Since the curl of the gradient of a scalar is zero, using (3.23), (3.22) can be written as

$$\begin{aligned}
\bar{H} &= \omega^2\mu_0\varepsilon_0\varepsilon_{j2}\bar{\Pi}_h + \nabla\phi_h \\
&= \nabla(\nabla \cdot \bar{\Pi}_h) - \nabla^2\bar{\Pi}_h
\end{aligned} \tag{3.24}$$

where ϕ_h is a scalar function. Solving for $\nabla^2\bar{\Pi}_h$ in (3.24) gives

$$\nabla^2\bar{\Pi}_h = \nabla(\nabla\cdot\bar{\Pi}_h - \phi_h) - \omega^2\mu_0\varepsilon_0\varepsilon_{j2}\bar{\Pi}_h. \tag{3.25}$$

Since ϕ_h is arbitrary, the following relation is defined: $\nabla\cdot\bar{\Pi}_h = \phi_h$. Substituting this into (3.25) gives

$$\nabla^2\bar{\Pi}_h + \omega^2\mu_0\varepsilon_0\varepsilon_{j2}\bar{\Pi}_h = 0. \tag{3.26}$$

Equations (3.20), (3.24) and (3.26) are all in terms of one unknown, $\bar{\Pi}_h$. These expressions represent the ordinary wave [34],[79].

Next, the following Fourier transform $\widetilde{\Phi}(\alpha, y, \beta)$ of the function $\Phi(x, y, z)$ is defined as [82]-[83]

$$\widetilde{\Phi}(\alpha, y, \beta) = \int_{-\infty}^{+\infty}\int_{-\infty}^{+\infty}\Phi(x, y, z)e^{-j(\alpha x+\beta z)}dxdz. \tag{3.27}$$

This then results in the following transform for the partial derivatives:

$$\frac{\partial\Phi}{\partial x} \Leftrightarrow j\alpha\widetilde{\Phi} \tag{3.28}$$

and

$$\frac{\partial\Phi}{\partial z} \Leftrightarrow j\beta\widetilde{\Phi}. \tag{3.29}$$

The inverse Fourier transform will then have the following definition:

$$\Phi(x, y, z) = \frac{1}{(2\pi)^2}\int_{-\infty}^{+\infty}\int_{-\infty}^{+\infty}\widetilde{\Phi}(\alpha, y, \beta)e^{j(\alpha x+\beta z)}d\alpha d\beta. \tag{3.30}$$

The Fourier transform is applied next to avoid the derivatives associated with the previously derived expressions. This greatly simplifies the numerical implementation of the equations.

First, the Fourier transform of (3.18) is evaluated. Expanding (3.18) for region j gives

$$\frac{\partial^2 \Pi_{ej}}{\partial x^2} + \frac{\varepsilon_{j2}}{\varepsilon_{j2}} \frac{\partial^2 \Pi_{ej}}{\partial y^2} + \frac{\partial^2 \Pi_{ej}}{\partial z^2} + \omega^2 \mu_0 \varepsilon_0 \varepsilon_{j1} \Pi_{ej} + (\varepsilon_{j1} - \varepsilon_{j2}) \frac{1}{\varepsilon_{j2}} \frac{\partial^2 \Pi_{ej}}{\partial y^2} = 0. \tag{3.31}$$

Simplifying (3.31) yields

$$\frac{\partial^2 \Pi_{ej}}{\partial x^2} + \frac{\varepsilon_{j1}}{\varepsilon_{j2}} \frac{\partial^2 \Pi_{ej}}{\partial y^2} + \frac{\partial^2 \Pi_{ej}}{\partial z^2} + \omega^2 \mu_0 \varepsilon_0 \varepsilon_{j1} \Pi_{ej} = 0. \tag{3.32}$$

Using (3.28) and (3.29), (3.32) transforms in the following manner:

$$-\alpha^2 \widetilde{\Pi}_{ej} + \frac{\varepsilon_{j1}}{\varepsilon_{j2}} \frac{\partial \widetilde{\Pi}^2_{ej}}{\partial y^2} - \beta^2 \widetilde{\Pi}_{ej} + \omega^2 \mu_0 \varepsilon_0 \varepsilon_{j1} \widetilde{\Pi}_{ej} = 0. \tag{3.33}$$

This then gives

$$\frac{\partial \widetilde{\Pi}^2_{ej}}{\partial y^2} - \gamma^2_{ej} \widetilde{\Pi}_{ej} = 0 \tag{3.34}$$

where

$$\gamma^2_{ej} = \frac{\varepsilon_{j2}}{\varepsilon_{j1}} (\alpha^2 + \beta^2 - \omega^2 \mu_0 \varepsilon_0 \varepsilon_{j1}). \tag{3.35}$$

Note that (3.34) is the same as Equation 3-27 in Nelson's work [71] even with the different Fourier transform defined in (3.27).

Similarly, expanding (3.26) for region j gives

$$\frac{\partial^2 \Pi_{hj}}{\partial x^2} + \frac{\partial^2 \Pi_{hj}}{\partial y^2} + \frac{\partial^2 \Pi_{hj}}{\partial z^2} + \omega^2 \mu_0 \varepsilon_0 \varepsilon_{j2} \Pi_{hj} = 0. \tag{3.36}$$

Using (3.28) and (3.29), (3.36) transforms in the following manner:

$$-\alpha^2 \widetilde{\Pi}_{hj} + \frac{\partial^2 \widetilde{\Pi}_{hj}}{\partial y^2} - \beta^2 \widetilde{\Pi}_{hj} + \omega^2 \mu_0 \varepsilon_0 \varepsilon_{j2} \widetilde{\Pi}_{hj} = 0. \tag{3.37}$$

This then gives

$$\frac{\partial \widetilde{\Pi}_{hj}^2}{\partial y^2} - \gamma_{hj}^2 \widetilde{\Pi}_{hj} = 0 \tag{3.38}$$

where

$$\gamma_{hj}^2 = (\alpha^2 + \beta^2 - \omega^2 \mu_0 \varepsilon_0 \varepsilon_{j2}). \tag{3.39}$$

Note that $j = 1, 2$ for (3.34) and (3.38) and that $\varepsilon_{j1} = \varepsilon_{j2} = 1$ for air. Since $\bar{\Pi}_{hj} = \Pi_{hj} \hat{a}_y$, (3.20) can be written in the j^{th} region as

$$\begin{aligned} \bar{E}_j &= -j\omega\mu_0 \nabla \times \bar{\Pi}_{hj} \\ &= -j\omega\mu_0 \bigg(- \frac{\partial \Pi_{hj}}{\partial z} \hat{a}_x + \frac{\partial \Pi_{hj}}{\partial x} \hat{a}_z \bigg). \end{aligned} \tag{3.40}$$

Using the definition of the Fourier transform in (3.27) results in the following expressions for the x-, y- and z-components of the electric field in the j^{th} region:

$$\widetilde{E}_{xj} = -\omega\mu_0 \beta \widetilde{\Pi}_{hj}, \tag{3.41}$$

$$\widetilde{E}_{yj} = 0, \tag{3.42}$$

$$\widetilde{E}_{zj} = \omega\mu_0 \alpha \widetilde{\Pi}_{hj}. \tag{3.43}$$

Notice that (3.40) has both x- and z-components. This is a direct result of using the y-component of the Hertz vector potential. Having x- and z-components enforces the tangential BC between the anisotropic dielectric layers. Similarly, (3.24) can be expanded for the j^{th} region in the following manner:

$$\begin{aligned} \bar{H}_j &= \nabla \bigg(\frac{\partial \Pi_{hj}}{\partial y} \bigg) - \frac{\partial^2 \bar{\Pi}_{hj}}{\partial x^2} - \frac{\partial^2 \bar{\Pi}_{hj}}{\partial y^2} - \frac{\partial^2 \bar{\Pi}_{hj}}{\partial z^2} \\ &= \frac{\partial^2 \Pi_{hj}}{\partial x \partial y} \hat{a}_x + \bigg(- \frac{\partial^2 \Pi_{hj}}{\partial x^2} - \frac{\partial^2 \Pi_{hj}}{\partial z^2} \bigg) \hat{a}_y - \frac{\partial^2 \Pi_{hj}}{\partial z \partial y} \hat{a}_z. \end{aligned} \tag{3.44}$$

Using the definition of the Fourier transform in (3.27) results in the following expressions for the x-, y- and z-components of the magnetic field in the j^{th} region:

$$\widetilde{H}_{xj} = j\alpha\frac{\partial\widetilde{\Pi}_{hj}}{\partial y}, \tag{3.45}$$

$$\widetilde{H}_{yj} = (\alpha^2+\beta^2)\widetilde{\Pi}_{hj}, \tag{3.46}$$

$$\widetilde{H}_{zj} = j\beta\frac{\partial\widetilde{\Pi}_{hj}}{\partial y}. \tag{3.47}$$

Next, the field expressions need to be derived in terms of $\bar{\Pi}_e = \Pi_{ej}\hat{a}_y$. Equation (3.6) results in

$$\bar{H}_j = j\omega\varepsilon_0\bigg(-\frac{\partial\Pi_{ej}}{\partial z}\hat{a}_x + \frac{\partial\Pi_{ej}}{\partial x}\hat{a}_z\bigg). \tag{3.48}$$

Using the definition of the Fourier transform in (3.27) results in the following expressions for the x-, y- and z-components of the magnetic field in the j^{th} region:

$$\widetilde{H}_{xj} = \omega\varepsilon_0\beta\widetilde{\Pi}_{ej}, \tag{3.49}$$

$$\widetilde{H}_{yj} = 0, \tag{3.50}$$

$$\widetilde{H}_{zj} = -\omega\varepsilon_0\alpha\widetilde{\Pi}_{ej}. \tag{3.51}$$

Next, expanding (3.19) gives

$$\begin{aligned}\bar{E}_j &= \omega^2\mu_0\varepsilon_0\Pi_{ej}\hat{a}_y + \frac{1}{\varepsilon_{j2}}\bigg(\frac{\partial^2\Pi_{ej}}{\partial x\partial y}\hat{a}_x + \frac{\partial^2\Pi_{ej}}{\partial y^2}\hat{a}_y + \frac{\partial^2\Pi_{ej}}{\partial z\partial y}\hat{a}_z\bigg)\\ &= \frac{1}{\varepsilon_{j2}}\frac{\partial^2\Pi_{ej}}{\partial x\partial y}\hat{a}_x + \bigg(\omega^2\mu_0\varepsilon_0\Pi_{ej}\hat{+}\frac{1}{\varepsilon_{j2}}\frac{\partial^2\Pi_{ej}}{\partial y^2}\bigg)\hat{a}_y + \frac{1}{\varepsilon_{j2}}\frac{\partial^2\Pi_{ej}}{\partial z\partial y}\hat{a}_z\bigg).\end{aligned} \tag{3.52}$$

Using the definition of the Fourier transform in (3.27) results in the following

expressions for the x-, y- and z-components of the electric field in the j^{th} region:

$$\widetilde{E}_{xj} = \frac{j\alpha}{\varepsilon_{j2}}\frac{\partial\widetilde{\Pi}_{ej}}{\partial y}, \tag{3.53}$$

$$\widetilde{E}_{yj} = \omega^2\mu_0\varepsilon_0\widetilde{\Pi}_{ej} + \frac{1}{\varepsilon_{j2}}\frac{\partial^2\widetilde{\Pi}_{ej}}{\partial y^2}, \tag{3.54}$$

$$\widetilde{E}_{zj} = \frac{j\beta}{\varepsilon_{j2}}\frac{\partial\widetilde{\Pi}_{ej}}{\partial y}. \tag{3.55}$$

Expressions for the x-, y- and z-components of the electric and magnetic fields in the j^{th} region in terms of $\widetilde{\Pi}_{ej}$ and $\widetilde{\Pi}_{hj}$ have been derived. The total electric and magnetic field in the j^{th} region is the superposition of the fields written in terms of $\widetilde{\Pi}_{ej}$ and $\widetilde{\Pi}_{hj}$ (i.e., the total field is the sum of the TM and TE modes represented by $\widetilde{\Pi}_{ej}$ and $\widetilde{\Pi}_{hj}$, respectively). Therefore, using (3.41)-(3.43), (3.45)-(3.47), (3.49)-(3.51) and (3.53)-(3.55), the total electric and magnetic fields in the j^{th} region can be written as:

$$\widetilde{E}_{xj} = -\omega\mu_0\beta\widetilde{\Pi}_{hj} + \frac{j\alpha}{\varepsilon_{j2}}\frac{\partial\widetilde{\Pi}_{ej}}{\partial y}, \tag{3.56}$$

$$\widetilde{E}_{yj} = \omega^2\mu_0\varepsilon_0\widetilde{\Pi}_{ej} + \frac{1}{\varepsilon_{j2}}\frac{\partial^2\widetilde{\Pi}_{ej}}{\partial y^2}, \tag{3.57}$$

$$\widetilde{E}_{zj} = \omega\mu_0\alpha\widetilde{\Pi}_{hj} + \frac{j\beta}{\varepsilon_{j2}}\frac{\partial\widetilde{\Pi}_{ej}}{\partial y}, \tag{3.58}$$

$$\widetilde{H}_{xj} = j\alpha\frac{\partial\widetilde{\Pi}_{hj}}{\partial y} + \omega\varepsilon_0\beta\widetilde{\Pi}_{ej}, \tag{3.59}$$

$$\widetilde{H}_{yj} = (\alpha^2+\beta^2)\widetilde{\Pi}_{hj}, \tag{3.60}$$

$$\widetilde{H}_{zj} = j\beta\frac{\partial\widetilde{\Pi}_{hj}}{\partial y} - \omega\varepsilon_0\alpha\widetilde{\Pi}_{ej}. \tag{3.61}$$

The expressions in (3.56)-(3.61) will be used to enforce the boundary conditions on the surfaces in Figure 15. The terms $\widetilde{\Pi}_{ej}$ and $\widetilde{\Pi}_{hj}$ will be found by solving the partial differential equations in (3.34) and (3.38) for each region. For the region below the

conducting patch (in the substrate) in Figure 15, the following solutions are assumed:

$$\widetilde{\Pi}_{hj} = A_j(\alpha,\beta)\sinh(\gamma_{hj}y) + A'_j(\alpha,\beta)\cosh(\gamma_{hj}y) \tag{3.62}$$

$$\widetilde{\Pi}_{ej} = B_j(\alpha,\beta)\cosh(\gamma_{ej}y) + B'_j(\alpha,\beta)\sinh(\gamma_{ej}y). \tag{3.63}$$

For the region above the substrate (air), the following solutions are assumed:

$$\widetilde{\Pi}_{hj} = A_j(\alpha,\beta)e^{-\gamma_0(y-d_1)} \tag{3.64}$$

$$\widetilde{\Pi}_{ej} = B_j(\alpha,\beta)e^{-\gamma_0(y-d_1)} \tag{3.65}$$

where

$$\gamma_0^2 = \alpha^2 + \beta^2 - \omega^2\mu_0\varepsilon_0. \tag{3.66}$$

Equations (3.62) and (3.63) represent a solution in a region that supports guided waves, hence the hyperbolic sines and cosines. Equations (3.64) and (3.65) represent a solution in a region that supports a decaying wave in the +y-direction, hence the decaying exponentials. The application of (3.56)-(3.61) to problems with printed conductors in stratified anisotropic material will be considered in the next sections.

3.3. One Anisotropic Layer

The first problem evaluated is the printed conductor on a single anisotropic layer shown in Figure 16. Region 2 is assumed to be air and region 1 has a permeability of μ_0, permittivity of $[\varepsilon_1]$ and has thickness d_1. The conducting patch is assumed to have an unknown current $\widetilde{\bar{J}}_1$. Note that $\widetilde{\bar{J}}_1$ is shown to exist on a single conducting patch in Figure 16. This is not necessarily the case for all problems. $\widetilde{\bar{J}}_1$ could be modified to represent a current on multiple conductors at d_1. But for ease of derivation, $\widetilde{\bar{J}}_1$ is defined on one printed conductor. Modifying $\widetilde{\bar{J}}_1$ for multiple conductors will be discussed later. Also note that $\widetilde{\bar{J}}_1$ is written as a vector in the transform domain.

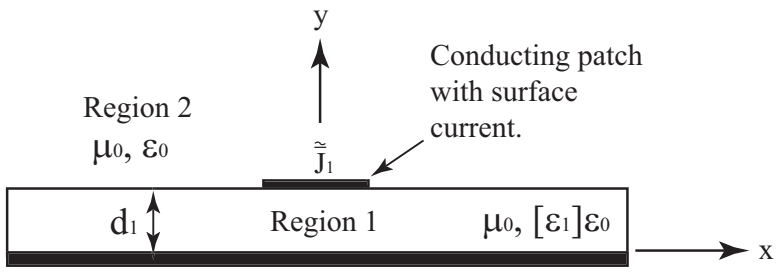

Figure 16. Printed conductor on a single grounded anisotropic substrate.

For the problem in Figure 16 the following tangential boundary conditions are enforced:

$$\widetilde{E}_{x1} = 0 \qquad y = 0 \tag{3.67}$$

$$\widetilde{E}_{z1} = 0 \qquad y = 0 \tag{3.68}$$

$$\widetilde{E}_{x1} = \widetilde{E}_{x2} \qquad y = d_1 \tag{3.69}$$

$$\widetilde{E}_{z1} = \widetilde{E}_{z2} \qquad y = d_1 \tag{3.70}$$

$$\widetilde{J}_{x1} = \widetilde{H}_{z2} - \widetilde{H}_{z1} \qquad y = d_1 \tag{3.71}$$

$$\widetilde{J}_{z1} = \widetilde{H}_{x1} - \widetilde{H}_{x2} \qquad y = d_1 \tag{3.72}$$

where $\widetilde{J}_{x1}$ and $\widetilde{J}_{z1}$ are the x- and z-components of the surface current $\widetilde{\bar{J}}_1$, respectively. Equations (3.56)-(3.61) will be used in terms of the electric and magnetic Hertz potentials to enforce the boundary conditions in (3.67)-(3.72). This will then lead to the spectral domain immittance functions that are similar to the expressions by Nelson [71].

3.3.1. Field expressions for region 1

In this section, the fields in region $j = 1$ will be written in terms of the Hertz

vector potential. Substituting (3.62) and (3.63) into (3.56) and using

$$\frac{\partial\widetilde{\Pi}_{e1}}{\partial y} = B_1(\alpha,\beta)\gamma_{e1}\sinh(\gamma_{e1}y) + B_1'(\alpha,\beta)\gamma_{e1}\cosh(\gamma_{e1}y) \tag{3.73}$$

gives:

$$\begin{aligned}\widetilde{E}_{x1}(\alpha,y,\beta) &= -\omega\mu_0\beta\Big[A_1(\alpha,\beta)\sinh(\gamma_{h1}y) + A_1'(\alpha,\beta)\cosh(\gamma_{h1}y)\Big] \\ &\quad +\frac{j\alpha}{\varepsilon_{12}}\Big[B_1(\alpha,\beta)\gamma_{e1}\sinh(\gamma_{e1}y) + B_1'(\alpha,\beta)\gamma_{e1}\cosh(\gamma_{e1}y)\Big]. \end{aligned}\tag{3.74}$$

Similarly, using

$$\frac{\partial\widetilde{\Pi}_{h1}}{\partial y} = A_1(\alpha,\beta)\gamma_{h1}\cosh(\gamma_{h1}y) + A_1'(\alpha,\beta)\gamma_{h1}\sinh(\gamma_{h1}y) \tag{3.75}$$

and substituting (3.62)-(3.63) into (3.58), (3.59) and (3.61) gives:

$$\begin{aligned}\widetilde{E}_{z1}(\alpha,y,\beta) &= \omega\mu_0\alpha\Big[A_1(\alpha,\beta)\sinh(\gamma_{h1}y) + A_1'(\alpha,\beta)\cosh(\gamma_{h1}y)\Big] \\ &\quad +\frac{j\beta}{\varepsilon_{12}}\Big[B_1(\alpha,\beta)\gamma_{e1}\sinh(\gamma_{e1}y) + B_1'(\alpha,\beta)\gamma_{e1}\cosh(\gamma_{e1}y)\Big], \end{aligned}\tag{3.76}$$

$$\begin{aligned}\widetilde{H}_{x1}(\alpha,y,\beta) &= j\alpha\Big[A_1(\alpha,\beta)\gamma_{h1}\cosh(\gamma_{h1}y) + A_1'(\alpha,\beta)\gamma_{h1}\sinh(\gamma_{h1}y)\Big] \\ &\quad +\omega\varepsilon_0\beta\Big[B_1(\alpha,\beta)\cosh(\gamma_{e1}y) + B_1'(\alpha,\beta)\sinh(\gamma_{e1}y)\Big], \end{aligned}\tag{3.77}$$

$$\begin{aligned}\widetilde{H}_{z1}(\alpha,y,\beta) &= j\beta\Big[A_1(\alpha,\beta)\gamma_{h1}\cosh(\gamma_{h1}y) + A_1'(\alpha,\beta)\gamma_{h1}\sinh(\gamma_{h1}y)\Big] \\ &\quad -\omega\varepsilon_0\alpha\Big[B_1(\alpha,\beta)\cosh(\gamma_{e1}y) + B_1'(\alpha,\beta)\sinh(\gamma_{e1}y)\Big]. \end{aligned}\tag{3.78}$$

Later, the expressions in (3.74) and (3.76)-(3.78) will be used to apply the boundary conditions for region 1 in (3.67)-(3.72).

3.3.2. Field expressions for region 2

In this section, the fields in region $j = 2$ will be written in terms of the Hertz

vector potential. Substituting (3.64) and (3.65) into (3.56) and using

$$\frac{\partial \widetilde{\Pi}_{e2}}{\partial y} = -\gamma_0 B_2(\alpha,\beta) e^{-\gamma_0(y-d_1)} \tag{3.79}$$

gives:

$$\widetilde{E}_{x2}(\alpha,y,\beta) = -\omega\mu_0\beta A_2(\alpha,\beta)e^{-\gamma_0(y-d_1)} - \frac{j\alpha}{\varepsilon_{22}}\gamma_0 B_2(\alpha,\beta)e^{-\gamma_0(y-d_1)}. \tag{3.80}$$

Similarly, using

$$\frac{\partial \widetilde{\Pi}_{h2}}{\partial y} = -\gamma_0 A_2(\alpha,\beta) e^{-\gamma_0(y-d_1)} \tag{3.81}$$

and substituting (3.64)-(3.65) into (3.58), (3.59) and (3.61) gives:

$$\widetilde{E}_{z2}(\alpha,y,\beta) = \omega\mu_0\alpha A_2(\alpha,\beta)e^{-\gamma_0(y-d_1)} - \frac{j\beta}{\varepsilon_{22}}\gamma_0 B_2(\alpha,\beta)e^{-\gamma_0(y-d_1)} \tag{3.82}$$

$$\widetilde{H}_{x2}(\alpha,y,\beta) = -j\alpha\gamma_0 A_2(\alpha,\beta)e^{-\gamma_0(y-d_1)} + \omega\varepsilon_0\beta B_2(\alpha,\beta)e^{-\gamma_0(y-d_1)} \tag{3.83}$$

$$\widetilde{H}_{z2}(\alpha,y,\beta) = -j\beta\gamma_0 A_2(\alpha,\beta)e^{-\gamma_0(y-d_1)} - \omega\varepsilon_0\alpha B_2(\alpha,\beta)e^{-\gamma_0(y-d_1)}. \tag{3.84}$$

The next section uses the expressions in (3.80) and (3.82)-(3.84) to apply the boundary conditions for region 2 in (3.67)-(3.72). This will result in solutions for A_1, A_1', B_1, B_1', A_2 and B_2 in (3.74), (3.76)-(3.78), (3.80) and (3.82)-(3.84).

3.3.3. The spectral domain immittance functions

In this section the boundary conditions in (3.67)-(3.72) will be enforced to solve for the coefficients in the field expressions. This process of substituting and solving for the coefficients is quite extensive. Because of this, the derivations for the following spectral domain immittance functions are shown in Appendix A and only the results are presented here. The x-component of the electric field at d_1 is:

$$\widetilde{E}_x(\alpha,d_1,\beta) = \widetilde{Z}_{xx}\widetilde{J}_{x1} + \widetilde{Z}_{xz}\widetilde{J}_{z1} \tag{3.85}$$

where

$$\widetilde{Z}_{xx} = \frac{\alpha^2}{\alpha^2+\beta^2}\left[-\frac{\gamma_{e1}\gamma_0}{j\omega\varepsilon_0[\gamma_{e1}+\varepsilon_{12}\gamma_0\coth(\gamma_{e1}d_1)]}\right] + \frac{\beta^2}{\alpha^2+\beta^2}\left[-\frac{j\omega\mu_0}{\gamma_0+\gamma_{h1}\coth(\gamma_{h1}d_1)}\right] \quad (3.86)$$

and

$$\widetilde{Z}_{xz} = \frac{\alpha\beta}{\alpha^2+\beta^2}\left[-\frac{\gamma_{e1}\gamma_0}{j\omega\varepsilon_0[\gamma_{e1}+\varepsilon_{12}\gamma_0\coth(\gamma_{h1}d_1)]} + \frac{j\omega\mu_0}{\gamma_0+\gamma_{h1}\coth(\gamma_{h1}d_1)}\right]. \quad (3.87)$$

Similarly, the z-component of the electric field at d_1 is:

$$\widetilde{E}_z(\alpha, d_1, \beta) = \widetilde{Z}_{zx}\widetilde{J}_{x1} + \widetilde{Z}_{zz}\widetilde{J}_{z1} \quad (3.88)$$

where

$$\widetilde{Z}_{zx} = \widetilde{Z}_{xz} \quad (3.89)$$

and

$$\widetilde{Z}_{zz} = \frac{\alpha^2}{\alpha^2+\beta^2}\left[-\frac{j\omega\mu_0}{\gamma_0+\gamma_{h1}\coth(\gamma_{h1}d_1)}\right] + \frac{\beta^2}{\alpha^2+\beta^2}\left[-\frac{\gamma_0\gamma_{e1}}{j\omega\varepsilon_0[\gamma_{e1}+\varepsilon_{12}\gamma_0\coth(\gamma_{e1}d_1)]}\right]. \quad (3.90)$$

Equations (3.85) and (3.88) are similar to 3-92 and 3-93 in Nelson's [71] work, respectively. The immittance functions have now been derived. The next section presents the spectral domain immittance functions for a problem with two anisotropic

layers.

The resulting derivations up to this point are a summary of previous work by Nelson *et al.* [34], Lee and Tripathi [33] and Krowne [35], although a small addition to the derivations of (3.85) and (3.88) was presented here by defining the substrate as anisotropic. This varies slightly from Nelson's *et al.* [34] original derivations of assuming an isotropic substrate. The following sections extend the derivations by Nelson *et al.* to include multiple conductors on different anisotropic layers.

3.4. Two Anisotropic Layers

The second problem evaluated is that of two printed conductors in the two anisotropic layers shown in Figure 17. Regions 1 and 2 have a permeability of μ_0 and relative permittivity of $[\varepsilon_1]$ and $[\varepsilon_2]$, respectively and region 3 is assumed to be air. Region 1 has thickness d_1 and region 2 has thickness d_2. The conducting patch between regions 1 and 2 is assumed to have an unknown current $\widetilde{\bar{J}}_1$ and the conducting patch between regions 2 and 3 is assumed to have an unknown current $\widetilde{\bar{J}}_2$. Note again that $\widetilde{\bar{J}}_1$ and $\widetilde{\bar{J}}_2$ are shown to each exist on single conducting patches in Figure 17. This is not necessarily the case for all problems. $\widetilde{\bar{J}}_1$ or $\widetilde{\bar{J}}_2$ could be modified to represent a current on multiple conductors at y = d_1 or y = d_{12}, respectively. But for ease of derivation, $\widetilde{\bar{J}}_1$ and $\widetilde{\bar{J}}_2$ are defined on one printed conductor. As mentioned in the previous section, modifying $\widetilde{\bar{J}}_1$ and $\widetilde{\bar{J}}_2$ for multiple conductors will be discussed later. Also note that $\widetilde{\bar{J}}_1$ and $\widetilde{\bar{J}}_2$ are written as vectors in the transform domain.

The following tangential boundary conditions are enforced in Figure 17:

$$\widetilde{E}_{x1} = 0 \qquad y = 0 \tag{3.91}$$

$$\widetilde{E}_{z1} = 0 \qquad y = 0 \tag{3.92}$$

$$\widetilde{E}_{x1} = \widetilde{E}_{x2} \qquad y = d_1 \tag{3.93}$$

$$\widetilde{E}_{z1} = \widetilde{E}_{z2} \qquad y = d_1 \tag{3.94}$$

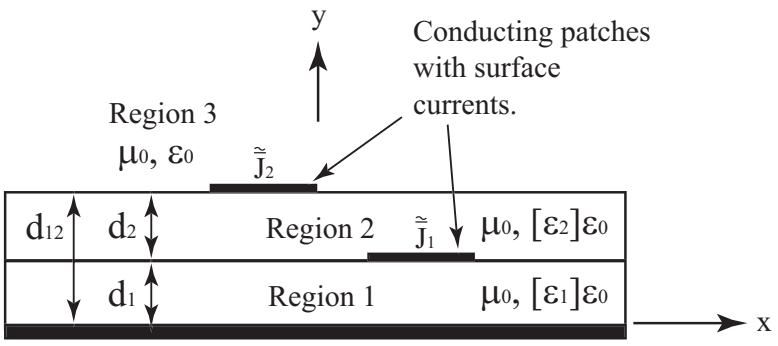

Figure 17. Printed conductors in two grounded anisotropic substrates.

$$\widetilde{E}_{x2} = \widetilde{E}_{x3} \qquad y = d_{12} \tag{3.95}$$

$$\widetilde{E}_{z2} = \widetilde{E}_{z3} \qquad y = d_{12} \tag{3.96}$$

$$\widetilde{J}_{x1} = \widetilde{H}_{z2} - \widetilde{H}_{z1} \qquad y = d_1 \tag{3.97}$$

$$\widetilde{J}_{z1} = \widetilde{H}_{x1} - \widetilde{H}_{x2} \qquad y = d_1 \tag{3.98}$$

$$\widetilde{J}_{x2} = \widetilde{H}_{z3} - \widetilde{H}_{z2} \qquad y = d_{12} \tag{3.99}$$

$$\widetilde{J}_{z2} = \widetilde{H}_{x2} - \widetilde{H}_{x3} \qquad y = d_{12} \tag{3.100}$$

where $\widetilde{J}_{x1}$ and $\widetilde{J}_{z1}$ are the x- and z-components, respectively, of the surface current $\widetilde{\vec{J}}_1$ and $\widetilde{J}_{x2}$ and $\widetilde{J}_{z2}$ are the x- and z-components, respectively, of the surface current $\widetilde{\vec{J}}_2$. Equations (3.56)-(3.61) will be written in terms of the electric and magnetic Hertz potentials to enforce the boundary conditions in (3.91)-(3.100). This will then lead to the spectral domain immittance functions that are similar to the expressions given by Nelson [71], except in this case there are two currents components on two different layers.

3.4.1. Field expressions for region 1

In this section, the fields in region $j = 1$ will be written in terms of the Hertz vector potential (similar to the previous sections). They will be presented for each

region for clarity. Substituting (3.62) and (3.63) into (3.56) and using

$$\frac{\partial\widetilde{\Pi}_{e1}}{\partial y} = B_1(\alpha,\beta)\gamma_{e1}\sinh(\gamma_{e1}y) + B_1'(\alpha,\beta)\gamma_{e1}\cosh(\gamma_{e1}y) \tag{3.101}$$

gives:

$$\begin{aligned}\widetilde{E}_{x1}(\alpha,y,\beta) &= -\omega\mu_0\beta\Big[A_1(\alpha,\beta)\sinh(\gamma_{h1}y) + A_1'(\alpha,\beta)\cosh(\gamma_{h1}y)\Big] \\ &\quad + \frac{j\alpha\gamma_{e1}}{\varepsilon_{12}}\Big[B_1(\alpha,\beta)\sinh(\gamma_{e1}y) + B_1'(\alpha,\beta)\cosh(\gamma_{e1}y)\Big]. \quad (3.102)\end{aligned}$$

Similarly, using

$$\frac{\partial\widetilde{\Pi}_{h1}}{\partial y} = A_1(\alpha,\beta)\gamma_{h1}\cosh(\gamma_{h1}y) + A_1'(\alpha,\beta)\gamma_{h1}\sinh(\gamma_{h1}y) \tag{3.103}$$

and substituting (3.62)-(3.63) into (3.58), (3.59) and (3.61) gives:

$$\begin{aligned}\widetilde{E}_{z1}(\alpha,y,\beta) &= \omega\mu_0\alpha\Big[A_1(\alpha,\beta)\sinh(\gamma_{h1}y) + A_1'(\alpha,\beta)\cosh(\gamma_{h1}y)\Big] \\ &\quad + \frac{j\beta\gamma_{e1}}{\varepsilon_{12}}\Big[B_1(\alpha,\beta)\sinh(\gamma_{e1}y) + B_1'(\alpha,\beta)\cosh(\gamma_{e1}y)\Big], \quad (3.104) \\ \widetilde{H}_{x1}(\alpha,y,\beta) &= j\alpha\Big[A_1(\alpha,\beta)\gamma_{h1}\cosh(\gamma_{h1}y) + A_1'(\alpha,\beta)\gamma_{h1}\sinh(\gamma_{h1}y)\Big] \\ &\quad + \omega\varepsilon_0\beta\Big[B_1(\alpha,\beta)\cosh(\gamma_{e1}y) + B_1'(\alpha,\beta)\sinh(\gamma_{e1}y)\Big], \quad (3.105) \\ \widetilde{H}_{z1}(\alpha,y,\beta) &= j\beta\Big[A_1(\alpha,\beta)\gamma_{h1}\cosh(\gamma_{h1}y) + A_1'(\alpha,\beta)\gamma_{h1}\sinh(\gamma_{h1}y)\Big] \\ &\quad - \omega\varepsilon_0\alpha\Big[B_1(\alpha,\beta)\cosh(\gamma_{e1}y) + B_1'(\alpha,\beta)\sinh(\gamma_{e1}y)\Big]. \quad (3.106)\end{aligned}$$

Later, the expressions in (3.102) and (3.104)-(3.106) will be used to apply the boundary conditions for region 1 given by (3.91)-(3.100).

3.4.2. Field expressions for region 2

In this section, the fields in region $j = 2$ will be written in terms of the Hertz

vector potential. Substituting (3.62) and (3.63) into (3.56) and using

$$\frac{\partial\widetilde{\Pi}_{e2}}{\partial y} = B_2(\alpha,\beta)\gamma_{e2}\sinh(\gamma_{e2}y) + B_2'(\alpha,\beta)\gamma_{e2}\cosh(\gamma_{e2}y) \tag{3.107}$$

gives:

$$\begin{aligned}\widetilde{E}_{x2}(\alpha,y,\beta) &= -\omega\mu_0\beta\Big[A_2(\alpha,\beta)\sinh(\gamma_{h2}y) + A_2'(\alpha,\beta)\cosh(\gamma_{h2}y)\Big] \\ &\quad + \frac{j\alpha\gamma_{e2}}{\varepsilon_{22}}\Big[B_2(\alpha,\beta)\sinh(\gamma_{e2}y) + B_2'(\alpha,\beta)\cosh(\gamma_{e2}y)\Big]. \quad (3.108)\end{aligned}$$

Similarly, using

$$\frac{\partial\widetilde{\Pi}_{h2}}{\partial y} = A_2(\alpha,\beta)\gamma_{h2}\cosh(\gamma_{h2}y) + A_2'(\alpha,\beta)\gamma_{h2}\sinh(\gamma_{h2}y) \tag{3.109}$$

and substituting (3.62)-(3.63) into (3.58), (3.59) and (3.61) gives:

$$\begin{aligned}\widetilde{E}_{z2}(\alpha,y,\beta) &= \omega\mu_0\alpha\Big[A_2(\alpha,\beta)\sinh(\gamma_{h2}y) + A_2'(\alpha,\beta)\cosh(\gamma_{h2}y)\Big] \\ &\quad + \frac{j\beta\gamma_{e2}}{\varepsilon_{22}}\Big[B_2(\alpha,\beta)\sinh(\gamma_{e2}y) + B_2'(\alpha,\beta)\cosh(\gamma_{e2}y)\Big], \quad (3.110) \\ \widetilde{H}_{x2}(\alpha,y,\beta) &= j\alpha\Big[A_2(\alpha,\beta)\gamma_{h2}\cosh(\gamma_{h2}y) + A_2'(\alpha,\beta)\gamma_{h2}\sinh(\gamma_{h2}y)\Big] \\ &\quad + \omega\varepsilon_0\beta\Big[B_2(\alpha,\beta)\cosh(\gamma_{e2}y) + B_2'(\alpha,\beta)\sinh(\gamma_{e2}y)\Big], \quad (3.111) \\ \widetilde{H}_{z2}(\alpha,y,\beta) &= j\beta\Big[A_2(\alpha,\beta)\gamma_{h2}\cosh(\gamma_{h2}y) + A_2'(\alpha,\beta)\gamma_{h2}\sinh(\gamma_{h2}y)\Big] \\ &\quad - \omega\varepsilon_0\alpha\Big[B_2(\alpha,\beta)\cosh(\gamma_{e2}y) + B_2'(\alpha,\beta)\sinh(\gamma_{e2}y)\Big]. \quad (3.112)\end{aligned}$$

Later, the expressions in (3.108) and (3.110)-(3.112) will be used to apply the boundary conditions for region 2 given by (3.91)-(3.100).

3.4.3. Field expressions for region 3

In this section, the fields in region $j = 3$ will be written in terms of the Hertz

vector potential. Substituting (3.64) and (3.65) into (3.56) and using

$$\frac{\partial \widetilde{\Pi}_{e3}}{\partial y} = -\gamma_0 B_3(\alpha,\beta) e^{-\gamma_0(y-d_{12})} \tag{3.113}$$

gives:

$$\widetilde{E}_{x3}(\alpha,y,\beta) = -\omega\mu_0\beta A_3(\alpha,\beta)e^{-\gamma_0(y-d_{12})} - \frac{j\alpha}{\varepsilon_{32}}\gamma_0 B_3(\alpha,\beta)e^{-\gamma_0(y-d_{12})}. \tag{3.114}$$

Similarly, using

$$\frac{\partial \widetilde{\Pi}_{h3}}{\partial y} = -\gamma_0 A_3(\alpha,\beta) e^{-\gamma_0(y-d_{12})} \tag{3.115}$$

and substituting (3.64)-(3.65) into (3.58), (3.59) and (3.61) gives:

$$\widetilde{E}_{z3}(\alpha,y,\beta) = \omega\mu_0\alpha A_3(\alpha,\beta)e^{-\gamma_0(y-d_{12})} - \frac{j\beta}{\varepsilon_{32}}\gamma_0 B_3(\alpha,\beta)e^{-\gamma_0(y-d_{12})} \tag{3.116}$$

$$\widetilde{H}_{x3}(\alpha,y,\beta) = -j\alpha\gamma_0 A_3(\alpha,\beta)e^{-\gamma_0(y-d_{12})} + \omega\varepsilon_0\beta B_3(\alpha,\beta)e^{-\gamma_0(y-d_{12})} \tag{3.117}$$

$$\widetilde{H}_{z3}(\alpha,y,\beta) = -j\beta\gamma_0 A_3(\alpha,\beta)e^{-\gamma_0(y-d_{12})} - \omega\varepsilon_0\alpha B_3(\alpha,\beta)e^{-\gamma_0(y-d_{12})}. \tag{3.118}$$

Next, the expressions in (3.114) and (3.116)-(3.118) will be used to apply the boundary conditions for region 3 given by (3.91)-(3.100). This will result in solutions for A_1, A_1', B_1, B_1', A_2, A_2', B_2, B_2', A_3 and B_3 in (3.102), (3.104)-(3.106), (3.108), (3.110)-(3.112), (3.114) and (3.116)-(3.118).

3.4.4. The spectral domain immittance functions

Again, since the derivations of the spectral domain immittance functions are quite extensive, only the functions will be presented in this section. The extensive derivations for the following spectral domain immittance functions are shown in Appendix B. The x-component of the electric field in *region 2* is:

$$\widetilde{E}_{x2}(\alpha,y,\beta) = \widetilde{J}_{x1}\widetilde{Z}_{xx1} + \widetilde{J}_{z1}\widetilde{Z}_{xz1} + \widetilde{J}_{x2}\widetilde{Z}_{xx2} + \widetilde{J}_{z2}\widetilde{Z}_{xz2} \tag{3.119}$$

where

$$\widetilde{Z}_{xx1} = \frac{\alpha^2}{\alpha^2+\beta^2}\left[\frac{\gamma_{e1}\gamma_{e2}\sinh(\gamma_{e1}d_1)}{-j\omega\varepsilon_0\varepsilon_{12}\varepsilon_{22}}(P_6-P_5)\right] + \frac{\beta^2}{\alpha^2+\beta^2}\left[j\omega\mu_0\sinh(\gamma_{h1}d_1)(P_4-P_3)\right], \tag{3.120}$$

$$\widetilde{Z}_{xz1} = \frac{\alpha\beta}{\alpha^2+\beta^2}\left[\frac{\gamma_{e1}\gamma_{e2}\sinh(\gamma_{e1}d_1)}{-j\omega\varepsilon_0\varepsilon_{12}\varepsilon_{22}}(P_6-P_5)\right] + \frac{\alpha\beta}{\alpha^2+\beta^2}\left[j\omega\mu_0\sinh(\gamma_{h1}d_1)(P_3-P_4)\right], \tag{3.121}$$

$$\widetilde{Z}_{xx2} = \frac{\alpha^2}{\alpha^2+\beta^2}\left[\frac{\gamma_0\gamma_{e2}}{-j\omega\varepsilon_0\varepsilon_{22}\varepsilon_{32}}(P_8-P_9)\right] + \frac{\beta^2}{\alpha^2+\beta^2}\left[-j\omega\mu_0(P_7+P_{10})\right], \tag{3.122}$$

$$\widetilde{Z}_{xz2} = \frac{\alpha\beta}{\alpha^2+\beta^2}\left[\frac{\gamma_0\gamma_{e2}}{-j\omega\varepsilon_0\varepsilon_{22}\varepsilon_{32}}(P_8-P_9)\right] + \frac{\alpha\beta}{\alpha^2+\beta^2}\left[j\omega\mu_0(P_7+P_{10})\right], \tag{3.123}$$

$$P_1 = N_1M_2 - N_2M_1, \tag{3.124}$$

$$P_2 = N_4M_3 + N_3M_4, \tag{3.125}$$

$$P_3 = \sinh(\gamma_{h2}y)\frac{N_3}{P_2}, \tag{3.126}$$

$$P_4 = \cosh(\gamma_{h2}y)\frac{M_3}{P_2}, \tag{3.127}$$

$$P_5 = \sinh(\gamma_{e2}y)\frac{N_2}{P_1}, \tag{3.128}$$

$$P_6 = \cosh(\gamma_{e2}y)\frac{M_2}{P_1}, \tag{3.129}$$

$$P_7 = \sinh(\gamma_{h2}y)\frac{N_4}{P_2}, \tag{3.130}$$

$$P_8 = \sinh(\gamma_{e2}y)\frac{N_1}{P_1}, \tag{3.131}$$

$$P_9 = \cosh(\gamma_{e2}y)\frac{M_1}{P_1}, \tag{3.132}$$

$$P_{10} = \cosh(\gamma_{h2}y)\frac{M_4}{P_2}, \tag{3.133}$$

$$M_1 = \frac{\gamma_{e2}}{\varepsilon_{22}}\cosh(\gamma_{e1}d_1)\sinh(\gamma_{e2}d_1) - \frac{\gamma_{e1}}{\varepsilon_{12}}\cosh(\gamma_{e2}d_1)\sinh(\gamma_{e1}d_1), \tag{3.134}$$

$$N_1 = \frac{\gamma_{e2}}{\varepsilon_{22}}\cosh(\gamma_{e1}d_1)\cosh(\gamma_{e2}d_1) - \frac{\gamma_{e1}}{\varepsilon_{12}}\sinh(\gamma_{e1}d_1)\sinh(\gamma_{e2}d_1), \tag{3.135}$$

$$M_2 = \cosh(\gamma_{e2}d_{12})\frac{\gamma_0}{\varepsilon_{32}} + \sinh(\gamma_{e2}d_{12})\frac{\gamma_{e2}}{\varepsilon_{22}}, \tag{3.136}$$

$$N_2 = \sinh(\gamma_{e2}d_{12})\frac{\gamma_0}{\varepsilon_{32}} + \cosh(\gamma_{e2}d_{12})\frac{\gamma_{e2}}{\varepsilon_{22}}, \tag{3.137}$$

$$M_3 = \gamma_0\sinh(\gamma_{h2}d_{12}) + \gamma_{h2}\cosh(\gamma_{h2}d_{12}), \tag{3.138}$$

$$N_3 = \gamma_0\cosh(\gamma_{h2}d_{12}) + \gamma_{h2}\sinh(\gamma_{h2}d_{12}), \tag{3.139}$$

$$M_4 = \gamma_{h1}\cosh(\gamma_{h1}d_1)\sinh(\gamma_{h2}d_1) - \gamma_{h2}\sinh(\gamma_{h1}d_1)\cosh(\gamma_{h2}d_1), \tag{3.140}$$

$$N_4 = -\gamma_{h1}\cosh(\gamma_{h2}d_1)\cosh(\gamma_{h1}d_1) + \gamma_{h2}\sinh(\gamma_{h2}d_1)\sinh(\gamma_{h1}d_1). \tag{3.141}$$

Finally, the z-component of the electric field in *region 2* is:

$$\widetilde{E}_{z2}(\alpha, y, \beta) = \widetilde{J}_{x1}\widetilde{Z}_{zx1} + \widetilde{J}_{z1}\widetilde{Z}_{zz1} + \widetilde{J}_{x2}\widetilde{Z}_{zx2} + \widetilde{J}_{z2}\widetilde{Z}_{zz2} \tag{3.142}$$

where

$$\widetilde{Z}_{zx1} = \widetilde{Z}_{xz1}, \tag{3.143}$$

$$\widetilde{Z}_{zz1} = \frac{\beta^2}{\alpha^2+\beta^2}\left[\frac{\gamma_{e1}\gamma_{e2}\sinh(\gamma_{e1}d_1)}{-j\omega\varepsilon_0\varepsilon_{12}\varepsilon_{22}}(P_6-P_5)\right] + \frac{\alpha^2}{\alpha^2+\beta^2}\left[j\omega\mu_0\sinh(\gamma_{h1}d_1)(P_4-P_3)\right], \quad (3.144)$$

$$\widetilde{Z}_{zx2} = \widetilde{Z}_{xz2}, \quad (3.145)$$

$$\widetilde{Z}_{zz2} = \frac{\beta^2}{\alpha^2+\beta^2}\left[\frac{\gamma_0\gamma_{e2}}{-j\omega\varepsilon_0\varepsilon_{22}\varepsilon_{32}}(P_8-P_9)\right] + \frac{\alpha^2}{\alpha^2+\beta^2}\left[-j\omega\mu_0(P_7+P_{10})\right]. \quad (3.146)$$

Equations (3.119) and (3.142) simplify down to (3.85) and (3.88) for single anisotropic case. The new spectral domain immittance functions have now been derived for the two layer case. The next section presents the spectral domain immittance functions for a problem with three anisotropic layers.

3.5. Three Anisotropic Layers

The third problem evaluated is that of two printed conductors on the three anisotropic layers as shown in Figure 18. Region 3 is an anisotropic superstrate, and region 4 is assumed to be air. Regions 1, 2 and 3 have a permeability of μ_0 and relative permittivity of $[\varepsilon_1]$, $[\varepsilon_2]$ and $[\varepsilon_3]$, respectively. Region 1 has thickness d_1, region 2 has thickness d_2 and region 3 has a thickness d_3. The conducting patch between regions 1 and 2 is assumed to have an unknown current $\widetilde{\bar{J}}_1$ and the conducting patch between regions 2 and 3 is assumed to have an unknown current $\widetilde{\bar{J}}_2$. Note again that $\widetilde{\bar{J}}_1$ and $\widetilde{\bar{J}}_2$ are shown to exist on a single conducting patch in Figure 18. This is not necessarily the case for all problems. $\widetilde{\bar{J}}_1$ or $\widetilde{\bar{J}}_2$ could be modified to represent a current on multiple

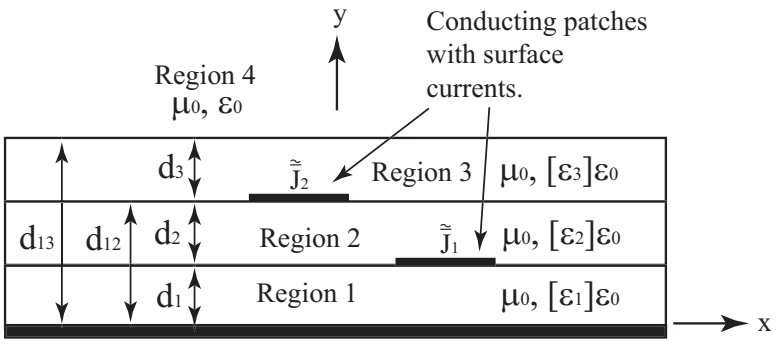

Figure 18. Two printed conductors in three grounded anisotropic substrates.

conductors at y = d_1 or y = d_{12}, respectively. But for ease of derivation, $\widetilde{\bar{J}}_1$ and $\widetilde{\bar{J}}_2$ are defined on one printed conductor. As mentioned in the previous sections, modifying $\widetilde{\bar{J}}_1$ and $\widetilde{\bar{J}}_2$ for multiple conductors will be discussed later. Also note that $\widetilde{\bar{J}}_1$ and $\widetilde{\bar{J}}_2$ are each written as a vector in the transform domain.

The following tangential boundary conditions in Figure 18 will be enforced:

$$\widetilde{E}_{x1} = 0 \qquad y = 0 \tag{3.147}$$

$$\widetilde{E}_{z1} = 0 \qquad y = 0 \tag{3.148}$$

$$\widetilde{E}_{x1} = \widetilde{E}_{x2} \qquad y = d_1 \tag{3.149}$$

$$\widetilde{E}_{z1} = \widetilde{E}_{z2} \qquad y = d_1 \tag{3.150}$$

$$\widetilde{E}_{x2} = \widetilde{E}_{x3} \qquad y = d_{12} \tag{3.151}$$

$$\widetilde{E}_{z2} = \widetilde{E}_{z3} \qquad y = d_{12} \tag{3.152}$$

$$\widetilde{E}_{x3} = \widetilde{E}_{x4} \qquad y = d_{13} \tag{3.153}$$

$$\widetilde{E}_{z3} = \widetilde{E}_{z4} \qquad y = d_{13} \tag{3.154}$$

$$\widetilde{H}_{x3} = \widetilde{H}_{x4} \qquad y = d_{13} \tag{3.155}$$

$$\widetilde{H}_{z3} = \widetilde{H}_{z4} \qquad y = d_{13} \tag{3.156}$$

$$\widetilde{J}_{x1} = \widetilde{H}_{z2} - \widetilde{H}_{z1} \qquad y = d_1 \tag{3.157}$$

$$\widetilde{J}_{z1} = \widetilde{H}_{x1} - \widetilde{H}_{x2} \qquad y = d_1 \tag{3.158}$$

$$\widetilde{J}_{x2} = \widetilde{H}_{z3} - \widetilde{H}_{z2} \qquad y = d_{12} \tag{3.159}$$

$$\widetilde{J}_{z2} = \widetilde{H}_{x2} - \widetilde{H}_{x3} \qquad y = d_{12} \tag{3.160}$$

where $\widetilde{J}_{x1}$ and $\widetilde{J}_{z1}$ are the x- and z-components, respectively, of the surface current $\widetilde{\bar{J}}_1$ and $\widetilde{J}_{x2}$ and $\widetilde{J}_{z2}$ are the x- and z-components, respectively, of the surface current $\widetilde{\bar{J}}_2$. Just as the previous sections, equations (3.56)-(3.61) will be written in terms of the electric and magnetic Hertz potentials to enforce the boundary conditions in (3.147)-(3.160). This will then lead to the spectral domain immittance functions that are similar to the expressions by Nelson [71], expect in this case there are two currents on two different layers.

3.5.1. Field expressions for region 1

In this section, the fields in region $j = 1$ will be written in terms of the Hertz vector potential similar to the previous sections. This process has been performed in the previous two sections and will be presented here for each region to be thorough. Substituting (3.62) and (3.63) into (3.56) and using

$$\frac{\partial \widetilde{\Pi}_{e1}}{\partial y} = B_1(\alpha,\beta)\gamma_{e1}\sinh(\gamma_{e1}y) + B_1'(\alpha,\beta)\gamma_{e1}\cosh(\gamma_{e1}y) \tag{3.161}$$

gives:

$$\begin{aligned}\widetilde{E}_{x1}(\alpha,y,\beta) &= -\omega\mu_0\beta\Big[A_1(\alpha,\beta)\sinh(\gamma_{h1}y) + A_1'(\alpha,\beta)\cosh(\gamma_{h1}y)\Big] \\ &\quad + \frac{j\alpha\gamma_{e1}}{\varepsilon_{12}}\Big[B_1(\alpha,\beta)\sinh(\gamma_{e1}y) + B_1'(\alpha,\beta)\cosh(\gamma_{e1}y)\Big].\end{aligned} \tag{3.162}$$

Similarly, using

$$\frac{\partial\widetilde{\Pi}_{h1}}{\partial y} = A_1(\alpha,\beta)\gamma_{h1}\cosh(\gamma_{h1}y) + A_1'(\alpha,\beta)\gamma_{h1}\sinh(\gamma_{h1}y) \tag{3.163}$$

and substituting (3.62)-(3.63) into (3.58), (3.59) and (3.61) gives:

$$\begin{aligned}
\widetilde{E}_{z1}(\alpha,y,\beta) &= \omega\mu_0\alpha\Big[A_1(\alpha,\beta)\sinh(\gamma_{h1}y) + A_1'(\alpha,\beta)\cosh(\gamma_{h1}y)\Big] \\
&\quad + \frac{j\beta\gamma_{e1}}{\varepsilon_{12}}\Big[B_1(\alpha,\beta)\sinh(\gamma_{e1}y) + B_1'(\alpha,\beta)\cosh(\gamma_{e1}y)\Big], \quad (3.164)\\
\widetilde{H}_{x1}(\alpha,y,\beta) &= j\alpha\Big[A_1(\alpha,\beta)\gamma_{h1}\cosh(\gamma_{h1}y) + A_1'(\alpha,\beta)\gamma_{h1}\sinh(\gamma_{h1}y)\Big] \\
&\quad + \omega\varepsilon_0\beta\Big[B_1(\alpha,\beta)\cosh(\gamma_{e1}y) + B_1'(\alpha,\beta)\sinh(\gamma_{e1}y)\Big], \quad (3.165)\\
\widetilde{H}_{z1}(\alpha,y,\beta) &= j\beta\Big[A_1(\alpha,\beta)\gamma_{h1}\cosh(\gamma_{h1}y) + A_1'(\alpha,\beta)\gamma_{h1}\sinh(\gamma_{h1}y)\Big] \\
&\quad - \omega\varepsilon_0\alpha\Big[B_1(\alpha,\beta)\cosh(\gamma_{e1}y) + B_1'(\alpha,\beta)\sinh(\gamma_{e1}y)\Big]. \quad (3.166)
\end{aligned}$$

Later, the expressions in (3.162) and (3.164)-(3.166) will be used to apply the boundary conditions for region 1 given by (3.147)-(3.160).

3.5.2. Field expressions for region 2

In this section, the fields in region $j = 2$ will be written in terms of the Hertz vector potential. Substituting (3.62) and (3.63) into (3.56) and using

$$\frac{\partial\widetilde{\Pi}_{e2}}{\partial y} = B_2(\alpha,\beta)\gamma_{e2}\sinh(\gamma_{e2}y) + B_2'(\alpha,\beta)\gamma_{e2}\cosh(\gamma_{e2}y) \tag{3.167}$$

gives:

$$\begin{aligned}
\widetilde{E}_{x2}(\alpha,y,\beta) &= -\omega\mu_0\beta\Big[A_2(\alpha,\beta)\sinh(\gamma_{h2}y) + A_2'(\alpha,\beta)\cosh(\gamma_{h2}y)\Big] \\
&\quad + \frac{j\alpha\gamma_{e2}}{\varepsilon_{22}}\Big[B_2(\alpha,\beta)\sinh(\gamma_{e2}y) + B_2'(\alpha,\beta)\cosh(\gamma_{e2}y)\Big]. \quad (3.168)
\end{aligned}$$

Similarly, using

$$\frac{\partial\widetilde{\Pi}_{h2}}{\partial y} = A_2(\alpha,\beta)\gamma_{h2}\cosh(\gamma_{h2}y) + A_2'(\alpha,\beta)\gamma_{h2}\sinh(\gamma_{h2}y) \tag{3.169}$$

and substituting (3.62)-(3.63) into (3.58), (3.59) and (3.61) gives:

$$\begin{aligned}
\widetilde{E}_{z2}(\alpha,y,\beta) &= \omega\mu_0\alpha\Big[A_2(\alpha,\beta)\sinh(\gamma_{h2}y) + A_2'(\alpha,\beta)\cosh(\gamma_{h2}y)\Big] \\
&\quad + \frac{j\beta\gamma_{e2}}{\varepsilon_{22}}\Big[B_2(\alpha,\beta)\sinh(\gamma_{e2}y) + B_2'(\alpha,\beta)\cosh(\gamma_{e2}y)\Big], \quad (3.170)\\
\widetilde{H}_{x2}(\alpha,y,\beta) &= j\alpha\Big[A_2(\alpha,\beta)\gamma_{h2}\cosh(\gamma_{h2}y) + A_2'(\alpha,\beta)\gamma_{h2}\sinh(\gamma_{h2}y)\Big] \\
&\quad + \omega\varepsilon_0\beta\Big[B_2(\alpha,\beta)\cosh(\gamma_{e2}y) + B_2'(\alpha,\beta)\sinh(\gamma_{e2}y)\Big], \quad (3.171)\\
\widetilde{H}_{z2}(\alpha,y,\beta) &= j\beta\Big[A_2(\alpha,\beta)\gamma_{h2}\cosh(\gamma_{h2}y) + A_2'(\alpha,\beta)\gamma_{h2}\sinh(\gamma_{h2}y)\Big] \\
&\quad - \omega\varepsilon_0\alpha\Big[B_2(\alpha,\beta)\cosh(\gamma_{e2}y) + B_2'(\alpha,\beta)\sinh(\gamma_{e2}y)\Big]. \quad (3.172)
\end{aligned}$$

Later, the expressions in (3.168) and (3.170)-(3.172) will be used to apply the boundary conditions for region 2 given by (3.147)-(3.160).

3.5.3. Field expressions for region 3

In this section, the fields in region $j = 3$ will be written in terms of the Hertz vector potential. Substituting (3.62) and (3.63) into (3.56) and using

$$\frac{\partial\widetilde{\Pi}_{e3}}{\partial y} = B_3(\alpha,\beta)\gamma_{e3}\sinh(\gamma_{e3}y) + B_3'(\alpha,\beta)\gamma_{e3}\cosh(\gamma_{e3}y) \tag{3.173}$$

gives:

$$\begin{aligned}
\widetilde{E}_{x3}(\alpha,y,\beta) &= -\omega\mu_0\beta\Big[A_3(\alpha,\beta)\sinh(\gamma_{h3}y) + A_3'(\alpha,\beta)\cosh(\gamma_{h3}y)\Big] \\
&\quad + \frac{j\alpha\gamma_{e3}}{\varepsilon_{32}}\Big[B_3(\alpha,\beta)\sinh(\gamma_{e3}y) + B_3'(\alpha,\beta)\cosh(\gamma_{e3}y)\Big]. \quad (3.174)
\end{aligned}$$

Similarly, using

$$\frac{\partial\widetilde{\Pi}_{h3}}{\partial y} = A_3(\alpha,\beta)\gamma_{h3}\cosh(\gamma_{h3}y) + A_3'(\alpha,\beta)\gamma_{h3}\sinh(\gamma_{h3}y) \tag{3.175}$$

and substituting (3.62)-(3.63) into (3.58), (3.59) and (3.61) gives:

$$\begin{aligned}
\widetilde{E}_{z3}(\alpha,y,\beta) &= \omega\mu_0\alpha\Big[A_3(\alpha,\beta)\sinh(\gamma_{h3}y) + A_3'(\alpha,\beta)\cosh(\gamma_{h3}y)\Big] \\
&\quad + \frac{j\beta\gamma_{e3}}{\varepsilon_{32}}\Big[B_3(\alpha,\beta)\sinh(\gamma_{e3}y) + B_3'(\alpha,\beta)\cosh(\gamma_{e3}y)\Big], \quad (3.176)\\
\widetilde{H}_{x3}(\alpha,y,\beta) &= j\alpha\Big[A_3(\alpha,\beta)\gamma_{h3}\cosh(\gamma_{h3}y) + A_3'(\alpha,\beta)\gamma_{h3}\sinh(\gamma_{h3}y)\Big] \\
&\quad + \omega\varepsilon_0\beta\Big[B_3(\alpha,\beta)\cosh(\gamma_{e3}y) + B_3'(\alpha,\beta)\sinh(\gamma_{e3}y)\Big], \quad (3.177)\\
\widetilde{H}_{z3}(\alpha,y,\beta) &= j\beta\Big[A_3(\alpha,\beta)\gamma_{h3}\cosh(\gamma_{h3}y) + A_3'(\alpha,\beta)\gamma_{h3}\sinh(\gamma_{h3}y)\Big] \\
&\quad - \omega\varepsilon_0\alpha\Big[B_3(\alpha,\beta)\cosh(\gamma_{e3}y) + B_3'(\alpha,\beta)\sinh(\gamma_{e3}y)\Big]. \quad (3.178)
\end{aligned}$$

Later, the expressions in (3.174) and (3.176)-(3.178) will be used to apply the boundary conditions for region 3 given by (3.147)-(3.160).

3.5.4. Field expressions for region 4

In this section, the fields in region $j = 4$ will be written in terms of the Hertz vector potential. Substituting (3.64) and (3.65) into (3.56) and using

$$\frac{\partial\widetilde{\Pi}_{e4}}{\partial y} = -\gamma_0 B_4(\alpha,\beta)e^{-\gamma_0(y-d_{13})} \tag{3.179}$$

gives:

$$\widetilde{E}_{x4}(\alpha,y,\beta) = -\omega\mu_0\beta A_4(\alpha,\beta)e^{-\gamma_0(y-d_{13})} - \frac{j\alpha}{\varepsilon_{42}}\gamma_0 B_4(\alpha,\beta)e^{-\gamma_0(y-d_{13})}. \tag{3.180}$$

Similarly, using

$$\frac{\partial \widetilde{\Pi}_{h4}}{\partial y} = -\gamma_0 A_4(\alpha,\beta) e^{-\gamma_0(y-d_{13})} \tag{3.181}$$

and substituting (3.64)-(3.65) into (3.58), (3.59) and (3.61) gives:

$$\widetilde{E}_{z4}(\alpha,y,\beta) = \omega\mu_0\alpha A_4(\alpha,\beta)e^{-\gamma_0(y-d_{13})} - \frac{j\beta}{\varepsilon_{42}}\gamma_0 B_4(\alpha,\beta)e^{-\gamma_0(y-d_{13})} \tag{3.182}$$

$$\widetilde{H}_{x4}(\alpha,y,\beta) = -j\alpha\gamma_0 A_4(\alpha,\beta)e^{-\gamma_0(y-d_{13})} + \omega\varepsilon_0\beta B_4(\alpha,\beta)e^{-\gamma_0(y-d_{13})} \tag{3.183}$$

$$\widetilde{H}_{z4}(\alpha,y,\beta) = -j\beta\gamma_0 A_4(\alpha,\beta)e^{-\gamma_0(y-d_{13})} - \omega\varepsilon_0\alpha B_4(\alpha,\beta)e^{-\gamma_0(y-d_{13})}. \tag{3.184}$$

Next, the expressions in (3.180) and (3.182)-(3.184) will be used to apply the boundary conditions for region 4 given by (3.147)-(3.160). This will result in solutions for A_1, A_1', B_1, B_1', A_2, A_2', B_2, B_2', A_3, A_3', B_3, B_3', A_4 and B_4 in (3.162), (3.164)-(3.166), (3.168), (3.170)-(3.172), (3.174), (3.176)-(3.178), (3.180) and (3.182)-(3.184).

3.5.5. The spectral domain immittance functions

Just as before, the derivations for the following spectral domain immittance functions are shown in Appendix C. The x-component of the electric field in *region 2* is:

$$\widetilde{E}_{x2}(\alpha,y,\beta) = \widetilde{J}_{x1}\widetilde{Z}_{xx1} + \widetilde{J}_{z1}\widetilde{Z}_{xz1} + \widetilde{J}_{x2}\widetilde{Z}_{xx2} + \widetilde{J}_{z2}\widetilde{Z}_{xz2} \tag{3.185}$$

where

$$\widetilde{Z}_{xx1} = \frac{\alpha^2}{\alpha^2+\beta^2}\left[\frac{\gamma_{e2}P_{30}\sinh(\gamma_{e2}y)}{j\omega\varepsilon_0\varepsilon_{22}} + \frac{\gamma_{e2}P_{32}\cosh(\gamma_{e2}y)}{-j\omega\varepsilon_0\varepsilon_{22}}\right] +$$

$$\frac{\beta^2}{\alpha^2+\beta^2}\left[j\omega\mu_0 P_{28}\cosh(\gamma_{h2}y) - j\omega\mu_0 P_{26}\sinh(\gamma_{h2}y)\right], \tag{3.186}$$

$$\widetilde{Z}_{xz1} = \frac{\alpha\beta}{\alpha^2+\beta^2}\left[\frac{\gamma_{e2}P_{32}\cosh(\gamma_{e2}y)}{-j\omega\varepsilon_0\varepsilon_{22}} + \frac{\gamma_{e2}P_{30}\sinh(\gamma_{e2}y)}{j\omega\varepsilon_0\varepsilon_{22}}\right] +$$

$$\frac{\alpha\beta}{\alpha^2+\beta^2}\left[j\omega\mu_0 P_{26}\sinh(\gamma_{h2}y) - j\omega\mu_0 P_{28}\cosh(\gamma_{h2}y)\right], \quad (3.187)$$

$$\widetilde{Z}_{xx2} = \frac{\alpha^2}{\alpha^2+\beta^2}\left[\frac{\gamma_{e2}P_{29}\sinh(\gamma_{e2}y)}{-j\omega\varepsilon_0\varepsilon_{22}} + \frac{\gamma_{e2}P_{31}\cosh(\gamma_{e2}y)}{-j\omega\varepsilon_0\varepsilon_{22}}\right] +$$

$$\frac{\beta^2}{\alpha^2+\beta^2}\left[-j\omega\mu_0 P_{25}\sinh(\gamma_{h2}y) - j\omega\mu_0 P_{27}\cosh(\gamma_{h2}y)\right], \quad (3.188)$$

$$\widetilde{Z}_{xz2} = \frac{\alpha\beta}{\alpha^2+\beta^2}\left[\frac{\gamma_{e2}P_{29}\sinh(\gamma_{e2}y)}{-j\omega\varepsilon_0\varepsilon_{22}} + \frac{\gamma_{e2}P_{31}\cosh(\gamma_{e2}y)}{-j\omega\varepsilon_0\varepsilon_{22}}\right] +$$

$$\frac{\alpha\beta}{\alpha^2+\beta^2}\left[j\omega\mu_0 P_{25}\sinh(\gamma_{h2}y) + j\omega\mu_0 P_{27}\cosh(\gamma_{h2}y)\right], \quad (3.189)$$

$$P_{11} = \frac{\gamma_{e3}}{\varepsilon_{32}}\cosh(\gamma_{e3}d_{12}) - \frac{M_6}{N_6}\frac{\gamma_{e3}}{\varepsilon_{32}}\sinh(\gamma_{e3}d_{12}), \quad (3.190)$$

$$P_{12} = \frac{\gamma_{e2}}{\varepsilon_{22}}\sinh(\gamma_{e2}d_{12}) - \frac{M_1}{N_1}\frac{\gamma_{e2}}{\varepsilon_{22}}\cosh(\gamma_{e2}d_{12}), \quad (3.191)$$

$$P_{13} = \cosh(\gamma_{h3}d_{12}) - \frac{M_7}{N_7}\sinh(\gamma_{h3}d_{12}), \quad (3.192)$$

$$P_{14} = \sinh(\gamma_{h2}d_{12}) + \frac{M_4}{N_4}\cosh(\gamma_{h2}d_{12}), \quad (3.193)$$

$$P_{15} = \frac{\gamma_{e1}\gamma_{e2}}{P_{11}N_1\varepsilon_{12}\varepsilon_{22}}\cosh(\gamma_{e2}d_{12})\sinh(\gamma_{e1}d_1), \quad (3.194)$$

$$P_{16} = \frac{M_6}{N_6}\cosh(\gamma_{e3}d_{12}) - \sinh(\gamma_{e3}d_{12}), \tag{3.195}$$

$$P_{17} = \frac{\gamma_{e1}}{N_1\varepsilon_{12}}\sinh(\gamma_{e1}d_1)\sinh(\gamma_{e2}d_{12}), \tag{3.196}$$

$$P_{18} = \frac{M_6P_{12}}{N_6P_{11}}\cosh(\gamma_{e3}d_{12}) - \frac{P_{12}}{P_{11}}\sinh(\gamma_{e3}d_{12}), \tag{3.197}$$

$$P_{19} = \cosh(\gamma_{e2}d_{12}) - \frac{M_1}{N_1}\sinh(\gamma_{e2}d_{12}), \tag{3.198}$$

$$P_{20} = \frac{\sinh(\gamma_{h1}d_1)\cosh(\gamma_{h2}d_{12})}{N_4P_{13}}, \tag{3.199}$$

$$P_{21} = \frac{M_7}{N_7}\gamma_{h3}\cosh(\gamma_{h3}d_{12}) - \gamma_{h3}\sinh(\gamma_{h3}d_{12}), \tag{3.200}$$

$$P_{22} = \frac{\gamma_{h2}\sinh(\gamma_{h1}d_1)\sinh(\gamma_{h2}d_{12})}{N_4}, \tag{3.201}$$

$$P_{23} = \frac{M_7P_{14}}{N_7P_{13}}\gamma_{h3}\cosh(\gamma_{h3}d_{12}) - \frac{P_{14}}{P_{13}}\gamma_{h3}\sinh(\gamma_{h3}d_{12}), \tag{3.202}$$

$$P_{24} = \frac{M_4}{N_4}\gamma_{h2}\sinh(\gamma_{h2}d_{12}) + \gamma_{h2}\cosh(\gamma_{h2}d_{12}), \tag{3.203}$$

$$P_{25} = \frac{1}{P_{23} + P_{24}}, \tag{3.204}$$

$$P_{26} = \frac{P_{20}P_{21} + P_{22}}{P_{23} + P_{24}}, \tag{3.205}$$

$$P_{27} = \frac{M_4}{N_4(P_{23} + P_{24})}, \tag{3.206}$$

$$P_{28} = \frac{\sinh(\gamma_{h1}d_1)}{N_4} - \frac{M_4(P_{20}P_{21} + P_{22})}{N_4(P_{23} + P_{24})}, \tag{3.207}$$

$$P_{29} = \frac{1}{P_{18} + P_{19}}, \tag{3.208}$$

$$P_{30} = \frac{P_{15}P_{16} + P_{17}}{P_{18} + P_{19}}, \tag{3.209}$$

$$P_{31} = \frac{-M_1P_{29}}{N1}, \tag{3.210}$$

$$P_{32} = \frac{M_1P_{30}}{N_1} + \frac{\gamma_{e1}\sinh(\gamma_{e1}d_1)}{N_1\varepsilon_{12}}, \tag{3.211}$$

$$M_6 = \frac{\gamma_0}{\varepsilon_{43}} \sinh(\gamma_{e3} d_{13}) + \frac{\gamma_{e3}}{\varepsilon_{32}} \cosh(\gamma_{e3} d_{13}), \tag{3.212}$$

$$N_6 = \frac{\gamma_0}{\varepsilon_{43}} \cosh(\gamma_{e3} d_{13}) + \frac{\gamma_{e3}}{\varepsilon_{32}} \sinh(\gamma_{e3} d_{13}), \tag{3.213}$$

$$M_7 = \gamma_0 \cosh(\gamma_{h3} d_{13}) + \gamma_{h3} \sinh(\gamma_{h3} d_{13}), \tag{3.214}$$

$$N_7 = \gamma_0 \sinh(\gamma_{h3} d_{13}) + \gamma_{h3} \cosh(\gamma_{h3} d_{13}), \tag{3.215}$$

with M_1, N_1, M_4 and N_4 defined in (3.134), (3.135), (3.140) and (3.141), respectively. Finally, the z-component of the electric field in *region 2* is:

$$\widetilde{E}_{z2}(\alpha, y, \beta) = \widetilde{J}_{x1}\widetilde{Z}_{zx1} + \widetilde{J}_{z1}\widetilde{Z}_{zz1} + \widetilde{J}_{x2}\widetilde{Z}_{zx2} + \widetilde{J}_{z2}\widetilde{Z}_{zz2} \tag{3.216}$$

where

$$\widetilde{Z}_{zx1} = \widetilde{Z}_{xz1}, \tag{3.217}$$

$$\begin{aligned} \widetilde{Z}_{zz1} \;=\; & \frac{\alpha^2}{\alpha^2+\beta^2}\Big[j\omega\mu_0 P_{28}\cosh(\gamma_{h2}y) - j\omega\mu_0 P_{26}\sinh(\gamma_{h2}y)\Big] + \\ & \frac{\beta^2}{\alpha^2+\beta^2}\left[\frac{\gamma_{e2}P_{30}\sinh(\gamma_{e2}y)}{j\omega\varepsilon_0\varepsilon_{22}} - \frac{\gamma_{e2}P_{32}\cosh(\gamma_{e2}y)}{j\omega\varepsilon_0\varepsilon_{22}}\right], \end{aligned} \tag{3.218}$$

$$\widetilde{Z}_{zx2} = \widetilde{Z}_{xz2}, \tag{3.219}$$

$$\widetilde{Z}_{zz2} = \frac{\alpha^2}{\alpha^2+\beta^2}\Big[- j\omega\mu_0 P_{25}\sinh(\gamma_{h2}y) - j\omega\mu_0 P_{27}\cosh(\gamma_{h2}y)\Big] +$$

$$\frac{\beta^2}{\alpha^2+\beta^2}\left[\frac{\gamma_{e2}P_{29}\sinh(\gamma_{e2}y)}{-j\omega\varepsilon_0\varepsilon_{22}} + \frac{\gamma_{e2}P_{31}\cosh(\gamma_{e2}y)}{-j\omega\varepsilon_0\varepsilon_{22}}\right]. \tag{3.220}$$

Now (3.185) and (3.216) can be used in the moment method to enforce the tangential boundary conditions on the conductors in Figure 18. This will then result in a solution to the unknown surface currents. Notice that certain hyperbolic sines and cosines in the immittance functions of (3.185) and (3.216) are written in terms of y and not set at a certain layer thickness. Leaving these terms arbitrary permits the definition of multiple conductors both above and below the second layer. Equations (3.185) and (3.216) can then be used to determine the mutual coupling between printed antennas on different layers. Since region 3 is a superstrate for conductors on top of region 2, the effect of an anisotropic dielectric cover on the mutual coupling between printed antennas can be investigated.

At this point, new spectral domain immittance functions have been derived. The new immittance functions will be used to evaluate problems with multiple printed antennas in layered anisotropic dielectrics. The moment method [80]-[81] will be used to solve for the unknown surface currents in these new spectral domain immittance functions. In particular, the spectral domain moment method will be used to solve for the unknown currents. The next chapter introduces the spectral domain moment method along with the numerical technique that will be used to solve for the unknown surface currents.

CHAPTER 4. SOLVING THE SPECTRAL DOMAIN IMMITTANCE FUNCTIONS USING THE MOMENT METHOD

4.1. Introduction to the Moment Method

The moment method is a linear algebra technique to approximate a solution to [80]-[81]

$$L(f) = g \tag{4.1}$$

where f is an unknown function, L is a linear operator, and g is a forcing function.

To solve (4.1), f is written in terms of known expansion functions denoted by f_n and an unknown amplitude denoted by α_n. This then gives

$$f \approx \tilde{f} = \sum_{n=1}^{N} f_n \alpha_n. \tag{4.2}$$

The expansion functions f_n are linearly independent in the *domain of the linear operator*. The approximation in (4.2) introduces an error between the exact solution and the approximate solution. This error is denoted by the residual $\tilde{R}$ and is written as

$$\tilde{R} = L(f) - L(\tilde{f}). \tag{4.3}$$

Substituting (4.1) into (4.3) results in

$$\tilde{R} = g - L(\tilde{f}). \tag{4.4}$$

To minimize $\tilde{R}$ the inner product ($\langle *, * \rangle$) will be taken with a set of known weighting functions, W_m. W_m is defined in the *range of the linear operator*. Using these weighting functions and (4.4) in the inner product, $\tilde{R}$ can be minimized by

letting

$$\langle W_m, \tilde{R} \rangle = 0 \tag{4.5}$$

for $m = 1, 2, ..., N$. Using (4.2) and (4.4) in (4.5) results in

$$\langle W_m, g - \sum_{n=1}^{N} \alpha_n L(f_n) \rangle = 0. \tag{4.6}$$

Rewriting (4.6) gives

$$\sum_{n=1}^{N} \alpha_n \langle W_m, L(f_n) \rangle = \langle W_m, g \rangle \tag{4.7}$$

for $m = 1, 2, ..., N$. Equation (4.7) can also be written in matrix form in the following manner:

$$\begin{bmatrix} \langle W_1, L(f_1) \rangle & \langle W_1, L(f_2) \rangle & \dots & \langle W_1, L(f_N) \rangle \\ \langle W_2, L(f_1) \rangle & \langle W_2, L(f_2) \rangle & \dots & \langle W_2, L(f_N) \rangle \\ \vdots & \vdots & \ddots & \vdots \\ \langle W_N, L(f_1) \rangle & \langle W_N, L(f_2) \rangle & \dots & \langle W_N, L(f_N) \rangle \end{bmatrix} \begin{bmatrix} \alpha_1 \\ \alpha_2 \\ \vdots \\ \alpha_N \end{bmatrix} = \begin{bmatrix} \langle W_1, g \rangle \\ \langle W_2, g \rangle \\ \vdots \\ \langle W_N, g \rangle \end{bmatrix}. \tag{4.8}$$

The matrix in (4.8) only contains the unknowns α_n because W_m were defined weighting functions, f_n were defined expansion functions, and the forcing function g is a known condition. Multiplying both sides of (4.8) by the inverse of the most left matrix in (4.8) determines the unknown values of α_n. This then gives

$$\begin{bmatrix} \alpha_1 \\ \alpha_2 \\ \vdots \\ \alpha_N \end{bmatrix} = \begin{bmatrix} \langle W_1, L(f_1) \rangle & \langle W_1, L(f_2) \rangle & \dots & \langle W_1, L(f_N) \rangle \\ \langle W_2, L(f_1) \rangle & \langle W_2, L(f_2) \rangle & \dots & \langle W_2, L(f_N) \rangle \\ \vdots & \vdots & \ddots & \vdots \\ \langle W_N, L(f_1) \rangle & \langle W_N, L(f_2) \rangle & \dots & \langle W_N, L(f_N) \rangle \end{bmatrix}^{-1} \begin{bmatrix} \langle W_1, g \rangle \\ \langle W_2, g \rangle \\ \vdots \\ \langle W_N, g \rangle \end{bmatrix}.$$

This is a short summary of the moment method. The next section introduces the

spectral domain moment method that will be used to solve for the unknown surface currents in the newly derived spectral domain immittance functions. The linear algebra and matrix operations introduced in this section will be used in the spectral domain moment method.

4.2. Introduction to the Spectral Domain Moment Method

The previous section introduced the fundamentals of the moment method in the frequency domain. This section introduces the moment method in the spectral or transform domain by summarizing some very good work given in a paper by Davidson and Aberle [84]. In this paper Davidson and Aberle introduce the spectral domain moment method formulation by evaluating the capacitance per unit length of an infinite microstrip line. Everything in this paper is meant to be used as a teaching tool to introduce this concept.

This section is only a summary of the paper, but several very important concepts were used in this research. In particular, the complex process of rearranging the terms in the spectral domain moment method to solve the spectral domain immittance functions is carefully presented. *This rearrangement is a very important aspect of this research.* It should also be mentioned that, since this is a summary, it is only natural that much of the discussion on this topic was left out and only the items relevant to this research are presented.

The main idea in the paper is to use the spectral domain moment method to transform the partial differential equations (PDE) in the spatial-frequency domain associated with solving a microstrip structure to the spatial domain. Davidson and Aberle also mention that in some literature this spatial-frequency domain is also called the spatial-spectral domain, wavenumber domain, transform domain, spectral domain or the k-space. To stay consistent with the work here, the spectral domain notation will be used to refer to the spatial-frequency domain notation used by Davidson and

Aberle. Next, consider the infinite microstrip structure in Figure 19. The grounded dielectric substrate is isotropic with thickness d. The microstrip is infinite along the z-axis, has a width w and zero thickness. To solve for the capacitance per unit length Davidson and Aberle introduce the unit charge problem in Figure 20. This problem will be solved using Poisson's equation:

$$\nabla^2\Phi(x,y) = -\frac{1}{\varepsilon}\delta(x)\delta(y-d) \tag{4.9}$$

where $\delta(x)\delta(y-d)$ is the spatially impulsive source of unit magnitude that represents the charge in Figure 20.

Davidson and Aberle transform (4.9) to the spectral domain to avoid evaluating the derivatives. For this, the following definition of the Fourier transform is used

$$\widetilde{\Phi}(k_x,y) = \int_{-\infty}^{+\infty}\Phi(x,y)e^{-jk_x x}dx. \tag{4.10}$$

This then results in the following transform for the partial derivatives:

$$\frac{\partial\Phi}{\partial x} \Leftrightarrow jk_x\widetilde{\Phi}. \tag{4.11}$$

Since there is no variation with respect to z, (4.9) simplifies to:

$$\nabla^2\Phi(x,y) = \frac{\partial^2\Phi(x,y)}{\partial^2 x^2} + \frac{\partial^2\Phi(x,y)}{\partial y^2} = -\frac{1}{\varepsilon}\delta(x)\delta(y-d). \tag{4.12}$$

Applying the Fourier transform property defined in (4.11) to (4.12) results in the

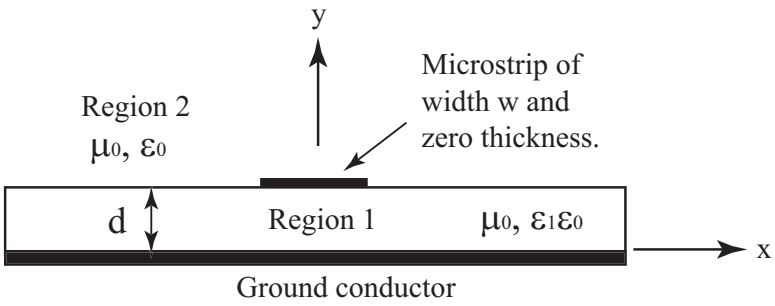

Figure 19. Infinite microstrip on a grounded isotropic dielectric substrate.

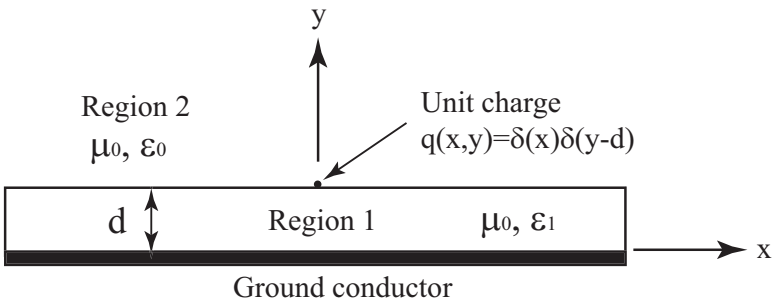

Figure 20. Unit charge on a grounded isotropic dielectric substrate.

following spectral expression:

$$\begin{aligned}(jk_x)^2\widetilde{\Phi}(k_x,y)+\frac{\partial^2\widetilde{\Phi}(k_x,y)}{\partial y^2} &= -\frac{1}{\varepsilon}*1*\delta(y-d)\\ &= \left[-k_x^2+\frac{\partial^2}{\partial y^2}\right]\widetilde{\Phi}(k_x,y). \qquad (4.13)\end{aligned}$$

This results in a second order, nonhomogeneous differential equation. This implies that the associated homogeneous differential equation of (4.13) is:

$$\left[-k_x^2+\frac{\partial^2}{\partial y^2}\right]\widetilde{\Phi}(k_x,y)=0 \qquad (4.14)$$

for all $y \neq d$.

The boundary conditions in this problem are a zero potential at y = 0 and ∞, continuous potential at y = d and the flux is discontinuous by the source singularity at y = d. The solution to (4.14) is assumed to have the following form:

$$\widetilde{\Phi}(k_x, y) = C_1 e^{\lambda_1 y} + C_2 e^{\lambda_2 y}. \tag{4.15}$$

This implies

$$\frac{\partial \widetilde{\Phi}(k_x, y)}{\partial y} = C_1 \lambda_1 e^{\lambda_1 y} + C_2 \lambda_2 e^{\lambda_2 y} \tag{4.16}$$

and

$$\frac{\partial^2 \widetilde{\Phi}(k_x, y)}{\partial y^2} = C_1 \lambda_1^2 e^{\lambda_1 y} + C_2 \lambda_2^2 e^{\lambda_2 y}. \tag{4.17}$$

To solve the homogeneous equation the following characteristic equation needs to be considered:

$$\lambda^2 - k_x^2 = 0. \tag{4.18}$$

This implies

$$\lambda = \pm\sqrt{k_x^2} = \pm|k_x|. \tag{4.19}$$

Therefore, $\widetilde{\Phi}(k_x, y)$ has the following form:

$$\widetilde{\Phi}(k_x, y) = C_1 e^{+|k_x|y} + C_2 e^{-|k_x|y} \tag{4.20}$$

where C_1 and C_2 are constants and need to be determined by applying the boundary conditions. If the dielectric is region 1, then

$$\widetilde{\Phi}_1(k_x, y) = A e^{+|k_x|y} + B e^{-|k_x|y} \tag{4.21}$$

and for the air in region 2,

$$\widetilde{\Phi}_2(k_x, y) = Ce^{+|k_x|y} + De^{-|k_x|y}. \tag{4.22}$$

Next, equations (4.21) and (4.22) will be used to enforce the following boundary conditions:

1. $\widetilde{\Phi}(k_x, y) = 0$ at y = 0 and $y \to \infty$.
2. $\widetilde{\rho_s} = \hat{n}_2 \cdot (\widetilde{D}_2 - \widetilde{D}_1)$.
3. $\widetilde{\Phi}(k_x, y)$ is continuous at y = d (i.e., $\widetilde{\Phi}_1(k_x, y) = \widetilde{\Phi}_2(k_x, y)$ at y = d).

Applying (4.21) in the first boundary condition gives $\widetilde{\Phi}_1(k_x, 0) = A + B = 0$. This implies $B = -A$. Next, applying (4.22) to the boundary condition in region 2 gives $\lim_{y\to\infty} \widetilde{\Phi}_2(k_x, y) = Ce^{+|k_x|y} + De^{-|k_x|y} = 0$. This forces $C = 0$ otherwise $\widetilde{\Phi}_2(k_x, y)$ will diverge and not satisfy the boundary condition. Substituting the constants into (4.21) and (4.22) gives:

$$\widetilde{\Phi}_1(k_x, y) = Ae^{+|k_x|y} - Ae^{-|k_x|y} \tag{4.23}$$

and

$$\widetilde{\Phi}_2(k_x, y) = De^{-|k_x|y}. \tag{4.24}$$

Next, the second boundary condition, $\widetilde{\rho_s} = \hat{n}_2 \cdot (\widetilde{D}_2 - \widetilde{D}_1) = 1$, will be applied at y = d. Also note that the normal component of both $\widetilde{D}_1$ and $\widetilde{D}_2$ is the y-component and $\widetilde{E}_1 = -\nabla\widetilde{\Phi}(k_x, y)$. This implies

$$\begin{aligned} \hat{n}_2 \cdot \widetilde{D}_1 &= -\varepsilon_0\varepsilon_r \frac{\partial\widetilde{\Phi}_1(k_x, y)}{\partial y} \\ &= -\varepsilon_0\varepsilon_r \big[A|k_x|e^{+|k_x|y} + A|k_x|e^{-|k_x|y}\big]. \end{aligned} \tag{4.25}$$

Similarly,

$$\begin{aligned} \hat{n}_2 \cdot \widetilde{D}_2 &= -\varepsilon_0 \frac{\partial \widetilde{\Phi}_2(k_x, y)}{\partial y} \\ &= \varepsilon_0 D|k_x| e^{-|k_x|y}. \end{aligned} \tag{4.26}$$

Substituting (4.25) and (4.26) into the second boundary condition gives:

$$\begin{aligned} D|k_x|e^{-|k_x|d} + A\varepsilon_r \left[e^{+|k_x|d} + e^{-|k_x|d} \right] &= D|k_x|e^{-|k_x|d} + A\varepsilon_r 2\cosh(|k_x|d) \\ &= \frac{1}{\varepsilon_0|k_x|}. \end{aligned} \tag{4.27}$$

Equation (4.27) is one equation with two unknowns. Now a second equation is needed. To get this, the third boundary condition will be applied. This is $\widetilde{\Phi}_1(k_x, d) = \widetilde{\Phi}_2(k_x, d)$. This implies that $Ae^{+|k_x|y} - Ae^{-|k_x|y} = De^{-|k_x|y}$. Solving for A gives

$$A = \frac{De^{-|k_x|d}}{2\sinh(|k_x|d)}. \tag{4.28}$$

Substituting (4.28) into (4.27) and solving for D gives

$$D = \frac{1}{\varepsilon_0|k_x|} \frac{1}{e^{-|k_x|d}} \frac{1}{1 + \varepsilon_r \coth(|k_x|d)}. \tag{4.29}$$

Substituting (4.28) into (4.23) and (4.29) into (4.24) gives:

$$\widetilde{\Phi}_1(k_x, y) = \frac{1}{\varepsilon_0|k_x|[1 + \varepsilon_r \coth(|k_x|d)]} \tag{4.30}$$

and

$$\widetilde{\Phi}_2(k_x, y) = \frac{e^{|k_x|(d-y)}}{\varepsilon_0|k_x|[1 + \varepsilon_r \coth(|k_x|d)]}. \tag{4.31}$$

(4.30) is the same as (6) in Davidson and Aberle's paper and (4.31) is the same as (5)

in Davidson and Aberle's paper. The steps leading to (5) and (6) in Davidson and Aberle's paper were not shown, but they have been shown here for clarity. Notice that the expressions in (4.30) and (4.31) are equal for $y = \mathrm{d}$ and *represent the Green's function in the spectral domain.* The definition of the inverse Fourier transform is used to obtain the following Green's function for the charge source at $x' = 0$ in Figure 20 in the space domain as:

$$G(x,0) = \frac{1}{2\pi}\int_{-\infty}^{+\infty} \widetilde{\Phi}_2(k_x,d)e^{jk_x x}dk_x. \tag{4.32}$$

Therefore, the following can be used for a source located anywhere along the x-axis:

$$G(x,x') = \frac{1}{2\pi}\int_{-\infty}^{+\infty} \widetilde{\Phi}_2(k_x,d)e^{jk_x(x-x')}dk_x. \tag{4.33}$$

Equation (4.33) represents the Green's function for a point charge on the x-axis and needs to be integrated to get the contribution from a line charge. This then gives the potential at d as

$$\Phi_2(x,d) = \int_{-\infty}^{\infty} G(x,x')\rho(x',d)dx' = \Phi_1(x,d). \tag{4.34}$$

Next, Davidson and Aberle calculated the capacitance per unit length for the dominant quasi-static TEM mode. This was done by doing the following:

1. Assume the microstrip is at potential V_o and the ground plane is at potential 0.
2. Determine ρ_s by setting up the appropriate integral equations and solve with the spectral domain moment mothod.
3. Evaluate the charge per unit length ρ_l by integrating the surface charge per unit length over the width of the conductor using $\rho_l = \int_L \rho_s dl$.

4. Evaluate the capacitance per unit length using $C = \frac{\rho_l}{V_o}$.

The potential due to the surface charge is determined using (4.34) and can be written as

$$V(x,y) = \int_{-W/2}^{W/2} G(x,y|x',d)\rho(x',d)dx'. \tag{4.35}$$

Applying the boundary condition on the strip results in the following integral equation:

$$V_o = \int_{-W/2}^{W/2} G(x,d|x',d)\rho(x',d)dx'. \tag{4.36}$$

The integral equation in (4.36) will be solved for the unknown charge using the spectral domain moment method. When applying Galerkin's method the unknown surface charge is expanded in terms of known basis functions. This then gives:

$$\rho(x') \approx \sum_{n=1}^{N} \rho_n \phi_n(x') \tag{4.37}$$

where ρ_n is the unknown magnitude and $\phi_n(x')$ is the known expansion function. Then defining the weighting function $w_m(x)$ and taking the inner product with these weighting functions results in the following matrix equation:

$$[A][f] = [g] \tag{4.38}$$

where $f_n = \rho_n$, $g_m = \int_{-W/2}^{W/2} w_m(x)V_o dx$ and

$$a_{m,n} = \int_{-W/2}^{W/2} w_m(x) \int_{-W/2}^{W/2} G(x,d|x',d)\phi_n(x',d)dx'dx. \tag{4.39}$$

Substituting (4.33) into (4.39) results in the following integral

$$a_{m,n} = \int_{-W/2}^{W/2} w_m(x) \int_{-W/2}^{W/2} \left[\frac{1}{2\pi}\int_{-\infty}^{+\infty} \widetilde{\Phi}_1(k_x,d)e^{jk_x(x-x')}dk_x\right]\phi_n(x')dx'dx \tag{4.40}$$

with the assumption that $\widetilde{\Phi}_1(k_x, d) = \widetilde{\Phi}_2(k_x, d)$. It can be seen that the integration in (4.40) could be very time consuming. The numerical infinite integration of k_x would have to be evaluated for every x and x'. This long integration can be avoided with some rearranging of (4.40). *This rearrangement is a very important step in this work and will be used later with the spectral domain immittance functions.* Thus, rearranging (because of uniform continuity) (4.40) and using the notation $\widetilde{G}$ gives

$$\begin{aligned} a_{m,n} &= \int_{-W/2}^{W/2} w_m(x) \int_{-W/2}^{W/2} \left[\frac{1}{2\pi} \int_{-\infty}^{+\infty} \widetilde{G}(k_x, d|d) e^{jk_x x} e^{-jk_x x'} dk_x \right] \phi_n(x') dx' dx \\ &= \frac{1}{2\pi} \int_{-\infty}^{+\infty} \left[\int_{-W/2}^{W/2} w_m(x) e^{jk_x x} dx \, \widetilde{G}(k_x, d|d) \int_{-W/2}^{W/2} \phi_n(x') e^{-jk_x x'} dx' \right] dk_x. \end{aligned} \quad (4.41)$$

From the definition in (4.10) it can be seen that $\int_{-W/2}^{W/2} w_m(x) e^{jk_x x} dx$ is the Fourier transform of $w_m(x)$ and is denoted as $\widetilde{w}_m(-k_x)$ and $\int_{-W/2}^{W/2} \phi_n(x') e^{-jk_x x'} dx'$ is the Fourier transform of $\phi_n(x')$ and is denoted as $\widetilde{\phi}_n(k_x)$. Note that the finite integration of $w_m(x)$ and $\phi_n(x')$ in (4.41) is the same as the infinite integration because of the finite support of the functions. This simplifies (4.41) to

$$a_{m,n} = \frac{1}{2\pi} \int_{-\infty}^{+\infty} \widetilde{w}_m(-k_x) \, \widetilde{G}(k_x, d|d) \widetilde{\phi}_n(k_x) dk_x. \quad (4.42)$$

Therefore, by starting with a basis or weighting function that has a known analytical Fourier transform, the transform of these functions can be substituted directly into (4.42) and the integral can be evaluated entirely in the spectral domain. Next, $w_m(x)$ and $\phi_n(x')$ need to be determined such that $\widetilde{w}_m(-k_x)$ and $\widetilde{\phi}_n(k_x)$ have closed forms. For simplicity Davidson and Aberle choose pulse functions as weighting

and basis functions. These can be written as

$$\phi_n(x') = \begin{cases} 1 & x \in (x_n, x_{n+1}) \\ 0 & \text{otherwise} \end{cases} \tag{4.43}$$

where N is the number of segments the microstrip is divided into and the nodal point x_n is defined in Figure 21. Applying the Fourier transform to (4.43) gives

$$\begin{aligned} \widetilde{\phi}_n(k_x) &= \int_{x_n}^{x_n+\Delta x} 1 e^{-jk_x x} dx \\ &= \frac{1}{-jk_x}\left[e^{-jk_x(x_n+\Delta x)} - e^{-jk_x x_n}\right] \\ &= \frac{1}{-jk_x} e^{-jk_x x_n} e^{-jk_x\frac{\Delta x}{2}}\left[e^{-jk_x\frac{\Delta x}{2}} - e^{jk_x\frac{\Delta x}{2}}\right] \\ &= \frac{1}{k_x} e^{-jk_x x_n} e^{-jk_x\frac{\Delta x}{2}} 2\sin(k_x\frac{\Delta x}{2}) \\ &= e^{-jk_x x_n}\frac{\Delta x \sin(k_x\frac{\Delta x}{2})}{(\frac{\Delta x k_x}{2})} e^{-jk_x\frac{\Delta x}{2}}. \end{aligned} \tag{4.44}$$

The expression in (4.44) is the Fourier transform of $\widetilde{\phi}_n(k_x)$. The Fourier transform of $\widetilde{w}_m(-k_x)$ can be found by simply substituting a $-k_x$ in for k_x in (4.44).

Equation (4.42) can be reduced even more. By noticing that $\widetilde{G}(-k_x, d|d) = \widetilde{G}(k_x, d|d)$ and using the identity $e^{jk_x x_m}e^{-jk_x x_n} + e^{-jk_x x_m}e^{jk_x x_n} = 2\cos(k_x(x_m - x_n))$, (4.42) reduces to

$$\begin{aligned} a_{mn} &= \frac{1}{2\pi}\int_0^\infty \widetilde{G}(k_x, d|d)[\widetilde{\phi}_m(-k_x)\widetilde{\phi}_n(k_x) + \widetilde{\phi}_m(k_x)\widetilde{\phi}_n(-k_x)]dk_x \\ &= \frac{1}{\pi}\int_0^\infty \widetilde{G}(k_x, d|d)\widetilde{\psi}^2(k_x)\cos(k_x(x_m - x_n))dx. \end{aligned} \tag{4.45}$$

where $\widetilde{\psi}(k_x) = \Delta x\frac{\sin(\frac{k_x\Delta x}{2})}{\frac{k_x\Delta x}{2}}$. This reduces the integration to the positive real line. Now (4.45) needs to be integrated. The numerical integration needs to be truncated at a point that approximates the infinite integration. To find the upper limit k_{max} is

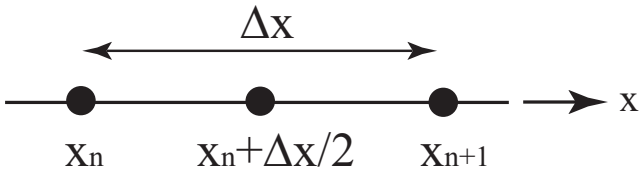

Figure 21. Definition of the nodal point.

chosen (upper limit of integration) such that the power contained in $\widetilde{\psi}(k_x)$ between 0 and k_{max} is a fraction of the total power of $\widetilde{\psi}(k_x)$ or

$$\frac{\int_0^{k_{max}} \widetilde{\psi}(k_x)dk_x}{\int_0^{\infty} \widetilde{\psi}(k_x)dk_x} \leq K \tag{4.46}$$

where $K < 1$. Solving for k_{max} in (4.46) gives $k_{max} = \frac{2}{\pi\Delta x}\frac{1}{1-k} = B_{max}\frac{1}{\Delta x}$ where $B_{max} = \frac{2}{\pi(1-k)}$ is a constant. This then allows an approximation for (4.45):

$$\begin{aligned} a_{mn} &= \frac{1}{\pi}\int_0^{\infty} \widetilde{G}(k_x, d|d)\widetilde{\psi}^2(k_x)\cos(k_x(x_m - x_n))dx \\ &\approx \frac{1}{\pi}\int_0^{k_{max}} \widetilde{G}(k_x, d|d)\widetilde{\psi}^2(k_x)\cos(k_x(x_m - x_n))dx \\ &\approx \frac{1}{\pi}\sum_{i=1}^{N_k} \widetilde{G}(k_i, d|d)\widetilde{\psi}^2(k_i)\cos(k_i(x_m - x_n))\Delta k \end{aligned} \tag{4.47}$$

where $\Delta k = \frac{k_max}{N_k}$, $k_i = (i-1)\Delta k$ and N_k is the number of segments the space is divided into. Also, since pulse weighting functions are used,

$$g_m = \int_{-W/2}^{W/2} w_m(x)V_o dx = V_o. \tag{4.48}$$

It can be seen that (4.47) is evaluated in the spectral domain, but the range, or values it takes on as a result of the integration is in the spatial domain. The integration in (4.48) is in the spatial domain and the values it takes on is also in the spatial domain. This allows us to equate (4.47) to (4.48) in the spectral domain

moment method and solve for the unknown charges. Noticing this is key to using the spectral domain moment method correctly in this case.

Davidson and Aberle evaluate the problem in Figure 19 with d = 10 mm, ε_r = 4.2, W = 10 mm, B_{max} = 10 and B_k = 50. A very thorough discussion on determining the number of B_{max} and B_k is presented by Davidson and Aberle and is not reproduced here. Davidson and Aberle also recommend choosing

$$N_k = B_k \left[\frac{1}{\pi} k_{max} W + \frac{1}{2} \right] \approx B_k \left[\frac{2}{\pi} k_{max} W \right]. \tag{4.49}$$

Matlab [85] was used to evaluate the matrix coefficients (4.47) and (4.48). Initially, the value of N_k was increased until the capacitance per unit length converged. These calculations are shown in Figure 22. It is shown that the solution converged after 40 segments. Therefore, defining N_k = 40 and integrating resulted in the charge distribution shown in Figure 23.

The results presented here compared very well with the results by Davidson and Aberle. The code for the calculations in Figures 22 and 23 is in Appendix D. Davidson and Aberle discuss many other aspects related to the application of the moment method in the spectral domain. These topics included classroom experience, implementation in Matlab and other hybrid techniques. These topics are very useful, but are not summarized here.

Two very significant points as a result of this discussion should be emphasized. The first one is the rearranging of a_{mn} to avoid the integration in both the space and spectral domain. This not only greatly reduced the numerical integration, but it also clearly showed the role of Green's function in this whole process. The second point is noticing that the range of a_{mn} and g_m are both in the spatial domain. The integration of a_{mn} may be in the spectral domain, but a_{mn} and g_m are *both* in the spatial domain and can be used to solve a physical problem using the moment method.

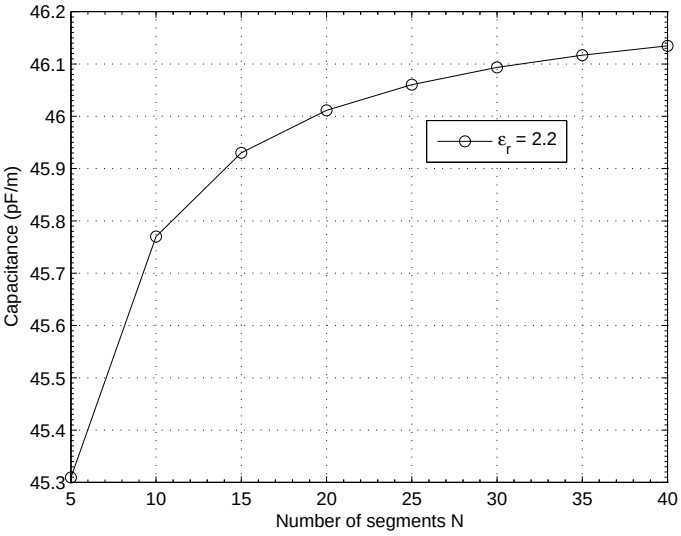

Figure 22. Convergence of the charge distribution along Davidson and Aberle's microstrip example.

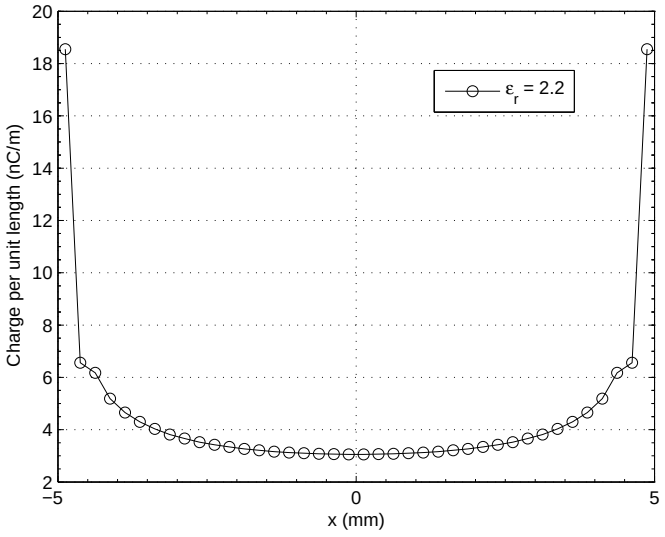

Figure 23. Charge distribution along Davidson and Aberle's microstrip example.

These two points are key to using the spectral domain moment method to solve for the unknown currents in the spectral domain immittance functions. The next section outlines the process of using the moment method to solve for the unknown currents.

4.3. Solving the Spectral Domain Immittance Functions

In this section the Green's function will be introduced and related to the spectral domain immittance functions. Then the use of the spectral domain moment method will be presented to solve for the unknown current.

The Green's function has many different applications to many different problems. An extensive discussion on the Green's Function can be found in Collin [79]. Only a brief introduction to the concept of the Green's function will be presented here. The Green's function $G(\bar{r}, \bar{r}')$ is an impulse response of a linear system to a point source of unit strength at $\bar{r}_0$ [79]. If the point source at $\bar{r}_0$ is denoted as $J(\bar{r}_0)$ then the electric field at x, y and z from $J(\bar{r}_0)$ can be written as [79]:

$$\bar{E}(x, y, z) = \int_{z'} \int_{y'} \int_{x'} G(\bar{r}, \bar{r}') \bar{J}(\bar{r}_0) dx' dy' dz'. \tag{4.50}$$

As mentioned in Chapter 4, the spectral domain immittance functions $\widetilde{Z}_{xx}$, $\widetilde{Z}_{xz}$, $\widetilde{Z}_{zx}$ and $\widetilde{Z}_{zz}$ represent the Green's function in the spectral domain. Therefore, the Green's function in the spatial domain is the inverse Fourier transform of $\widetilde{Z}_{xx}$, $\widetilde{Z}_{xz}$, $\widetilde{Z}_{zx}$ and $\widetilde{Z}_{zz}$.

Using Z_{xx}, Z_{xz}, Z_{zx} and Z_{zz} the x- and z-component of the electric field in each region can be written in the spatial domain as [31]

$$E_x(x, y, z) = \int_{z'} \int_{x'} \Big[Z_{xx}(x - x', z - z') J_x(x', z') + Z_{xz}(x - x', z - z') J_z(x', z') \Big] dx' dz' \tag{4.51}$$

and

$$E_z(x,y,z) = \int_{z'}\int_{x'}\Big[Z_{zx}(x-x',z-z')J_x(x',z') + Z_{zz}(x-x',z-z')J_z(x',z')\Big]dx'dz', \tag{4.52}$$

respectively. Since Z_{xx}, Z_{xz}, Z_{zx} and Z_{zz} in (4.51) and (4.52) are in the spatial domain, the inverse Fourier transform defined in (3.30) will need to be applied to $\widetilde{Z}_{xx}$, $\widetilde{Z}_{xz}$, $\widetilde{Z}_{zx}$ and $\widetilde{Z}_{zz}$. This will then result in representations of the Green's functions in the spatial domain. Note that when referring to the work by Davidson and Aberle in the previous section, the k_x variable is associated with the α variable in this work. If a two-dimensional integral had been used in Davidson and Aberle's work, the k_z variable would be related to the β variable in this work. Proceeding in this manner, the x-component of the electric field can be written as

$$\begin{aligned} E_x(x,y,z) &= \frac{1}{(2\pi)^2}\int_{z'}\int_{x'}\Bigg[\int_{-\infty}^{\infty}\int_{-\infty}^{\infty}\widetilde{Z}_{xx}(\alpha,\beta)e^{j[\alpha(x-x')+\beta(z-z')]}d\alpha d\beta J_x(x',z') \\ &+ \int_{-\infty}^{\infty}\int_{-\infty}^{\infty}\widetilde{Z}_{xz}(\alpha,\beta)e^{j[\alpha(x-x')+\beta(z-z')]}d\alpha d\beta J_z(x',z')\Bigg]dx'dz'. \end{aligned} \tag{4.53}$$

Next, define the current in terms of basis functions as

$$J_x(x',z') = \sum_{n=1}^{N} I_{xn} r_{xn}(x',z') \tag{4.54}$$

and

$$J_z(x',z') = \sum_{n=1}^{N} I_{zn} r_{zn}(x',z') \tag{4.55}$$

where I_{xn} and I_{zn} are the unknown magnitudes of the x- and z-components of the surface current, respectively. The known expansion functions are $r_{xn}(x',z')$ and $r_{zn}(x',z')$. Since Galerkin's method is being used, the weighting functions $w_{xm}(x,z)$

and $w_{zm}(x,z)$ will be defined to be the same as the expansion functions $r_{xn}(x',z')$ and $r_{zn}(x',z')$, respectively. The weighting functions will be indexed by the variable m and are defined at x and z.

Substituting (4.54) and (4.55) into (4.53), taking the inner product $\langle w_{xm}(x,z), E_x(x,y,z)\rangle$ and factoring gives

$$\begin{aligned}\langle w_{xm}(x,z), E_x(x,y,z)\rangle &= \\ &\frac{1}{(2\pi)^2}\int_{-\infty}^{\infty}\int_{-\infty}^{\infty}\Bigg[\int_z\int_x w_{xm}(x,z)e^{j\alpha x}e^{j\beta z}dxdz * \widetilde{Z}_{xx}(\alpha,\beta) * \\ &\int_{z'}\int_{x'} r_{xn}(x',z')e^{-j\alpha x'}e^{-j\beta z'}dx'dz'\Bigg]d\alpha d\beta \\ &+ \frac{1}{(2\pi)^2}\int_{-\infty}^{\infty}\int_{-\infty}^{\infty}\Bigg[\int_z\int_x w_{xm}(x,z)e^{j\alpha x}e^{j\beta z}dxdz * \widetilde{Z}_{xz}(\alpha,\beta) * \\ &\int_{z'}\int_{x'} r_{zn}(x',z')e^{-j\alpha x'}e^{-j\beta z'}dx'dz'\Bigg]d\alpha d\beta. \qquad (4.56)\end{aligned}$$

Similarly, for the z-component:

$$\begin{aligned}\langle w_{zm}(x,z), E_z(x,y,z)\rangle &= \\ &\frac{1}{(2\pi)^2}\int_{-\infty}^{\infty}\int_{-\infty}^{\infty}\Bigg[\int_z\int_x w_{zm}(x,z)e^{j\alpha x}e^{j\beta z}dxdz * \widetilde{Z}_{zx}(\alpha,\beta) * \\ &\int_{z'}\int_{x'} r_{xn}(x',z')e^{-j\alpha x'}e^{-j\beta z'}dx'dz'\Bigg]d\alpha d\beta \\ &+ \frac{1}{(2\pi)^2}\int_{-\infty}^{\infty}\int_{-\infty}^{\infty}\Bigg[\int_z\int_x w_{zm}(x,z)e^{j\alpha x}e^{j\beta z}dxdz * \widetilde{Z}_{zz}(\alpha,\beta) * \\ &\int_{z'}\int_{x'} r_{zn}(x',z')e^{-j\alpha x'}e^{-j\beta z'}dx'dz'\Bigg]d\alpha d\beta. \qquad (4.57)\end{aligned}$$

Notice the following expression is contained in (4.56):

$$\int_{z'}\int_{x'} r_{xn}(x',z')e^{-j\alpha x'}e^{-j\beta z'}dx'dz'. \tag{4.58}$$

This expression is the Fourier transform of the basis function r_{xn}, denoted as $\widetilde{r}_{xn}$. Therefore, if the basis functions are chosen appropriately, an analytical expression for (4.58) could be derived and substituted directly back into (4.56). Since the Galerkin's method is being used, this substitution could be done for both the weighting and expansion functions. Continuing in this manner, (4.56) and (4.57) simplify to the following:

$$\begin{aligned}\langle w_{xm}(x,z), E_x(x,y,z)\rangle &= \frac{1}{(2\pi)^2}\int_{-\infty}^{\infty}\int_{-\infty}^{\infty}\left[\widetilde{w}_{xm}(-\alpha,-\beta)\widetilde{\widetilde{Z}}_{xx}(\alpha,\beta)\widetilde{r}_{xn}(\alpha,\beta)\right]d\alpha d\beta \\ &+ \frac{1}{(2\pi)^2}\int_{-\infty}^{\infty}\int_{-\infty}^{\infty}\left[\widetilde{w}_{xm}(-\alpha,-\beta)\widetilde{\widetilde{Z}}_{xz}(\alpha,\beta)\widetilde{r}_{zn}(\alpha,\beta)\right]d\alpha d\beta\end{aligned} \tag{4.59}$$

and

$$\begin{aligned}\langle w_{zm}(x,z), E_z(x,y,z)\rangle &= \frac{1}{(2\pi)^2}\int_{-\infty}^{\infty}\int_{-\infty}^{\infty}\left[\widetilde{w}_{zm}(-\alpha,-\beta)\widetilde{\widetilde{Z}}_{zx}(\alpha,\beta)\widetilde{r}_{xn}(\alpha,\beta)\right]d\alpha d\beta \\ &+ \frac{1}{(2\pi)^2}\int_{-\infty}^{\infty}\int_{-\infty}^{\infty}\left[\widetilde{w}_{zm}(-\alpha,-\beta)\widetilde{\widetilde{Z}}_{zz}(\alpha,\beta)\widetilde{r}_{zn}(\alpha,\beta)\right]d\alpha d\beta\end{aligned} \tag{4.60}$$

.

The steps leading to (4.59) and (4.60) are key to implementing the spectral domain immittance functions in electromagnetics problems. Notice that the integration of (4.59) and (4.60) is entirely in the spectral domain and the electric field values are in the spatial domain. These steps simplified the numerical implementation of the

spectral domain immittance functions greatly. Notice that the expressions in (4.59) and (4.60) do not contain a numerical derivative. This is another great advantage of this technique. The next section discusses the basis functions used in this work.

4.4. The Basis Functions

4.4.1. Spatial domain

The basis functions defined are for the printed dipole in Figure 24. Since the surfaces in this research are planar, a two-dimensional piecewise sinusoidal (PWS) basis function is chosen. It is assumed that the current on the dipole in Figure 24 does not vary with respect to the width of the conductor and only varies with respect to the length. Therefore thin-wire assumptions are enforced. This then allows the PWS to be constant with respect to the z-axis and vary sinusoidally with respect to the x-axis. The PWS basis functions are shown in Figure 25 and are defined as

$$r_i(x',z') = \begin{cases} \frac{\sin[k(\Delta x - x_i + x')]}{\sin(k\Delta x)} U(z'), & x_i - d \leq x' \leq x_i; \\ \frac{\sin[k(\Delta x - x' + x_i)]}{\sin(k\Delta x)} U(z'), & x_i < x' \leq x_i + d; \\ 0, & \text{otherwise} \end{cases} \tag{4.61}$$

where $U(z')$ is a unit pulse defined over the width of the conductor (i.e., in the z-direction) and zero otherwise. Equation (4.61) will be used to represent the unknown surface current $\bar{J}_s$ in the dipole problems.

4.4.2. Spectral domain

In this section the two-dimensional Fourier Transform defined in (3.27) will be applied to (4.61) to determine the basis function in the transform domain. This gives

$$\begin{aligned} \widetilde{r}_i(\alpha,\beta) &= \left[\int_{x_i-\Delta x}^{x_i} \frac{\sin[k(\Delta x - x_i + x')]}{\sin(k\Delta x)} e^{-j\alpha x'} dx' \right. \\ &\quad \left. + \int_{x_i}^{x_i+\Delta x} \frac{\sin[k(\Delta x - x' + x_i)]}{\sin(k\Delta x)} e^{-j\alpha x'} dx' \right] * \int_{z_i-W/2}^{z_i+W/2} 1 e^{-j\beta z'} dz' \end{aligned}$$

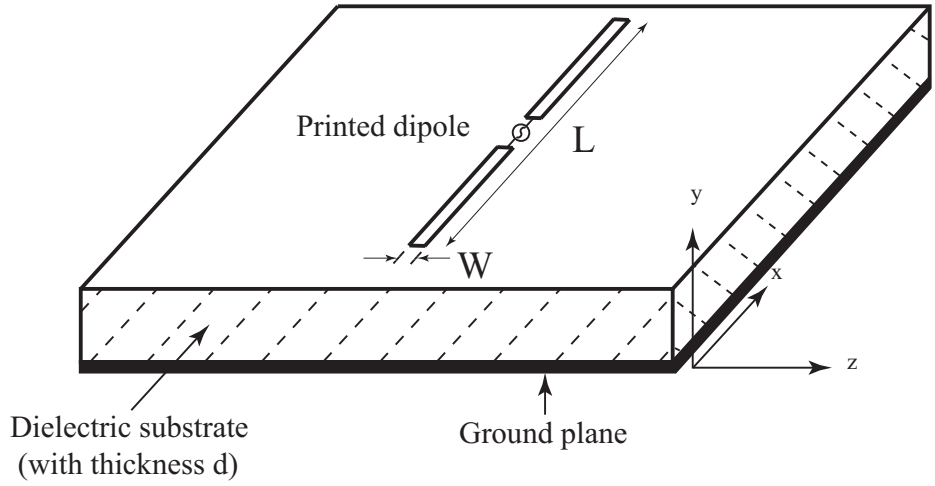

Figure 24. The "conducting strip" printed dipole that is equivalent to the cylindrical dipole.

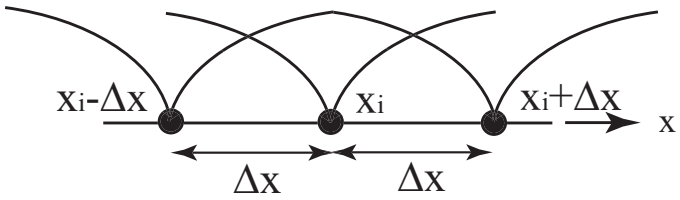

Figure 25. Piecewise sinusoidal basis functions used in the numerical computations.

$$= \frac{2}{\sin(k\Delta x)}\left(\frac{1}{k+\alpha}+\frac{1}{k-\alpha}\right)e^{-j\alpha x_i}\sin\left(\frac{\Delta x(k+\alpha)}{2}\right)\sin\left(\frac{\Delta x(k-\alpha)}{2}\right)*$$

$$e^{-j\beta z_i}\frac{\Delta z\sin(\beta\Delta z/2)}{\Delta z\beta/2}e^{-j\beta\Delta z/2} \tag{4.62}$$

where Δz has been substituted for W to generalize the expression. A closed form solution for the basis functions in the transform domain has now been derived. This can now be substituted directly into (4.59) and (4.60) and then be used to represent

the unknown current in the spectral or transform domain. Notice that the last expression in (4.62) is in the form of a sinc function and needs to be defined at the origin. Also, notice that a singularity exists at $\alpha = \pm k$. The two-dimensional numerical integration will have to be modified to avoid these poles.

4.5. Numerical Integration

The first step for the numerical integration is to define the $\alpha - \beta$ plane on which the numerical integration of the spectral domain immittance functions is performed. In the Fourier transform the x-variable is associated with the α-variable and the z-variable is associated with the β-variable. This association results in the $\alpha - \beta$ plane shown in Figure 26 on which the numerical integration routine is defined. The association of the x- and z-variable with spectral variables α and β, respectively, is an important one. For example, if the spatial definition of the basis functions is much smaller in the z-direction than the x-direction, then the spectral content in the β-direction will be much more than the content in the α-direction. This is important to remember when numerically integrating the expressions in (4.59) and (4.60).

Several poles exist in the functions that are numerically integrated over the spectral plane. It is very important that these poles are avoided by the numerical integration. The location of these poles has led to the use of polar integration from the origin to a circle of radius k. Then rectangular integration is performed on the remainder of the plane. Both types of numerical integration are shown in Figure 26. The first pole is in the denominator of (3.86) and has the form $\gamma_{e1} + \varepsilon_{12}\gamma_0 \coth(\gamma_{e1} d_1)$. The secant method is used to find the root to this equation, and it is located somewhere between k_0 and k. The location of this pole is shown in Figure 26. Similarly, it can be seen in (4.62) that a pole exists at $\pm k$. This is also shown in Figure 26. Finally, in all the immittance functions derived in Chapter 3, it can be seen that a pole is located at the origin. This is also illustrated in Figure 26.

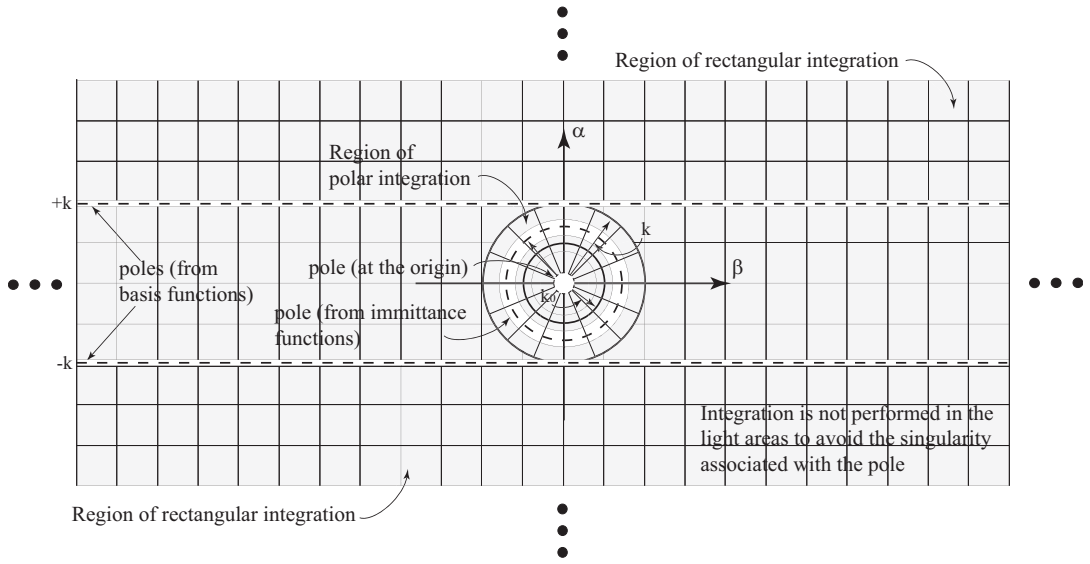

Figure 26. The numerical integration mesh definitions (polar and rectangular) and the location of the poles on the $\alpha - \beta$ plane.

The shaded areas in Figure 26 indicate the region of the plane in which the numerical integration is performed. The regions around the poles are removed from the numerical integration to avoid the singularity associated with the expressions. This deleted region is indicated by the white areas with the poles shown by dotted lines.

4.6. The Delta Source

The expression for the tangential components of the electric field on the conductors can be written as $\bar{E}^s_{\tan} + \bar{E}^i_{\tan} = 0$ where $\bar{E}^s_{\tan}$ is the tangential component of the scattered field and $\bar{E}^i_{\tan}$ is the tangential component of the incident field. $\bar{E}^s_{\tan}$ is represented by the spectral domain immittance functions and $\bar{E}^i_{\tan}$ will be generated by a delta source [22]. This type of source is probably the most common source implemented in the MOM and is shown in Figure 27. The delta source generates an electric field by defining a voltage source V_A across several of the full-wave segments. The voltage points can be seen in Figure 27. The electric potential between points a

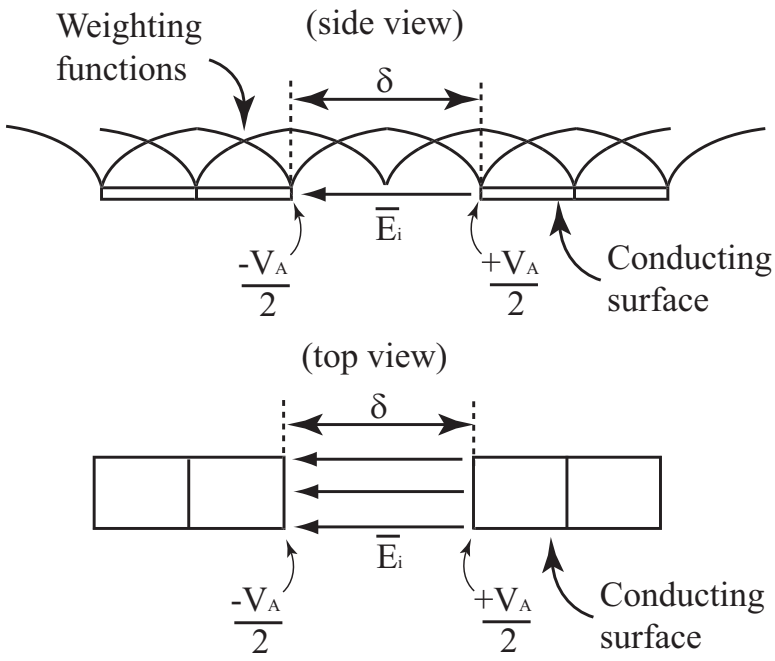

Figure 27. The delta source used to represent an incident field on the printed dipole.

and b can be written as

$$V_b - V_a = -\int_a^b \bar{E}^i_{\tan} \cdot d\bar{l}. \tag{4.63}$$

Assuming $\bar{E}^i_{\tan}$ is constant, (4.63) can be integrated across the δ-gap in Figure 27 giving $V_A = E_i\delta$; which then gives

$$E_i = \frac{V_A}{\delta}. \tag{4.64}$$

It is assumed that the δ-gap is small enough such that no fringing of the electric field exists. Equation (4.64) has two known values, V_A and δ, and can be implemented in the MOM to satisfy the expression for $\bar{E}^s_{\tan} + \bar{E}^i_{\tan} = 0$ on the conductor. Delta sources are a good way to simulate the fields from an antenna when it is driven at a single point with a voltage source. From the calculated currents the input impedance

Z_{in} at the k^{th} driving point can then be determined by

$$Z_{in} = \frac{V_A}{I_k}. \tag{4.65}$$

Notice that the delta source is defined across two conductor segments in Figure 27. Because of this, three different weighting functions are used to enforce the incident field boundary conditions. This then requires three elements in the voltage matrix to be calculated. The middle location of the three voltage matrix elements is determined with the normal weighting function calculation, but the two adjacent matrix elements are only half of the value of the middle element. This is because only half of the adjacent weighting functions are defined across the delta gap. This is very important to remember and can easily be forgotten during the code writing process.

CHAPTER 5. NUMERICAL AND MEASUREMENT RESULTS

The printed dipole was the antenna primarily investigated in this work. The following sections present measurements and numerical results for a printed dipole in one, two and three isotropic and anisotropic dielectric layers. In each section the results are presented first followed by a discussion.

5.1. Measurements of a Printed Dipole in Several Layers of Isotropic and Anisotropic Dielectrics

The first step was to validate the results from the immittance functions and ADS [86] with measurements. A wire monopole with radius a = 0.4 mm and length L = 60 mm, similar to the one presented in [28], was placed above a 1.58 mm substrate made of FR-4 material. It was assumed that the FR-4 material had a permittivity of $\varepsilon_r = 4.35$. The material and wire monopole was then placed vertically above a ground plane and driven with a coax. Pictures of the setup is shown in Figures 28-30 and a diagram is shown in Figure 31. It has been shown by others [87] that this test setup provides accurate measurements. The resonant frequency of the monopole was measured for various superstrates with a calibrated Agilent E5071C ENA series network analyzer. The results from these measurements are shown in Table 1. Layer 1 refers to the substrate, layer two refers to the superstrate immediately above the monopole (i.e., superstrate touching the monopole) and layer 3 refers to the superstrate above layer 2 (i.e., the superstrate between layer 2 and the surround air). The anisotropic Epsilam-10 material had a thickness of 0.635 mm, $\varepsilon_x = \varepsilon_z = 13$ and $\varepsilon_y = 10.2$. The isotropic Rogers RT/Duroid 5880 had a thickness of 0.7874 mm and $\varepsilon_r = 2.2$.

An equivalent problem of a flat printed monopole with the same length and width of $W = 4a$ was defined to be evaluated by ADS and the immittance functions.

Figure 28. Picture of the monopole being measured above an FR-4 substrate.

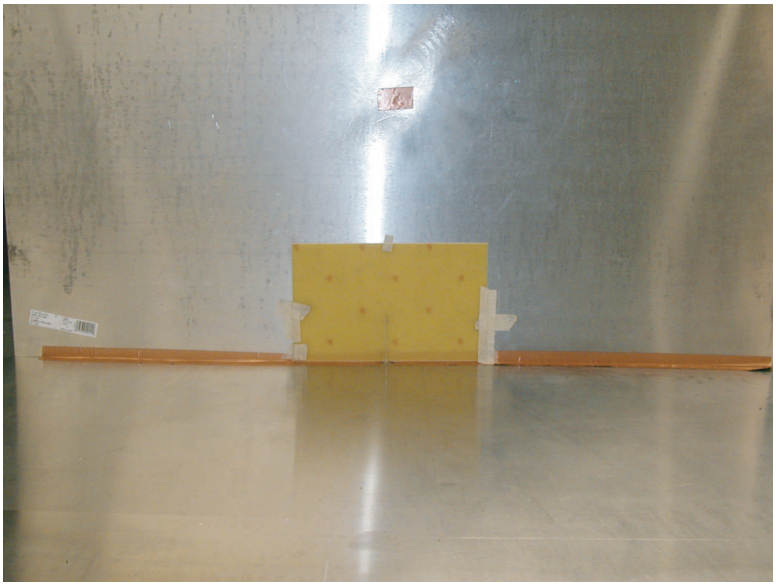

Figure 29. Picture of the monopole being measured above an FR-4 substrate showing the ground plane.

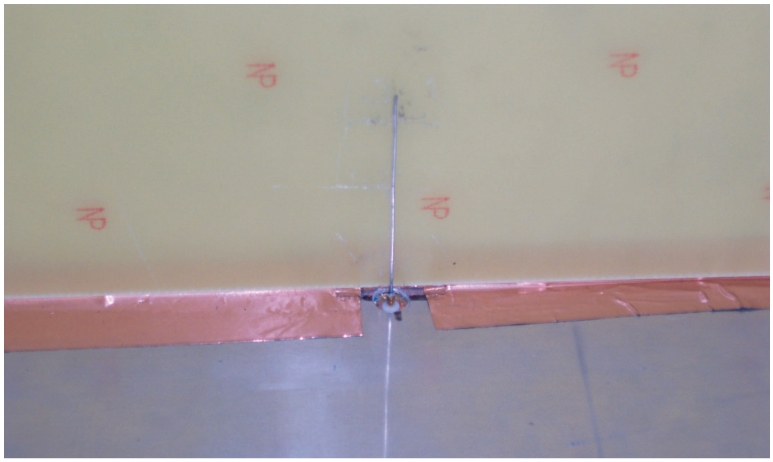

Figure 30. Picture of the sma connector feeding the monopole above an FR-4 substrate.

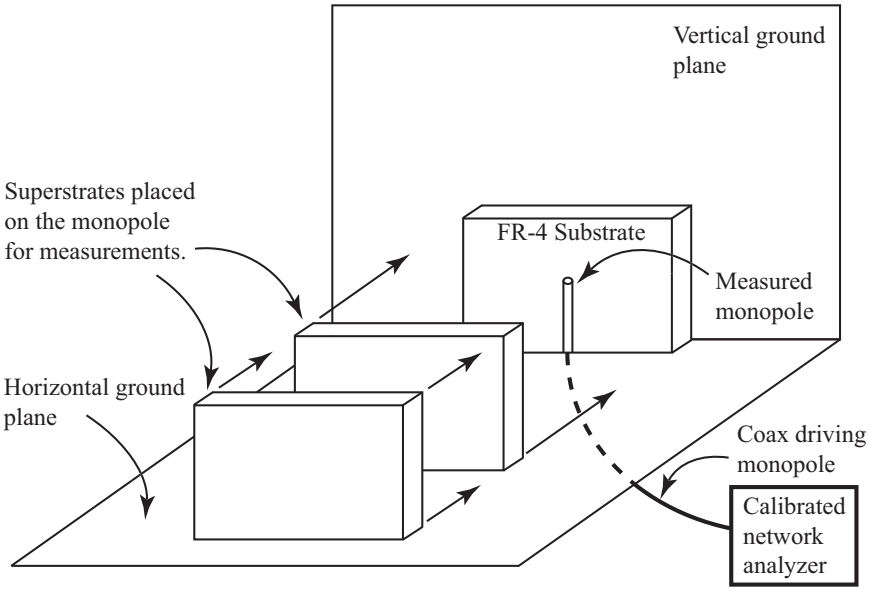

Figure 31. Diagram of the experimental validation using the monopole.

Table 1. Measured resonant frequency of a monopole in layered material.

Layer Information	ADS	Matlab	Measured
Layer 1: FR-4, Layer 2: Air, Layer 3: Air	704 MHz	704 MHz	706 MHz
Layer 1: FR-4, Layer 2: FR-4, Layer 3: Air	615 MHz	615 MHz	617 MHz
Layer 1: FR-4, Layer 2: Rogers 5880, Layer 3: Air	673 MHz	674 MHz	676 MHz
Layer 1: FR-4, Layer 2: Epsilam-10, Layer 3: Air	X	564 MHz	566 MHz
Layer 1: FR-4, Layer 2: Epsilam-10, Layer 3: Rogers 5880	X	555 MHz	554 MHz
Layer 1: FR-4, Layer 2: Epsilam-10, Layer 3: FR-4	X	539 MHz	540 MHz

It has been shown that a flat printed "strip" conductor with a width of $W = 4a$ can be used to approximate a thin-wire cylindrical conductor with radius a [22]. The numerical results from ADS and the immittance functions are shown in Table 1.

Table 1 shows that very good agreement exists between the measurements and numerical results from the spectral domain immittance functions and ADS. In fact, all simulations and measurement values were within one-half of a percent. These measurements illustrate that the immittance functions are accurately calculating various properties of the printed dipole and that ADS can be used as a good tool to validate the results from the immittance functions. From this point on, ADS will be used exclusively to validate the isotropic results from the immittance funcitons.

5.2. Numerical Results of a Single Printed Dipole On a Single Anisotropic Layer

The next problem evaluated by the spectral domain immittance functions was the printed dipole on the anisotropic substrate shown in Figure 32. In particular, the resonant frequency and input impedance were determined for various values of substrate thickness d_1 and anisotropic ratios. The values computed by the spectral

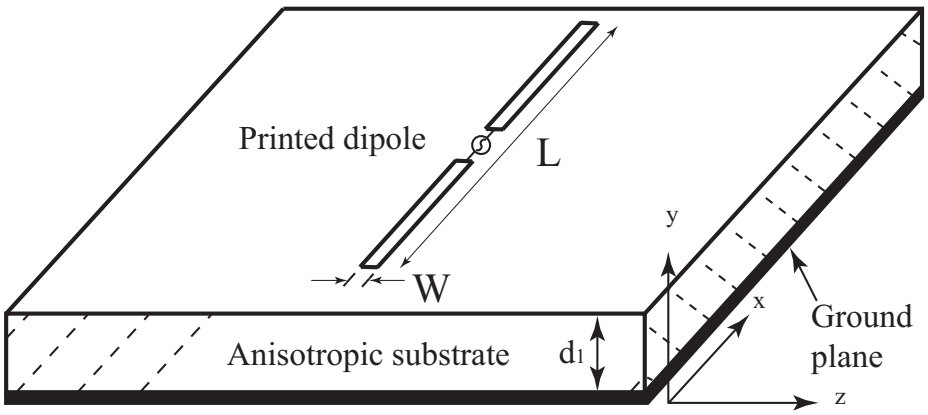

Figure 32. A printed dipole on a single anisotropic substrate.

domain immittance functions were compared to computations by ADS and published literature.

In the first problem, the dipole in Figure 32 was defined to have a length of 15 cm, a width of 0.5 mm and driven at the center with a delta source. The thickness d_1 was set at 1.58 mm and an isotropic substrate with a permittivity of ε_1 was defined. This intermediate isotropic case was computed first because the results from the immittance functions could be compared to ADS for accuracy. Figure 33 shows the resonant frequency of the dipole as ε_1 was increased from 1 to 13. The results from the immittance functions are compared to the results from ADS and good agreement was shown to exist. The resistance at resonance is shown in Figure 34 and good agreement between the immittance functions and ADS exists. This shows that the values calculated by the immittance functions are accurate for isotropic substrates. The next problem investigated the resonant frequency of the printed dipole in Figure 32 as the depth of the substrate was varied. The results are shown in Figure 35 for various values of ε_1. Again, it can be seen that good agreement exists between ADS and the immittance functions.

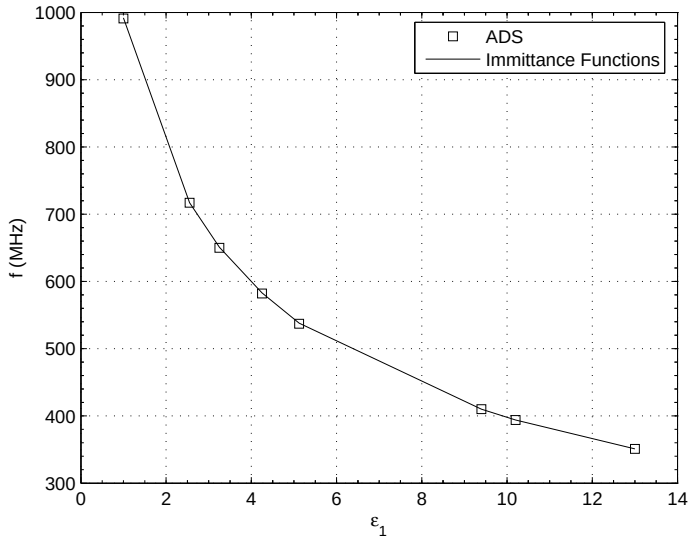

Figure 33. Resonant frequency of a printed dipole on a single isotropic substrate for various values of ε_1, L = 15 cm, W = 0.5 mm and d_1 = 1.58 mm.

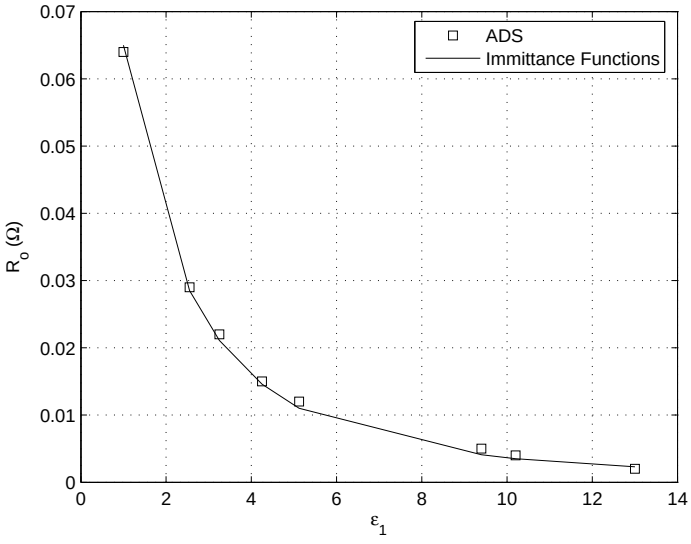

Figure 34. Resistance at resonance of a printed dipole on a single isotropic substrate for various values of ε_1, L = 15 cm, W = 0.5 mm and d_1 = 1.58 mm.

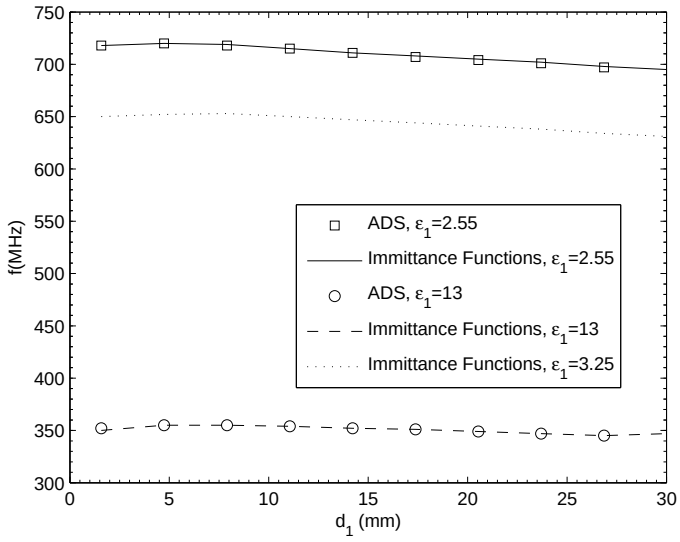

Figure 35. Resonant frequency of a printed dipole on a single isotropic substrate for various values of d_1, L = 15 cm and W = 0.5 mm.

Next, an anisotropic substrate was defined below the dipole. This time the anisotropy ratio was varied in both directions while the thickness was set at 1.58 mm. First, ε_{y1} was varied while ε_{x1} was set at $\varepsilon_{x1} = 2.55$. Then ε_{x1} was varied while ε_{y1} was set at $\varepsilon_{y1} = 2.55$. The results for these sweeps are shown in Figures 36 and 37. It can be seen in both figures that the isotropic case corresponds well with the results from ADS. Also note that the resonant frequency shown in Figure 37 was plotted with respect to the anisotropy ratio $n = \sqrt{\varepsilon_x/\varepsilon_y}$. Finally, an anisotropic substrate of boron nitride, sapphire and Epsilam-10 was defined and the resonant frequency of the dipole was calculated as the thickness of the substrate was increased. The results are shown in Figure 38.

The next problem reproduced the results by Rana and Alexopoulos [28]. Rana and Alexopoulos calculate the input impedance for various lengths of a printed dipole with an isotropic substrate. Instead of the printed dipole defined in Figure 32, Rana and Alexopoulos defined a thin-wire dipole with radius a = $0.0001\lambda_0$ on an isotropic

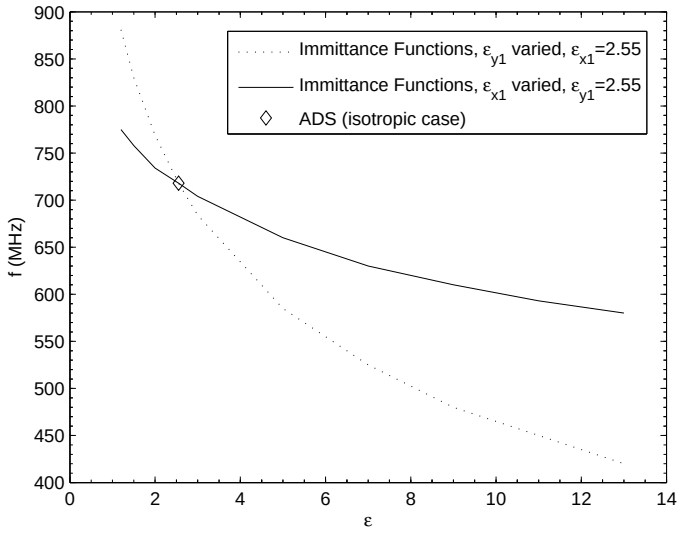

Figure 36. Resonant frequency of a printed dipole on a single anisotropic substrate for various values of $[\varepsilon_1]$, L = 15 cm, W = 0.5 mm and $d_1 = 1.58$ mm.

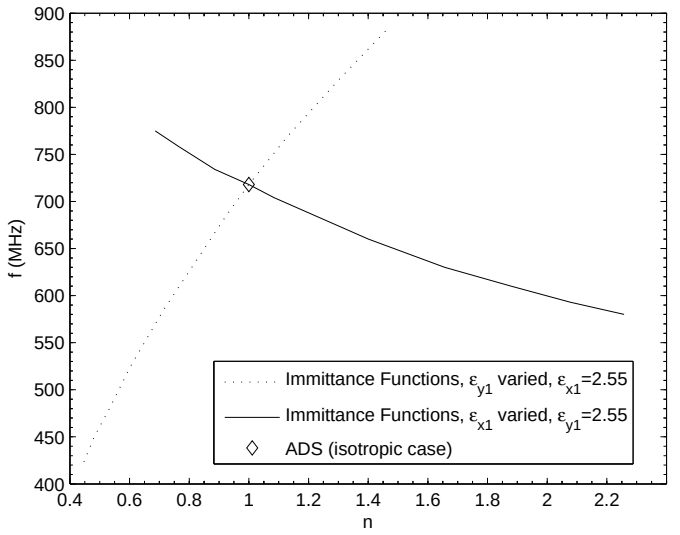

Figure 37. Resonant frequency of a printed dipole on a single anisotropic substrate for various values of n, L = 15 cm, W = 0.5 mm and $d_1 = 1.58$ mm.

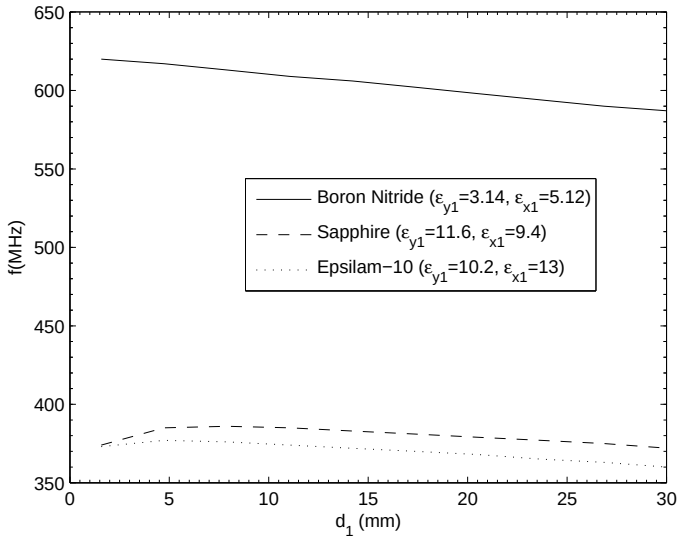

Figure 38. Resonant frequency of a printed dipole on boron nitride, sapphire and Epsilam-10 for various values of d_1, L = 15 cm and W = 0.5 mm.

substrate with thickness $d_1 = 0.1016\ \lambda_0$. An equivalent problem of a flat printed dipole with the same length and width $W = 4a$ was defined to be evaluated by the immittance functions. The results computed by the immittance functions are compared to the results by Rana and Alexopoulos and ADS for the isotropic case in Figures 39 and 40 followed by the convergence plot in Figure 41. The value of $[\varepsilon_1]$ was also changed and the input impedance was calculated. This is also shown in Figures 39 and 40. Good agreement exists between the computations by the immittance functions and published results by Rana and Alexopoulos. A convergence plot is also shown in Figure 41 to ensure that the results in Figures 39 and 40 converged. The code for the previous computations is shown in Appendix E.

It can be seen in Figures 33 and 36 that the resonant frequency significantly decreases as the value of permittivity is increased. For the anisotropic case, the resonant frequency was reduced by either 461 MHz or 195 MHz, depending on the

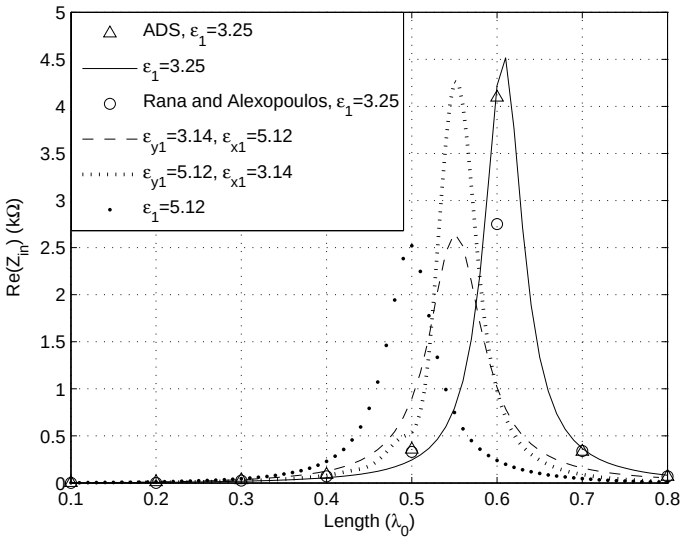

Figure 39. Input resistance for a printed dipole on an anisotropic substrate for various values of $[\varepsilon_1]$, d_1 = $0.1016\lambda_0$, W = 4a and a = $0.0001\lambda_0$.

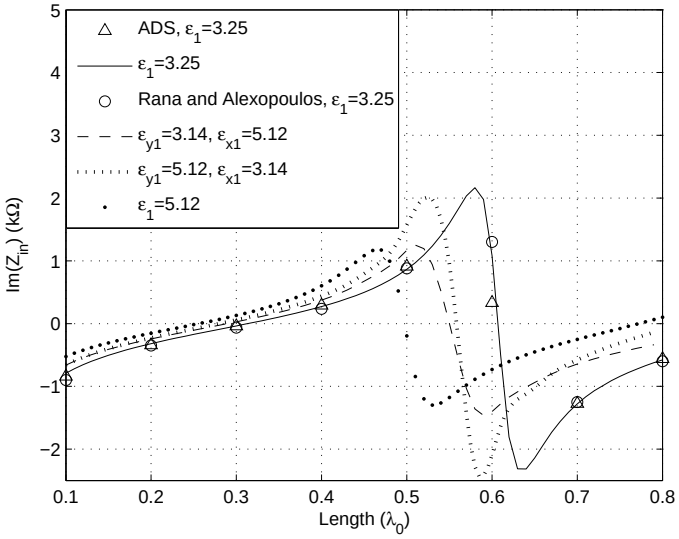

Figure 40. Input reactance for a printed dipole on an anisotropic substrate for various values of $[\varepsilon_1]$, d_1 = $0.1016\lambda_0$, W = 4a and a = $0.0001\lambda_0$.

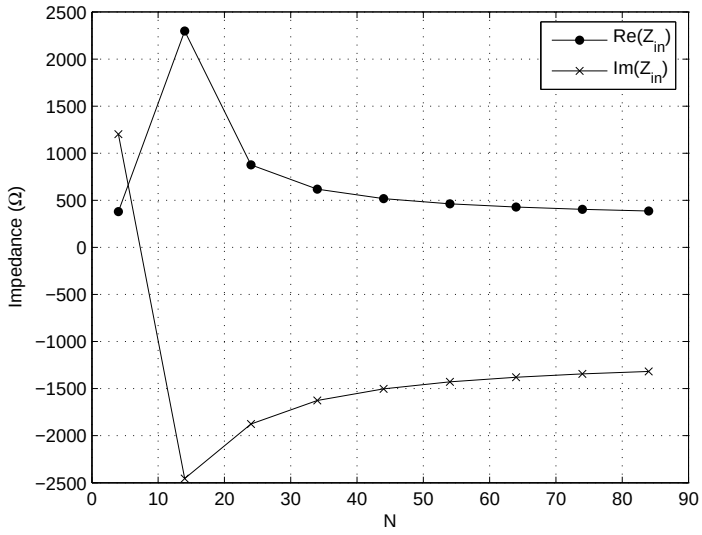

Figure 41. Input impedance convergence for a $0.7\lambda_0$ dipole on an isotropic substrate with $\varepsilon_1 = 3.25$, $d_1 = 0.1016\lambda_0$, W = 4a and a = $0.0001\lambda_0$.

changing variable. It is shown in Figure 36 that the resonant frequency was mostly affected by the y-component of $[\varepsilon_1]$. This is because, for substrates of this thickness, only the dominant TM_0 mode with a field component in the y-direction is present [12].

It is shown in Figures 35 and 38 that the thickness of the substrate has little effect on the resonant frequency. Thus it is believed that ε_{y1} is not effectively increasing the substrate thickness but causing the printed dipole to resonate at half of a wavelength of the wave *in* the material and not the free-space wavelength. For example, in Figure 33 the dipole resonates at 991 MHz for $\varepsilon_1 = 1$. A frequency of 991 MHz has a free-space wavelength of 30.2 cm and the dipole length was 15 cm, about half of the free-space wavelength. For $\varepsilon_1 = 10.2$ the dipole resonated at 394 MHz. A frequency of 394 MHz has a free-space wavelength of 76.1 cm and a wavelength of 76.1 cm/$\sqrt{10.2}$ = 23.8 cm in the material. This frequency has a half-wavelength of 11.9

cm in the material, which was close to the length of the dipole. Also, it is believed that the x- and z-components of $[\varepsilon_1]$ were increasing the edge effect of the printed dipole and thus have much less of an effect on the resonant frequency of the dipole. Similar effects are shown in Figures 39 and 40. It is shown that the dipole resonates at a lower frequency for the case where $\varepsilon_1 = 5.12$ and the case where $\varepsilon_{y1} = 5.12$ and $\varepsilon_{x1} = 3.14$. These values correspond to the permittivity in the direction of the optical axis and the TM_0 mode.

5.3. Numerical Results for the Mutual Coupling Between Two Printed Dipoles On a Single Anisotropic Layer

The next problem was an investigation of the mutual coupling between two printed dipoles using the newly derived spectral domain immittance functions from Chapter 3. The problem in Figure 42 was used to calculate the mutual coupling between these printed dipoles. The problem consisted of two printed dipoles of length L and width W on a grounded anisotropic substrate. The separation between the dipoles along the z- and x-axis was represented by the variables S and G, respectively. Expression (3.85) was used to solve for the unknown currents and the mutual coupling between the printed dipoles.

The mutual coupling between the two printed dipoles was calculated for various values of S, G, d_1 and $[\varepsilon_1]$. Several different expressions are used in literature to represent the mutual coupling between printed antennas. Authors use $20\log(|Z_{12}|^2)$, $20\log(|S_{12}|^2)$, $\log(|Z_{12}|)$ or $|I_2|/|I_1|$ [12], [44], [88]. Each expression represents mutual coupling in its own manner with no apparent advantage of one particular expression over another. For the work presented here the mutual coupling was calculated as $20\log(|Z_{12}|^2)$ where Z_{12} was the mutual impedance between the two printed dipoles. Z_{12} was calculated by computing the input impedance Z_{oc} of the driven dipole with the second dipole removed and computing the input impedance Z_{sc} of the driven

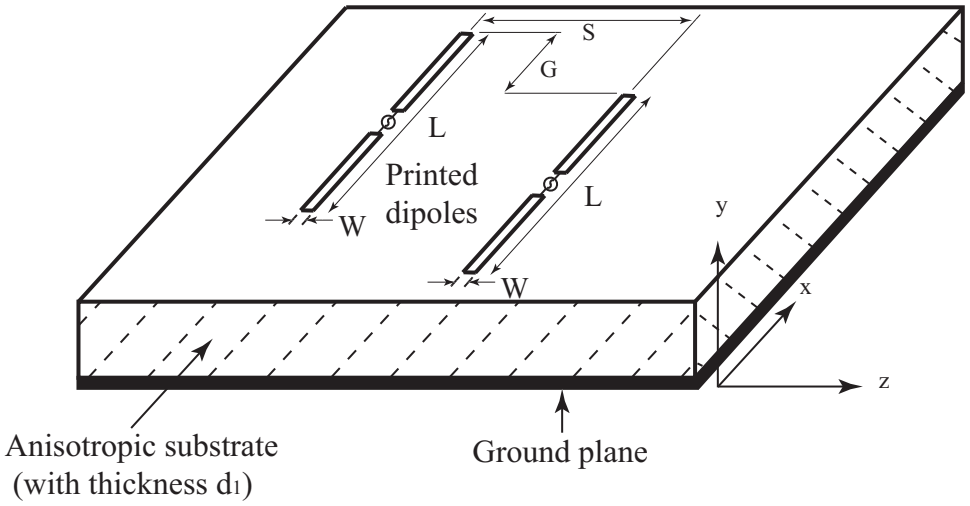

Figure 42. Expanded view of two printed dipoles with an anisotropic substrate.

dipole with the second dipole in place with a short-circuited port. Then Z_{12} was calculated by using [22]

$$Z_{12} = \sqrt{Z_{oc}(Z_{oc} - Z_{sc})}. \tag{5.1}$$

In the first configurations the substrate was set at 1.58 mm and the anisotropy ratio was varied. Each dipole had a length of 15 cm, a width of 0.5 mm and a source frequency of 500MHz. The separation between the dipoles was then varied for the broadside, collinear and echelon configurations. An example of these three configurations is shown in Figure 43.

The mutual coupling between the printed dipoles can be seen in Figures 44, 45 and 46. Figure 44 shows the mutual coupling between two broadside printed dipoles. The value of S was varied from 2 mm to 30 mm with $G = 0$ and good agreement with ADS is shown. Figure 45 shows the mutual coupling for the collinear orientations. The value of G was varied from 152 mm to 350 mm with $S = 0$. Figure 46 shows the mutual coupling between two echelon printed dipoles. The value of S was set at 10 mm and G was varied from 0 to 200 mm.

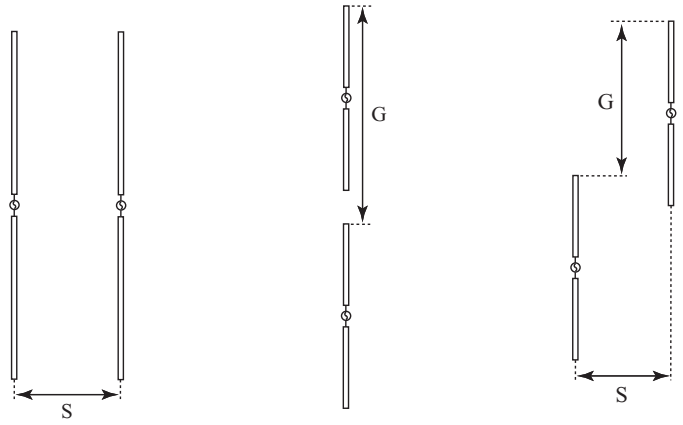

Figure 43. Broadside, collinear and echelon orientations.

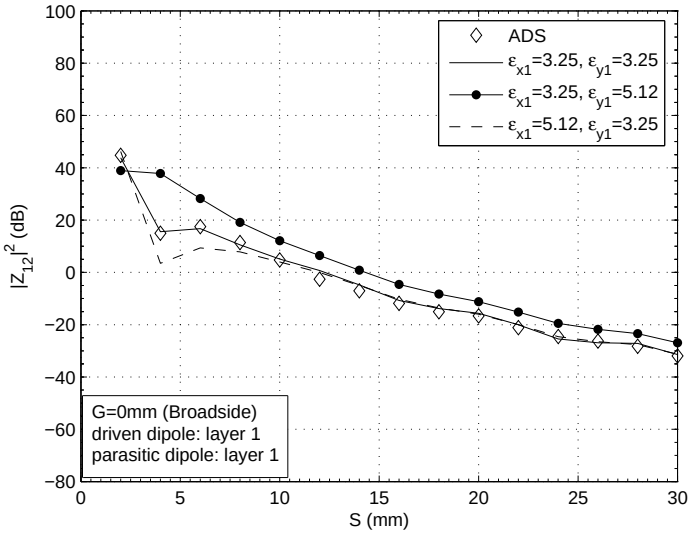

Figure 44. Mutual coupling between printed dipoles on an anisotropic substrate for various values of $[\varepsilon_1]$, L = 15 cm, W = 0.5 mm, f = 500 MHz and $d_1 = 1.58$ mm (broadside).

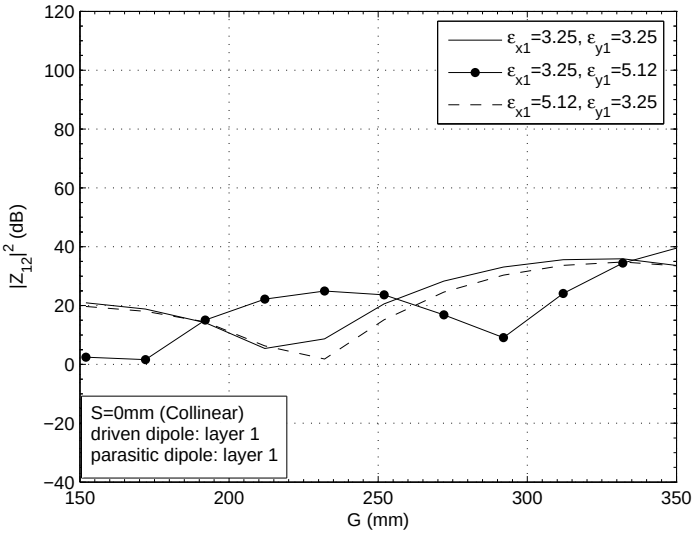

Figure 45. Mutual coupling between printed dipoles on an anisotropic substrate for various values of $[\varepsilon_1]$, L = 15 cm, W = 0.5 mm, f = 500 MHz and d_1 = 1.58 mm (collinear).

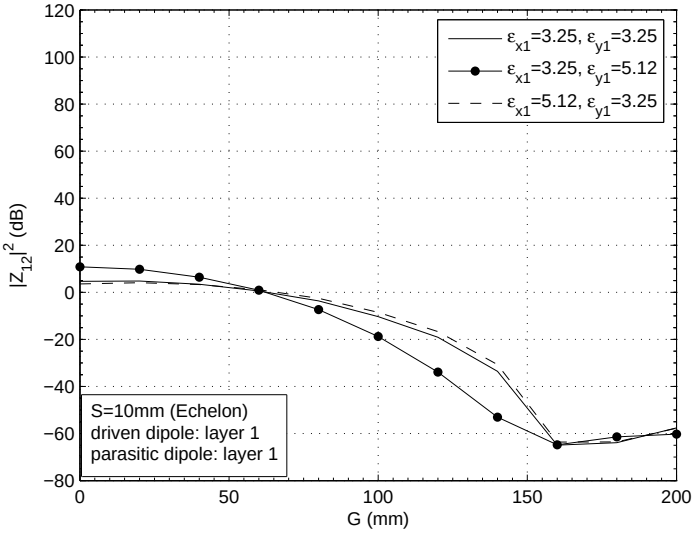

Figure 46. Mutual coupling between printed dipoles on an anisotropic substrate for various values of $[\varepsilon_1]$, L = 15 cm, W = 0.5 mm, f = 500 MHz and d_1 = 1.58 mm (echelon).

The next configuration set the values of $[\varepsilon_1]$ at $\varepsilon_{y1} = 5.12$ and $\varepsilon_{x1} = 3.25$ and the thickness of the substrate at 1.58 mm, 7.9 mm and 15.8 mm. The mutual coupling between the printed dipoles for these configurations can be seen in Figures 47, 48 and 49. Figure 47 shows the mutual coupling between two broadside printed dipoles. The value of S was varied from 2 mm to 30 mm with $G = 0$. Figure 48 shows the mutual coupling for the collinear orientations. The value of G was varied from 152 mm to 350 mm. Figure 49 shows the mutual coupling between two echelon printed dipoles. The value of S was set at 10 mm and G was varied from 0 to 200 mm.

The code for the mutual coupling computations is shown in Appendix F. The code was modified slightly to move the source and match points around the surface of the anisotropic substrate to represent the three configurations. Then different "for loops" were used to step through the appropriate spacing used in the computations.

It can be seen that the mutual coupling between the broadside dipoles in Figure 44 was increased for $\varepsilon_{x1} = 3.25$ and $\varepsilon_{y1} = 5.12$. This is because the TM_0 mode is the dominant mode in the substrate with no cutoff frequency. The TM_0 mode has a y-directed electric field component which corresponds to the direction of the optical axis and the larger $\varepsilon_{y1} = 5.12$ value. The large coupling is due to the surface wave being coupled to the substrate as a result of a larger value of permittivity in the direction of the optical axis. This coupling is also evident in the collinear and echelon configurations in Figures 45 and 46. The collinear results shown in Figure 45 show a growing mutual coupling as the dipoles move further apart. This is because in close proximity the coupling is mainly due to direct coupling (i.e., capacitive and inductive) between the elements [40]. Then as the dipoles move apart the quasi-periodic coupling due to the surface waves mainly contributes to the coupling. The greatest coupling for the echelon configuration occurs when the dipoles are broadside. Then, as the dipoles move apart, the mutual coupling reduces to a quasi-periodic nature. This

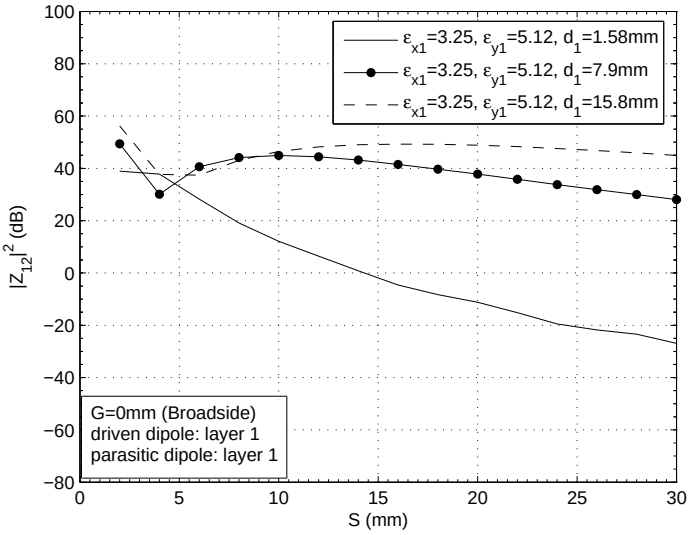

Figure 47. Mutual coupling between printed dipoles on an anisotropic substrate for various values of d_1, L = 15 cm, W = 0.5 mm and f = 500 MHz (broadside).

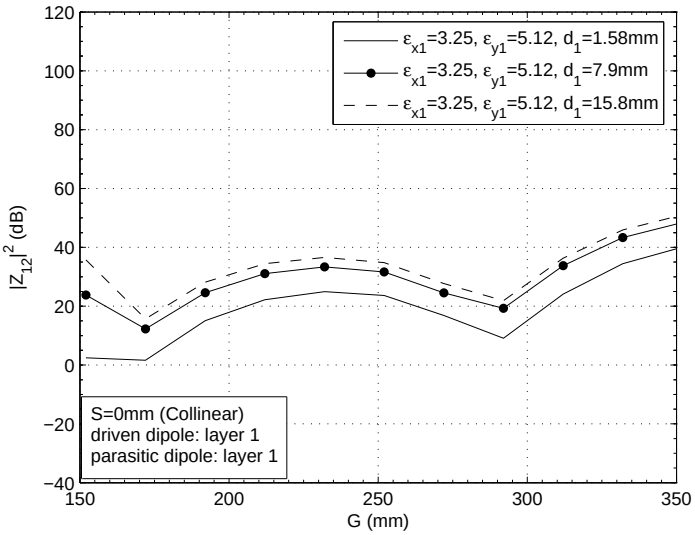

Figure 48. Mutual coupling between printed dipoles on an anisotropic substrate for various values of d_1, L = 15 cm, W = 0.5 mm and f = 500 MHz (collinear).

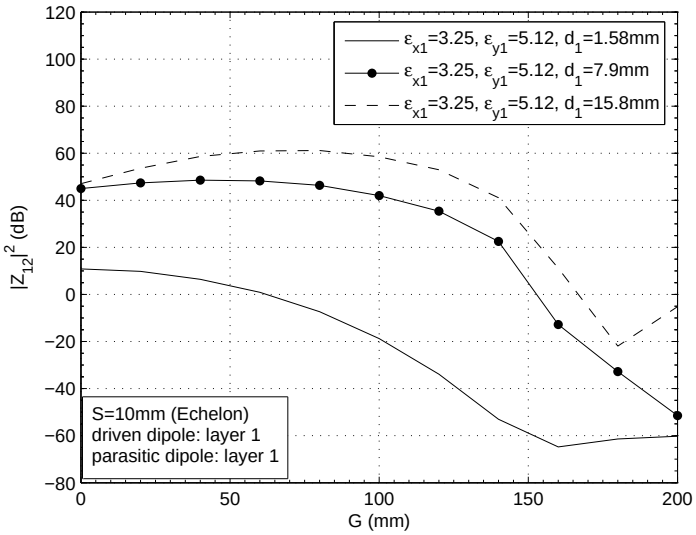

Figure 49. Mutual coupling between printed dipoles on an anisotropic substrate for various values of d_1, L = 15 cm, W = 0.5 mm and f = 500 MHz (echelon).

is due to the configuration moving from a broadside orientation to a collinear orientation. The increased coupling as a result of a larger substrate thickness is due to the increased surface wave modes and space waves. As the dipoles are separated from the ground plane as a result of larger substrates, a stronger space and surface wave mode is launched. This results in more power being radiated and more effect on parasitic elements in proximity to the dipoles.

5.4. Numerical Results of a Single Printed Dipole In Two Anisotropic Layers

In this section the resonant length and input impedance was computed for a printed dipole in two anisotropic layers. The expanded view of the two-layer anisotropic structure is shown in Figure 50.

Again, the printed dipole was defined to have a length of 15 cm and a width W of 0.5 mm. Initially, an isotropic substrate and superstrate were defined around

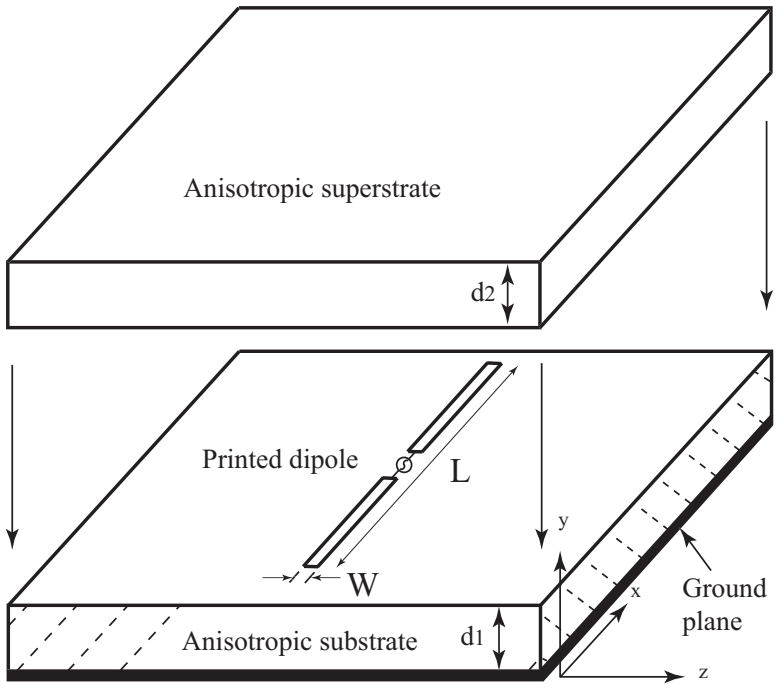

Figure 50. Expanded view of a printed dipole in two layers of anisotropic material.

the antenna in Figure 50. This isotropic case was investigated first because the immittance functions could then be compared to results from ADS for further validation. The first example sets the depth of the substrate and superstrate at $d_1 = 1.58$ mm and $d_2 = 1.58$ mm, respectively. Figures 51 and 52 show the resonant frequency and resonant resistance, respectively, for various substrate and superstrate permittivities. For the bottom curves, $\varepsilon_1 = 9.4$ and ε_2 was varied and, for the top curves, $\varepsilon_1 = 2.55$ and ε_2 was varied. It is shown that good agreement exists between the values computed by the immittance functions and ADS.

In the next problem an anisotropic superstrate was located over an isotropic substrate with $\varepsilon_1 = 2.55$ and $d_1 = d_2 = 1.58$ mm. The dipole was placed between the two regions, and ε_{y2} and ε_{x2} were varied in the superstrate. The printed dipole length and width remained at 15 cm and 0.5 mm, respectively. The computed resonant

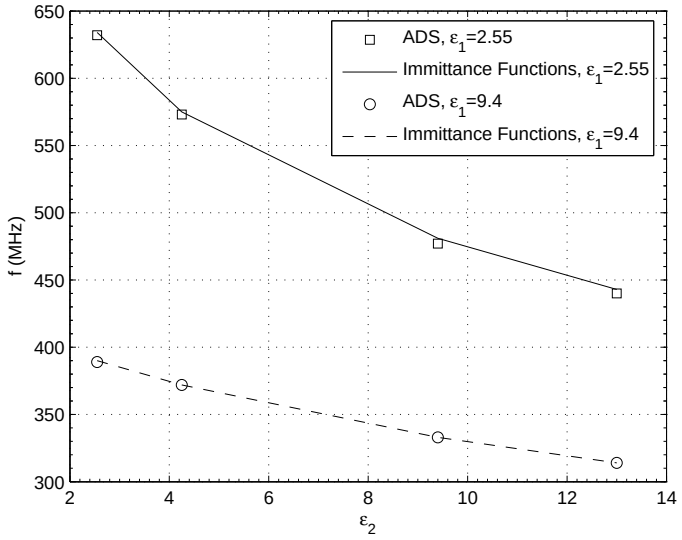

Figure 51. Resonant frequency of a printed dipole in two isotropic layers for various values of ε_1, various values of ε_2, L = 15 cm, W = 0.5 mm and $d_1 = d_2 =$ 1.58 mm.

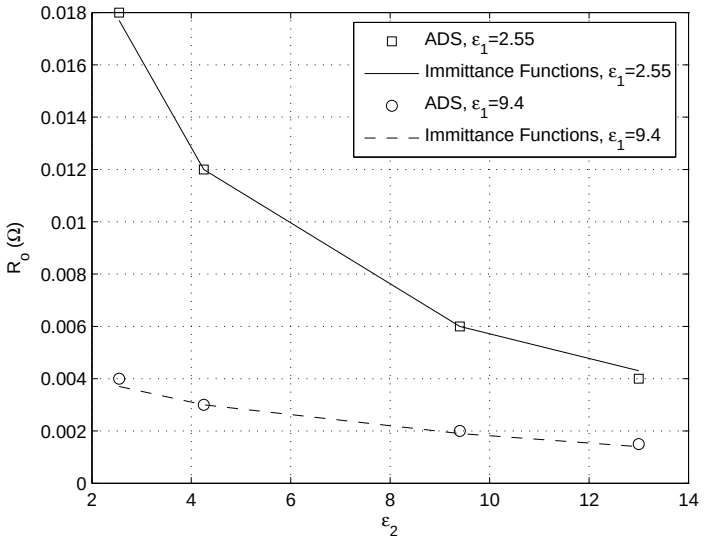

Figure 52. Resistance at resonance of a printed dipole in two isotropic layers for various values of ε_1, various values of ε_2, L = 15 cm, W = 0.5 mm and $d_1 = d_2 =$ 1.58 mm.

frequency for the dipole is shown in Figure 53. It can be seen in Figure 53 that the isotopic case agrees well with the results from ADS. The next problem computed the resonant length of the dipole for an increasing superstrate thickness. First, an isotropic substrate and superstrate were defined. Again, the substrate had a thickness of $d_1 = 1.58$ mm and $\varepsilon_1 = 2.55$. The superstrate had a thickness that varied from 1.58 mm to 30.02 mm. The computed resonant frequency for various values of ε_2 are shown in Figure 54 with good agreement with ADS. Finally, the superstrate was replaced by anisotropic materials of boron nitride ($\varepsilon_{x2} = 5.12$ and $\varepsilon_{y2} = 3.14$), sapphire ($\varepsilon_{x2} = 9.4$ and $\varepsilon_{y2} = 11.6$) and Epsilam-10 ($\varepsilon_{x2} = 13$ and $\varepsilon_{y2} = 10.2$). The thickness of the superstrate was increased and the resonant frequency was calculated. The results are shown in Figure 55 for $\varepsilon_1 = 2.55$ and $d_1 = 1.58$ mm.

Next, the input impedance of the printed dipole was computed for various values of $[\varepsilon_2]$. For these computations the following dimensions were defined: $d_1 = d_2 = 1.58$ mm, L = 15 cm and W = 0.5 mm. Again, the isotropic case was compared to ADS for accuracy. The computed results are shown in Figures 56 and 57 for $\varepsilon_1 = 3.25$ and $\varepsilon_2 = 5.12$. It is shown that the real part of the input impedance is fairly well behaved up to the region between 1 GHz and 1.1 GHz. At this point the resistance increases to an extremely large value. Also, it can be seen in Figure 57 that the reactance is also very dynamic between 1 GHz and 1.1 GHz. These results are similar to the results of Monferrer and Kishk [89]. Fortunately, the region of interest is around the resonant frequency. This region is much more well behaved and outlined in Figure 57. In both figures it is shown that the results from ADS and the immittance functions are in good agreement. Next, the anisotropy ratio of the superstrate was changed and the input impedance around the resonant frequency was computed for all cases with $\varepsilon_1 = 3.25$ and $d_1 = d_2 = 1.58$ mm. The results from these computations are shown in Figures 58 and 59.

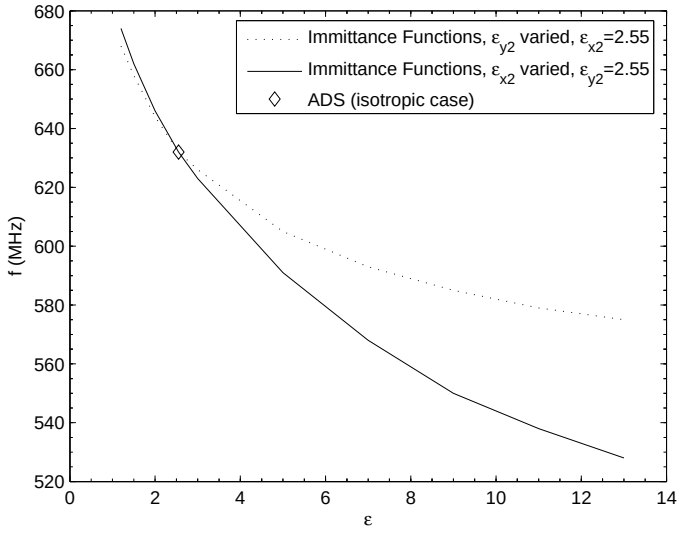

Figure 53. Resonant frequency of a printed dipole with an anisotropic superstrate for various values of ε_{x2}, various values of ε_{y2}, $\varepsilon_1 = 2.55$, L = 15 cm, W = 0.5 mm and $d_1 = d_2 = 1.58$ mm.

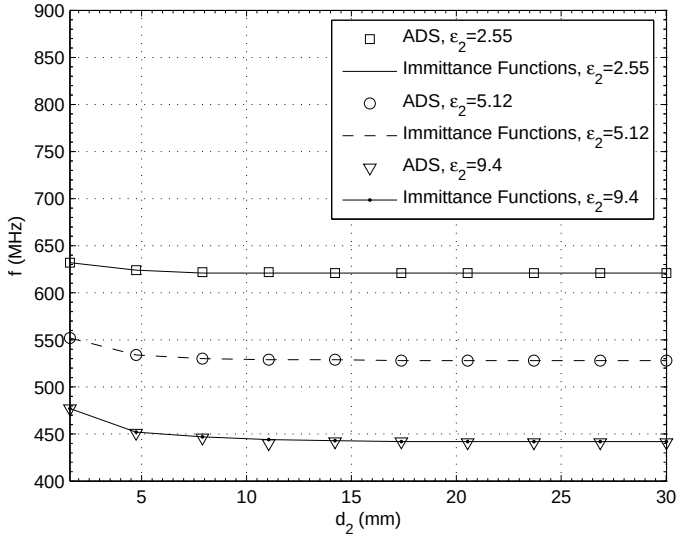

Figure 54. Resonant frequency of a printed dipole in two isotropic layers for various values of ε_2, various values of d_2, $\varepsilon_1 = 2.55$, L = 15 cm, W = 0.5 mm and $d_1 = 1.58$ mm.

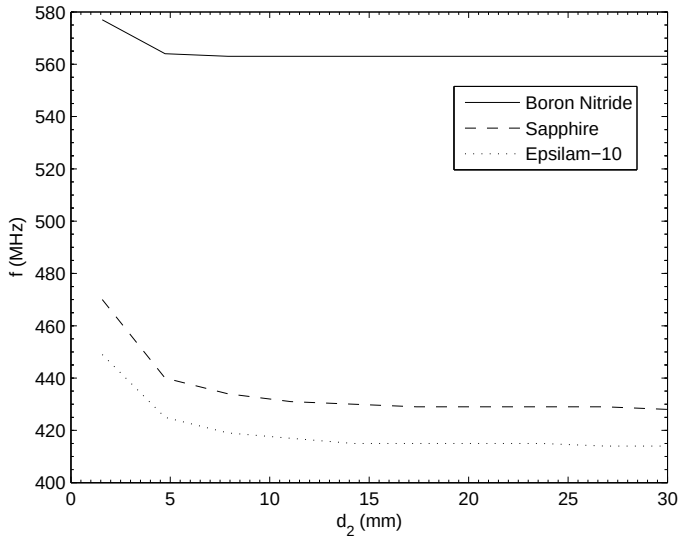

Figure 55. Resonant frequency of a printed dipole with an anisotropic superstrate for various values of d_2, $\varepsilon_1 = 2.55$, L = 15 cm, W = 0.5 mm and $d_1 = 1.58$ mm.

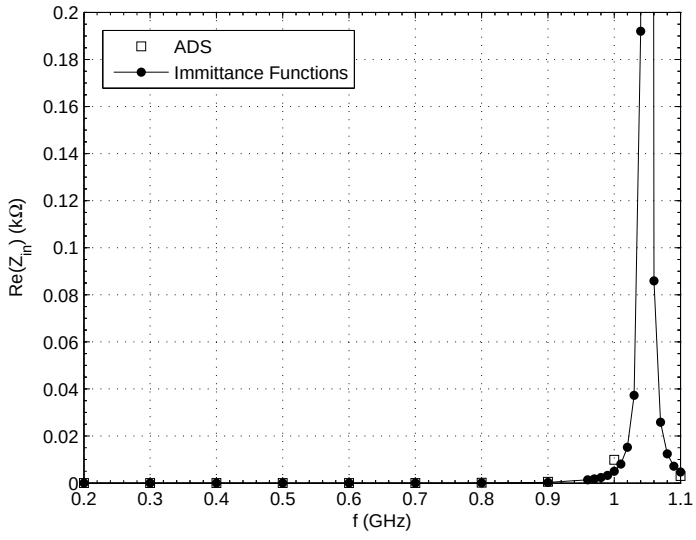

Figure 56. Input resistance of a printed dipole in two isotropic layers for $\varepsilon_1 = 3.25$, $\varepsilon_2 = 5.12$, L = 15 cm, W = 0.5 mm and $d_1 = d_2 = 1.58$ mm.

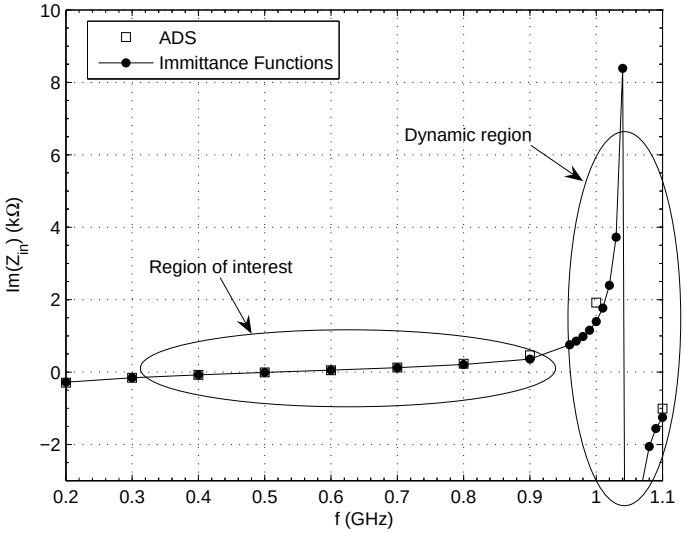

Figure 57. Input reactance of a printed dipole in two isotropic layers for $\varepsilon_1 = 3.25$, $\varepsilon_2 = 5.12$, L = 15 cm, W = 0.5 mm and $d_1 = d_2 = 1.58$ mm.

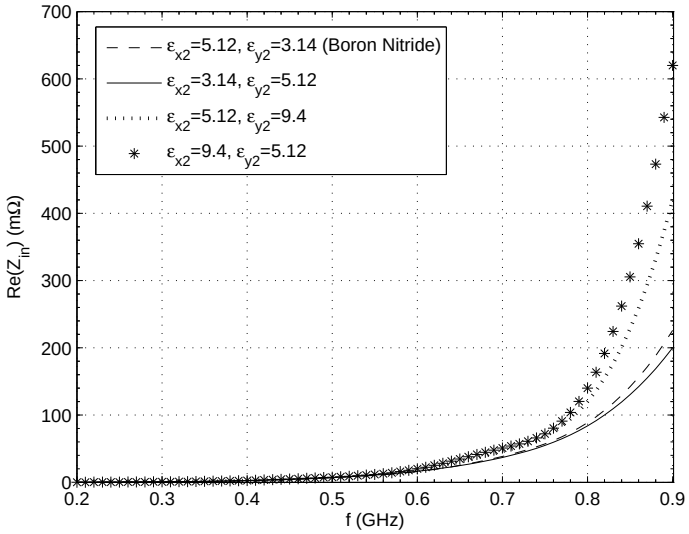

Figure 58. Input resistance of a printed dipole with an anisotropic superstrate for various values of $[\varepsilon_2]$, ε_1 = 3.25, L = 15 cm, W = 0.5 mm and $d_1 = d_2 = 1.58$ mm.

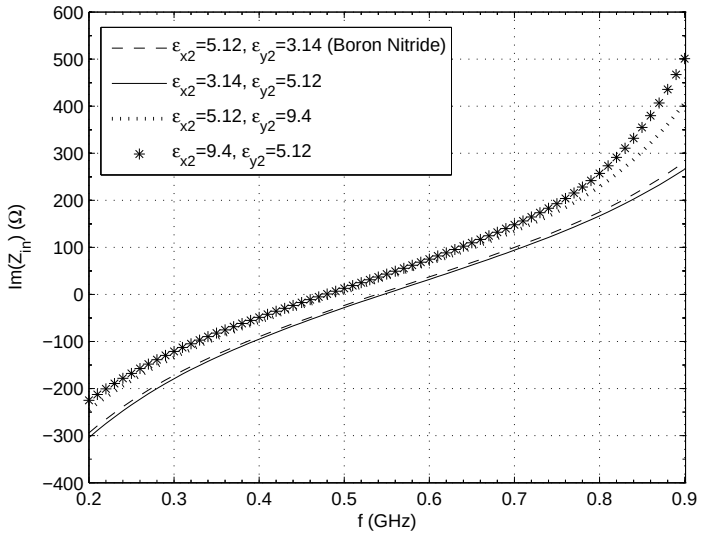

Figure 59. Input reactance of a printed dipole with an anisotropic superstrate for various values of $[\varepsilon_2]$, $\varepsilon_1 = 3.25$, L = 15 cm, W = 0.5 mm and $d_1 = d_2 = 1.58$ mm.

The code for all the previous results is shown in Appendix G. The code was modified appropriately to search for the resonant frequency and compute the input impedance for the appropriate layer properties.

It is clear from the previous figures that the immittance functions and ADS results compare very well. It can be seen in Figure 53 that the effect that layer 2 has on the resonant frequency of the dipole has to do with the space waves and surface waves launched from the dipole [28]. For a layer thickness of 1.58 mm it can be assumed that only the TM_0 mode is present as a surface mode. For this case the electric field has the strongest component along the axis of the dipole with a component of the electric field orthogonal to the direction of propagation in a position broadside to the dipole [28] . In all these cases the electric field has a component in the x-z plane (Figure 60) which corresponds to the greater impact ε_{x2} and ε_{z2} have on the resonant frequency and input impedance, and not ε_{y2}.

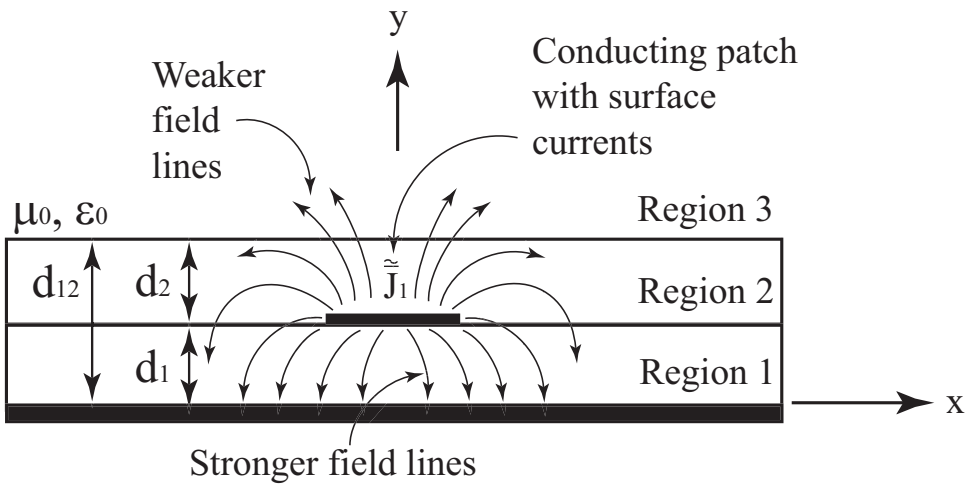

Figure 60. Field lines around a printed dipole.

The effects that the two layers have on the resonant frequency and input impedance of the dipole are very different. The field lines in Figure 60 that are directly below the printed dipole couple strongly to the ground plane. The fields above the dipole in region two are mostly responsible for launching the space (radiation) and surface waves. These fields along the boundary between regions 1 and 2 have components in the x-z plane. This corresponds to the effects that ε_{x2} and ε_{z2} have on the resonant frequency. As mentioned before, the fields immediately below the printed dipole have a component in the y-direction which correspond to the direction of the optical axis. This is why the value of ε_{y1} significantly impacts the results in the previous single layer results. When the results in Figure 36 are compared to the results in Figure 53, it can be seen that the permittivity in the direction of the optical axis has a much more significant impact on the resonant frequency than the permittivity in the direction orthogonal to the optical axis. This is believed to be a result of the stronger fields that are present below the printed dipole. These strong fields are related to the currents on the printed dipole and hence on both the input impedance and resonant frequency.

5.5. Numerical Results for the Mutual Coupling Between Two Printed Dipoles In Two Anisotropic Layers

In the next problem, the mutual coupling between the printed dipoles in Figures 61 and 62 was calculated. In Figure 61 the two dipoles are both located on the top of layer 1, and, in Figure 62, one dipole was on the top of layer 1, and the other dipole was on the top of layer 2. In both cases the dipoles were separated by a distance S and shifted from the broadside orientation by a distance G. The problem in Figure 61 studied how the superstrate values of $[\varepsilon_2]$ and layer thickness effected the mutual coupling between two printed dipoles on the same layer. The problem in Figure 62 placed an anisotropic layer between the two printed dipoles and studied how $[\varepsilon_2]$ effected the mutual coupling between the printed dipoles.

The problem in Figure 62 was computed first. Both layer thicknesses were set at 1.58 mm and several values were chosen for $[\varepsilon_2]$. The length of each dipole was set at 15 cm, the width of each dipole was set at 0.5 mm and the source frequency was 500 MHz. The distances S and G were varied and the substrate permittivity was $\varepsilon_1 = 3.25$. The mutual coupling between the dipoles for the broadside case ($G = 0$) is shown in Figure 63. As a check, the mutual coupling between the printed dipoles was calculated by ADS. It is shown in Figure 63 that good agreement exists between the immittance functions and ADS for the isotropic results. The next problem placed the dipoles in Figure 62 in a collinear arrangement (i.e., $S = 0$), and the value of G was varied. The dipoles were directly above and below each other for $G = 0$, and the top dipole moved along the x-axis as G was increased to 200 mm. The mutual coupling results are shown in Figure 64. It is shown that the isotropic results agree very well with ADS. Next, the dipoles in Figure 62 were placed in an echelon arrangement. The value of S was set at $S = 10$ mm and G was varied. The mutual coupling results are shown in Figure 65.

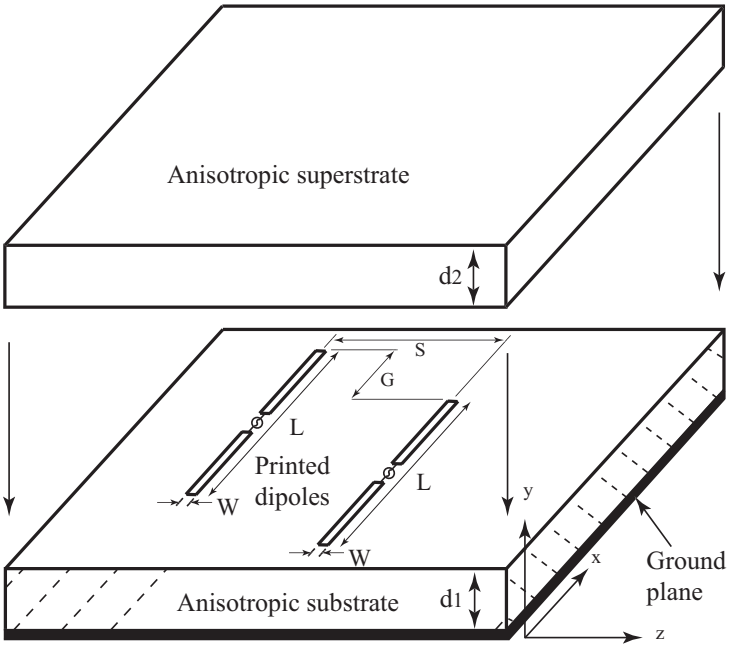

Figure 61. Expanded view of two printed dipoles with an anisotropic superstrate.

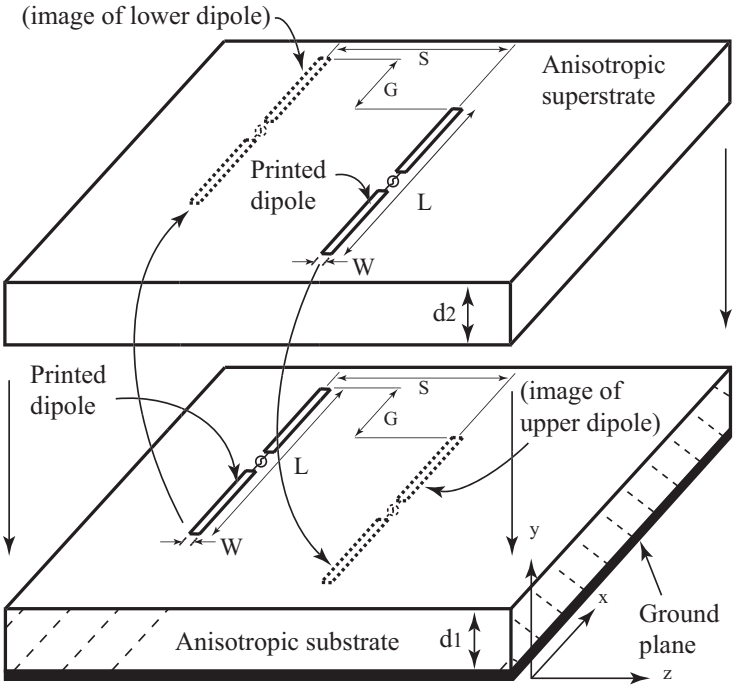

Figure 62. Expanded view of two printed dipoles separated by a layer of anisotropic material.

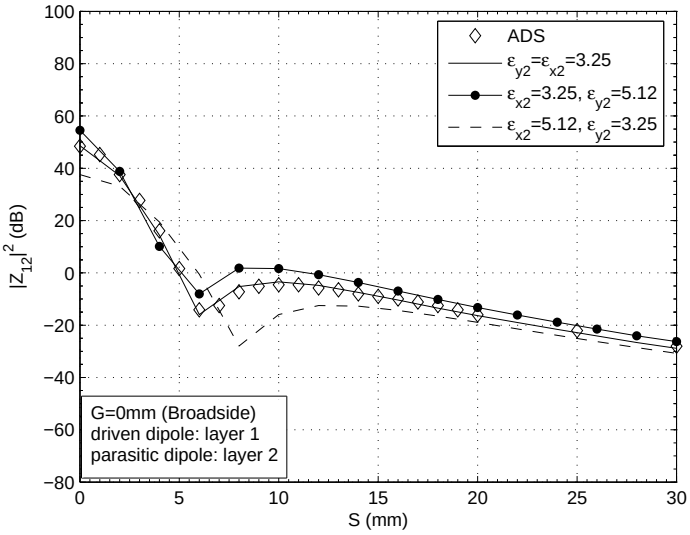

Figure 63. Mutual coupling between printed dipoles separated by an anisotropic layer for various values of $[\varepsilon_2]$, $\varepsilon_1 = 3.25$, L = 15 cm, W = 0.5 mm, f = 500 MHz and $d_1 = d_2 = 1.58$ mm (broadside).

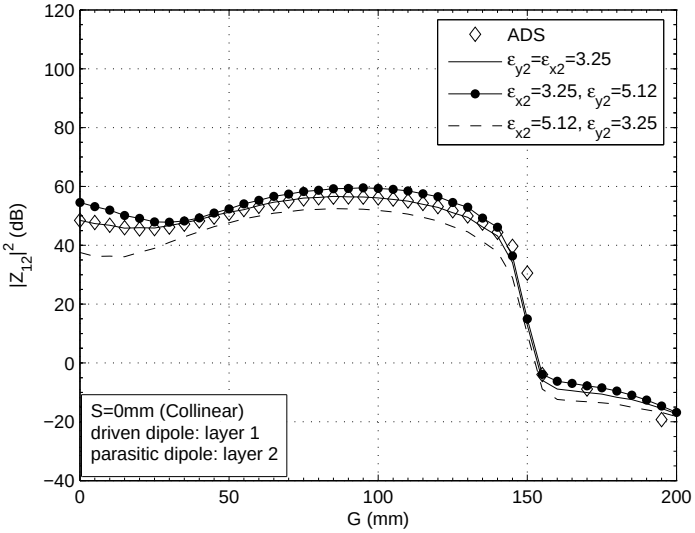

Figure 64. Mutual coupling between printed dipoles separated by an anisotropic layer for various values of $[\varepsilon_2]$, $\varepsilon_1 = 3.25$, L = 15 cm, W = 0.5 mm, f = 500 MHz and $d_1 = d_2 = 1.58$ mm (collinear).

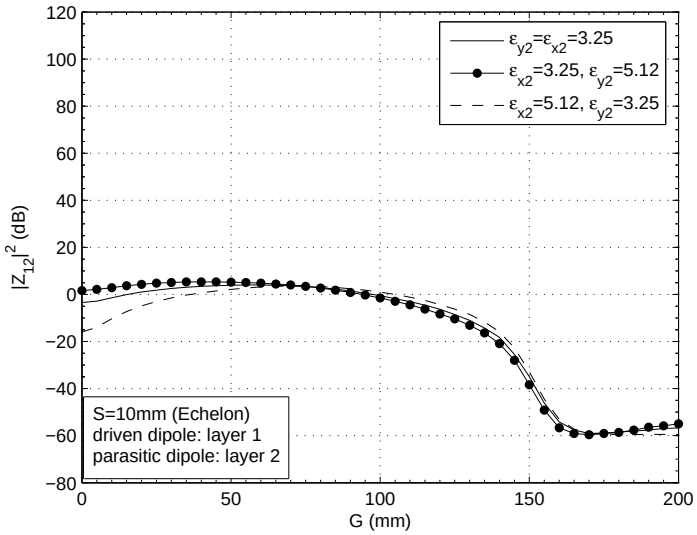

Figure 65. Mutual coupling between printed dipoles separated by an anisotropic layer for various values of $[\varepsilon_2]$, $\varepsilon_1 = 3.25$, L = 15 cm, W = 0.5 mm, f = 500 MHz and $d_1 = d_2 = 1.58$ mm (echelon).

The results in Figures 63 and 64 validate the immittance functions in a very thorough manner. This is because both immittance functions are included in the calculations for the first time. By comparing the numerical results to ADS it is shown that both the immittance functions are correct and can be used to calculate problems that contain antennas on different layers.

The problem in Figure 61 was computed next. The length of each dipole was set again at 15 cm, the width of each dipole was set again at 0.5 mm and the source frequency was 500 MHz. The thickness of the substrate was set at 1.58 mm. Several values of $[\varepsilon_2]$ and d_2 were chosen and the distances S and G were varied. The substrate permittivity was $\varepsilon_1 = 3.25$. The mutual coupling between the dipoles for the broadside case ($G = 0$) can be seen in Figure 66. S was increased from 2 mm to 30 mm and d_2 was set at 1.58 mm. The next problem set the superstrate permittivity at $\varepsilon_{x2} = 3.25$ and $\varepsilon_{y2} = 5.12$ while d_2 was defined at 1.58 mm, 7.9 mm

and 15.8 mm. Again, S was varied from 2 mm to 30 mm. The mutual coupling between the printed dipoles is shown in Figure 67. Next, the dipoles were placed in a collinear orientation ($S = 0$) and the value of G was varied from 152 mm to 350 mm. Initially, d_2 was set at 1.58 mm and $[\varepsilon_2]$ was varied. The mutual coupling results for this configuration are shown in Figure 68. Next, the superstrate permittivity was set at $\varepsilon_{x2} = 3.25, \varepsilon_{y2} = 5.12$ and the thickness of d_2 was defined at 1.58 mm, 7.9 mm and 15.8 mm. The results from these computations are shown in Figure 69. Finally, the dipoles were placed in an echelon orientation with $S = 10$ mm. The value of G was varied from 0 to 200 mm. Initially, d_2 was set at 1.58 mm and $[\varepsilon_2]$ was varied. The mutual coupling results for this configuration are shown in Figure 70. Next, the superstrate permittivity was set at $\varepsilon_{x2} = 3.25, \varepsilon_{y2} = 5.12$ and the thickness of d_2 was defined at 1.58 mm, 7.9 mm and 15.8 mm. The results are shown in Figure 71.

The code for the mutual coupling computations is shown in Appendix H. Again, the code was modified to move the source and match points around the surfaces.

The results in this section look at the effects a second anisotropic layer has on the mutual coupling between two printed antennas. In the first case the two printed dipoles were separated by an anisotropic layer. Looking at this problem resulted in two important results relating to mutual coupling. The first is illustrated in Figures 63-65. For $\varepsilon_{x2} = 3.25$ and $\varepsilon_{y2} = 5.12$ the mutual coupling is generally increased over all the orientations. This is believed to be a result of the $\varepsilon_{y2} = 5.12$ value in the layer below the dipole on the top of layer 2. By increasing ε_{y2} the TM_0 mode is coupled more strongly to the substrate by the dipole on the top of layer 2 and hence increases the mutual coupling. The second important result shows that the second anisotropic layer can be used to isolate the two printed dipoles by increasing the permittivity in the direction orthogonal to the optical axis.

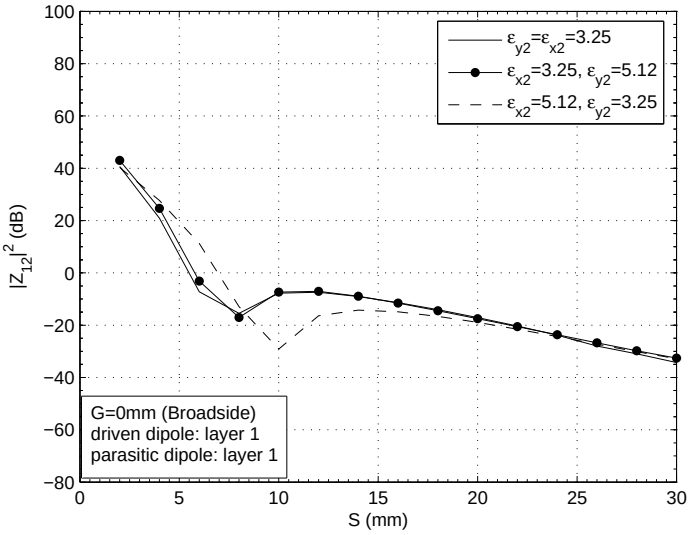

Figure 66. Mutual coupling between printed dipoles on the same anisotropic layer for various values of $[\varepsilon_2]$, $\varepsilon_1 = 3.25$, L = 15 cm, W = 0.5 mm, f = 500 MHz and $d_1 = d_2 = 1.58$ mm (broadside).

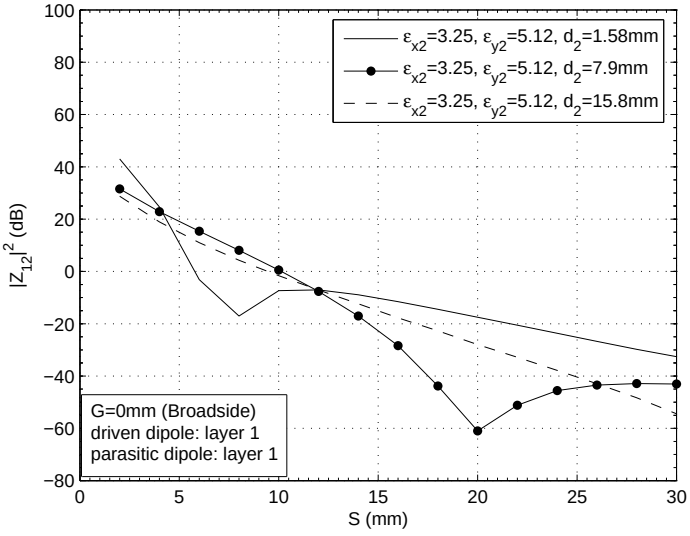

Figure 67. Mutual coupling between printed dipoles on the same anisotropic layer for various values of d_2, $\varepsilon_1 = 3.25$, L = 15 cm, W = 0.5 mm, f = 500 MHz and $d_1 = 1.58$ mm (broadside).

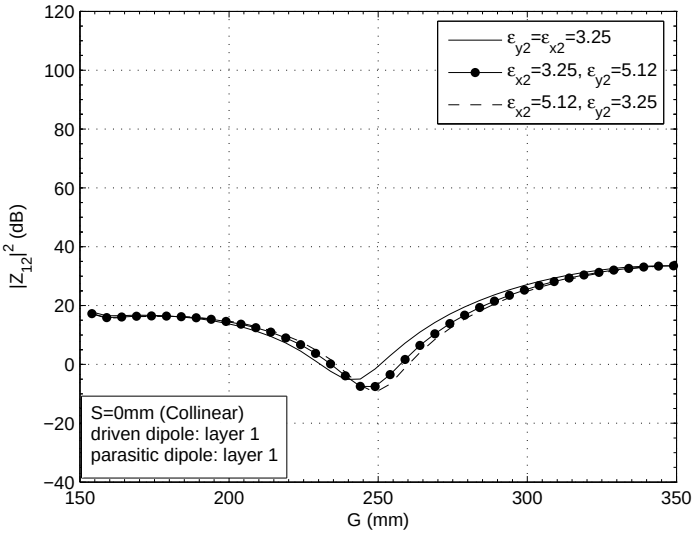

Figure 68. Mutual coupling between printed dipoles on the same anisotropic layer for various values of $[\varepsilon_2]$, $\varepsilon_1 = 3.25$, L = 15 cm, W = 0.5 mm, f = 500 MHz and $d_1 = d_2 = 1.58$ mm (collinear).

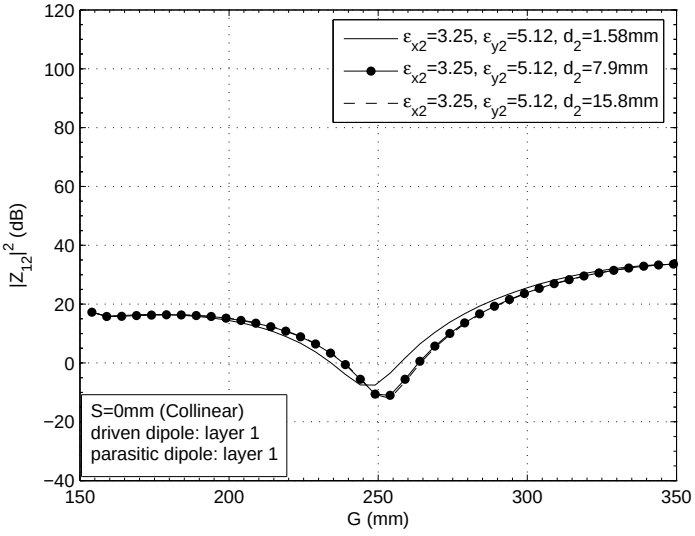

Figure 69. Mutual coupling between printed dipoles on the same anisotropic layer for various values of d_2, $\varepsilon_1 = 3.25$, L = 15 cm, W = 0.5 mm, f = 500 MHz and $d_1 = 1.58$ mm (collinear).

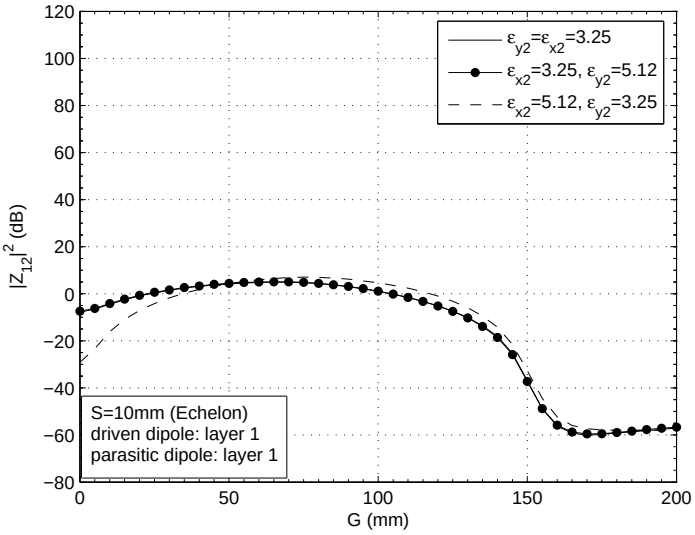

Figure 70. Mutual coupling between printed dipoles on the same anisotropic layer for various values of $[\varepsilon_2]$, $\varepsilon_1 = 3.25$, L = 15 cm, W = 0.5 mm, f = 500 MHz and $d_1 = d_2 = 1.58$ mm (echelon).

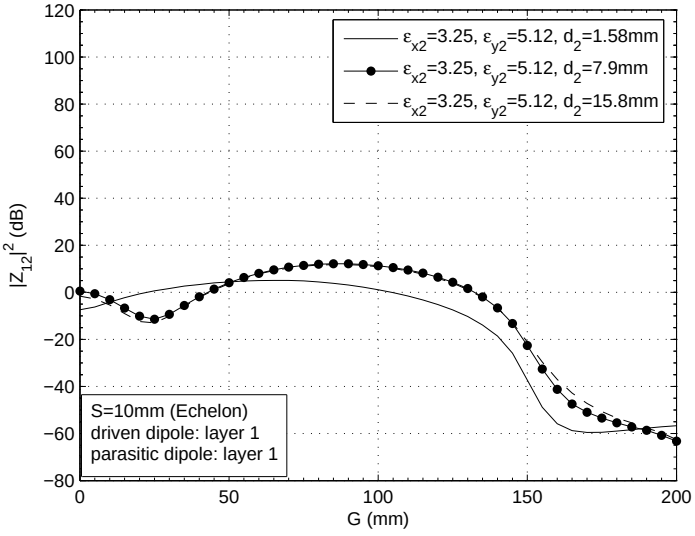

Figure 71. Mutual coupling between printed dipoles on the same anisotropic layer for various values of d_2, $\varepsilon_1 = 3.25$, L = 15 cm, W = 0.5 mm, f = 500 MHz and $d_1 = 1.58$ mm (echelon).

Several comments can be made about the case when both of the printed dipoles were on layer 1 and the second layer was anisotropic (i.e., the dipoles had an anisotropic cover). In general, the overall coupling between the printed dipoles was reduced by the introduction of the anisotropic cover. In particular, when referring to the anisotropic cover, the coupling was reduced when the value of permittivity in the direction orthogonal to the optical axis was increased while an increase in permittivity in the direction of the optical axis had little or no impact on the coupling. Finally, when the cover thickness was increased the effect on the coupling significantly reduced.

5.6. Numerical Results of a Single Printed Dipole In Three Anisotropic Layers

In the next case, the printed dipole in the three-layer structure shown in Figure 72 was evaluated. The printed dipole was between the second and third layers of anisotropic material. The first layer was next to the ground plane, the second layer was under the dipole and the third layer was the superstrate above the dipole.

The first three layer problem had three isotropic layers defined. Again, this problem was chosen to compare the results of the immittance functions with ADS. The depth of each layer was set at 1.58 mm and the dipole had a length of 15 cm with a width of 0.5 mm. The isotropic layer next to the ground plane (layer 1) had a permittivity of $\varepsilon_1 = 2.55$. The value of ε_3 was varied, and ε_2 was set at $\varepsilon_2 = 5.12$. Then the value of ε_2 was varied, and ε_3 was set at $\varepsilon_3 = 5.12$. The resonant frequency of the antenna was calculated for both of these cases, and the results are shown in Figure 73. Again, good agreement between the immittance functions and ADS was observed. Next, the anisotropy ratio of the layers above and below the dipole was changed. The computational results for this case is shown in Figure 74.

Next, the input impedance of a printed dipole with a length of 15 cm and a width of 0.5 mm was computed over the frequency range of 200 MHz to 800 MHz.

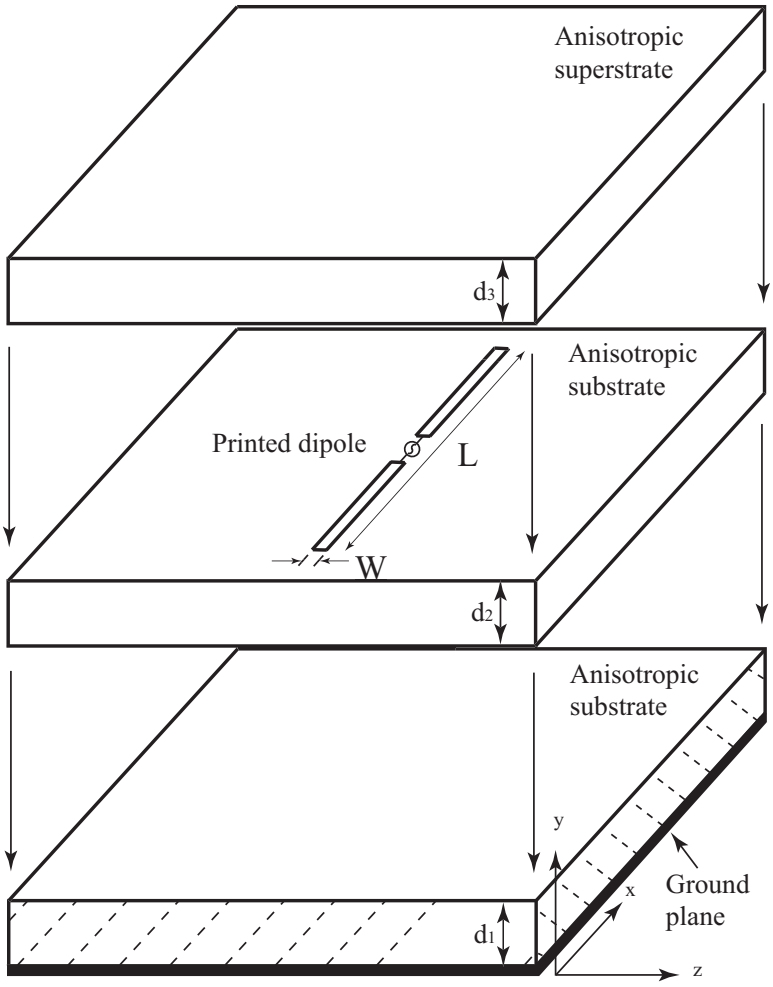

Figure 72. Expanded view of a printed dipole in three layers of anisotropic material.

Each layer had a thickness of 1.58 mm and the dipole was placed on the top of layer 2. This resulted in two anisotropic substrates and a single anisotropic superstrate. For the results in Figures 75 and 76, the permittivity of layer 1 was set at $\varepsilon_1 = 3.25$ and the values of $[\varepsilon_2]$ and $[\varepsilon_3]$ were varied. The isotropic results from ADS are also included in Figures 75 and 76. It is shown that the isotropic results from the immittance functions compare very well with the results from ADS. The code for the results in this section is shown in Appendix I.

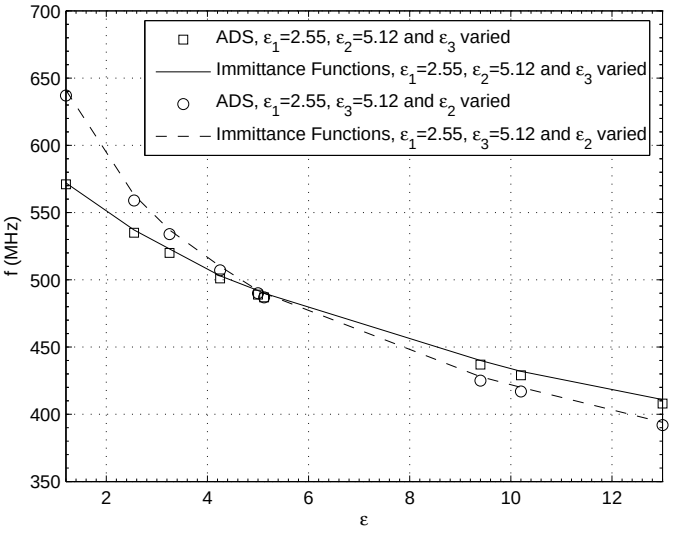

Figure 73. Resonant frequency of a printed dipole in three isotropic layers for various values of ε_2, various values of ε_3, L = 15 cm, W = 0.5 mm and $d_1 = d_2 = d_3 = 1.58$ mm.

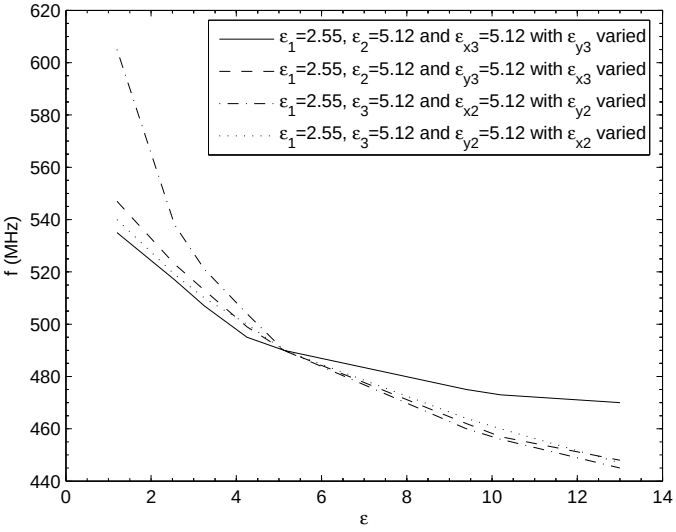

Figure 74. Resonant frequency of a printed dipole in three anisotropic layers for various values of $[\varepsilon_2]$, various values of $[\varepsilon_3]$, L = 15 cm, W = 0.5 mm and $d_1 = d_2 = d_3 = 1.58$ mm.

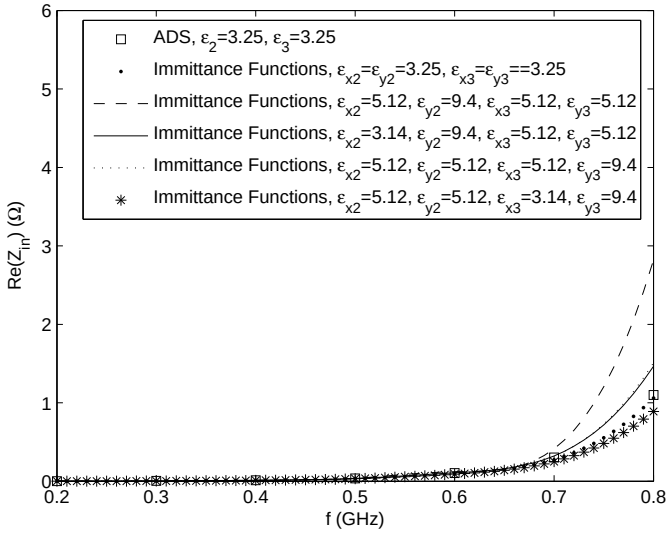

Figure 75. Input resistance of a printed dipole with an anisotropic substrate and superstrate for various values of $[\varepsilon_2]$, various values of $[\varepsilon_3]$, $\varepsilon_1 = 3.25$, L = 15 cm, W = 0.5 mm and $d_1 = d_2 = d_3 = 1.58$ mm.

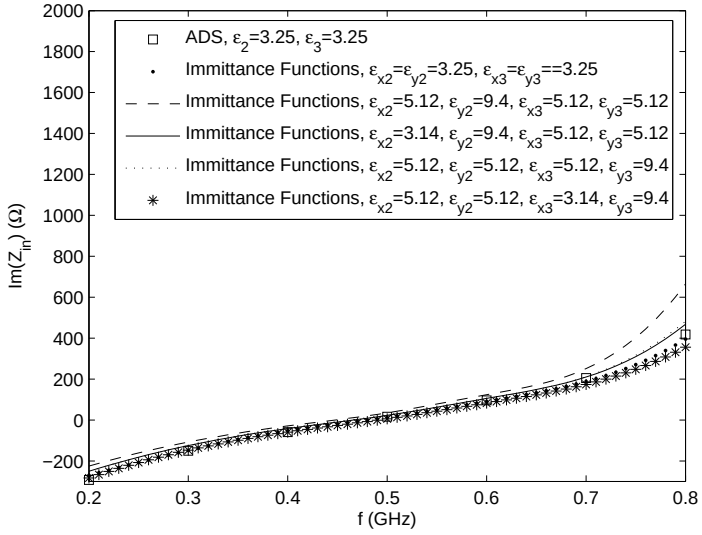

Figure 76. Input reactance of a printed dipole with an anisotropic substrate and superstrate for various values of $[\varepsilon_2]$, various values of $[\varepsilon_3]$, $\varepsilon_1 = 3.25$, L = 15 cm, W = 0.5 mm and $d_1 = d_2 = d_3 = 1.58$ mm.

The results from these three-layer problems correspond to the one- and two-layer problems. The results in Figure 74 show that ε_{y2} effects the resonant frequency much more significantly than all the other characteristics of layers 2 and 3. The reason for this was discussed in the single-layer problem and is related to the dominant TM_0 mode below the printed dipole. When looking at the effects of ε_{x3} and ε_{y3} on the resonant frequency, it is evident that ε_{x3} has much more of an impact on the resonant frequency than ε_{y3}. As ε_{x3} was varied the resonant frequency was changed by 99 MHz while ε_{y3} changed the resonant frequency by 65 MHz. Similar results are shown in Figures 75 and 76. The input resistance is largest when $\varepsilon_{x2} = 5.12$, $\varepsilon_{y2} = 9.4$ and $\varepsilon_{x3} = \varepsilon_{y3} = 5.12$. This corresponds to the largest value of permittivity in the direction of the optical axis in the layer immediately below the dipole. The larger real part of Z_{in} corresponds to a lower resonance of the dipole and a stronger space and surface wave being launched from the dipole. The larger resistance associated with changing $[\varepsilon_3]$ corresponds to $\varepsilon_{x2} = 5.12$, $\varepsilon_{y2} = 5.12$, $\varepsilon_{x3} = 5.12$ and $\varepsilon_{y3} = 9.4$, which are the results with the largest ε_{x3} values.

5.7. Numerical Results for the Mutual Coupling Between Two Printed Dipoles In Three Anisotropic Layers

The last problem evaluated was the mutual coupling between two printed dipoles in three layers of anisotropic dielectrics. The three-layer problem is shown in Figure 77. One dipole was located on the top of layer 1, and one dipole was located on the top of layer 2. The dipoles are separated by a distance S and shifted from the broadside orientation by a distance G. This three-layer problem is similar to the two-layer problem in Figure 62 with another anisotropic layer defined. Defining the third anisotropic layer leads to the study of how another superstrate will affect the mutual coupling between the two dipoles.

The length of each dipole was set again at 15 cm and the width of each dipole

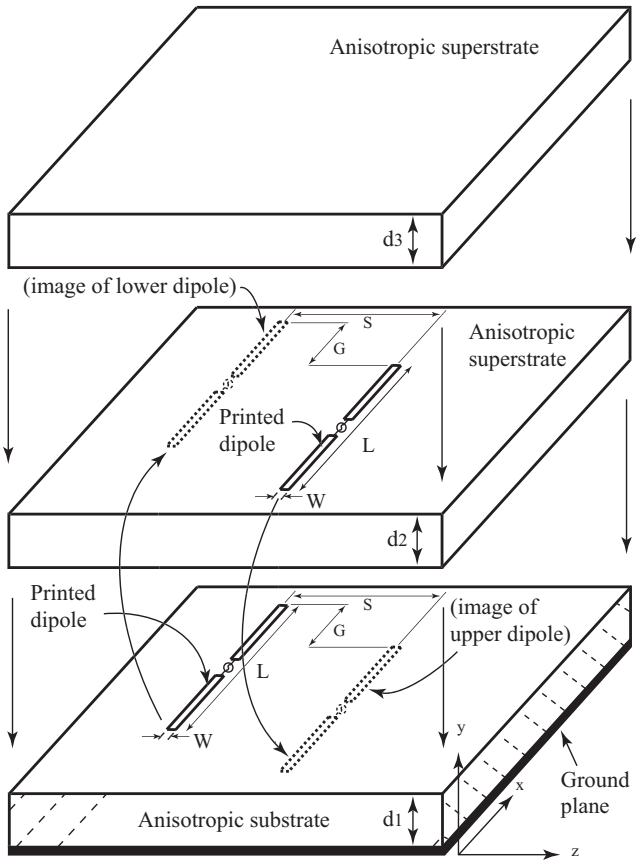

Figure 77. Expanded view of two printed dipoles in three layers of anisotropic layers.

was set again at 0.5 mm. The thickness of each layer was set at $d_1 = d_2 = d_3 = 1.58$ mm, and the permittivities of layers 1 and 2 were defined to be 3.25. The source frequency was 500 MHz. Several values of $[\varepsilon_3]$ and d_3 were chosen, and the distances S and G were varied. The mutual coupling between the dipoles for the broadside case ($G = 0$) can be seen in Figure 78. S was increased from 2 mm to 30 mm and d_3 was set at 1.58 mm. Good agreement between the results from ADS and the immittance functions for the isotropic case is also shown. The next problem sets the superstrate permittivity at $\varepsilon_{x3} = 3.25$ and $\varepsilon_{y3} = 5.12$ while d_3 was defined at 1.58 mm, 7.9 mm and 15.8 mm. Again, S was varied from 2 mm to 30 mm. The mutual coupling between the printed dipoles is shown in Figure 79. Next, the dipoles are placed in

a collinear orientation ($S = 0$) and the value of G was varied from 0 to 200 mm. Initially, d_3 was set at 1.58 mm and $[\varepsilon_3]$ was varied. The mutual coupling results for this configuration are shown in Figure 80. Next, the superstrate permittivity was set at $\varepsilon_{x3} = 3.25$, $\varepsilon_{y3} = 5.12$ and the thickness of d_3 was defined at 1.58 mm, 7.9 mm and 15.8 mm. The results from these computations are shown in Figure 81. Next, the dipoles were placed in an echelon orientation with $S = 10$ mm. The value of G was varied from 0 to 200 mm. The thickness of each layer was set at $d_1 = d_2 = d_3 = 1.58$ mm and the permittivities of layers 1 and 2 were defined to be 3.25. Initially, $[\varepsilon_3]$ was varied. The mutual coupling results for this configuration are shown in Figure 82. Next, the superstrate permittivity was set at $\varepsilon_{x3} = 3.25$, $\varepsilon_{y3} = 5.12$, and the thickness of d_3 was defined at 1.58 mm, 7.9 mm and 15.8 mm. The results from these computations are shown in Figure 83. The code for the mutual coupling computations is shown in Appendix J.

The only significant change as a result of the third layer was in the broadside configuration. When comparing the broadside results for the two-layer problem in Figure 63 to the three-layer results in Figure 78, it is observed that the third layer reduces the coupling between the two dipoles. This general reduction was not as significant in the collinear and echelon results in Figures 80 and 82. In general the mutual coupling was the greatest for the superstrate values of $\varepsilon_{x3} = 4.25$ and $\varepsilon_{y3} = 5.12$. When the thickness of layer 3 was increased the mutual coupling was increased. This is believed to be a result of the guided waves supported by the increased layer thickness [90]. In general it is difficult to make observations that are consistent with all three dipole orientations. In the cases presented here the behavior of the permittivities in the direction of the optical axis and orthogonal to the optical axis seemed to effect the mutual coupling the same for all configurations. This will be very useful for many antenna design situations.

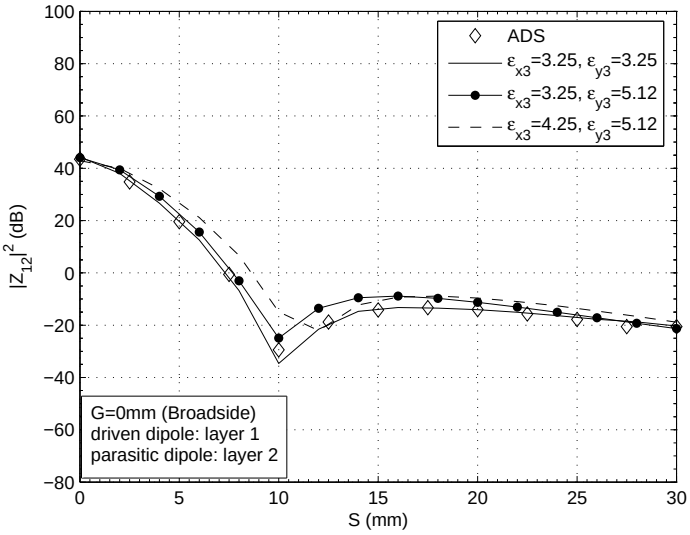

Figure 78. Mutual coupling between printed dipoles separated by an anisotropic layer for various values of $[\varepsilon_3]$, $\varepsilon_1 = \varepsilon_2 = 3.25$, L = 15 cm, W = 0.5 mm, f = 500 MHz and $d_1 = d_2 = d_3 = 1.58$ mm (broadside).

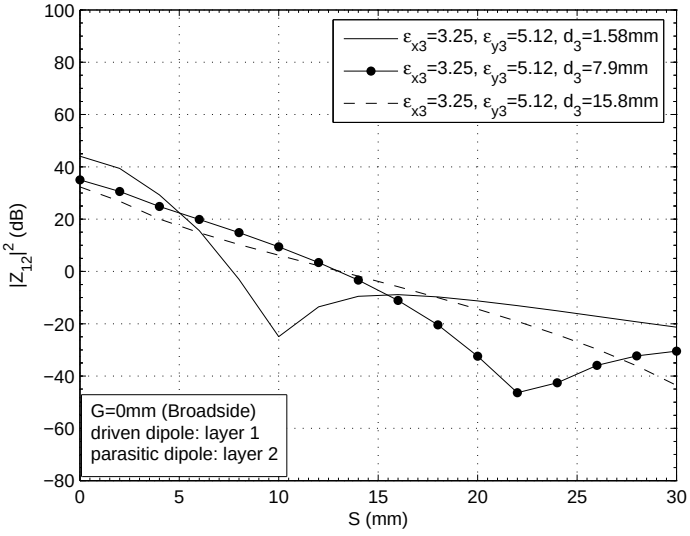

Figure 79. Mutual coupling between printed dipoles separated by an anisotropic layer for various values of d_3, $\varepsilon_1 = \varepsilon_2 = 3.25$, L = 15 cm, W = 0.5 mm, f = 500 MHz and $d_1 = d_2 = 1.58$ mm (broadside).

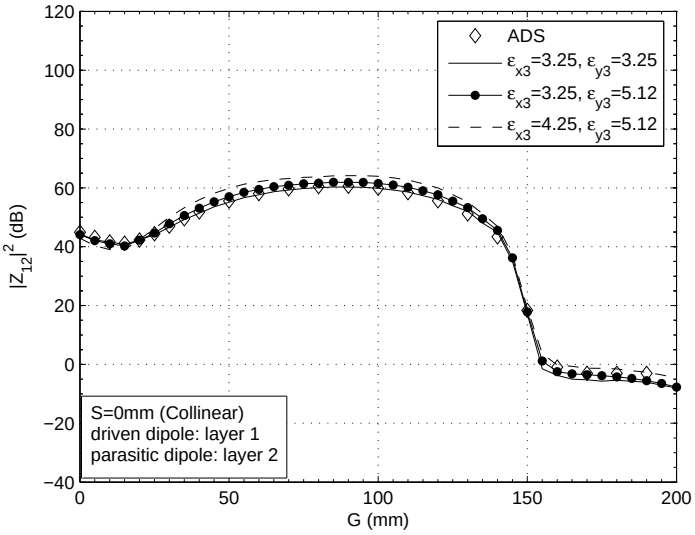

Figure 80. Mutual coupling between printed dipoles separated by an anisotropic layer for various values of $[\varepsilon_3]$, $\varepsilon_1 = \varepsilon_2 = 3.25$, L = 15 cm, W = 0.5 mm, f = 500 MHz and $d_1 = d_2 = d_3 = 1.58$ mm (collinear).

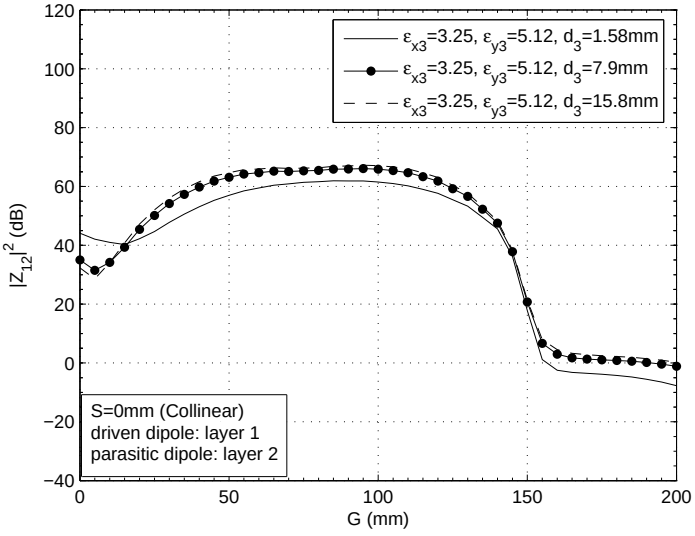

Figure 81. Mutual coupling between printed dipoles separated by an anisotropic layer for various values of d_3, $\varepsilon_1 = \varepsilon_2 = 3.25$, L = 15 cm, W = 0.5 mm, f = 500 MHz and $d_1 = d_2 = 1.58$ mm (collinear).

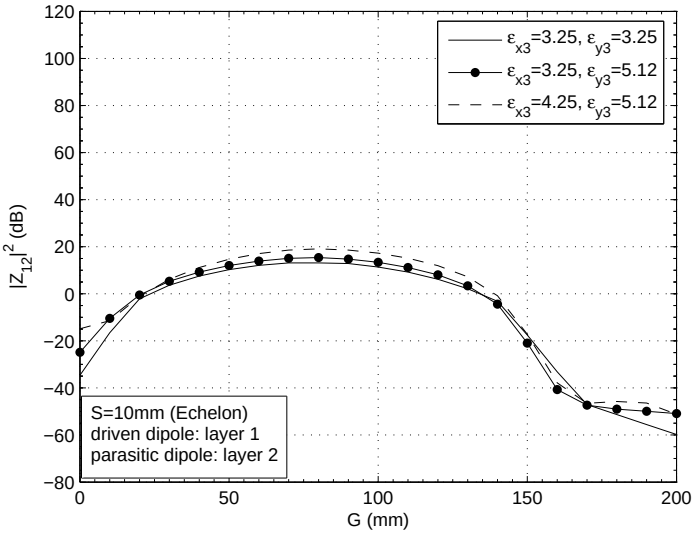

Figure 82. Mutual coupling between printed dipoles separated by an anisotropic layer for various values of $[\varepsilon_3]$, $\varepsilon_1 = \varepsilon_2 = 3.25$, L = 15 cm, W = 0.5 mm, f = 500 MHz and $d_1 = d_2 = d_3 = 1.58$ mm (echelon).

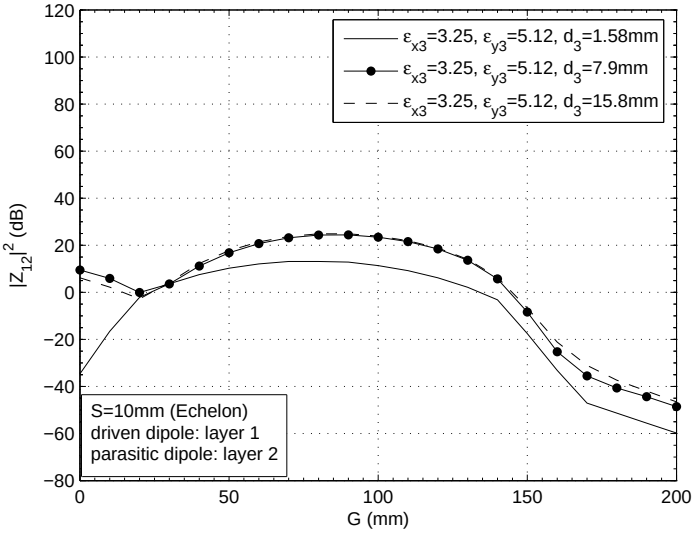

Figure 83. Mutual coupling between printed dipoles separated by an anisotropic layer for various values of d_3, $\varepsilon_1 = \varepsilon_2 = 3.25$, L = 15 cm, W = 0.5 mm, f = 500 MHz and $d_1 = d_2 = 1.58$ mm (echelon).

5.8. The Printed Rectangular Microstrip Patch - A Discussion

The results in the previous sections can be directly applied to a rectangular microstrip antenna. Pozar [29] mentions that the current on an edge-fed rectangular microstrip patch can be represented as a current with one component in the direction away from the feed point. This is illustrated in Figure 84. Pozar uses one PWS expansion function that is sinusoidal in the direction of the current and constant orthogonal to the direction of the current to represent the current on the patch. Pozar mentions that this single current representation provides reasonable results. This was also later shown by Zhu *et al.* [91] to be a good approximation of the current.

The results in this present work assume a similar current representation on the surface of the printed dipole. The PWS expansion functions are sinusoidal in the direction of the current and constant orthogonal to the direction of the current. Because of this similarity in the currents, the results outlined in this work can be applied to rectangular patches. Many characteristics of the results in the work presented here agree with existing published literature on the rectangular microstrip antenna. The work by Nelson [71] shows how the resonant frequency of a rectangular patch is affected by various anisotropic layers. Many of the results in Nelson's work correspond to the results here. Similarly, Pozar [37] investigates the radiation and scattering of a rectangular patch on a single anisotropic substrate. The characteristics of the modes associated with the anisotropic substrate in Pozar's work correspond to the results in this work. Oliveira and D'Assunção [38] investigate the input impedance of a rectangular patch in several layers of anisotropic dielectrics. Their results correspond well to the results in this work.

The isotropic mutual coupling results presented in this work have the same characteristics as much of the published literature [29], [39]-[50], [88]. A comparison

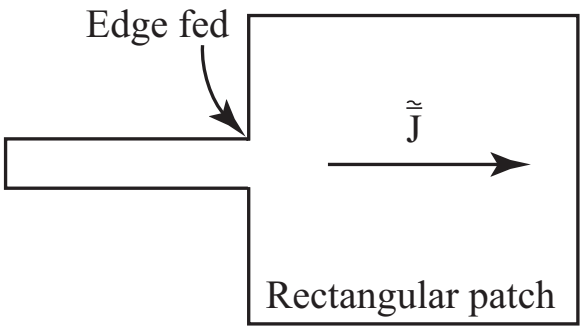

Figure 84. Current on an edge-fed rectangular patch.

between the work here and published literature for an anisotropic mutual coupling problem was not found because the work here is the first investigation of these types of coupling problems.

5.9. Overall Discussion and Design Guidelines

The following original and useful comments can be made about the results from this work.

1) The resonant frequency, input impedance and mutual coupling of the printed dipoles were mostly affected by the value of permittivity in the direction of the optical axis in the layer immediately below each individual dipole. This is because the dominant mode in the problems was the TM_0 mode. This mode had an electric field component in the direction of the optical axis.

2) The permittivity in the direction orthogonal to the optical axis in the anisotropic layer immediately above a printed antenna has the next most significant effect on all the properties associated with that particular antenna. This is because the electric field has components in the x-z plane, which is the plane containing the boundary between the two anisotropic layers.

3) Another new observation from this work is related to the mutual coupling. Generally the mutual coupling was reduced between the printed dipoles by placing

an anisotropic layer above both dipoles. In particular, an increase in the permittivity in the anisotropic cover in the direction orthogonal to the optical axis reduced the coupling between the dipoles in all configurations while an increase in the permittivity in the direction of the optical axis generally had no effect on the coupling. From a designers point of view, this is very useful because the permittivity in the direction of the optical axis below the dipole could be used to design a specific resonant frequency for a given dipole and the permittivity orthogonal to the optical axis in the layer above the dipole could be used to control mutual coupling.

4) As thickness of the anisotropic layers were increased, the effect of the resonant frequency was significantly reduced. This showed that the introduction of very thin anisotropic layers above printed dipoles can have a very significant impact on the resonant frequency of a printed dipole.

5) As the thickness of the anisotropic layers were increased, the effect on the mutual coupling was generally reduced. In some cases (collinear, Figure 69) the mutual coupling was not affected much.

6) When the permittivity in the direction of the optical axis was increased in the anisotropic layer separating the printed dipoles, the mutual coupling was generally increased. The mutual coupling was then reduced by increasing the permittivity in the direction orthogonal to the optical axis in the anisotropic layer separating the printed dipoles.

7) When an anisotropic layer was placed above the printed dipoles separated by an anisotropic layer, the anisotropy ratio had little effect on the mutual coupling between the dipoles.

8) In general, when the thickness of an anisotropic layer placed above the printed dipoles separated by an anisotropic layer was increased, the mutual coupling was affected very little after a point.

9) When considering radiation resistance, it is shown that the largest radiation resistance values in the anisotropic results are associated with the larger values of permittivity in the direction of the optical axis in the layers below the dipole.

10) Finally, the radiation resistance of a dipole with an anisotropic superstrate was the largest when the permittivity orthogonal to the optical axis in the superstrate was the largest.

Keeping these anisotropic layer properties in mind will be very useful in many different printed antenna designs.

CHAPTER 6. CONCLUSION

In this work, spectral domain immittance functions, based on the Hertz vector potentials, have been derived to investigate the properties of printed dipoles in stratified uniaxial anisotropic dielectrics. A complete derivation of the immittance functions for a single conductor found in published literature was performed. Then these immittance functions were extended for the first time to include multiple conductors on different layers of anisotropic dielectrics. In this study the current on each dipole was not assumed and solved for using the Moment Method. This differs from all of the previous printed dipole research associated with anisotropic dielectrics because in previous work the printed dipoles were assumed to be Hertzian (i.e., constant current) or had an assumed sinusoidal current distribution.

The input impedance and resonant frequency of a single printed dipole was investigated in one-, two- and three-layered anisotropic structures. Then the mutual coupling between two printed dipoles in one-, two- and three-layered anisotropic structures was determined for the first time. The single printed dipole results were validated with commercial software, published literature and measurements while the isotropic mutual coupling results were validated by commercial software. In all cases excellent agreement was observed between the immittance functions, measurements, published literature and commercial software.

The following novel and valuable comments are a brief summary about the results from this work. The resonant frequency, input impedance and mutual coupling of the printed dipoles were mostly effected by the value of permittivity in the direction of the optical axis in the layer immediately below each individual dipole. This is because the dominant mode in the problems was the TM_0 mode. This mode had an electric field component in the direction of the optical axis. Another new observation from this work is related to the mutual coupling. Generally the mutual coupling

was reduced between the printed dipoles by placing an anisotropic layer above both dipoles. In particular, an increase in the permittivity in the anisotropic cover in the direction orthogonal to the optical axis reduced the coupling between the dipoles in all configurations while an increase in the permittivity in the direction of the optical axis generally had no effect on the coupling. From a designers point of view, this is very useful because the permittivity in the direction of the optical axis below the dipole could be used to design a specific resonant frequency for a given dipole and the permittivity orthogonal to the optical axis in the layer above the dipole could be used to control mutual coupling. Finally, the effect of layer thicknesses on the the resonant frequency and mutual coupling was generally reduced as the thickness of the anisotropic layers increased. This showed that the introduction of very thin anisotropic layers above printed dipoles can have a very significant initial impact on the resonant frequency and mutual coupling.

Many avenues of research could be taken as a result of the work here. Two immediate applications would be to investigate the mutual coupling between rectangular patches and ultra wide-band (UWB) antennas in layered anisotropic material. As system frequencies and transmission distances increase, array applications become more important. The use of rectangular patches and UWB antennas in arrays is becoming more common, and understanding the coupling between elements is very important.

Another topic of interest is to study the effect that mutual coupling has on the performance of RFID tags in very close proximity to each other. In many cases RFID tags need to be embedded in stratified material. By using the results from this work, a designer could use the anisotropic properties of the stratified material to control the mutual coupling between the RFID tags to improve the read range.

The mathematical aspect is another very significant area of research associated

with this work. Many integration limits, poles and convergence questions have not been answered. The limit of integration seemed to be associated with the problem definition. Understanding this could be used to increase the computational accuracy and speed significantly. Also, the poles associated with the immittance functions are related to surface wave modes, leaky waves and radiation. A complete and formal mathematical understanding of this topic would be very valuable.

Many novel and useful results associated with printed dipoles have been presented in this work. A comprehensive understanding of the effect of the individual anisotropic properties on the resonant frequency, input impedance and mutual coupling was achieved. This has led to original design guidelines that will help with printed antenna design. Even though new problems have been investigated and discussed, it is evident that much more work could be done.

BIBLIOGRAPHY

[1] Sanford P. Bordeau, *Volts to Hertz...the rise of electricity,* Burgess Publishing Company, Minneapolis, MN, 1982.

[2] John Tyndall, *Faraday as a Discoverer,* D. Appleton and Co., New York, NY, 1874.

[3] Silvanus P. Thompson, *Michael Faraday: His Life and Work,* Cassel and Co., Ltd., New York, NY, 1901.

[4] James Clerk Maxwell, *A Treatise on Electricity and Magnetism,* Dover Publications, Inc., Mineola, NY, 1954.

[5] Rollo Appleyard, *Pioneers of Electrical Communications,* Books for Libraries Press, Freeport, NY, 1968.

[6] W. L. Stutzman, "Bibliography for antennas: a list of every English-language antenna book ever written," *IEEE Antennas and Propagation Magazine,* vol. 50, no. 4, pp. 128-143, August 2008.

[7] James G. Crowther, *Six Great Inventors,* Hamish Hamilton, London, England, 1957.

[8] Orrin E. Dunlap Jr., *Marconi: The Man and His Wireless,* The Macmillan Co., New York, NY, 1937.

[9] Julius Adams Stratton, *Electromagnetic Theory,* 1^{st} Ed., McGraw-Hill Book Company, New York, NY, 1941, pp. 464-468.

[10] R. W. P. King, *The Theory of Linear Antennas with Charts and Table for Practical Applications,* Harvard University Press, Cambridge, MA, 1956.

[11] G. A. Deschamps, "Microstrip Microwave Antennas," presented at the *3rd USAF Symposium on Antennas*, 1953.

[12] David M. Pozar and Daniel H. Schaubert, *Microstrip Antennas: The analysis and Design of Microstrip Antennas and Arrays,* IEEE Press, Piscataway, NJ, 1995.

[13] K. Finkenzeller, *RFID Handbook: Fundamentals and Applications in Contactless Smart Cards and Identification,* John Wiley and Sons, West Sussex, England, 2003.

[14] B. D. Braaten, G. J. Owen, D. Vaselaar, R. M. Nelson, C. Bauer-Reich, J. Glower, B. Morlock, M. Reich and A. Reinholz, "A Printed Rampart-line antenna with a dielectric superstrate for UHF RFID applications," *IEEE International Conference on RFID,* The Venetian, Las Vegas, NV, April 16-17, 2008.

[15] A. Sundaram, M. Maddela and R. Ramados, "Koch-Fractal Folded-Slot Antenna Characteristics," *IEEE Antennas and Wireless Propagation Letters,* vol. 6, pp. 219-222, 2007.

[16] C. Calabrese and G. Marrocco, "Meandered-slot antennas for sensor-RFID tags," *IEEE Antennas and Wireless Propagation Letters,* vol. 7, pp. 5-8, 2008.

[17] J-P Curty, M. Declercq, C. Dehollain and N. Joehl, *Design and Optimization of Passive UHF RFID Systems,* Springer-Verlag New York, LLC, 2006.

[18] E. Cooney, *RFID+: The Complete Review of Radio Frequency Identification,* Cengage Delmar Learning, 2006.

[19] D. Paret, R. Riesco, R. Riesco, *RFID and Contactless Smart Card Applications,* John Wiley and Sons, Inc., 2005.

[20] V. D. Hunt, A. Puglia, and M. Puglia, *RFID-A Guide to Radio Frequency Identification,* John Wiley and Sons, Inc., 2007.

[21] E. W. Schuster, S. J. Allen and D. L. Brock, *Global RFID: The Value of the EPCglobal Network for Supply Chain Management,* Springer-Verlag New York, LLC, 2006.

[22] Warren L. Stutzman and Gary A. Thiele, *Antenna Theory and Design,* 2nd ed., John Wiley and Sons, Inc., New York, NY, 1998.

[23] Constantine A. Balanis, *Antenna Theory: Analysis and Design,* Harper and Row, Publishers, New York, NY, 1982.

[24] R. E. Munson, "Conformal microstrip antennas and microstrip phased arrays," *IEEE Transactions on Antennas and Propagation,* vol. 22, no. 1, pp. 74-78, January 1974.

[25] T. G. Campbell, *An extremely thin omnidirectional microwave antenna array for spacecraft applications,* NASA Technical Note D-5539, November 1969.

[26] J. Q. Howell, "Microstrip antennas," *IEEE Transactions on Antennas and Propagation,* vol. 14, no. 1, pp. 90-93, January 1975.

[27] N. K. Uzunoglu, N. G. Alexopoulos and J. G. Fikioris, "Radiation properties of microstrip dipoles," *IEEE Transactions on Antennas and Propagation,* vol. 27, no. 6, pp. 853-858, November 1979.

[28] I. E. Rana and N. G. Alexopoulos, "Current distribution and input impedance of printed dipoles," *IEEE Transactions on Antennas and Propagation,* vol. 29, no. 1, pp. 99-105, January 1981.

[29] D. M. Pozar, "Input impedance and mutual coupling of rectangular microstrip antennas," *IEEE Transactions on Antennas and Propagation,* vol. 30, no. 6, pp. 1191-1196, November 1982.

[30] T. Itoh, "Spectral domain immitance approach for dispersion characteristics of generalized printed transmission lines," *IEEE Transactions on Antennas and Propagation,* vol. 28, no. 7, pp. 733-736, July 1980.

[31] T. Itoh and W. Menzel, "A full-wave analysis method for open microstrip structures," *IEEE Transactions on Microwave Theory and Techniques,* vol. 29, no. 1, pp. 63-68, January 1981.

[32] I. J. Bahl, P. Bhartia and S. S. Stuchly, "Design of microstrip antennas covered with a dielectric layer," *IEEE Transactions on Antennas and Propagation,* vol. 30, no. 2, pp. 314-318, March 1982.

[33] H. Lee and V. K. Tripathi, "Spectral domain analysis of frequency dependent propagation characteristics of planar structures on uniaxial medium," *IEEE Transactions on Microwave Theory and Techniques,* vol. 30, no. 8, pp. 1188-1193, August 1982.

[34] R. M. Nelson, D. A. Rogers and A. G. D'Assuncao, "Resonant frequency of a rectangular microstrip patch on several uniaxial substrates," *IEEE Transactions on Antennas and Propagation,* vol. 38, no. 7, pp. 973-981, July 1990.

[35] C. M. Krowne, "Green's function in the spectral domain for biaxial and uniaxial anisotropic planar dielectric structures," *IEEE Transactions on Antennas and Propagation,* vol. 32, no. 12, pp. 1273-1281, December 1984.

[36] C. M. Krowne, "Determination of the Green's function in the spectral domain using a matrix method: application to radiators or resonators immersed in

a complex anisotropic layered medium," *IEEE Transactions on Antennas and Propagation,* vol. 34, no. 2, pp. 247-253, February 1986.

[37] D. M. Pozar, "Radiation and scattering from a microstrip patch on a uniaxial substrate," *IEEE Transactions on Antennas and Propagation,* vol. 35, no. 6, pp. 613-621, June 1987.

[38] J. R. S. Oliveira and A. G. D'Assuncao, "Input impedance of microstrip patch antennas on anisotropic dielectric substrates," *Antennas and Propagation Society International Symposium Digest,* vol. 2, July 21-26, 1996, pp. 1066-1069.

[39] H. C. Baker and A. H. LaGrone, "Digital computation of the mutual impedance between thin dipoles," *IRE Transactions on Antennas and Propagation,* pp. 172-178, March 1962.

[40] N. G. Alexopoulos and I. E. Rana, "Mutual impedance computation between printed dipoles," *IEEE Transactions on Antennas and Propagation,* vol. 29, no. 1, pp. 106-112, January 1981.

[41] R. P. Jedlicka, M. T. Poe and K. R. Carver, "Measured mutual coupling between microstrip antennas," *IEEE Transactions on Antennas and Propagation,* vol. 29, no. 1, pp. 147-149, January 1981.

[42] E. H. Newman, J. H. Richmond and B. W. Kwan, "Mutual impedance computation between microstrip antennas," *IEEE Transactions on Microwave Theory and Techniques,* vol. 31, no. 11, pp. 941-945, November 1983.

[43] E. H. V. Lil and A. R. V. DeCapelle, "Transmission line model for mutual coupling between microstrip antennas," *IEEE Transactions on Antennas and Propagation,* vol. 32, no. 8, pp. 816-821, August 1984.

[44] V. Hansen and M. Patzold, "Input impedance and mutual coupling of rectangular microstrip patch antennas with a dielectric cover," *16th European Microwave Conference* October 1986, pp. 643-648.

[45] P. B. Katehi, "Mutual coupling between microstrip dipoles in multielement arrays," *IEEE Transactions on Antennas and Propagation,* vol. 37, no. 3, pp. 275-280, March 1989.

[46] A. H. Mohammadian, N. M. Martin and D. W. Griffin, "A theoretical and experimental study of mutual coupling in microstrip antenna arrays," *IEEE Transactions on Antennas and Propagation,* vol. 37, no. 10, pp. 1217-1223, October 1989.

[47] A. Benalla and K. C. Gupta, "Mutual coupling between rectangular microstrip patches covered with a dielectric cover layer," *Antennas and Propagation Society International Symposium, Merging Technologies for the 90's' Digest,* vol. 1, May 7-11 1990, pp. 358-361.

[48] C. Terret, S. Assailly, K. Mahdjoubi and M. Edimo, "Mutual coupling between stacked square microstrip antennas fed on their diagonal," *IEEE Transactions on Antennas and Propagation,* vol. 39, no. 7, pp. 1049-1051, July 1991.

[49] S. G. Pan and I. Wolff, "Computation of mutual coupling between slot-coupled microstrip patches in a finite array," *IEEE Transactions on Antennas and Propagation,* vol. 40, no. 9, pp. 1047-1053, September 1992.

[50] P. F. Wahid and T. Voor, "Mutual impedance between skewed patch antennas," *IEEE Transactions on Antennas and Propagation,* vol. 42, no. 5, pp. 754-756, May 1994.

[51] M. D. Deshpande and M. C. Bailey, "Input impedance of microstrip antennas," *IEEE Transactions on Antennas and Propagation,* vol. 30, no. 4, pp. 645-650, July 1982.

[52] W. Y. Tam, A. K. Y. Lai and K. M. Luk, "Mutual coupling between cylindrical rectangular microstrip antennas," *IEEE Transactions on Antennas and Propagation,* vol. 43, no. 8, pp. 897-899, August 1995.

[53] A. K. Verma and Nasimuddin, "Input impedance of rectangular microstrip patch antenna with iso/anisotropic substrate-superstrate," *IEEE Microwave and Wireless Components Letters,* vol. 11, no. 11, pp. 456-458, November 2001.

[54] W. J. Wang, *Multilayered printed antennas with biaxial anisotropic dielectric substrates: general analysis and case studies,* Ph.D. Dissertation, Polytechnic University, January 2002.

[55] V. D. Costa, I. Bianchi, J. C. da S. Lacava and L. Cividances, "Analysis of electromagnetically coupled microstrip antennas printed on anisotropic substrates," *Proceedings of the 2003 SBMO/IEEE MTT-S International Microwave and Optoelectronics Conference, IMOC ,* vol. 1, September 20-23, 2003, pp. 317-322.

[56] R. B. Waterhouse, S. D. Targonski and D. M. Kokotoff, "Design and performance of small printed antennas," *IEEE Transactions on Antennas and Propagation,* vol. 46, no. 11, pp. 1629-1633, November 1998.

[57] C. Y. Chiu, C. H. Chan and K. M. Luk, "Study of a small wide-band patch antenna with double shorting walls," *IEEE Antennas and Wireless Propagation Letters,* vol. 3, pp. 230-231, 2004.

[58] A. Shackelford, K. F. Lee, D. Chatterjee, Y. X. Guo, K. M. Luk and R. Chair, "Small-size wide-bandwidth microstrip patch antennas," *IEEE Antennas and Propagation Society International Symposium Digest,* vol. 1, July 8-13, 2001, pp. 86-89.

[59] Y. Li, R. Chair, K. M. Luk and K. F. Lee, "Broadband triangular patch antenna with a folding shorting wall," *IEEE Antennas and Wireless Propagation Letters,* vol. 3, pp. 189-192, 2004.

[60] R. L. Li, G. DeJean, E. Tsai, E. Tentzeris and J. Laskar, "Novel small folded shorted-patch antennas," *IEEE Antennas and Propagation Society International Symposium Digest,* vol. 4, June 16-21, 2002, pp. 26-29.

[61] A. F. Sheta, H. Boghdady, A. Mohra and S. F. Mahmound, "A Novel dual-band small size microstrip antenna," *ACES Journal,* vol. 21, no. 2, pp. 135-142, July 2006.

[62] L. Markley and G. V. Eleftheriades, "A negative-refractive-index metamaterial for incident plane waves of arbitrary polarization," *IEEE Antennas and Wireless Propagation Letters,* vol. 6, pp. 28-32, 2007.

[63] P. Baccarelli, P. Burghignoli, F. Frezza, A. Galli, P. Lampariello, G. Lovat and S. Paulitto, "Fundamental modal properties of surface waves on metamaterial grounded slabs," *IEEE Transactions on Microwave Theory and Techniques,* vol. 53, no. 4, pp. 1431-1442, April 2005.

[64] K. Buell, H. Mosallaei and K. Sarabandi, "Metamaterial insulator enabled superdirective array," *IEEE Transactions on Antennas and Propagation,* vol. 55, no. 4, pp. 1074-1085, April 2007.

[65] K. G. Balmain, A. A. E. Luttgen and P. C. Kremer, "Resonance cone formation, reflection, refraction, and focusing in a planar anisotropic metamaterial," *IEEE Antennas and Wireless Propagation Letters,* vol. 1, pp. 146-149, 2002.

[66] K. G. Balmain, A. A. E. Luttgen and P. C. Kremer, "Power flow for resonance cone phenomena in planar anisotropic metamaterials," *IEEE Transactions on Antennas and Propagation,* vol. 51, no. 10, pp. 2612-2618, October 2003.

[67] F. Yang and Y. Rahmatt-Samii "Microstrip antennas integrated with electromagnetic band-gap (EBG) structures: a low mutual coupling design for array applications," *IEEE Transactions on Antennas and Propagation,* vol. 51, no. 10, pp. 2936-2946, October 2003.

[68] R. Chair, A. A. Kishk and K.-F. Lee, "Comparative study on the mutual coupling between different sized cylindrical dielectric resonators antennas and circular microstrip patch antennas," *IEEE Transactions on Antennas and Propagation,* vol. 53, no. 3, pp. 1011-1019, March 2005.

[69] Zeland Software, Inc, February 2009, [Online]. www.zeland.com.

[70] Fawwaz T. Ulaby, *Fundamentals of Applied Electromagnetics,* 1999 Ed., Prentice Hall, Upper Saddle River, NJ, 1999, p. 162.

[71] R. M. Nelson, *Rectangular microstrip patch resonators on several anisotropic substrates,* Ph.D. Dissertation, North Dakota State University, Fargo ND, 1987.

[72] N. G. Alexopoulus, "Integrated-circuit structures on anisotropic substrates," *IEEE Transactions on Microwave Theory and Techniques,* vol. 33, no. 10, pp. 847-881, October 1985.

[73] I. J. Bahl and P. Bhartia *Microstrip Antennas,* Artech House, Inc. Dedham, MA, 1980, pp.214-215.

[74] Y. Chen and B. Beker, "Analysis of an array of four microstrip patch resonators printed on an anisotropic substrate," *IEEE Transactions on Microwave Theory and Techniques,* vol. 43, no. 2, pp. 460-463, February 1995.

[75] F. J. Harackiewicz and D. M. Pozar, "Radiation and scattering by infinite microstrip patch arrays on anisotropic substrates," *Antennas and Propagation Society International Symposium Digest,* vol. 1, June 6-10, 1988, pp. 10-13.

[76] A. L. P. S. Campos an A. G. D'Assuncao, "Scattering parameters of a frequency selective surface between anisotropic dielectric layers for incident co-polarized plane waves," *Antennas and Propagation Society International Symposium Digest,* 4, July 8-13, 2001, pp. 382-385.

[77] A. L. P. S. Campos an A. G. D'Assuncao, "Scattering by FSS on anisotropic substrate for TE and TM excitation," *IEEE Transactions on Microwave Theory and Techniques,* vol. 50, pp. 72-76, January 2002.

[78] A. L. P. S. Campos an A. G. D'Assuncao, "Hertz vector potential analysis of FSS on anisotropic substrates," *Proceedings of the 2003 SBMO/IEEE MTT-S International Microwave and Optoelectronics Conference, 2003* vol. 1, September 20-23, 2003, pp. 473-477.

[79] Robert E. Collin, *Field Theory of Guided Waves,* 2nd ed., IEEE Press-John Wiley and Sons, Inc., New York, 1991.

[80] Roger F. Harrington, *Field Computation by Moment Methods,* Robert E. Krieger Publishing Company, Inc., Malabar, FL, 1982, pp. 62-80.

[81] Roger F. Harrington, *Matrix Methods for Field Problems, Proceedings of the IEEE*, vol. 55, no. 2, pp. 136-149, February 1967.

[82] Yitzhak Katznelson, *An Introduction to Harmonic Analysis,* 2nd ed., Dover Publications, Inc., New York, NY, 1976, p. 120.

[83] Walter Rudin, *Functional Analysis,* McGraw-Hill Book Company, New York, NY, 1973, p. 167.

[84] D. B. Davidson and J. T. Aberle, "An introduction to the spectral domain method-of-moments formulations," *IEEE Antennas and Propagation Magazine,* vol. 46, no. 3, pp. 11-19, June 2004.

[85] William Palm III, *Introduction to MATLAB 6 for Engineers,* 1^{st} Ed., McGraw-Hill Book Company, New York, NY, 2001, pp. 419-505.

[86] Advanced Design System-ADS 2004A, Agilent Technologies.

[87] R. G. Olsen, G. L. Hower, and P. D. Mannikko, "A Hybrid Method for Combining Quasi-Static and Full-Wave Techniques for Electromagnetic Scattering Problems," *IEEE Transactions on Antennas and Propagation*, vol. 36, no. 8, pp. 1180-1184, August 1988.

[88] P. R. Haddad and D. M. Pozar, "Anomalous mutual coupling between microstrip antennas," *IEEE Transactions on Antennas and Propagation,* vol. 42, no. 11, pp. 1545-1549, November 1994.

[89] F. A. Monferrer and A. A. Kishk, "Green's functions analysis of planar thin-wire structures in a two layer grounded medium," *IEEE Antennas and Propagation Society International Symposium Digest,* vol. 3, June 24-28, 1991, pp. 1360-1363.

[90] N. G. Alexopoulos and D. R. Jackson, "Fundamental superstrate (cover) effects on printed circuit antennas," *IEEE Transactions on Antennas and Propagation,* vol. 32, no. 8, pp. 807-816, August 1981.

[91] L. Zhu, E. Yamashita and I. Joishi, "Generalized modeling of microstrip-fed patch antennas using an equivalent delta voltage source backed by a perfect electric wall," *IEEE Antennas and Propagation Society International Symposium Digest,* vol. 2, July 21-26, 1996, pp. 1082-1085 .

APPENDIX A. DERIVATIONS FOR ONE ANISOTROPIC LAYER

This appendix contains the derivations of the spectral domain immittance functions for a single anisotropic dielectric layer. The first boundary condition applied will be (3.67). Applying (3.74) at y = 0 gives:

$$\begin{aligned} \widetilde{E}_{x1}(\alpha, 0, \beta) &= 0 \\ &= -\omega\mu_0\beta A_1'(\alpha, \beta) + \frac{j\alpha}{\varepsilon_{12}} B_1'(\alpha, \beta)\gamma_{e1}. \end{aligned} \tag{A.1}$$

Next, the boundary condition applied will be (3.68). Applying (3.76) at y = 0 gives:

$$\begin{aligned} \widetilde{E}_{z1}(\alpha, 0, \beta) &= 0 \\ &= \omega\mu_0\alpha A_1'(\alpha, \beta) + \frac{j\beta}{\varepsilon_{12}} B_1'(\alpha, \beta)\gamma_{e1}. \end{aligned} \tag{A.2}$$

Solving for $A_1'(\alpha, \beta)$ in (A.1) and substituting into (A.2) gives:

$$-\alpha^2 B_1'(\alpha, \beta) = \beta^2 B_1'(\alpha, \beta). \tag{A.3}$$

The only solution to (A.3) is

$$B_1'(\alpha, \beta) = 0. \tag{A.4}$$

Substituting (A.4) back into (A.1) implies

$$A_1'(\alpha, \beta) = 0. \tag{A.5}$$

The third boundary condition applied will be (3.69). Equating (3.74) to (3.80) at d_1

and substituting in (A.4) and (A.5) gives:

$$\begin{aligned}\widetilde{E}_{x1}(\alpha, d_1, \beta) &= -\omega\mu_0\beta A_1(\alpha,\beta)\sinh(\gamma_{h1}d_1) + \frac{j\alpha}{\varepsilon_{12}}B_1(\alpha,\beta)\gamma_{e1}\sinh(\gamma_{e1}d_1) \\ &= -\omega\mu_0\beta A_2(\alpha,\beta) - \frac{j\alpha}{\varepsilon_{22}}\gamma_0 B_2(\alpha,\beta) \\ &= \widetilde{E}_{x2}(\alpha, d_1, \beta). \end{aligned} \tag{A.6}$$

Factoring out the coefficients results in:

$$\begin{aligned} A_1(\alpha,\beta)\Big[-\omega\mu_0\beta\sinh(\gamma_{h1}d_1)\Big] &+ B_1(\alpha,\beta)\left[\frac{j\alpha}{\varepsilon_{12}}\gamma_{e1}\sinh(\gamma_{e1}d_1)\right] \\ +A_2(\alpha,\beta)\Big[\omega\mu_0\beta\Big] &+ B_2(\alpha,\beta)\left[\frac{j\alpha}{\varepsilon_{22}}\gamma_0\right] = 0. \end{aligned} \tag{A.7}$$

The fourth boundary condition applied will be (3.70). Equating (3.76) to (3.82) at d_1 and substituting in (A.4) and (A.5) gives:

$$\begin{aligned}\widetilde{E}_{z1}(\alpha, d_1, \beta) &= \omega\mu_0\alpha A_1(\alpha,\beta)\sinh(\gamma_{h1}d_1) + \frac{j\beta}{\varepsilon_{12}}B_1(\alpha,\beta)\gamma_{e1}\sinh(\gamma_{e1}d_1) \\ &= \omega\mu_0\alpha A_2(\alpha,\beta) - \frac{j\beta}{\varepsilon_{22}}\gamma_0 B_2(\alpha,\beta) \\ &= \widetilde{E}_{z2}(\alpha, d_1, \beta). \end{aligned} \tag{A.8}$$

Factoring out the coefficients results in:

$$\begin{aligned} A_1(\alpha,\beta)\Big[\omega\mu_0\alpha\sinh(\gamma_{h1}d_1)\Big] &+ B_1(\alpha,\beta)\left[\frac{j\beta}{\varepsilon_{12}}\gamma_{e1}\sinh(\gamma_{e1}d_1)\right] \\ -A_2(\alpha,\beta)\Big[\omega\mu_0\alpha\Big] &+ B_2(\alpha,\beta)\left[\frac{j\beta}{\varepsilon_{22}}\gamma_0\right] = 0. \end{aligned} \tag{A.9}$$

Next, multiplying (A.7) by α and (A.9) by β and adding gives:

$$B_1(\alpha,\beta)\left[\frac{j\alpha^2}{\varepsilon_{12}}\gamma_{e1}\sinh(\gamma_{e1}d_1) \;+\; \frac{j\beta^2}{\varepsilon_{12}}\gamma_{e1}\sinh(\gamma_{e1}d_1)\right] + B_2(\alpha,\beta)\left[\frac{j\alpha^2}{\varepsilon_{22}}\gamma_0+\frac{j\beta^2}{\varepsilon_{22}}\gamma_0\right]=0. \quad \text{(A.10)}$$

Factoring out an $j(\alpha^2+\beta^2)$ gives:

$$B_1(\alpha,\beta)\left[\frac{\gamma_{e1}}{\varepsilon_{12}}\sinh(\gamma_{e1}d_1)\right]+B_2(\alpha,\beta)\left[\frac{\gamma_0}{\varepsilon_{22}}\right]=0. \quad \text{(A.11)}$$

Next, multiplying (A.7) by β and (A.9) by $-\alpha$ and adding gives:

$$A_1(\alpha,\beta)\left[-\omega\mu_0\beta^2\sinh(\gamma_{h1}d_1) \;-\; \omega\mu_0\alpha^2\sinh(\gamma_{h1}d_1)\right] + A_2(\alpha,\beta)\left[\omega\mu_0\beta^2+\omega\mu_0\alpha^2\right]=0. \quad \text{(A.12)}$$

Factoring out a $\omega\mu_0(\alpha^2+\beta^2)$ gives:

$$-A_1(\alpha,\beta)\sinh(\gamma_{h1}d_1)+A_2(\alpha,\beta)=0. \quad \text{(A.13)}$$

The next boundary condition applied will be (3.71). Equating the subtraction of (3.78) from (3.84) at d_1 to $\widetilde{J}_{x1}$ and substituting in (A.4) and (A.5) gives:

$$\widetilde{J}_{x1} = -\; A_1(\alpha,\beta)\left[j\beta\gamma_{h1}\cosh(\gamma_{h1}d_1)\right]+B_1(\alpha,\beta)\left[\omega\varepsilon_0\alpha\cosh(\gamma_{e1}d_1)\right] + A_2(\alpha,\beta)\left[-j\beta\gamma_0\right]-B_2(\alpha,\beta)\left[\omega\varepsilon_0\alpha\right]. \quad \text{(A.14)}$$

Similarly, the next boundary condition applied will be (3.72). Equating the subtrac-

tion of (3.83) from (3.77) at d_1 to $\widetilde{J}_{z1}$ and substituting in (A.4) and (A.5) gives:

$$\begin{aligned}\widetilde{J}_{z1} &= A_1(\alpha,\beta)\Big[j\alpha\gamma_{h1}\cosh(\gamma_{h1}d_1)\Big] + B_1(\alpha,\beta)\Big[\omega\varepsilon_0\beta\cosh(\gamma_{e1}d_1)\Big] \\ &+ A_2(\alpha,\beta)\Big[j\alpha\gamma_0\Big] - B_2(\alpha,\beta)\Big[\omega\varepsilon_0\beta\Big]. \qquad \text{(A.15)}\end{aligned}$$

Next, multiply (A.14) by α and (A.15) by β and add:

$$\begin{aligned}\alpha\widetilde{J}_{x1} + \beta\widetilde{J}_{z1} &= B_1(\alpha,\beta)\Big[\omega\varepsilon_0\alpha^2 + \omega\varepsilon_0\beta^2\Big]\cosh(\gamma_{e1}d_1) - B_2(\alpha,\beta)\Big[\omega\varepsilon_0\alpha^2 + \omega\varepsilon_0\beta^2\Big] \\ &= (\alpha^2+\beta^2)B_1(\alpha,\beta)\omega\varepsilon_0\cosh(\gamma_{e1}d_1) - (\alpha^2+\beta^2)B_2(\alpha,\beta)\omega\varepsilon_0. \qquad \text{(A.16)}\end{aligned}$$

This implies

$$\frac{\alpha\widetilde{J}_{x1} + \beta\widetilde{J}_{z1}}{\omega\varepsilon_0(\alpha^2+\beta^2)} = B_1(\alpha,\beta)\cosh(\gamma_{e1}d_1) - B_2(\alpha,\beta). \qquad \text{(A.17)}$$

Next, multiply (A.14) by β and (A.15) by $-\alpha$ and add. This gives

$$\begin{aligned}\beta\widetilde{J}_{x1} - \alpha\widetilde{J}_{z1} &= A_2(\alpha,\beta)\Big[-j\beta^2\gamma_0 - j\alpha^2\gamma_0\Big] \\ &\quad + A_1(\alpha,\beta)\Big[-j\beta^2\gamma_{h1}\cosh(\gamma_{h1}d_1) - j\alpha^2\gamma_{h1}\cosh(\gamma_{h1}d_1)\Big] \\ &= -(\alpha^2+\beta^2)\Big[A_1(\alpha,\beta)j\gamma_{h1}\cosh(\gamma_{h1}d_1) + A_2(\alpha,\beta)j\gamma_0\Big]. \qquad \text{(A.18)}\end{aligned}$$

This implies

$$\frac{\alpha\widetilde{J}_{z1} - \beta\widetilde{J}_{x1}}{\alpha^2+\beta^2} = A_1(\alpha,\beta)j\gamma_{h1}\cosh(\gamma_{h1}d_1) + A_2(\alpha,\beta)j\gamma_0. \qquad \text{(A.19)}$$

Next, multiply (A.11) by $-\cosh(\gamma_{e1}d_1)$ and (A.17) by $\frac{\gamma_{e1}}{\varepsilon_{12}}\sinh(\gamma_{e1}d_1)$ and add. This

gives

$$\begin{aligned}\frac{\alpha\widetilde{J}_{x1}+\beta\widetilde{J}_{z1}}{\omega\varepsilon_0(\alpha^2+\beta^2)}\frac{\gamma_{e1}}{\varepsilon_{12}}\sinh(\gamma_{e1}d_1) &= -B_2(\alpha,\beta)\frac{\gamma_0}{\varepsilon_{22}}\cosh(\gamma_{e1}d_1) - B_2(\alpha,\beta)\frac{\gamma_{e1}}{\varepsilon_{12}}\sinh(\gamma_{e1}d_1) \\ &= -B_2(\alpha,\beta)M_1 \end{aligned} \tag{A.20}$$

where

$$M_1 = \frac{\gamma_0}{\varepsilon_{22}}\cosh(\gamma_{e1}d_1) + \frac{\gamma_{e1}}{\varepsilon_{12}}\sinh(\gamma_{e1}d_1). \tag{A.21}$$

Then, solving for $B_2(\alpha,\beta)$ gives:

$$B_2(\alpha,\beta) = -\frac{\alpha\widetilde{J}_{x1}+\beta\widetilde{J}_{z1}}{M_1\omega\varepsilon_0(\alpha^2+\beta^2)}\frac{\gamma_{e1}}{\varepsilon_{12}}\sinh(\gamma_{e1}d_1). \tag{A.22}$$

Next, substituting (A.22) back into (A.17)

$$\begin{aligned}\frac{\alpha\widetilde{J}_{x1}+\beta\widetilde{J}_{z1}}{\omega\varepsilon_0(\alpha^2+\beta^2)} &= B_1(\alpha,\beta)\cosh(\gamma_{e1}d_1) \\ &\quad + \frac{\alpha\widetilde{J}_{x1}+\beta\widetilde{J}_{z1}}{M_1\omega\varepsilon_0(\alpha^2+\beta^2)}\frac{\gamma_{e1}}{\varepsilon_{12}}\sinh(\gamma_{e1}d_1). \end{aligned} \tag{A.23}$$

Solving for $B_1(\alpha,\beta)$ gives:

$$B_1(\alpha,\beta) = \frac{\alpha\widetilde{J}_{x1}+\beta\widetilde{J}_{z1}}{\omega\varepsilon_0(\alpha^2+\beta^2)\cosh(\gamma_{e1}d_1)}\left[1 - \frac{\gamma_{e1}}{M_1\varepsilon_{12}}\sinh(\gamma_{e1}d_1)\right]. \tag{A.24}$$

Now we will solve for the $A_1(\alpha,\beta)$ and $A_2(\alpha,\beta)$ constants. Multiplying (A.13) by $-j\gamma_0$ and adding to (A.19) gives:

$$\frac{\alpha\widetilde{J}_{z1}-\beta\widetilde{J}_{x1}}{\alpha^2+\beta^2} = A_1(\alpha,\beta)\left[j\gamma_0\sinh(\gamma_{h1}d_1) + j\gamma_{h1}\cosh(\gamma_{h1}d_1)\right]. \tag{A.25}$$

Solving for $A_1(\alpha,\beta)$ in (A.25) gives:

$$A_1(\alpha,\beta) = \frac{\alpha\widetilde{J}_{z1} - \beta\widetilde{J}_{x1}}{j(\alpha^2+\beta^2)} \frac{1}{\gamma_0 \sinh(\gamma_{h1}d_1) + \gamma_{h1}\cosh(\gamma_{h1}d_1)}. \tag{A.26}$$

Substituting (A.26) into (A.13) and solving for $A_2(\alpha,\beta)$ gives:

$$A_2(\alpha,\beta) = \frac{\alpha\widetilde{J}_{z1} - \beta\widetilde{J}_{x1}}{j(\alpha^2+\beta^2)} \frac{\sinh(\gamma_{h1}d_1)}{\gamma_0 \sinh(\gamma_{h1}d_1) + \gamma_{h1}\cosh(\gamma_{h1}d_1)}. \tag{A.27}$$

Next, substituting (A.4), (A.5), (A.24) and (A.26) into (3.74), we get the following x-component of the electric field at d_1:

$$\begin{aligned}
\widetilde{E}_x(\alpha,d_1,\beta) &= -\omega\mu_0\beta\left[\frac{\alpha\widetilde{J}_{z1} - \beta\widetilde{J}_{x1}}{j(\alpha^2+\beta^2)} \frac{1}{\gamma_0 \sinh(\gamma_{h1}d_1) + \gamma_{h1}\cosh(\gamma_{h1}d_1)} \sinh(\gamma_{h1}d_1)\right] \\
&+ \frac{j\alpha}{\varepsilon_{12}}\gamma_{e1}\sinh(\gamma_{e1}d_1)\frac{\alpha\widetilde{J}_{x1} + \beta\widetilde{J}_{z1}}{\omega\varepsilon_0(\alpha^2+\beta^2)\cosh(\gamma_{e1}d_1)}\left[1 - \frac{\gamma_{e1}}{M_1\varepsilon_{12}}\sinh(\gamma_{e1}d_1)\right] \\
&= \widetilde{J}_{x1}\left[\frac{\beta^2}{j(\alpha^2+\beta^2)}\frac{\omega\mu_0}{\gamma_0 + \gamma_{h1}\coth(\gamma_{h1}d_1)}\right] \\
&+ \widetilde{J}_{x1}\left[\frac{j\alpha^2}{\varepsilon_{12}}\frac{\gamma_{e1}\sinh(\gamma_{e1}d_1)}{\omega\varepsilon_0(\alpha^2+\beta^2)}\frac{\frac{\varepsilon_{12}}{\varepsilon_{22}}\gamma_0}{\frac{\varepsilon_{12}}{\varepsilon_{22}}\gamma_0\cosh(\gamma_{e1}d_1) + \gamma_{e1}\sinh(\gamma_{e1}d_1)}\right] \\
&+ \widetilde{J}_{z1}\left[\frac{-\alpha\beta}{j(\alpha^2+\beta^2)}\frac{\omega\mu_0}{\gamma_0 + \gamma_{h1}\coth(\gamma_{h1}d_1)}\right] \\
&+ \widetilde{J}_{z1}\left[\frac{j\alpha\beta}{\varepsilon_{12}}\frac{\gamma_{e1}\sinh(\gamma_{e1}d_1)}{\omega\varepsilon_0(\alpha^2+\beta^2)}\frac{\frac{\varepsilon_{12}}{\varepsilon_{22}}\gamma_0}{\frac{\varepsilon_{12}}{\varepsilon_{22}}\gamma_0\cosh(\gamma_{e1}d_1) + \gamma_{e1}\sinh(\gamma_{e1}d_1)}\right]
\end{aligned} \tag{A.28}$$

Note, it can be shown that

$$1 - \frac{\gamma_{e1}}{M_1\varepsilon_{12}}\sinh(\gamma_{e1}d_1) = \frac{\frac{\varepsilon_{12}}{\varepsilon_{22}}\gamma_0}{\frac{\varepsilon_{12}}{\varepsilon_{22}}\gamma_0\cosh(\gamma_{e1}d_1) + \gamma_{e1}\sinh(\gamma_{e1}d_1)}.$$

Equation (A.28) is written for an anisotropic superstrate. Since region 2 is air we have $\varepsilon_{22} = 1$. This simplifies (A.28) to

$$\begin{aligned}
\widetilde{E}_x(\alpha, d_1, \beta) &= \widetilde{J}_{x1}\Bigg[\frac{\beta^2}{j(\alpha^2+\beta^2)}\frac{\omega\mu_0}{\gamma_0 + \gamma_{h1}\coth(\gamma_{h1}d_1)} \\
&\qquad + \frac{j\alpha^2\gamma_{e1}}{\omega\varepsilon_0(\alpha^2+\beta^2)}\frac{\gamma_0}{\gamma_{e1} + \varepsilon_{12}\gamma_0\coth(\gamma_{e1}d_1)}\Bigg] \\
&+ \widetilde{J}_{z1}\Bigg[\frac{-\alpha\beta}{j(\alpha^2+\beta^2)}\frac{\omega\mu_0}{\gamma_0 + \gamma_{h1}\coth(\gamma_{h1}d_1)} \\
&\qquad + j\alpha\beta\frac{\gamma_{e1}}{\omega\varepsilon_0(\alpha^2+\beta^2)}\frac{\gamma_0}{\gamma_{e1} + \varepsilon_{12}\gamma_0\coth(\gamma_{e1}d_1)}\Bigg] \\
&= \widetilde{J}_{x1}\Bigg[\frac{\beta^2}{\alpha^2+\beta^2}\frac{-j\omega\mu_0}{\gamma_0 + \gamma_{h1}\coth(\gamma_{h1}d_1)} \\
&\qquad + \frac{\alpha^2}{\alpha^2+\beta^2}\frac{\gamma_{e1}\gamma_0}{-j\omega\varepsilon_0[\gamma_{e1} + \varepsilon_{12}\gamma_0\coth(\gamma_{e1}d_1)]}\Bigg] \\
&+ \widetilde{J}_{z1}\Bigg[\frac{\alpha\beta}{\alpha^2+\beta^2}\Bigg[\frac{\gamma_{e1}\gamma_0}{-j\omega\varepsilon_0[\gamma_{e1} + \varepsilon_{12}\gamma_0\coth(\gamma_{h1}d_1)]} \\
&\qquad + \frac{j\omega\mu_0}{\gamma_0 + \gamma_{h1}\coth(\gamma_{h1}d_1)}\Bigg]\Bigg]. \qquad \text{(A.29)}
\end{aligned}$$

Writing (A.29) in terms of the spectral domain immittance functions gives:

$$\widetilde{E}_x(\alpha, d_1, \beta) = \widetilde{Z}_{xx}\widetilde{J}_{x1} + \widetilde{Z}_{xz}\widetilde{J}_{z1} \qquad \text{(A.30)}$$

where

$$\widetilde{Z}_{xx} = \frac{\alpha^2}{\alpha^2+\beta^2}\left[-\frac{\gamma_{e1}\gamma_0}{j\omega\varepsilon_0[\gamma_{e1}+\varepsilon_{12}\gamma_0\coth(\gamma_{e1}d_1)]}\right] + \frac{\beta^2}{\alpha^2+\beta^2}\left[-\frac{j\omega\mu_0}{\gamma_0+\gamma_{h1}\coth(\gamma_{h1}d_1)}\right] \quad \text{(A.31)}$$

and

$$\widetilde{Z}_{xz} = \frac{\alpha\beta}{\alpha^2+\beta^2}\left[-\frac{\gamma_{e1}\gamma_0}{j\omega\varepsilon_0[\gamma_{e1}+\varepsilon_{12}\gamma_0\coth(\gamma_{h1}d_1)]} + \frac{j\omega\mu_0}{\gamma_0+\gamma_{h1}\coth(\gamma_{h1}d_1)}\right]. \quad \text{(A.32)}$$

Equations (A.31) and (A.32) are the same as 3-90 and 3-91 in Nelson's [71] work, respectively. Next, we will write an expression similar to (A.30) for the z-component of the electric field. Substituting (A.4), (A.5), (A.24) and (A.26) into (3.76), we get the following electric field at d_1:

$$\begin{aligned}
\widetilde{E}_z(\alpha,d_1,\beta) &= \omega\mu_0\alpha\left[\frac{\alpha\widetilde{J}_{z1}-\beta\widetilde{J}_{x1}}{j(\alpha^2+\beta^2)}\frac{1}{\gamma_0\sinh(\gamma_{h1}d_1)+\gamma_{h1}\cosh(\gamma_{h1}d_1)}\sinh(\gamma_{h1}d_1)\right] \\
&+ \frac{j\beta}{\varepsilon_{12}}\gamma_{e1}\sinh(\gamma_{e1}d_1)\frac{\alpha\widetilde{J}_{x1}+\beta\widetilde{J}_{z1}}{\omega\varepsilon_0(\alpha^2+\beta^2)\cosh(\gamma_{e1}d_1)}\left[1-\frac{\gamma_{e1}}{M_1\varepsilon_{12}}\sinh(\gamma_{e1}d_1)\right] \\
&= \widetilde{J}_{z1}\left[\frac{\alpha^2}{j(\alpha^2+\beta^2)}\frac{\omega\mu_0\sinh(\gamma_{h1}d_1)}{\gamma_0\sinh(\gamma_{h1}d_1)+\gamma_{h1}\cosh(\gamma_{h1}d_1)}\right] \\
&+ \widetilde{J}_{z1}\left[\frac{j\beta^2}{\alpha^2+\beta^2}\frac{\gamma_{e1}\sinh(\gamma_{e1}d_1)}{\omega\varepsilon_0}\frac{\gamma_0}{\gamma_0\varepsilon_{12}\cosh(\gamma_{e1}d_1)+\gamma_{e1}\sinh(\gamma_{e1}d_1)}\right]
\end{aligned}$$

$$+ \quad \widetilde{J}_{x1}\left[\frac{j\alpha\beta}{\alpha^2+\beta^2}\frac{\gamma_{e1}\sinh(\gamma_{e1}d_1)}{\omega\varepsilon_0}\frac{\gamma_0}{\varepsilon_{12}\gamma_0\cosh(\gamma_{e1}d1)+\gamma_{e1}\sinh(\gamma_{e1}d_1)}\right]$$

$$+ \quad \widetilde{J}_{x1}\left[\frac{-\alpha\beta}{j(\alpha^2+\beta^2)}\frac{\omega\mu_0\sinh(\gamma_{h1}d_1)}{\gamma_0\sinh(\gamma_{h1}d_1)+\gamma_{h1}\cosh(\gamma_{h1}d_1)}\right]. \tag{A.33}$$

Factoring and writing (A.33) in terms of the spectral domain immittance functions gives:

$$\widetilde{E}_z(\alpha, d_1, \beta) = \widetilde{Z}_{zx}\widetilde{J}_{x1} + \widetilde{Z}_{zz}\widetilde{J}_{z1} \tag{A.34}$$

where

$$\widetilde{Z}_{zx} = \widetilde{Z}_{xz} \tag{A.35}$$

and

$$\widetilde{Z}_{zz} \quad = \quad \frac{\alpha^2}{\alpha^2+\beta^2}\left[-\frac{j\omega\mu_0}{\gamma_0+\gamma_{h1}\coth(\gamma_{h1}d_1)}\right]$$

$$+\frac{\beta^2}{\alpha^2+\beta^2}\left[-\frac{\gamma_0\gamma_{e1}}{j\omega\varepsilon_0[\gamma_{e1}+\varepsilon_{12}\gamma_0\coth(\gamma_{e1}d_1)]}\right]. \tag{A.36}$$

Again, (A.35) and (A.36) are the same as 3-92 and 3-93 in Nelson's [71] work, respectively. The immittance functions have now been derived. The next step is to apply the Moment method to (A.30) and (A.34) to solve for the unknown currents.

APPENDIX B. DERIVATIONS FOR TWO ANISOTROPIC LAYERS

This appendix contains the derivations of the spectral domain immittance functions for two anisotropic dielectric layers. The first boundary condition applied will be (3.91). Applying (3.102) at y = 0 gives:

$$\begin{aligned} \widetilde{E}_{x1}(\alpha, 0, \beta) &= 0 \\ &= -\omega\mu_0\beta A_1'(\alpha, \beta) + \frac{j\alpha}{\varepsilon_{12}} B_1'(\alpha, \beta)\gamma_{e1}. \end{aligned} \tag{B.1}$$

Next, the boundary condition applied will be (3.92). Applying (3.104) at y = 0 gives:

$$\begin{aligned} \widetilde{E}_{z1}(\alpha, 0, \beta) &= 0 \\ &= \omega\mu_0\alpha A_1'(\alpha, \beta) + \frac{j\beta}{\varepsilon_{12}} B_1'(\alpha, \beta)\gamma_{e1}. \end{aligned} \tag{B.2}$$

Solving for $A_1'(\alpha, \beta)$ in (B.1) and substituting into (B.2) gives:

$$-\alpha^2 B_1'(\alpha, \beta) = \beta^2 B_1'(\alpha, \beta). \tag{B.3}$$

The only solution to (B.3) is

$$B_1'(\alpha, \beta) = 0. \tag{B.4}$$

Substituting (B.4) back into (B.1) implies

$$A_1'(\alpha, \beta) = 0. \tag{B.5}$$

The third boundary condition applied will be (3.93). Equating (3.102) to (3.108) at

d_1 and substituting in (B.4) and (B.5) gives:

$$\begin{aligned}\widetilde{E}_{x1}(\alpha, d_1, \beta) &= -\omega\mu_0\beta A_1(\alpha,\beta)\sinh(\gamma_{h1}d_1) + \frac{j\alpha}{\varepsilon_{12}}B_1(\alpha,\beta)\gamma_{e1}\sinh(\gamma_{e1}d_1) \\ &= -\omega\mu_0\beta A_2(\alpha,\beta)\sinh(\gamma_{h2}d_1) + \frac{j\alpha}{\varepsilon_{22}}B_2(\alpha,\beta)\gamma_{e2}\sinh(\gamma_{e2}d_1) \\ &\quad -\omega\mu_0\beta A_2'(\alpha,\beta)\cosh(\gamma_{h2}d_1) + \frac{j\alpha}{\varepsilon_{22}}B_2'(\alpha,\beta)\gamma_{e2}\cosh(\gamma_{e2}d_1) \\ &= \widetilde{E}_{x2}(\alpha, d_1, \beta). \end{aligned} \tag{B.6}$$

Factoring out the coefficients results in:

$$\begin{aligned} A_1(\alpha,\beta)\Big[-\omega\mu_0\beta\sinh(\gamma_{h1}d_1)\Big] &+ B_1(\alpha,\beta)\left[\frac{j\alpha}{\varepsilon_{12}}\gamma_{e1}\sinh(\gamma_{e1}d_1)\right] \\ +A_2(\alpha,\beta)\Big[\omega\mu_0\beta\sinh(\gamma_{h2}d_1)\Big] &- B_2(\alpha,\beta)\left[\frac{j\alpha}{\varepsilon_{22}}\gamma_{e2}\sinh(\gamma_{e2}d_1)\right] \\ +A_2'(\alpha,\beta)\Big[\omega\mu_0\beta\cosh(\gamma_{h2}d_1)\Big] &- B_2'(\alpha,\beta)\left[\frac{j\alpha}{\varepsilon_{22}}\gamma_{e2}\cosh(\gamma_{e2}d_1)\right] = 0. \end{aligned} \tag{B.7}$$

The fourth boundary condition applied will be (3.94). Equating (3.104) to (3.110) at d_1 and substituting in (B.4) and (B.5) gives:

$$\begin{aligned}\widetilde{E}_{z1}(\alpha, d_1, \beta) &= \omega\mu_0\alpha A_1(\alpha,\beta)\sinh(\gamma_{h1}d_1) + \frac{j\beta}{\varepsilon_{12}}B_1(\alpha,\beta)\gamma_{e1}\sinh(\gamma_{e1}d_1) \\ &= \omega\mu_0\alpha A_2(\alpha,\beta)\sinh(\gamma_{h2}d_1) + \frac{j\beta}{\varepsilon_{22}}B_2(\alpha,\beta)\gamma_{e2}\sinh(\gamma_{e2}d_1) \\ &= \widetilde{E}_{z2}(\alpha, d_1, \beta). \end{aligned} \tag{B.8}$$

Factoring out the coefficients results in:

$$\begin{aligned} A_1(\alpha,\beta)\Big[\omega\mu_0\alpha\sinh(\gamma_{h1}d_1)\Big] &+ B_1(\alpha,\beta)\left[\frac{j\beta}{\varepsilon_{12}}\gamma_{e1}\sinh(\gamma_{e1}d_1)\right] \\ - A_2(\alpha,\beta)\Big[\omega\mu_0\alpha\sinh(\gamma_{h2}d_1)\Big] &- A_2'(\alpha,\beta)\Big[\omega\mu_0\alpha\cosh(\gamma_{h2}d_1)\Big] \\ - B_2(\alpha,\beta)\left[\frac{j\beta}{\varepsilon_{22}}\gamma_{e2}\sinh(\gamma_{e2}d_1)\right] &- B_2'(\alpha,\beta)\left[\frac{j\beta}{\varepsilon_{22}}\gamma_{e2}\cosh(\gamma_{e2}d_1)\right] = 0. \end{aligned} \tag{B.9}$$

Next, multiplying (B.7) by α and (B.9) by β, and adding gives:

$$\begin{aligned} & B_1(\alpha,\beta)\left[\frac{j\alpha^2}{\varepsilon_{12}}\gamma_{e1}\sinh(\gamma_{e1}d_1)+\frac{j\beta^2}{\varepsilon_{12}}\gamma_{e1}\sinh(\gamma_{e1}d_1)\right] \\ - \quad & B_2(\alpha,\beta)\left[\frac{j\alpha^2}{\varepsilon_{22}}\gamma_{e2}\sinh(\gamma_{e2}d_1)+\frac{j\beta^2}{\varepsilon_{22}}\gamma_{e2}\sinh(\gamma_{e2}d_1)\right] \\ - \quad & B_2'(\alpha,\beta)\left[\frac{j\alpha^2}{\varepsilon_{22}}\gamma_{e2}\cosh(\gamma_{e2}d_1)+\frac{j\beta^2}{\varepsilon_{22}}\gamma_{e2}\cosh(\gamma_{e2}d_1)\right]=0. \end{aligned} \tag{B.10}$$

Factoring out an $j(\alpha^2+\beta^2)$ gives:

$$B_1(\alpha,\beta)\left[\frac{\gamma_{e1}}{\varepsilon_{12}}\sinh(\gamma_{e1}d_1)\right]-B_2(\alpha,\beta)\left[\frac{\gamma_{e2}}{\varepsilon_{22}}\sinh(\gamma_{e2}d_1)\right]-B_2'(\alpha,\beta)\left[\frac{\gamma_{e2}}{\varepsilon_{22}}\cosh(\gamma_{e2}d_1)\right]=0. \tag{B.11}$$

Next, multiplying (B.7) by β and (B.9) by $-\alpha$, and adding gives:

$$\begin{aligned} & A_1(\alpha,\beta)\Big[-\omega\mu_0\beta^2\sinh(\gamma_{h1}d_1)-\omega\mu_0\alpha^2\sinh(\gamma_{h1}d_1)\Big] \\ + \quad & A_2(\alpha,\beta)\Big[\omega\mu_0\beta^2\sinh(\gamma_{h2}d_1)+\omega\mu_0\alpha^2\sinh(\gamma_{h2}d_1)\Big] \\ + \quad & A_2'(\alpha,\beta)\Big[\omega\mu_0\beta^2\cosh(\gamma_{h2}d_1)+\omega\mu_0\alpha^2\cosh(\gamma_{h2}d_1)\Big]=0. \end{aligned} \tag{B.12}$$

Factoring out a $\omega\mu_0(\alpha^2+\beta^2)$ gives:

$$-A_1(\alpha,\beta)\sinh(\gamma_{h1}d_1)+A_2(\alpha,\beta)\sinh(\gamma_{h2}d_1)+A_2'(\alpha,\beta)\cosh(\gamma_{h2}d_1)=0. \tag{B.13}$$

The next boundary condition applied will be (3.97). Equating the subtraction of (3.106) from (3.112) at d_1 to $\widetilde{J}_{x1}$ and substituting in (B.4) and (B.5) gives:

$$\begin{aligned} \widetilde{J}_{x1} = \quad & - \quad A_1(\alpha,\beta)\Big[j\beta\gamma_{h1}\cosh(\gamma_{h1}d_1)\Big]+B_1(\alpha,\beta)\Big[\omega\varepsilon_0\alpha\cosh(\gamma_{e1}d_1)\Big] \\ & + \quad A_2(\alpha,\beta)\Big[j\beta\gamma_{h2}\cosh(\gamma_{h2}d_1)\Big]+A_2'(\alpha,\beta)\Big[j\beta\gamma_{h2}\sinh(\gamma_{h2}d_1)\Big] \end{aligned}$$

$$- \quad B_2(\alpha,\beta)\Big[\omega\varepsilon_0\alpha\cosh(\gamma_{e2}d_1)\Big] - B_2'(\alpha,\beta)\Big[\omega\varepsilon_0\alpha\sinh(\gamma_{e2}d_1)\Big]. \quad \text{(B.14)}$$

Similarly, the next boundary condition applied will be (3.98). Equating the subtraction of (3.111) from (3.105) at d_1 to $\widetilde{J}_{z1}$ and substituting in (B.4) and (B.5) gives:

$$\begin{aligned}\widetilde{J}_{z1} = \quad & A_1(\alpha,\beta)\Big[j\alpha\gamma_{h1}\cosh(\gamma_{h1}d_1)\Big] + B_1(\alpha,\beta)\Big[\omega\varepsilon_0\beta\cosh(\gamma_{e1}d_1)\Big] \\ - \quad & A_2(\alpha,\beta)\Big[j\alpha\gamma_{h2}\cosh(\gamma_{h2}d_1)\Big] - A_2'(\alpha,\beta)\Big[j\alpha\gamma_{h2}\sinh(\gamma_{h2}d_1)\Big] \\ - \quad & B_2(\alpha,\beta)\Big[\omega\varepsilon_0\beta\cosh(\gamma_{e2}d_1)\Big] - B_2'(\alpha,\beta)\Big[\omega\varepsilon_0\beta\sinh(\gamma_{e2}d_1)\Big]. \quad \text{(B.15)}\end{aligned}$$

Next, multiply (B.14) by α and (B.15) by β and add:

$$\begin{aligned}\alpha\widetilde{J}_{x1} + \beta\widetilde{J}_{z1} \quad = \quad & B_1(\alpha,\beta)\omega\varepsilon_0\cosh(\gamma_{e1}d_1)(\alpha^2+\beta^2) \\ & -B_2(\alpha,\beta)\omega\varepsilon_0\cosh(\gamma_{e2}d_1)(\alpha^2+\beta^2) \\ & -B_2'(\alpha,\beta)\omega\varepsilon_0\sinh(\gamma_{e2}d_1)(\alpha^2+\beta^2). \quad \text{(B.16)}\end{aligned}$$

This implies

$$\frac{\alpha\widetilde{J}_{x1} + \beta\widetilde{J}_{z1}}{\omega\varepsilon_0(\alpha^2+\beta^2)} = B_1(\alpha,\beta)\cosh(\gamma_{e1}d_1) - B_2(\alpha,\beta)\cosh(\gamma_{e2}d_1) - B_2'(\alpha,\beta)\sinh(\gamma_{e2}d_1). \quad \text{(B.17)}$$

Next, multiply (B.14) by β and (B.15) by $-\alpha$ and add. This gives

$$\begin{aligned}\beta\widetilde{J}_{x1} - \alpha\widetilde{J}_{z1} \quad = \quad & -A_1(\alpha,\beta)j\gamma_{h1}\cosh(\gamma_{h1}d_1)(\alpha^2+\beta^2) \\ & +A_2(\alpha,\beta)j\gamma_{h2}\cosh(\gamma_{h2}d_1)(\alpha^2+\beta^2) \\ & +A_2'(\alpha,\beta)j\gamma_{h2}\sinh(\gamma_{h2}d_1)(\alpha^2+\beta^2). \quad \text{(B.18)}\end{aligned}$$

This implies

$$\frac{\beta\widetilde{J}_{x1}-\alpha\widetilde{J}_{z1}}{j(\alpha^2+\beta^2)} = \quad -A_1(\alpha,\beta)\gamma_{h1}\cosh(\gamma_{h1}d_1)+A_2(\alpha,\beta)\gamma_{h2}\cosh(\gamma_{h2}d_1) \\ +A_2'(\alpha,\beta)\gamma_{h2}\sinh(\gamma_{h2}d_1). \tag{B.19}$$

Next, multiplying (B.11) by $-\cosh(\gamma_{e1}d_1)$ and (B.17) by $\frac{\gamma_{e1}}{\varepsilon_{12}}\sinh(\gamma_{e1}d_1)$, and adding gives:

$$\begin{aligned}\frac{\gamma_{e1}}{\varepsilon_{12}}\sinh(\gamma_{e1}d_1)\left[\frac{\alpha\widetilde{J}_{x1}+\beta\widetilde{J}_{z1}}{\omega\varepsilon_0(\alpha^2+\beta^2)}\right] &= B_2(\alpha,\beta)\left[\frac{\gamma_{e2}}{\varepsilon_{22}}\cosh(\gamma_{e1}d_1)\sinh(\gamma_{e2}d_1)\right. \\ &\quad \left.-\frac{\gamma_{e1}}{\varepsilon_{12}}\cosh(\gamma_{e2}d_1)\sinh(\gamma_{e1}d_1)\right] \\ &\quad +B_2'(\alpha,\beta)\left[\frac{\gamma_{e2}}{\varepsilon_{22}}\cosh(\gamma_{e1}d_1)\cosh(\gamma_{e2}d_1)\right. \\ &\quad \left.-\frac{\gamma_{e1}}{\varepsilon_{12}}\sinh(\gamma_{e1}d_1)\sinh(\gamma_{e2}d_1)\right]. \end{aligned}\tag{B.20}$$

Solving for $B_2(\alpha,\beta)$ in (B.20) gives:

$$B_2(\alpha,\beta) = -B_2'(\alpha,\beta)\frac{N_1}{M_1}+\frac{\gamma_{e1}}{\varepsilon_{12}M_1}\sinh(\gamma_{e1}d_1)\left[\frac{\alpha\widetilde{J}_{x1}+\beta\widetilde{J}_{z1}}{\omega\varepsilon_0(\alpha^2+\beta^2)}\right] \tag{B.21}$$

where

$$N_1 = \frac{\gamma_{e2}}{\varepsilon_{22}}\cosh(\gamma_{e1}d_1)\cosh(\gamma_{e2}d_1)-\frac{\gamma_{e1}}{\varepsilon_{12}}\sinh(\gamma_{e1}d_1)\sinh(\gamma_{e2}d_1) \tag{B.22}$$

and

$$M_1 = \frac{\gamma_{e2}}{\varepsilon_{22}}\cosh(\gamma_{e1}d_1)\sinh(\gamma_{e2}d_1)-\frac{\gamma_{e1}}{\varepsilon_{12}}\cosh(\gamma_{e2}d_1)\sinh(\gamma_{e1}d_1). \tag{B.23}$$

Again, multiply (B.11) by $-\cosh(\gamma_{e2}d_1)$ and (B.17) by $\frac{\gamma_{e2}}{\varepsilon_{22}}\sinh(\gamma_{e2}d_1)$ and add. This

results in

$$\frac{\gamma_{e2}}{\varepsilon_{22}}\sinh(\gamma_{e2}d_1)\left[\frac{\alpha\widetilde{J}_{x1}+\beta\widetilde{J}_{z1}}{\omega\varepsilon_0(\alpha^2+\beta^2)}\right] = B_1(\alpha,\beta)\left[\frac{\gamma_{e2}}{\varepsilon_{22}}\cosh(\gamma_{e1}d_1)\sinh(\gamma_{e2}d_1) - \frac{\gamma_{e1}}{\varepsilon_{12}}\cosh(\gamma_{e2}d_1)\sinh(\gamma_{e1}d_1)\right] + B_2'(\alpha,\beta)\left[\frac{\gamma_{e2}}{\varepsilon_{22}}\right]. \quad \text{(B.24)}$$

Solving for $B_1(\alpha,\beta)$ in (B.24) gives:

$$B_1(\alpha,\beta) = -B_2'(\alpha,\beta)\frac{\gamma_{e2}}{\varepsilon_{22}M_1} + \frac{\gamma_{e2}}{\varepsilon_{22}M_1}\sinh(\gamma_{e2}d_1)\left[\frac{\alpha\widetilde{J}_{x1}+\beta\widetilde{J}_{z1}}{\omega\varepsilon_0(\alpha^2+\beta^2)}\right]. \quad \text{(B.25)}$$

Next, multiply (B.13) by $\gamma_{h2}\sinh(\gamma_{h2}d_1)$ and (B.19) by $-\cosh(\gamma_{h2}d_1)$ and add. This results in

$$-\cosh(\gamma_{h2}d_1)\left[\frac{\beta\widetilde{J}_{x1}-\alpha\widetilde{J}_{z1}}{j(\alpha^2+\beta^2)}\right] = A_1(\alpha,\beta)\Big[-\gamma_{h2}\sinh(\gamma_{h2}d_1)\sinh(\gamma_{h1}d_1) + \gamma_{h1}\cosh(\gamma_{h2}d_1)\cosh(\gamma_{h1}d_1)\Big] + A_2(\alpha,\beta)[\gamma_{h2}]. \quad \text{(B.26)}$$

Solving for $A_1(\alpha,\beta)$ in (B.26) gives

$$A_1(\alpha,\beta) = A_2(\alpha,\beta)\frac{\gamma_{h2}}{N_4} + \frac{\cosh(\gamma_{h2}d_1)}{N_4}\left[\frac{\beta\widetilde{J}_{x1}-\alpha\widetilde{J}_{z1}}{j(\alpha^2+\beta^2)}\right] \quad \text{(B.27)}$$

where

$$N_4 = -\gamma_{h1}\cosh(\gamma_{h2}d_1)\cosh(\gamma_{h1}d_1) + \gamma_{h2}\sinh(\gamma_{h2}d_1)\sinh(\gamma_{h1}d_1). \quad \text{(B.28)}$$

Next, multiply (B.13) by $\gamma_{h1}\cosh(\gamma_{h1}d_1)$ and (B.19) by $-\sinh(\gamma_{h1}d_1)$ and add. This

results in

$$
\begin{aligned}
-\sinh(\gamma_{h1}d_1)\left[\frac{\beta\widetilde{J}_{x1}-\alpha\widetilde{J}_{z1}}{j(\alpha^2+\beta^2)}\right] &= A_2'(\alpha,\beta)\Big[\gamma_{h1}\cosh(\gamma_{h1}d_1)\cosh(\gamma_{h2}d_1) \\
&\quad -\gamma_{h2}\sinh(\gamma_{h1}d_1)\sinh(\gamma_{h2}d_1)\Big] \\
&\quad +A_2(\alpha,\beta)\Big[\gamma_{h1}\cosh(\gamma_{h1}d_1)\sinh(\gamma_{h2}d_1) \\
&\quad -\gamma_{h2}\sinh(\gamma_{h1}d_1)\cosh(\gamma_{h2}d_1)\Big]. \qquad \text{(B.29)}
\end{aligned}
$$

Solving for $A_2'(\alpha,\beta)$ in (B.26) gives

$$
A_2'(\alpha,\beta) = A_2(\alpha,\beta)\frac{M_4}{N_4} + \frac{\sinh(\gamma_{h1}d_1)}{N_4}\left[\frac{\beta\widetilde{J}_{x1}-\alpha\widetilde{J}_{z1}}{j(\alpha^2+\beta^2)}\right] \qquad \text{(B.30)}
$$

where

$$
M_4 = \gamma_{h1}\cosh(\gamma_{h1}d_1)\sinh(\gamma_{h2}d_1) - \gamma_{h2}\sinh(\gamma_{h1}d_1)\cosh(\gamma_{h2}d_1). \qquad \text{(B.31)}
$$

The next boundary condition enforced is (3.95). Equating (3.108) and (3.114) gives:

$$
\begin{aligned}
\widetilde{E}_{x2}(\alpha,d_{12},\beta) &= -\omega\mu_0\beta\Big[A_2(\alpha,\beta)\sinh(\gamma_{h2}d_{12}) + A_2'(\alpha,\beta)\cosh(\gamma_{h2}d_{12})\Big] \\
&\quad +\frac{j\alpha\gamma_{e2}}{\varepsilon_{22}}\Big[B_2(\alpha,\beta)\sinh(\gamma_{e2}d_{12}) + B_2'(\alpha,\beta)\cosh(\gamma_{e2}d_{12})\Big] \\
&= -\omega\mu_0\beta A_3(\alpha,\beta) - \frac{j\alpha}{\varepsilon_{32}}\gamma_0 B_3(\alpha,\beta) \\
&= \widetilde{E}_{x3}(\alpha,d_{12},\beta). \qquad \text{(B.32)}
\end{aligned}
$$

Factoring out the coefficients in (B.32) gives

$$\begin{aligned}
&A_2(\alpha,\beta)\Big[-\omega\mu_0\beta\sinh(\gamma_{h2}d_{12})\Big]+A_2'(\alpha,\beta)\Big[-\omega\mu_0\beta\cosh(\gamma_{h2}d_{12})\Big]\\
&+B_2(\alpha,\beta)\left[\frac{j\alpha\gamma_{e2}}{\varepsilon_{22}}\sinh(\gamma_{e2}d_{12})\right]+B_2'(\alpha,\beta)\left[\frac{j\alpha\gamma_{e2}}{\varepsilon_{22}}\cosh(\gamma_{e2}d_{12})\right]\\
&+A_3(\alpha,\beta)\Big[\omega\mu_0\beta\Big]+B_3(\alpha,\beta)\left[\frac{j\alpha}{\varepsilon_{32}}\gamma_0\right]=0..
\end{aligned}\tag{B.33}$$

Next, using (3.110) and (3.116), enforcing the boundary condition in (3.96) and factoring gives:

$$\begin{aligned}
&A_2(\alpha,\beta)\Big[\omega\mu_0\alpha\sinh(\gamma_{h2}d_{12})\Big]+A_2'(\alpha,\beta)\Big[\omega\mu_0\alpha\cosh(\gamma_{h2}d_{12})\Big]\\
&+B_2(\alpha,\beta)\left[\frac{j\beta\gamma_{e2}}{\varepsilon_{22}}\sinh(\gamma_{e2}d_{12})\right]+B_2'(\alpha,\beta)\left[\frac{j\beta\gamma_{e2}}{\varepsilon_{22}}\cosh(\gamma_{e2}d_{12})\right]\\
&-A_3(\alpha,\beta)\Big[\omega\mu_0\alpha\Big]+B_3(\alpha,\beta)\left[\frac{j\beta}{\varepsilon_{32}}\gamma_0\right]=0..
\end{aligned}\tag{B.34}$$

Next, multiply (B.33) by α and (B.34) by β and add. This results in the following:

$$B_2(\alpha,\beta)\left[\frac{\gamma_{e2}}{\varepsilon_{22}}\sinh(\gamma_{e2}d_{12})\right]+B_2'(\alpha,\beta)\left[\frac{\gamma_{e2}}{\varepsilon_{22}}\cosh(\gamma_{e2}d_{12})\right]+B_3(\alpha,\beta)\left[\frac{\gamma_0}{\varepsilon_{32}}\right]=0.\tag{B.35}$$

Next, multiply (B.33) by β and (B.34) by $-\alpha$ and add. This results in the following:

$$-A_2(\alpha,\beta)\sinh(\gamma_{h2}d_{12})-A_2'(\alpha,\beta)\cosh(\gamma_{h2}d_{12})+A_3(\alpha,\beta)=0.\tag{B.36}$$

Next, we enforce the boundary condition in (3.99) by subtracting (3.112) from (3.118)

and equating to $\widetilde{J}_{x2}$. This gives

$$\begin{aligned}\widetilde{J}_{x2} &= A_3(\alpha,\beta)\Big[-j\beta\gamma_0\Big] + B_3(\alpha,\beta)\Big[-\omega\varepsilon_0\alpha\Big] \\ &+ A_2(\alpha,\beta)\Big[-j\beta\gamma_{h2}\cosh(\gamma_{h2}d_{12})\Big] + A_2'(\alpha,\beta)\Big[-j\beta\gamma_{h2}\sinh(\gamma_{h2}d_{12})\Big] \\ &+ B_2(\alpha,\beta)\Big[\omega\varepsilon_0\alpha\cosh(\gamma_{e2}d_{12})\Big] + B_2'(\alpha,\beta)\Big[\omega\varepsilon_0\alpha\sinh(\gamma_{e2}d_{12})\Big]. \qquad \text{(B.37)}\end{aligned}$$

Next, we enforce the boundary condition in (3.100) by subtracting (3.117) from (3.111) and equating to $\widetilde{J}_{z2}$. This gives

$$\begin{aligned}\widetilde{J}_{z2} &= A_3(\alpha,\beta)\Big[j\alpha\gamma_0\Big] + B_3(\alpha,\beta)\Big[-\omega\varepsilon_0\beta\Big] \\ &+ A_2(\alpha,\beta)\Big[j\alpha\gamma_{h2}\cosh(\gamma_{h2}d_{12})\Big] + A_2'(\alpha,\beta)\Big[j\alpha\gamma_{h2}\sinh(\gamma_{h2}d_{12})\Big] \\ &+ B_2(\alpha,\beta)\Big[\omega\varepsilon_0\beta\cosh(\gamma_{e2}d_{12})\Big] + B_2'(\alpha,\beta)\Big[\omega\varepsilon_0\beta\sinh(\gamma_{e2}d_{12})\Big]. \qquad \text{(B.38)}\end{aligned}$$

Next, multiply (B.37) by α and (B.38) by β and add. This results in

$$\frac{\alpha\widetilde{J}_{x2}+\beta\widetilde{J}_{z2}}{\omega\varepsilon_0(\alpha^2+\beta^2)} = B_2(\alpha,\beta)\cosh(\gamma_{e2}d_{12}) + B_2'(\alpha,\beta)\sinh(\gamma_{e2}d_{12}) - B_3(\alpha,\beta). \qquad \text{(B.39)}$$

Next, multiply (B.37) by β and (B.38) by $-\alpha$ and add. This results in

$$\frac{\beta\widetilde{J}_{x2}-\alpha\widetilde{J}_{z2}}{-j(\alpha^2+\beta^2)} = A_2(\alpha,\beta)[\gamma_{h2}\cosh(\gamma_{h2}d_{12})] + A_2'(\alpha,\beta)[\gamma_{h2}\sinh(\gamma_{h2}d_{12})] + A_3(\alpha,\beta)[\gamma_0]. \qquad \text{(B.40)}$$

Next, multiply (B.35) by $-\cosh(\gamma_{e2}d_{12})$ and (B.39) by $\frac{\gamma_{e2}}{\varepsilon_{22}}\sinh(\gamma_{e2}d_{12})$ and add. This

results in

$$B_3(\alpha,\beta)\Bigg[-\cosh(\gamma_{e2}d_{12})\frac{\gamma_0}{\varepsilon_{32}}-\sinh(\gamma_{e2}d_{12})\frac{\gamma_{e2}}{\varepsilon_{22}}\Bigg]+$$
$$B_2'(\alpha,\beta)\Bigg[-\cosh(\gamma_{e2}d_{12})\cosh(\gamma_{e2}d_{12})\frac{\gamma_{e2}}{\varepsilon_{22}}+\sinh(\gamma_{e2}d_{12})\sinh(\gamma_{e2}d_{12})\frac{\gamma_{e2}}{\varepsilon_{22}}\Bigg]$$
$$=\frac{\gamma_{e2}}{\varepsilon_{22}}\sinh(\gamma_{e2}d_{12})\Bigg[\frac{\alpha\widetilde{J}_{x2}+\beta\widetilde{J}_{z2}}{\omega\varepsilon_0(\alpha^2+\beta^2)}\Bigg]. \tag{B.41}$$

Solving for $B_3(\alpha,\beta)$ in (B.41) gives

$$B_3(\alpha,\beta)=\frac{-\gamma_{e2}\sinh(\gamma_{e2}d_{12})}{\varepsilon_{22}M_2}\frac{\alpha\widetilde{J}_{x2}+\beta\widetilde{J}_{z2}}{\omega\varepsilon_0(\alpha^2+\beta^2)}-B_2'(\alpha,\beta)\frac{\gamma_{e2}}{\varepsilon_{22}M_2} \tag{B.42}$$

where

$$M_2=\cosh(\gamma_{e2}d_{12})\frac{\gamma_0}{\varepsilon_{32}}+\sinh(\gamma_{e2}d_{12})\frac{\gamma_{e2}}{\varepsilon_{22}}. \tag{B.43}$$

Next, multiply (B.39) by $\gamma_0/\varepsilon_{32}$ and add to (B.35). This results in

$$B_2(\alpha,\beta)\Bigg[\cosh(\gamma_{e2}d_{12})\frac{\gamma_0}{\varepsilon_{32}}+\sinh(\gamma_{e2}d_{12})\frac{\gamma_{e2}}{\varepsilon_{22}}\Bigg]+$$
$$B_2'(\alpha,\beta)\Bigg[\sinh(\gamma_{e2}d_{12})\frac{\gamma_0}{\varepsilon_{32}}+\cosh(\gamma_{e2}d_{12})\frac{\gamma_{e2}}{\varepsilon_{22}}\Bigg]$$
$$=\frac{\gamma_0}{\varepsilon_{32}}\Bigg[\frac{\alpha\widetilde{J}_{x2}+\beta\widetilde{J}_{z2}}{\omega\varepsilon_0(\alpha^2+\beta^2)}\Bigg]. \tag{B.44}$$

Solving for $B_2(\alpha,\beta)$ in (B.44) gives

$$B_2(\alpha,\beta)=\frac{\gamma_0}{\varepsilon_{32}M_2}\frac{\alpha\widetilde{J}_{x2}+\beta\widetilde{J}_{z2}}{\omega\varepsilon_0(\alpha^2+\beta^2)}-B_2'(\alpha,\beta)\frac{N_2}{M_2} \tag{B.45}$$

where M_2 is given in (B.43) and

$$N_2=\sinh(\gamma_{e2}d_{12})\frac{\gamma_0}{\varepsilon_{32}}+\cosh(\gamma_{e2}d_{12})\frac{\gamma_{e2}}{\varepsilon_{22}}. \tag{B.46}$$

Next, equate (B.45) and (B.21)

$$\begin{aligned} B_2(\alpha,\beta) &= \frac{\gamma_0}{\varepsilon_{32}M_2}\frac{\alpha\widetilde{J}_{x2}+\beta\widetilde{J}_{z2}}{\omega\varepsilon_0(\alpha^2+\beta^2)} - B_2'(\alpha,\beta)\frac{N_2}{M_2} \\ &= -B_2'(\alpha,\beta)\frac{N_1}{M_1} + \frac{\gamma_{e1}}{\varepsilon_{12}M_1}\sinh(\gamma_{e1}d_1)\frac{\alpha\widetilde{J}_{x1}+\beta\widetilde{J}_{z1}}{\omega\varepsilon_0(\alpha^2+\beta^2)}. \end{aligned} \tag{B.47}$$

Solving for $B_2'(\alpha,\beta)$ in (B.47) gives

$$B_2'(\alpha,\beta) = \frac{M_1M_2}{N_1M_2-N_2M_1}\left[\frac{\gamma_{e1}}{\varepsilon_{12}M_1}\sinh(\gamma_{e1}d_1)\frac{\alpha\widetilde{J}_{x1}+\beta\widetilde{J}_{z1}}{\omega\varepsilon_0(\alpha^2+\beta^2)} - \frac{\gamma_0}{\varepsilon_{32}M_2}\frac{\alpha\widetilde{J}_{x2}+\beta\widetilde{J}_{z2}}{\omega\varepsilon_0(\alpha^2+\beta^2)}\right]. \tag{B.48}$$

Substituting (B.48) in (B.25) and rearranging results in

$$\begin{aligned} B_1(\alpha,\beta) &= \left[\frac{\gamma_{e2}}{\varepsilon_{22}}\sinh(\gamma_{e2}d_1) - \frac{M_2}{N_1M_2-N_2M_1}\frac{\gamma_{e1}\gamma_{e2}}{\varepsilon_{12}\varepsilon_{22}}\sinh(\gamma_{e1}d_1)\right]\frac{\alpha\widetilde{J}_{x1}+\beta\widetilde{J}_{z1}}{M_1\omega\varepsilon_0(\alpha^2+\beta^2)} + \\ &\quad \left[\frac{1}{N_1M_2-N_2M_1}\frac{\gamma_0\gamma_{e2}}{\varepsilon_{32}\varepsilon_{22}}\right]\frac{\alpha\widetilde{J}_{x2}+\beta\widetilde{J}_{z2}}{\omega\varepsilon_0(\alpha^2+\beta^2)}. \end{aligned} \tag{B.49}$$

Similarly, substituting (B.48) into (B.21) results in

$$\begin{aligned} B_2(\alpha,\beta) &= \left[\frac{\gamma_{e1}}{\varepsilon_{12}}\sinh(\gamma_{e1}d_1) - \frac{N_1M_2}{N_1M_2-N_2M_1}\frac{\gamma_{e1}}{\varepsilon_{12}}\sinh(\gamma_{e1}d_1)\right]\frac{\alpha\widetilde{J}_{x1}+\beta\widetilde{J}_{z1}}{M_1\omega\varepsilon_0(\alpha^2+\beta^2)} + \\ &\quad \left[\frac{N_1}{N_1M_2-N_2M_1}\frac{\gamma_0}{\varepsilon_{32}}\right]\frac{\alpha\widetilde{J}_{x2}+\beta\widetilde{J}_{z2}}{\omega\varepsilon_0(\alpha^2+\beta^2)}. \end{aligned} \tag{B.50}$$

Next, substituting (B.48) into (B.42) gives

$$\begin{aligned} B_3(\alpha,\beta) &= \left[\frac{M_1}{N_1M_2-N_2M_1}\frac{\gamma_0\gamma_{e2}}{\varepsilon_{32}\varepsilon_{22}} - \frac{\gamma_{e2}}{\varepsilon_{22}}\sinh(\gamma_{e2}d_{12})\right]\frac{\alpha\widetilde{J}_{x2}+\beta\widetilde{J}_{z2}}{M_2\omega\varepsilon_0(\alpha^2+\beta^2)} - \\ &\quad \left[\frac{\gamma_{e1}\gamma_{e2}}{\varepsilon_{12}\varepsilon_{22}}\frac{\sinh(\gamma_{e1}d_1)}{N_1M_2-N_2M_1}\right]\frac{\alpha\widetilde{J}_{x1}+\beta\widetilde{J}_{z1}}{\omega\varepsilon_0(\alpha^2+\beta^2)}. \end{aligned} \tag{B.51}$$

Next, multiply (B.36) by $\gamma_{h2}\sinh(\gamma_{h2}d_{12})$ and (B.40) by $\cosh(\gamma_{h2}d_{12})$ and add. This

results in

$$\begin{aligned}
&-A_2(\alpha,\beta)[\gamma_{h2}\sinh^2(\gamma_{h2}d_{12})] + A_3(\alpha,\beta)[\gamma_{h2}\sinh(\gamma_{h2}d_{12})] \\
&+A_2(\alpha,\beta)[\gamma_{h2}\cosh^2(\gamma_{h2}d_{12})] + A_3(\alpha,\beta)[\gamma_0\cosh(\gamma_{h2}d_{12})] \\
&= \cosh(\gamma_{h2}d_{12})\frac{\beta\widetilde{J}_{x2} - \alpha\widetilde{J}_{z2}}{-j(\alpha^2+\beta^2)}.
\end{aligned} \tag{B.52}$$

Solving for $A_3(\alpha,\beta)$ in (B.52) results in

$$A_3(\alpha,\beta) = \frac{\cosh(\gamma_{h2}d_{12})}{N_3}\frac{\beta\widetilde{J}_{x2} - \alpha\widetilde{J}_{z2}}{-j(\alpha^2+\beta^2)} - A_2(\alpha,\beta)\frac{\gamma_{h2}}{N_3} \tag{B.53}$$

where

$$N_3 = \gamma_0\cosh(\gamma_{h2}d_{12}) + \gamma_{h2}\sinh(\gamma_{h2}d_{12}). \tag{B.54}$$

Next, multiply (B.36) by $-\gamma_0$ and add to (B.40). This results in

$$\begin{aligned}
&A_2(\alpha,\beta)[\gamma_0\sinh(\gamma_{h2}d_{12})] + A_2'(\alpha,\beta)[\gamma_0\cosh(\gamma_{h2}d_{12})] \\
&+A_2(\alpha,\beta)[\gamma_{h2}\cosh(\gamma_{h2}d_{12})] + A_2'(\alpha,\beta)[\gamma_{h2}\sinh(\gamma_{h2}d_{12})] \\
&= \frac{\beta\widetilde{J}_{x2} - \alpha\widetilde{J}_{z2}}{-j(\alpha^2+\beta^2)}.
\end{aligned} \tag{B.55}$$

Solving for $A_2'(\alpha,\beta)$ in (B.55) results in

$$A_2'(\alpha,\beta) = \frac{1}{N_3}\frac{\beta\widetilde{J}_{x2} - \alpha\widetilde{J}_{z2}}{-j(\alpha^2+\beta^2)} - A_2(\alpha,\beta)\frac{M_3}{N_3} \tag{B.56}$$

where

$$M_3 = \gamma_0\sinh(\gamma_{h2}d_{12}) + \gamma_{h2}\cosh(\gamma_{h2}d_{12}). \tag{B.57}$$

Then equating (B.56) and (B.30) gives

$$\frac{1}{N_3}\frac{\beta\widetilde{J}_{x2}-\alpha\widetilde{J}_{z2}}{-j(\alpha^2+\beta^2)}-A_2(\alpha,\beta)\frac{M_3}{N_3}=A_2(\alpha,\beta)\frac{M_4}{N_4}+\frac{\sinh(\gamma_{h1}d_1)}{N_4}\left[\frac{\beta\widetilde{J}_{x1}-\alpha\widetilde{J}_{z1}}{j(\alpha^2+\beta^2)}\right]. \quad \text{(B.58)}$$

Solving for $A_2(\alpha,\beta)$ in (B.58) gives

$$A_2(\alpha,\beta)=-\frac{N_3\sinh(\gamma_{h1}d_1)}{N_4M_3+N_3M_4}\left[\frac{\beta\widetilde{J}_{x1}-\alpha\widetilde{J}_{z1}}{j(\alpha^2+\beta^2)}\right]+\frac{N_4}{N_4M_3+N_3M_4}\left[\frac{\beta\widetilde{J}_{x2}-\alpha\widetilde{J}_{z2}}{-j(\alpha^2+\beta^2)}\right]. \quad \text{(B.59)}$$

Substituting (B.59) into (B.27) gives

$$\begin{aligned}A_1(\alpha,\beta) &= \left[\frac{\gamma_{h2}}{N_4}\frac{-N_3\sinh(\gamma_{h1}d_1)}{N_4M_3+N_3M_4}+\frac{\cosh(\gamma_{h2}d_1)}{N_4}\right]\frac{\beta\widetilde{J}_{x1}-\alpha\widetilde{J}_{z1}}{j(\alpha^2+\beta^2)}\\ &\quad+\left[\frac{\gamma_{h2}}{N_4M_3+N_3M_4}\right]\frac{\beta\widetilde{J}_{x2}-\alpha\widetilde{J}_{z2}}{-j(\alpha^2+\beta^2)}. \quad \text{(B.60)}\end{aligned}$$

Similarly, substituting (B.59) into (B.30) gives

$$\begin{aligned}A_2'(\alpha,\beta) &= \left[\frac{1}{N_4}-\frac{M_4}{N_4}\frac{N_3}{N_4M_3+N_3M_4}\right]\sinh(\gamma_{h1}d_1)\frac{\beta\widetilde{J}_{x1}-\alpha\widetilde{J}_{z1}}{j(\alpha^2+\beta^2)}\\ &\quad+\left[\frac{M_4}{N_4M_3+N_3M_4}\right]\frac{\beta\widetilde{J}_{x2}-\alpha\widetilde{J}_{z2}}{-j(\alpha^2+\beta^2)}. \quad \text{(B.61)}\end{aligned}$$

Substituting (B.59) into (B.53) gives

$$\begin{aligned}A_3(\alpha,\beta) &= \left[\frac{\cosh(\gamma_{h2}d_{12})}{N_3}-\frac{\gamma_{h2}}{N_3}\frac{N_4}{N_4M_3+N_3M_4}\right]\frac{\beta\widetilde{J}_{x2}-\alpha\widetilde{J}_{z2}}{j(\alpha^2+\beta^2)}\\ &\quad+\left[\frac{\gamma_{h2}\sinh(\gamma_{h1}d_1)}{N_4M_3+N_3M_4}\right]\frac{\beta\widetilde{J}_{x1}-\alpha\widetilde{J}_{z1}}{-j(\alpha^2+\beta^2)}. \quad \text{(B.62)}\end{aligned}$$

Next, substituting (B.48), (B.50), (B.59) and (B.61) in (3.108) we get the following

x-component for the electric field anywhere in region 2:

$$\widetilde{E}_{x2}(\alpha, y, \beta) =$$

$$-\omega\mu_0\beta\Bigg[\Bigg(-\frac{N_3\sinh(\gamma_{h1}d_1)}{N_4M_3+N_3M_4}\left[\frac{\beta\widetilde{J}_{x1}-\alpha\widetilde{J}_{z1}}{j(\alpha^2+\beta^2)}\right]$$

$$+\frac{N_4}{N_4M_3+N_3M_4}\left[\frac{\beta\widetilde{J}_{x2}-\alpha\widetilde{J}_{z2}}{-j(\alpha^2+\beta^2)}\right]\Bigg)\sinh(\gamma_{h2}y)$$

$$+\Bigg(\left[\frac{1}{N_4}-\frac{M_4}{N_4}\frac{N_3}{N_4M_3+N_3M_4}\right]\sinh(\gamma_{h1}d_1)\frac{\beta\widetilde{J}_{x1}-\alpha\widetilde{J}_{z1}}{j(\alpha^2+\beta^2)}$$

$$+\left[\frac{M_4}{N_4M_3+N_3M_4}\right]\frac{\beta\widetilde{J}_{x2}-\alpha\widetilde{J}_{z2}}{-j(\alpha^2+\beta^2)}\Bigg)\cosh(\gamma_{h2}y)\Bigg]$$

$$+\frac{j\alpha}{\varepsilon_{22}}\Bigg[\Bigg(\left[\frac{\gamma_{e1}}{\varepsilon_{12}}\sinh(\gamma_{e1}d_1)-\frac{N_1M_2}{N_1M_2-N_2M_1}\frac{\gamma_{e1}}{\varepsilon_{12}}\sinh(\gamma_{e1}d_1)\right]\frac{\alpha\widetilde{J}_{x1}+\beta\widetilde{J}_{z1}}{M_1\omega\varepsilon_0(\alpha^2+\beta^2)}$$

$$+\left[\frac{N_1}{N_1M_2-N_2M_1}\frac{\gamma_0}{\varepsilon_{32}}\right]\frac{\alpha\widetilde{J}_{x2}+\beta\widetilde{J}_{z2}}{\omega\varepsilon_0(\alpha^2+\beta^2)}\Bigg)\gamma_{e2}\sinh(\gamma_{e2}y)$$

$$+\Bigg(\frac{M_1M_2}{N_1M_2-N_2M_1}\Bigg[\left[\frac{\gamma_{e1}}{\varepsilon_{12}M_1}\sinh(\gamma_{e1}d_1)\right]\frac{\alpha\widetilde{J}_{x1}+\beta\widetilde{J}_{z1}}{\omega\varepsilon_0(\alpha^2+\beta^2)}$$

$$-\left[\frac{\gamma_0}{\varepsilon_{32}M_2}\right]\frac{\alpha\widetilde{J}_{x2}+\beta\widetilde{J}_{z2}}{\omega\varepsilon_0(\alpha^2+\beta^2)}\Bigg]\Bigg)\gamma_{e2}\cosh(\gamma_{e2}y)\Bigg]. \qquad \text{(B.63)}$$

Grouping the current terms and simplifying, (B.63) becomes

$$\widetilde{E}_{x2}(\alpha, y, \beta) =$$

$$\widetilde{J}_{x1}\Bigg[\frac{\beta^2}{\alpha^2+\beta^2} j\omega\mu_0 \sinh(\gamma_{h1}d_1)\left(\frac{-N_3\sinh(\gamma_{h2}y)}{N_4M_3+N_3M_4}+\frac{M_3\cosh(\gamma_{h2}y)}{N_4M_3+N_3M_4}\right)+$$

$$\frac{\alpha^2}{\alpha^2+\beta^2}\frac{\gamma_{e1}\gamma_{e2}\sinh(\gamma_{e1}d_1)}{-j\omega\varepsilon_0\varepsilon_{12}\varepsilon_{22}}\left(\frac{-N_2\sinh(\gamma_{e2}y)}{N_1M_2-N_2M_1}+\frac{M_2\cosh(\gamma_{e2}y)}{N_1M_2-N_2M_1}\right)\Bigg]+$$

$$\widetilde{J}_{z1}\Bigg[\frac{\alpha\beta}{\alpha^2+\beta^2} j\omega\mu_0 \sinh(\gamma_{h1}d_1)\left(\frac{N_3\sinh(\gamma_{h2}y)}{N_4M_3+N_3M_4}-\frac{M_3\cosh(\gamma_{h2}y)}{N_4M_3+N_3M_4}\right)+$$

$$\frac{\alpha\beta}{\alpha^2+\beta^2}\frac{\gamma_{e1}\gamma_{e2}\sinh(\gamma_{e1}d_1)}{-j\omega\varepsilon_0\varepsilon_{12}\varepsilon_{22}}\left(\frac{-N_2\sinh(\gamma_{e2}y)}{N_1M_2-N_2M_1}+\frac{M_2\cosh(\gamma_{e2}y)}{N_1M_2-N_2M_1}\right)\Bigg]+$$

$$\widetilde{J}_{x2}\Bigg[\frac{\beta^2}{\alpha^2+\beta^2} j\omega\mu_0\left(\frac{-N_4\sinh(\gamma_{h2}y)}{N_4M_3+N_3M_4}-\frac{M_4\cosh(\gamma_{h2}y)}{N_4M_3+N_3M_4}\right)+$$

$$\frac{\alpha^2}{\alpha^2+\beta^2}\frac{\gamma_0\gamma_{e2}}{-j\omega\varepsilon_0\varepsilon_{22}\varepsilon_{32}}\left(\frac{N_1\sinh(\gamma_{e2}y)}{N_1M_2-N_2M_1}-\frac{M_1\cosh(\gamma_{e2}y)}{N_1M_2-N_2M_1}\right)\Bigg]+$$

$$\widetilde{J}_{z2}\Bigg[\frac{\alpha\beta}{\alpha^2+\beta^2} j\omega\mu_0\left(\frac{N_4\sinh(\gamma_{h2}y)}{N_4M_3+N_3M_4}+\frac{M_4\cosh(\gamma_{h2}y)}{N_4M_3+N_3M_4}\right)+$$

$$\frac{\alpha\beta}{\alpha^2+\beta^2}\frac{\gamma_0\gamma_{e2}}{-j\omega\varepsilon_0\varepsilon_{22}\varepsilon_{32}}\left(\frac{N_1\sinh(\gamma_{e2}y)}{N_1M_2-N_2M_1}-\frac{M_1\cosh(\gamma_{e2}y)}{N_1M_2-N_2M_1}\right)\Bigg]. \tag{B.64}$$

Finally, rearranging the terms and simplifying, (B.64) becomes

$$\widetilde{E}_{x2}(\alpha, y, \beta) = \widetilde{J}_{x1}\widetilde{Z}_{xx1} + \widetilde{J}_{z1}\widetilde{Z}_{xz1} + \widetilde{J}_{x2}\widetilde{Z}_{xx2} + \widetilde{J}_{z2}\widetilde{Z}_{xz2} \tag{B.65}$$

where

$$\widetilde{Z}_{xx1} = \frac{\alpha^2}{\alpha^2+\beta^2}\left[\frac{\gamma_{e1}\gamma_{e2}\sinh(\gamma_{e1}d_1)}{-j\omega\varepsilon_0\varepsilon_{12}\varepsilon_{22}}(P_6-P_5)\right] + \frac{\beta^2}{\alpha^2+\beta^2}\left[j\omega\mu_0\sinh(\gamma_{h1}d_1)(P_4-P_3)\right], \tag{B.66}$$

$$\widetilde{Z}_{xz1} = \frac{\alpha\beta}{\alpha^2+\beta^2}\left[\frac{\gamma_{e1}\gamma_{e2}\sinh(\gamma_{e1}d_1)}{-j\omega\varepsilon_0\varepsilon_{12}\varepsilon_{22}}(P_6-P_5)\right] + \frac{\alpha\beta}{\alpha^2+\beta^2}\left[j\omega\mu_0\sinh(\gamma_{h1}d_1)(P_3-P_4)\right], \tag{B.67}$$

$$\widetilde{Z}_{xx2} = \frac{\alpha^2}{\alpha^2+\beta^2}\left[\frac{\gamma_0\gamma_{e2}}{-j\omega\varepsilon_0\varepsilon_{22}\varepsilon_{32}}(P_8-P_9)\right] + \frac{\beta^2}{\alpha^2+\beta^2}\left[-j\omega\mu_0(P_7+P_{10})\right], \tag{B.68}$$

$$\widetilde{Z}_{xz2} = \frac{\alpha\beta}{\alpha^2+\beta^2}\left[\frac{\gamma_0\gamma_{e2}}{-j\omega\varepsilon_0\varepsilon_{22}\varepsilon_{32}}(P_8-P_9)\right] + \frac{\alpha\beta}{\alpha^2+\beta^2}\left[j\omega\mu_0(P_7+P_{10})\right], \tag{B.69}$$

$$P_1 = N_1M_2 - N_2M_1, \tag{B.70}$$

$$P_2 = N_4 M_3 + N_3 M_4, \tag{B.71}$$

$$P_3 = \sinh(\gamma_{h2} y)\frac{N_3}{P_2}, \tag{B.72}$$

$$P_4 = \cosh(\gamma_{h2} y)\frac{M_3}{P_2}, \tag{B.73}$$

$$P_5 = \sinh(\gamma_{e2} y)\frac{N_2}{P_1}, \tag{B.74}$$

$$P_6 = \cosh(\gamma_{e2} y)\frac{M_2}{P_1}, \tag{B.75}$$

$$P_7 = \sinh(\gamma_{h2} y)\frac{N_4}{P_2}, \tag{B.76}$$

$$P_8 = \sinh(\gamma_{e2} y)\frac{N_1}{P_1}, \tag{B.77}$$

$$P_9 = \cosh(\gamma_{e2} y)\frac{M_1}{P_1}, \tag{B.78}$$

$$P_{10} = \cosh(\gamma_{h2} y)\frac{M_4}{P_2}. \tag{B.79}$$

Next, substituting (B.48), (B.50), (B.59) and (B.61) in (3.110) and rearranging we get the following z-component for the electric field anywhere in region 2:

$$\widetilde{E}_{z2}(\alpha, y, \beta) =$$

$$\widetilde{J}_{x1}\left[\frac{\alpha\beta}{\alpha^2+\beta^2}(-j\omega\mu_0)\sinh(\gamma_{h1}d_1)\left(\frac{-N_3\sinh(\gamma_{h2}y)}{N_4M_3+N_3M_4}+\frac{M_3\cosh(\gamma_{h2}y)}{N_4M_3+N_3M_4}\right)+\right.$$

$$\left.\frac{\alpha\beta}{\alpha^2+\beta^2}\frac{\gamma_{e1}\gamma_{e2}\sinh(\gamma_{e1}d_1)}{-j\omega\varepsilon_0\varepsilon_{12}\varepsilon_{22}}\left(\frac{-N_2\sinh(\gamma_{e2}y)}{N_1M_2-N_2M_1}+\frac{M_2\cosh(\gamma_{e2}y)}{N_1M_2-N_2M_1}\right)\right]+$$

$$\widetilde{J}_{z1}\left[\frac{\alpha^2}{\alpha^2+\beta^2}(-j\omega\mu_0)\sinh(\gamma_{h1}d_1)\left(\frac{N_3\sinh(\gamma_{h2}y)}{N_4M_3+N_3M_4}-\frac{M_3\cosh(\gamma_{h2}y)}{N_4M_3+N_3M_4}\right)+\right.$$

$$\frac{\beta^2}{\alpha^2+\beta^2}\frac{\gamma_{e1}\gamma_{e2}\sinh(\gamma_{e1}d_1)}{-j\omega\varepsilon_0\varepsilon_{12}\varepsilon_{22}}\left(\frac{-N_2\sinh(\gamma_{e2}y)}{N_1M_2-N_2M_1}+\frac{M_2\cosh(\gamma_{e2}y)}{N_1M_2-N_2M_1}\right)\Bigg]+$$

$$\widetilde{J}_{x2}\Bigg[\frac{\alpha\beta}{\alpha^2+\beta^2}(-j\omega\mu_0)\left(\frac{-N_4\sinh(\gamma_{h2}y)}{N_4M_3+N_3M_4}-\frac{M_4\cosh(\gamma_{h2}y)}{N_4M_3+N_3M_4}\right)+$$

$$\frac{\alpha\beta}{\alpha^2+\beta^2}\frac{\gamma_0\gamma_{e2}}{-j\omega\varepsilon_0\varepsilon_{22}\varepsilon_{32}}\left(\frac{N_1\sinh(\gamma_{e2}y)}{N_1M_2-N_2M_1}-\frac{M_1\cosh(\gamma_{e2}y)}{N_1M_2-N_2M_1}\right)\Bigg]+$$

$$\widetilde{J}_{z2}\Bigg[\frac{\alpha^2}{\alpha^2+\beta^2}(-j\omega\mu_0)\left(\frac{N_4\sinh(\gamma_{h2}y)}{N_4M_3+N_3M_4}+\frac{M_4\cosh(\gamma_{h2}y)}{N_4M_3+N_3M_4}\right)+$$

$$\frac{\beta^2}{\alpha^2+\beta^2}\frac{\gamma_0\gamma_{e2}}{-j\omega\varepsilon_0\varepsilon_{22}\varepsilon_{32}}\left(\frac{N_1\sinh(\gamma_{e2}y)}{N_1M_2-N_2M_1}-\frac{M_1\cosh(\gamma_{e2}y)}{N_1M_2-N_2M_1}\right)\Bigg]. \tag{B.80}$$

Finally, rearranging the terms and simplifying, (B.80) becomes

$$\widetilde{E}_{z2}(\alpha,y,\beta)=\widetilde{J}_{x1}\widetilde{Z}_{zx1}+\widetilde{J}_{z1}\widetilde{Z}_{zz1}+\widetilde{J}_{x2}\widetilde{Z}_{zx2}+\widetilde{J}_{z2}\widetilde{Z}_{zz2} \tag{B.81}$$

where

$$\widetilde{Z}_{zx1}=\widetilde{Z}_{xz1}, \tag{B.82}$$

$$\begin{aligned}\widetilde{Z}_{zz1} &= \frac{\beta^2}{\alpha^2+\beta^2}\Bigg[\frac{\gamma_{e1}\gamma_{e2}\sinh(\gamma_{e1}d_1)}{-j\omega\varepsilon_0\varepsilon_{12}\varepsilon_{22}}(P_6-P_5)\Bigg]\\ &\quad+\frac{\alpha^2}{\alpha^2+\beta^2}\Bigg[j\omega\mu_0\sinh(\gamma_{h1}d_1)(P_4-P_3)\Bigg],\end{aligned} \tag{B.83}$$

$$\widetilde{Z}_{zx2}=\widetilde{Z}_{xz2}, \tag{B.84}$$

$$\widetilde{Z}_{zz2} = \frac{\beta^2}{\alpha^2+\beta^2}\left[\frac{\gamma_0\gamma_{e2}}{-j\omega\varepsilon_0\varepsilon_{22}\varepsilon_{32}}(P_8-P_9)\right]$$

$$+\frac{\alpha^2}{\alpha^2+\beta^2}\left[-j\omega\mu_0(P_7+P_{10})\right]. \qquad \text{(B.85)}$$

APPENDIX C. DERIVATIONS FOR THREE ANISOTROPIC LAYERS

This appendix contains the derivations of the spectral domain immittance functions for three anisotropic dielectric layers. The first boundary condition applied will be (3.147). Applying (3.162) at y = 0 gives:

$$\begin{aligned} \widetilde{E}_{x1}(\alpha, 0, \beta) &= 0 \\ &= -\omega\mu_0\beta A_1'(\alpha, \beta) + \frac{j\alpha}{\varepsilon_{12}} B_1'(\alpha, \beta)\gamma_{e1}. \end{aligned} \tag{C.1}$$

Next, the boundary condition applied will be (3.148). Applying (3.164) at y = 0 gives:

$$\begin{aligned} \widetilde{E}_{z1}(\alpha, 0, \beta) &= 0 \\ &= \omega\mu_0\alpha A_1'(\alpha, \beta) + \frac{j\beta}{\varepsilon_{12}} B_1'(\alpha, \beta)\gamma_{e1}. \end{aligned} \tag{C.2}$$

Solving for $A_1'(\alpha, \beta)$ in (C.1) and substituting into (C.2) gives:

$$-\alpha^2 B_1'(\alpha, \beta) = \beta^2 B_1'(\alpha, \beta). \tag{C.3}$$

The only solution to (C.3) is

$$B_1'(\alpha, \beta) = 0. \tag{C.4}$$

Substituting (C.4) back into (C.1) implies

$$A_1'(\alpha, \beta) = 0. \tag{C.5}$$

The third boundary condition applied will be (3.149). Equating (3.162) to (3.168) at

d_1 and substituting in (C.4) and (C.5) gives:

$$\begin{aligned}\widetilde{E}_{x1}(\alpha, d_1, \beta) &= -\omega\mu_0\beta A_1(\alpha,\beta)\sinh(\gamma_{h1}d_1) + \frac{j\alpha}{\varepsilon_{12}}B_1(\alpha,\beta)\gamma_{e1}\sinh(\gamma_{e1}d_1) \\ &= -\omega\mu_0\beta A_2(\alpha,\beta)\sinh(\gamma_{h2}d_1) + \frac{j\alpha}{\varepsilon_{22}}B_2(\alpha,\beta)\gamma_{e2}\sinh(\gamma_{e2}d_1) \\ &\quad -\omega\mu_0\beta A_2'(\alpha,\beta)\cosh(\gamma_{h2}d_1) + \frac{j\alpha}{\varepsilon_{22}}B_2'(\alpha,\beta)\gamma_{e2}\cosh(\gamma_{e2}d_1) \\ &= \widetilde{E}_{x2}(\alpha, d_1, \beta). \end{aligned} \tag{C.6}$$

Factoring out the coefficients results in:

$$\begin{aligned} A_1(\alpha,\beta)\Big[-\omega\mu_0\beta\sinh(\gamma_{h1}d_1)\Big] &+ B_1(\alpha,\beta)\left[\frac{j\alpha}{\varepsilon_{12}}\gamma_{e1}\sinh(\gamma_{e1}d_1)\right] \\ +A_2(\alpha,\beta)\Big[\omega\mu_0\beta\sinh(\gamma_{h2}d_1)\Big] &- B_2(\alpha,\beta)\left[\frac{j\alpha}{\varepsilon_{22}}\gamma_{e2}\sinh(\gamma_{e2}d_1)\right] \\ +A_2'(\alpha,\beta)\Big[\omega\mu_0\beta\cosh(\gamma_{h2}d_1)\Big] &- B_2'(\alpha,\beta)\left[\frac{j\alpha}{\varepsilon_{22}}\gamma_{e2}\cosh(\gamma_{e2}d_1)\right] = 0. \end{aligned} \tag{C.7}$$

The fourth boundary condition applied will be (3.150). Equating (3.164) to (3.170) at d_1 and substituting in (C.4) and (C.5) gives:

$$\begin{aligned}\widetilde{E}_{z1}(\alpha, d_1, \beta) &= \omega\mu_0\alpha A_1(\alpha,\beta)\sinh(\gamma_{h1}d_1) + \frac{j\beta}{\varepsilon_{12}}B_1(\alpha,\beta)\gamma_{e1}\sinh(\gamma_{e1}d_1) \\ &= \omega\mu_0\alpha A_2(\alpha,\beta)\sinh(\gamma_{h2}d_1) + \frac{j\beta}{\varepsilon_{22}}B_2(\alpha,\beta)\gamma_{e2}\sinh(\gamma_{e2}d_1) \\ &= \widetilde{E}_{z2}(\alpha, d_1, \beta). \end{aligned} \tag{C.8}$$

Factoring out the coefficients results in:

$$\begin{aligned} A_1(\alpha,\beta)\Big[\omega\mu_0\alpha\sinh(\gamma_{h1}d_1)\Big] &+ B_1(\alpha,\beta)\left[\frac{j\beta}{\varepsilon_{12}}\gamma_{e1}\sinh(\gamma_{e1}d_1)\right] \\ - A_2(\alpha,\beta)\Big[\omega\mu_0\alpha\sinh(\gamma_{h2}d_1)\Big] &- A_2'(\alpha,\beta)\Big[\omega\mu_0\alpha\cosh(\gamma_{h2}d_1)\Big] \\ - B_2(\alpha,\beta)\left[\frac{j\beta}{\varepsilon_{22}}\gamma_{e2}\sinh(\gamma_{e2}d_1)\right] &- B_2'(\alpha,\beta)\left[\frac{j\beta}{\varepsilon_{22}}\gamma_{e2}\cosh(\gamma_{e2}d_1)\right] = 0. \end{aligned} \tag{C.9}$$

Next, multiplying (C.7) by α and (C.9) by β, and adding gives:

$$\begin{aligned} & B_1(\alpha,\beta)\left[\frac{j\alpha^2}{\varepsilon_{12}}\gamma_{e1}\sinh(\gamma_{e1}d_1)+\frac{j\beta^2}{\varepsilon_{12}}\gamma_{e1}\sinh(\gamma_{e1}d_1)\right] \\ - \quad & B_2(\alpha,\beta)\left[\frac{j\alpha^2}{\varepsilon_{22}}\gamma_{e2}\sinh(\gamma_{e2}d_1)+\frac{j\beta^2}{\varepsilon_{22}}\gamma_{e2}\sinh(\gamma_{e2}d_1)\right] \\ - \quad & B_2'(\alpha,\beta)\left[\frac{j\alpha^2}{\varepsilon_{22}}\gamma_{e2}\cosh(\gamma_{e2}d_1)+\frac{j\beta^2}{\varepsilon_{22}}\gamma_{e2}\cosh(\gamma_{e2}d_1)\right]=0. \end{aligned} \tag{C.10}$$

Factoring out an $j(\alpha^2+\beta^2)$ gives:

$$B_1(\alpha,\beta)\left[\frac{\gamma_{e1}}{\varepsilon_{12}}\sinh(\gamma_{e1}d_1)\right]-B_2(\alpha,\beta)\left[\frac{\gamma_{e2}}{\varepsilon_{22}}\sinh(\gamma_{e2}d_1)\right]-B_2'(\alpha,\beta)\left[\frac{\gamma_{e2}}{\varepsilon_{22}}\cosh(\gamma_{e2}d_1)\right]=0. \tag{C.11}$$

Next, multiplying (C.7) by β and (C.9) by $-\alpha$, and adding gives:

$$\begin{aligned} & A_1(\alpha,\beta)\Big[-\omega\mu_0\beta^2\sinh(\gamma_{h1}d_1)-\omega\mu_0\alpha^2\sinh(\gamma_{h1}d_1)\Big] \\ + \quad & A_2(\alpha,\beta)\Big[\omega\mu_0\beta^2\sinh(\gamma_{h2}d_1)+\omega\mu_0\alpha^2\sinh(\gamma_{h2}d_1)\Big] \\ + \quad & A_2'(\alpha,\beta)\Big[\omega\mu_0\beta^2\cosh(\gamma_{h2}d_1)+\omega\mu_0\alpha^2\cosh(\gamma_{h2}d_1)\Big]=0. \end{aligned} \tag{C.12}$$

Factoring out a $\omega\mu_0(\alpha^2+\beta^2)$ gives:

$$-A_1(\alpha,\beta)\sinh(\gamma_{h1}d_1)+A_2(\alpha,\beta)\sinh(\gamma_{h2}d_1)+A_2'(\alpha,\beta)\cosh(\gamma_{h2}d_1)=0. \tag{C.13}$$

The next boundary condition applied will be (3.157). Equating the subtraction of (3.166) from (3.172) at d_1 to $\widetilde{J}_{x1}$ and substituting in (C.4) and (C.5) gives:

$$\begin{aligned} \widetilde{J}_{x1} = \quad & - \quad A_1(\alpha,\beta)\Big[j\beta\gamma_{h1}\cosh(\gamma_{h1}d_1)\Big]+B_1(\alpha,\beta)\Big[\omega\varepsilon_0\alpha\cosh(\gamma_{e1}d_1)\Big] \\ & + \quad A_2(\alpha,\beta)\Big[j\beta\gamma_{h2}\cosh(\gamma_{h2}d_1)\Big]+A_2'(\alpha,\beta)\Big[j\beta\gamma_{h2}\sinh(\gamma_{h2}d_1)\Big] \end{aligned}$$

$$- \quad B_2(\alpha,\beta)\Big[\omega\varepsilon_0\alpha\cosh(\gamma_{e2}d_1)\Big] - B_2'(\alpha,\beta)\Big[\omega\varepsilon_0\alpha\sinh(\gamma_{e2}d_1)\Big]. \quad \text{(C.14)}$$

Similarly, the next boundary condition applied will be (3.158). Equating the subtraction of (3.171) from (3.165) at d_1 to $\widetilde{J}_{z1}$ and substituting in (C.4) and (C.5) gives:

$$\begin{aligned}\widetilde{J}_{z1} = \quad & A_1(\alpha,\beta)\Big[j\alpha\gamma_{h1}\cosh(\gamma_{h1}d_1)\Big] + B_1(\alpha,\beta)\Big[\omega\varepsilon_0\beta\cosh(\gamma_{e1}d_1)\Big] \\ - \quad & A_2(\alpha,\beta)\Big[j\alpha\gamma_{h2}\cosh(\gamma_{h2}d_1)\Big] - A_2'(\alpha,\beta)\Big[j\alpha\gamma_{h2}\sinh(\gamma_{h2}d_1)\Big] \\ - \quad & B_2(\alpha,\beta)\Big[\omega\varepsilon_0\beta\cosh(\gamma_{e2}d_1)\Big] - B_2'(\alpha,\beta)\Big[\omega\varepsilon_0\beta\sinh(\gamma_{e2}d_1)\Big]. \quad \text{(C.15)}\end{aligned}$$

Next, multiply (C.14) by α and (C.15) by β and add:

$$\begin{aligned}\alpha\widetilde{J}_{x1} + \beta\widetilde{J}_{z1} \quad = \quad & B_1(\alpha,\beta)\omega\varepsilon_0\cosh(\gamma_{e1}d_1)(\alpha^2+\beta^2) \\ & -B_2(\alpha,\beta)\omega\varepsilon_0\cosh(\gamma_{e2}d_1)(\alpha^2+\beta^2) \\ & -B_2'(\alpha,\beta)\omega\varepsilon_0\sinh(\gamma_{e2}d_1)(\alpha^2+\beta^2). \quad \text{(C.16)}\end{aligned}$$

This implies

$$\frac{\alpha\widetilde{J}_{x1} + \beta\widetilde{J}_{z1}}{\omega\varepsilon_0(\alpha^2+\beta^2)} = B_1(\alpha,\beta)\cosh(\gamma_{e1}d_1) - B_2(\alpha,\beta)\cosh(\gamma_{e2}d_1) - B_2'(\alpha,\beta)\sinh(\gamma_{e2}d_1). \quad \text{(C.17)}$$

Next, multiply (C.14) by β and (C.15) by $-\alpha$ and add. This gives

$$\begin{aligned}\beta\widetilde{J}_{x1} - \alpha\widetilde{J}_{z1} \quad = \quad & -A_1(\alpha,\beta)j\gamma_{h1}\cosh(\gamma_{h1}d_1)(\alpha^2+\beta^2) \\ & +A_2(\alpha,\beta)j\gamma_{h2}\cosh(\gamma_{h2}d_1)(\alpha^2+\beta^2) \\ & +A_2'(\alpha,\beta)j\gamma_{h2}\sinh(\gamma_{h2}d_1)(\alpha^2+\beta^2). \quad \text{(C.18)}\end{aligned}$$

This implies

$$\begin{aligned}\frac{\beta\widetilde{J}_{x1}-\alpha\widetilde{J}_{z1}}{j(\alpha^2+\beta^2)} = \quad & -A_1(\alpha,\beta)\gamma_{h1}\cosh(\gamma_{h1}d_1)+A_2(\alpha,\beta)\gamma_{h2}\cosh(\gamma_{h2}d_1) \\ & +A_2'(\alpha,\beta)\gamma_{h2}\sinh(\gamma_{h2}d_1). \end{aligned} \tag{C.19}$$

Next, multiplying (C.11) by $-\cosh(\gamma_{e1}d_1)$ and (C.17) by $\frac{\gamma_{e1}}{\varepsilon_{12}}\sinh(\gamma_{e1}d_1)$, and adding gives:

$$\begin{aligned}\frac{\gamma_{e1}}{\varepsilon_{12}}\sinh(\gamma_{e1}d_1)\left[\frac{\alpha\widetilde{J}_{x1}+\beta\widetilde{J}_{z1}}{\omega\varepsilon_0(\alpha^2+\beta^2)}\right] = \quad & B_2(\alpha,\beta)\left[\frac{\gamma_{e2}}{\varepsilon_{22}}\cosh(\gamma_{e1}d_1)\sinh(\gamma_{e2}d_1)\right. \\ & \left.-\frac{\gamma_{e1}}{\varepsilon_{12}}\cosh(\gamma_{e2}d_1)\sinh(\gamma_{e1}d_1)\right] \\ & +B_2'(\alpha,\beta)\left[\frac{\gamma_{e2}}{\varepsilon_{22}}\cosh(\gamma_{e1}d_1)\cosh(\gamma_{e2}d_1)\right. \\ & \left.-\frac{\gamma_{e1}}{\varepsilon_{12}}\sinh(\gamma_{e1}d_1)\sinh(\gamma_{e2}d_1)\right]. \end{aligned} \tag{C.20}$$

Solving for $B_2'(\alpha,\beta)$ in (C.20) gives:

$$B_2'(\alpha,\beta)=\frac{\gamma_{e1}}{\varepsilon_{12}N_1}\sinh(\gamma_{e1}d_1)\left[\frac{\alpha\widetilde{J}_{x1}+\beta\widetilde{J}_{z1}}{\omega\varepsilon_0(\alpha^2+\beta^2)}\right]-B_2(\alpha,\beta)\frac{N_1}{M_1} \tag{C.21}$$

where

$$N_1=\frac{\gamma_{e2}}{\varepsilon_{22}}\cosh(\gamma_{e1}d_1)\cosh(\gamma_{e2}d_1)-\frac{\gamma_{e1}}{\varepsilon_{12}}\sinh(\gamma_{e1}d_1)\sinh(\gamma_{e2}d_1) \tag{C.22}$$

and

$$M_1=\frac{\gamma_{e2}}{\varepsilon_{22}}\cosh(\gamma_{e1}d_1)\sinh(\gamma_{e2}d_1)-\frac{\gamma_{e1}}{\varepsilon_{12}}\cosh(\gamma_{e2}d_1)\sinh(\gamma_{e1}d_1). \tag{C.23}$$

Again, multiply (C.11) by $-\cosh(\gamma_{e2}d_1)$ and (C.17) by $\frac{\gamma_{e2}}{\varepsilon_{22}}\sinh(\gamma_{e2}d_1)$ and add. This

results in

$$\frac{\gamma_{e2}}{\varepsilon_{22}}\sinh(\gamma_{e2}d_1)\left[\frac{\alpha\widetilde{J}_{x1}+\beta\widetilde{J}_{z1}}{\omega\varepsilon_0(\alpha^2+\beta^2)}\right] = B_1(\alpha,\beta)\left[\frac{\gamma_{e2}}{\varepsilon_{22}}\cosh(\gamma_{e1}d_1)\sinh(\gamma_{e2}d_1) - \frac{\gamma_{e1}}{\varepsilon_{12}}\cosh(\gamma_{e2}d_1)\sinh(\gamma_{e1}d_1)\right] + B_2'(\alpha,\beta)\left[\frac{\gamma_{e2}}{\varepsilon_{22}}\right]. \quad \text{(C.24)}$$

Solving for $B_2'(\alpha,\beta)$ in (C.24) gives:

$$B_2'(\alpha,\beta) = \sinh(\gamma_{e2}d_1)\left[\frac{\alpha\widetilde{J}_{x1}+\beta\widetilde{J}_{z1}}{\omega\varepsilon_0(\alpha^2+\beta^2)}\right] - B_1(\alpha,\beta)\frac{\varepsilon_{22}M_1}{\gamma_{e2}}. \quad \text{(C.25)}$$

Next, multiply (C.13) by $\gamma_{h2}\sinh(\gamma_{h2}d_1)$ and (C.19) by $-\cosh(\gamma_{h2}d_1)$ and add. This results in

$$-\cosh(\gamma_{h2}d_1)\left[\frac{\beta\widetilde{J}_{x1}-\alpha\widetilde{J}_{z1}}{j(\alpha^2+\beta^2)}\right] = A_1(\alpha,\beta)\Big[-\gamma_{h2}\sinh(\gamma_{h2}d_1)\sinh(\gamma_{h1}d_1) + \gamma_{h1}\cosh(\gamma_{h2}d_1)\cosh(\gamma_{h1}d_1)\Big] + A_2(\alpha,\beta)[\gamma_{h2}]. \quad \text{(C.26)}$$

Solving for $A_1(\alpha,\beta)$ in (C.26) gives

$$A_1(\alpha,\beta) = A_2(\alpha,\beta)\frac{\gamma_{h2}}{N_4} + \frac{\cosh(\gamma_{h2}d_1)}{N_4}\left[\frac{\beta\widetilde{J}_{x1}-\alpha\widetilde{J}_{z1}}{j(\alpha^2+\beta^2)}\right] \quad \text{(C.27)}$$

where

$$N_4 = -\gamma_{h1}\cosh(\gamma_{h2}d_1)\cosh(\gamma_{h1}d_1) + \gamma_{h2}\sinh(\gamma_{h2}d_1)\sinh(\gamma_{h1}d_1). \quad \text{(C.28)}$$

Next, multiply (C.13) by $\gamma_{h1}\cosh(\gamma_{h1}d_1)$ and (C.19) by $-\sinh(\gamma_{h1}d_1)$ and add. This

results in

$$
\begin{aligned}
-\sinh(\gamma_{h1}d_1)\left[\frac{\beta\widetilde{J}_{x1}-\alpha\widetilde{J}_{z1}}{j(\alpha^2+\beta^2)}\right] &= A_2'(\alpha,\beta)\Big[\gamma_{h1}\cosh(\gamma_{h1}d_1)\cosh(\gamma_{h2}d_1) \\
&\quad -\gamma_{h2}\sinh(\gamma_{h1}d_1)\sinh(\gamma_{h2}d_1)\Big] \\
&\quad +A_2(\alpha,\beta)\Big[\gamma_{h1}\cosh(\gamma_{h1}d_1)\sinh(\gamma_{h2}d_1) \\
&\quad -\gamma_{h2}\sinh(\gamma_{h1}d_1)\cosh(\gamma_{h2}d_1)\Big]. \quad \text{(C.29)}
\end{aligned}
$$

Solving for $A_2'(\alpha,\beta)$ in (C.29) gives

$$
A_2'(\alpha,\beta) = A_2(\alpha,\beta)\frac{M_4}{N_4} + \frac{\sinh(\gamma_{h1}d_1)}{N_4}\left[\frac{\beta\widetilde{J}_{x1}-\alpha\widetilde{J}_{z1}}{j(\alpha^2+\beta^2)}\right] \qquad \text{(C.30)}
$$

where

$$
M_4 = \gamma_{h1}\cosh(\gamma_{h1}d_1)\sinh(\gamma_{h2}d_1) - \gamma_{h2}\sinh(\gamma_{h1}d_1)\cosh(\gamma_{h2}d_1). \qquad \text{(C.31)}
$$

The seventh boundary condition applied will be (3.151). Equating (3.168) to (3.174) at d_{12} and factoring gives:

$$
\begin{aligned}
-A_2(\alpha,\beta)\left[\omega\mu_0\beta\sinh(\gamma_{h2}d_{12})\right] &+ B_2(\alpha,\beta)\left[\frac{j\alpha}{\varepsilon_{22}}\gamma_{e2}\sinh(\gamma_{e2}d_{12})\right] \\
-A_2'(\alpha,\beta)\left[\omega\mu_0\beta\cosh(\gamma_{h2}d_{12})\right] &+ B_2'(\alpha,\beta)\left[\frac{j\alpha}{\varepsilon_{22}}\gamma_{e2}\cosh(\gamma_{e2}d_{12})\right] \\
+A_3(\alpha,\beta)\left[\omega\mu_0\beta\sinh(\gamma_{h3}d_{12})\right] &- B_3(\alpha,\beta)\left[\frac{j\alpha}{\varepsilon_{32}}\gamma_{e3}\sinh(\gamma_{e3}d_{12})\right] \\
+A_3'(\alpha,\beta)\left[\omega\mu_0\beta\cosh(\gamma_{h3}d_{12})\right] &- B_3'(\alpha,\beta)\left[\frac{j\alpha}{\varepsilon_{32}}\gamma_{e3}\cosh(\gamma_{e3}d_{12})\right] = 0. \quad \text{(C.32)}
\end{aligned}
$$

The eighth boundary condition applied will be (3.152). Equating (3.170) to (3.176)

at d_{12} and factoring gives:

$$\begin{aligned} A_2(\alpha,\beta)\left[\omega\mu_0\alpha\sinh(\gamma_{h2}d_{12})\right] &+ B_2(\alpha,\beta)\left[\frac{j\beta}{\varepsilon_{22}}\gamma_{e2}\sinh(\gamma_{e2}d_{12})\right] \\ +A_2'(\alpha,\beta)\left[\omega\mu_0\alpha\cosh(\gamma_{h2}d_{12})\right] &+ B_2'(\alpha,\beta)\left[\frac{j\beta}{\varepsilon_{22}}\gamma_{e2}\cosh(\gamma_{e2}d_{12})\right] \\ -A_3(\alpha,\beta)\left[\omega\mu_0\alpha\sinh(\gamma_{h3}d_{12})\right] &- B_3(\alpha,\beta)\left[\frac{j\beta}{\varepsilon_{32}}\gamma_{e3}\sinh(\gamma_{e3}d_{12})\right] \\ -A_3'(\alpha,\beta)\left[\omega\mu_0\alpha\cosh(\gamma_{h3}d_{12})\right] &- B_3'(\alpha,\beta)\left[\frac{j\beta}{\varepsilon_{32}}\gamma_{e3}\cosh(\gamma_{e3}d_{12})\right] = 0. \end{aligned} \quad \text{(C.33)}$$

Next, multiplying (C.32) by α and (C.33) by β, adding and factoring out $j(\alpha^2+\beta^2)$ gives:

$$\begin{aligned} & B_2(\alpha,\beta)\left[\frac{\gamma_{e2}}{\varepsilon_{22}}\sinh(\gamma_{e2}d_{12})\right] + B_2'(\alpha,\beta)\left[\frac{\gamma_{e2}}{\varepsilon_{22}}\cosh(\gamma_{e2}d_{12})\right] \\ - \; & B_3(\alpha,\beta)\left[\frac{\gamma_{e3}}{\varepsilon_{32}}\sinh(\gamma_{e3}d_{12})\right] - B_3'(\alpha,\beta)\left[\frac{\gamma_{e3}}{\varepsilon_{32}}\cosh(\gamma_{e3}d_{12})\right] = 0. \end{aligned} \quad \text{(C.34)}$$

Next, multiplying (C.32) by β and (C.33) by $-\alpha$, add and factoring out $\omega\mu_0(\alpha^2+\beta^2)$ gives:

$$\begin{aligned} & A_2(\alpha,\beta)\sinh(\gamma_{h2}d_{12}) + A_2'(\alpha,\beta)\cosh(\gamma_{h2}d_{12}) \\ - \; & A_3(\alpha,\beta)\sinh(\gamma_{h3}d_{12}) - A_3'(\alpha,\beta)\cosh(\gamma_{h3}d_{12}) = 0. \end{aligned} \quad \text{(C.35)}$$

The next boundary condition applied will be (3.159). Equating the subtraction of (3.172) from (3.178) at d_{12} to $\widetilde{J}_{x2}$ and factoring gives:

$$\begin{aligned} \widetilde{J}_{x2} \;=\; & -A_2(\alpha,\beta)\left[j\beta\gamma_{h2}\cosh(\gamma_{h2}d_{12})\right] + B_2(\alpha,\beta)\left[\omega\varepsilon_0\alpha\cosh(\gamma_{e2}d_{12})\right] \\ & -A_2'(\alpha,\beta)\left[j\beta\gamma_{h2}\sinh(\gamma_{h2}d_{12})\right] + B_2'(\alpha,\beta)\left[\omega\varepsilon_0\alpha\sinh(\gamma_{e2}d_{12})\right] \\ & +A_3(\alpha,\beta)\left[j\beta\gamma_{h3}\cosh(\gamma_{h3}d_{12})\right] - B_3(\alpha,\beta)\left[\omega\varepsilon_0\alpha\cosh(\gamma_{e3}d_{12})\right] \end{aligned}$$

$$+A_3'(\alpha,\beta)\Big[j\beta\gamma_{h3}\sinh(\gamma_{h3}d_{12})\Big] - B_3'(\alpha,\beta)\Big[\omega\varepsilon_0\alpha\sinh(\gamma_{e3}d_{12})\Big]. \quad \text{(C.36)}$$

Similarly, the next boundary condition applied will be (3.160). Equating the subtraction of (3.177) from (3.171) at d_{12} to $\widetilde{J}_{z2}$ and factoring gives:

$$\begin{aligned}\widetilde{J}_{z2} \;=\;& A_2(\alpha,\beta)\Big[j\alpha\gamma_{h2}\cosh(\gamma_{h2}d_{12})\Big] + B_2(\alpha,\beta)\Big[\omega\varepsilon_0\beta\cosh(\gamma_{e2}d_{12})\Big]\\ &+A_2'(\alpha,\beta)\Big[j\alpha\gamma_{h2}\sinh(\gamma_{h2}d_{12})\Big] + B_2'(\alpha,\beta)\Big[\omega\varepsilon_0\beta\sinh(\gamma_{e2}d_{12})\Big]\\ &-A_3(\alpha,\beta)\Big[j\alpha\gamma_{h3}\cosh(\gamma_{h3}d_{12})\Big] - B_3(\alpha,\beta)\Big[\omega\varepsilon_0\beta\cosh(\gamma_{e3}d_{12})\Big]\\ &-A_3'(\alpha,\beta)\Big[j\alpha\gamma_{h3}\sinh(\gamma_{h3}d_{12})\Big] - B_3'(\alpha,\beta)\Big[\omega\varepsilon_0\beta\sinh(\gamma_{e3}d_{12})\Big]. \quad \text{(C.37)}\end{aligned}$$

Next, multiply (C.36) by α and (C.37) by β and add. After factoring, this yields

$$\begin{aligned}\frac{\alpha\widetilde{J}_{x2}+\beta\widetilde{J}_{z2}}{\omega\varepsilon_0(\alpha^2+\beta^2)} \;=\;& B_2(\alpha,\beta)\cosh(\gamma_{e2}d_{12}) + B_2'(\alpha,\beta)\sinh(\gamma_{e2}d_{12})\\ &-B_3(\alpha,\beta)\cosh(\gamma_{e3}d_{12}) - B_3'(\alpha,\beta)\sinh(\gamma_{e3}d_{12}). \quad \text{(C.38)}\end{aligned}$$

Next, multiply (C.36) by β and (C.37) by $-\alpha$ and add. After factoring, this yields

$$\begin{aligned}\frac{\beta\widetilde{J}_{x2}-\alpha\widetilde{J}_{z2}}{-j(\alpha^2+\beta^2)} \;=\;& A_2(\alpha,\beta)\Big[\gamma_{h2}\cosh(\gamma_{h2}d_{12})\Big] + A_2'(\alpha,\beta)\Big[\gamma_{h2}\sinh(\gamma_{h2}d_{12})\Big]\\ &-A_3(\alpha,\beta)\Big[\gamma_{h3}\cosh(\gamma_{h3}d_{12})\Big] - A_3'(\alpha,\beta)\Big[\gamma_{h3}\sinh(\gamma_{h3}d_{12})\Big]. \quad \text{(C.39)}\end{aligned}$$

The next boundary condition applied will be (3.153). Equating (3.174) to (3.180) at d_{13} and factoring results in:

$$\begin{aligned}-\;& A_3(\alpha,\beta)\Big[\omega\mu_0\beta\sinh(\gamma_{h3}d_{13})\Big] + B_3(\alpha,\beta)\Big[\frac{j\alpha}{\varepsilon_{32}}\gamma_{e3}\sinh(\gamma_{e3}d_{13})\Big]\\ -\;& A_3'(\alpha,\beta)\Big[\omega\mu_0\beta\cosh(\gamma_{h3}d_{13})\Big] + B_3'(\alpha,\beta)\Big[\frac{j\alpha}{\varepsilon_{32}}\gamma_{e3}\cosh(\gamma_{e3}d_{13})\Big]\end{aligned}$$

$$+A_4(\alpha,\beta)\left[\omega\mu_0\beta\right] + B_4(\alpha,\beta)\left[\frac{j\alpha}{\varepsilon_{42}}\gamma_0\right] = 0. \tag{C.40}$$

The next boundary condition applied will be (3.154). Equating (3.176) to (3.182) at d_{13} and factoring results in:

$$\begin{aligned} & A_3(\alpha,\beta)\left[\omega\mu_0\alpha\sinh(\gamma_{h3}d_{13})\right] + B_3(\alpha,\beta)\left[\frac{j\beta}{\varepsilon_{32}}\gamma_{e3}\sinh(\gamma_{e3}d_{13})\right] \\ + \;& A_3'(\alpha,\beta)\left[\omega\mu_0\alpha\cosh(\gamma_{h3}d_{13})\right] + B_3'(\alpha,\beta)\left[\frac{j\beta}{\varepsilon_{32}}\gamma_{e3}\cosh(\gamma_{e3}d_{13})\right] \\ - \;& A_4(\alpha,\beta)\left[\omega\mu_0\alpha\right] + B_4(\alpha,\beta)\left[\frac{j\beta}{\varepsilon_{42}}\gamma_0\right] = 0. \end{aligned} \tag{C.41}$$

Next, multiplying (C.40) by α and (C.41) by β, adding and factoring out $j(\alpha^2+\beta^2)$ gives:

$$B_3(\alpha,\beta)\left[\frac{\gamma_{e3}}{\varepsilon_{32}}\sinh(\gamma_{e3}d_{13})\right] + B_3'(\alpha,\beta)\left[\frac{\gamma_{e3}}{\varepsilon_{32}}\cosh(\gamma_{e3}d_{13})\right] + B_4(\alpha,\beta)\left[\frac{\gamma_0}{\varepsilon_{42}}\right] = 0. \tag{C.42}$$

Next, multiplying (C.40) by β and (C.41) by $-\alpha$, adding and factoring out a $\omega\mu_0(\alpha^2+\beta^2)$ gives:

$$A_3(\alpha,\beta)\sinh(\gamma_{h3}d_{13}) + A_3'(\alpha,\beta)\cosh(\gamma_{h3}d_{13}) - A_4(\alpha,\beta) = 0. \tag{C.43}$$

The next boundary condition applied will be (3.155). Equating (3.177) to (3.183) at d_{13} and factoring results in:

$$\begin{aligned} & A_3(\alpha,\beta)\left[j\alpha\gamma_{h3}\cosh(\gamma_{h3}d_{13})\right] + B_3(\alpha,\beta)\left[\omega\varepsilon_0\beta\cosh(\gamma_{e3}d_{13})\right] \\ + \;& A_3'(\alpha,\beta)\left[j\alpha\gamma_{h3}\sinh(\gamma_{h3}d_{13})\right] + B_3'(\alpha,\beta)\left[\omega\varepsilon_0\beta\sinh(\gamma_{e3}d_{13})\right] \\ + \;& A_4(\alpha,\beta)\left[j\alpha\gamma_0\right] - B_4(\alpha,\beta)\left[\omega\varepsilon_0\beta\right] = 0. \end{aligned} \tag{C.44}$$

The final boundary condition applied will be (3.156). Equating (3.178) to (3.184) at d_{13} and factoring results in:

$$\begin{aligned} & A_3(\alpha,\beta)\Big[j\beta\gamma_{h3}\cosh(\gamma_{h3}d_{13})\Big] - B_3(\alpha,\beta)\Big[\omega\varepsilon_0\alpha\cosh(\gamma_{e3}d_{13})\Big] \\ + \quad & A_3'(\alpha,\beta)\Big[j\beta\gamma_{h3}\sinh(\gamma_{h3}d_{13})\Big] - B_3'(\alpha,\beta)\Big[\omega\varepsilon_0\alpha\sinh(\gamma_{e3}d_{13})\Big] \\ + \quad & A_4(\alpha,\beta)\Big[j\beta\gamma_0\Big] + B_4(\alpha,\beta)\Big[\omega\varepsilon_0\alpha\Big] = 0. \end{aligned} \tag{C.45}$$

Next, multiplying (C.44) by α and (C.45) by β, adding and factoring gives:

$$A_3(\alpha,\beta)\Big[\gamma_{h3}\cosh(\gamma_{h3}d_{13})\Big] + A_3'(\alpha,\beta)\Big[\gamma_{h3}\sinh(\gamma_{h3}d_{13})\Big] + A_4(\alpha,\beta)\Big[\gamma_0\Big] = 0. \tag{C.46}$$

Next, multiplying (C.44) by β and (C.45) by $-\alpha$, adding and factoring gives:

$$B_3(\alpha,\beta)\cosh(\gamma_{e3}d_{13}) + B_3'(\alpha,\beta)\sinh(\gamma_{e3}d_{13}) - B_4(\alpha,\beta) = 0. \tag{C.47}$$

Next, multiply (C.47) by $\frac{\gamma_0}{\varepsilon_{42}}$ and add to (C.42). This yields

$$B_3(\alpha,\beta)N_6 + B_3'(\alpha,\beta)M_6 = 0 \tag{C.48}$$

where

$$M_6 = \frac{\gamma_0}{\varepsilon_{42}}\sinh(\gamma_{e3}d_{13}) + \frac{\gamma_{e3}}{\varepsilon_{32}}\cosh(\gamma_{e3}d_{13}) \tag{C.49}$$

$$N_6 = \frac{\gamma_0}{\varepsilon_{42}}\cosh(\gamma_{e3}d_{13}) + \frac{\gamma_{e3}}{\varepsilon_{32}}\sinh(\gamma_{e3}d_{13}). \tag{C.50}$$

Next, multiply (C.43) by γ_0 and add to (C.46). This yields

$$A_3(\alpha,\beta)N_7 + A_3'(\alpha,\beta)M_7 = 0 \tag{C.51}$$

where

$$M_7 = \gamma_0 \cosh(\gamma_{h3} d_{13}) + \gamma_{h3} \sinh(\gamma_{h3} d_{13}) \tag{C.52}$$

$$N_7 = \gamma_0 \sinh(\gamma_{h3} d_{13}) + \gamma_{h3} \cosh(\gamma_{h3} d_{13}). \tag{C.53}$$

Next, multiply (C.47) by $-\frac{\gamma_{e3}}{\varepsilon_{32}} \sinh(\gamma_{e3} d_{13})$ and (C.42) by $\cosh(\gamma_{e3} d_{13})$ and add. This yields

$$B_3'(\alpha, \beta) \frac{\gamma_{e3}}{\varepsilon_{32}} + B_4(\alpha, \beta) N_6 = 0. \tag{C.54}$$

Next, multiply (C.43) by $-\gamma_{h3} \cosh(\gamma_{h3} d_{13})$ and (C.46) $\sinh(\gamma_{h3} d_{13})$ and add. This yields

$$-A_3'(\alpha, \beta) \gamma_{h3} + A_4(\alpha, \beta) N_7 = 0. \tag{C.55}$$

Solving for $B_3(\alpha, \beta)$ in (C.48) gives:

$$B_3(\alpha, \beta) = -\frac{M_6}{N_6} B_3'(\alpha, \beta). \tag{C.56}$$

Solving for $A_3(\alpha, \beta)$ in (C.51) gives:

$$A_3(\alpha, \beta) = -\frac{M_7}{N_7} A_3'(\alpha, \beta). \tag{C.57}$$

Solving for $B_4(\alpha, \beta)$ in (C.54) gives:

$$B_4(\alpha, \beta) = -\frac{\gamma_{e3}}{N_6 \varepsilon_{32}} B_3'(\alpha, \beta). \tag{C.58}$$

Solving for $A_4(\alpha, \beta)$ in (C.55) gives:

$$A_4(\alpha, \beta) = \frac{\gamma_{h3}}{N_7} A_3'(\alpha, \beta). \tag{C.59}$$

Next, substitute (C.21) and (C.56) into (C.34). After factoring, this yields

$$B_3'(\alpha,\beta) = \frac{P_{12}}{P_{11}} B_2(\alpha,\beta) + \left[\frac{\gamma_{e1}\gamma_{e2}\sinh(\gamma_{e1}d_1)\cosh(\gamma_{e2}d_{12})}{P_{11}N_1\varepsilon_{12}\varepsilon_{22}}\right]\frac{\alpha\widetilde{J}_{x1}+\beta\widetilde{J}_{z1}}{\omega\varepsilon_0(\alpha^2+\beta^2)} \tag{C.60}$$

where

$$P_{11} = \frac{\gamma_{e3}}{\varepsilon_{32}}\cosh(\gamma_{e3}d_{12}) - \frac{M_6}{N_6}\frac{\gamma_{e3}}{\varepsilon_{32}}\sinh(\gamma_{e3}d_{12}) \tag{C.61}$$

$$P_{12} = \frac{\gamma_{e2}}{\varepsilon_{22}}\sinh(\gamma_{e2}d_{12}) - \frac{M_1}{N_1}\frac{\gamma_{e2}}{\varepsilon_{22}}\cosh(\gamma_{e2}d_{12}). \tag{C.62}$$

Next, substitute (C.30) and (C.57) into (C.35). After factoring this yields

$$A_3'(\alpha,\beta) = \frac{P_{14}}{P_{13}} A_2(\alpha,\beta) + \left[\frac{\sinh(\gamma_{h1}d_1)\cosh(\gamma_{h2}d_{12})}{P_{13}N_4}\right]\frac{\beta\widetilde{J}_{x1}-\alpha\widetilde{J}_{z1}}{j(\alpha^2+\beta^2)} \tag{C.63}$$

where

$$P_{13} = \cosh(\gamma_{h3}d_{12}) - \frac{M_7}{N_7}\sinh(\gamma_{h3}d_{12}) \tag{C.64}$$

$$P_{14} = \sinh(\gamma_{h2}d_{12}) + \frac{M_4}{N_4}\cosh(\gamma_{h2}d_{12}). \tag{C.65}$$

Next, substitute (C.56), (C.60) and (C.21) into (C.38). After factoring and simplifying this yields

$$B_2'(\alpha,\beta) = P_{29}\frac{\alpha\widetilde{J}_{x2}+\beta\widetilde{J}_{z2}}{\omega\varepsilon_0(\alpha^2+\beta^2)} - P_{30}\frac{\alpha\widetilde{J}_{x1}+\beta\widetilde{J}_{z1}}{\omega\varepsilon_0(\alpha^2+\beta^2)} \tag{C.66}$$

where

$$P_{15} = \frac{\gamma_{e1}\gamma_{e2}}{P_{11}N_1\varepsilon_{12}\varepsilon_{22}}\cosh(\gamma_{e2}d_{12})\sinh(\gamma_{e1}d_1) \tag{C.67}$$

$$P_{16} = \frac{M_6}{N_6}\cosh(\gamma_{e3}d_{12}) - \sinh(\gamma_{e3}d_{12}) \tag{C.68}$$

$$P_{17} = \frac{\gamma_{e1}}{N_1\varepsilon_{12}}\sinh(\gamma_{e1}d_1)\sinh(\gamma_{e2}d_{12}) \tag{C.69}$$

$$P_{18} = \frac{M_6 P_{12}}{N_6 P_{11}} \cosh(\gamma_{e3} d_{12}) - \frac{P_{12}}{P_{11}} \sinh(\gamma_{e3} d_{12}) \tag{C.70}$$

$$P_{19} = \cosh(\gamma_{e2} d_{12}) - \frac{M_1}{N_1} \sinh(\gamma_{e2} d_{12}), \tag{C.71}$$

$$P_{29} = \frac{1}{P_{18} + P_{19}}, \tag{C.72}$$

$$P_{30} = \frac{P_{15} P_{16} + P_{17}}{P_{18} + P_{19}}. \tag{C.73}$$

Next, substitute (C.30), (C.57) and (C.63) into (C.39). After factoring and simplifying this yields

$$A_2(\alpha, \beta) = \left[\frac{1}{P_{23} + P_{24}}\right] \frac{\beta \widetilde{J}_{x2} - \alpha \widetilde{J}_{z2}}{-j(\alpha^2 + \beta^2)} - \left[\frac{P_{22} + P_{20} P_{21}}{P_{23} + P_{24}}\right] \frac{\beta \widetilde{J}_{x1} - \alpha \widetilde{J}_{z1}}{j(\alpha^2 + \beta^2)} \tag{C.74}$$

where

$$P_{20} = \frac{\sinh(\gamma_{h1} d_1) \cosh(\gamma_{h2} d_{12})}{N_4 P_{13}} \tag{C.75}$$

$$P_{21} = \frac{M_7}{N_7} \gamma_{h3} \cosh(\gamma_{h3} d_{12}) - \gamma_{h3} \sinh(\gamma_{h3} d_{12}) \tag{C.76}$$

$$P_{22} = \frac{\gamma_{h2} \sinh(\gamma_{h1} d_1) \sinh(\gamma_{h2} d_{12})}{N_4} \tag{C.77}$$

$$P_{23} = \frac{M_7 P_{14}}{N_7 P_{13}} \gamma_{h3} \cosh(\gamma_{h3} d_{12}) - \frac{P_{14}}{P_{13}} \gamma_{h3} \sinh(\gamma_{h3} d_{12}) \tag{C.78}$$

$$P_{24} = \frac{M_4}{N_4} \gamma_{h2} \sinh(\gamma_{h2} d_{12}) + \gamma_{h2} \cosh(\gamma_{h2} d_{12}). \tag{C.79}$$

Next we have the coefficients in (C.66) and (C.74) written in terms of the material properties only. We will now use these expressions to solve for the other coefficients. Substituting (C.66) into (C.21), and (C.60) and factoring, results in the following coefficients

$$B_2'(\alpha, \beta) = P_{32} \frac{\alpha \widetilde{J}_{x1} + \beta \widetilde{J}_{z1}}{\omega \varepsilon_0 (\alpha^2 + \beta^2)} + P_{31} \frac{\alpha \widetilde{J}_{x2} + \beta \widetilde{J}_{z2}}{\omega \varepsilon_0 (\alpha^2 + \beta^2)}, \tag{C.80}$$

$$B_3'(\alpha,\beta) = \left[\frac{\gamma_{e1}\gamma_{e2}\sinh(\gamma_{e1}d_1)\cosh(\gamma_{e2}d_{12})}{P_{11}N_1\varepsilon_{12}\varepsilon_{22}} - \frac{P_{12}(P_{15}P_{16}+P_{17})}{P_{11}(P_{18}+P_{19})}\right]\frac{\alpha\widetilde{J}_{x1}+\beta\widetilde{J}_{z1}}{\omega\varepsilon_0(\alpha^2+\beta^2)}$$

$$+\left[\frac{P_{12}}{P_{11}(P_{18}+P_{19})}\right]\frac{\alpha\widetilde{J}_{x2}+\beta\widetilde{J}_{z2}}{\omega\varepsilon_0(\alpha^2+\beta^2)} \tag{C.81}$$

where

$$P_{31} = \frac{-M_1P_{29}}{N1}, \tag{C.82}$$

$$P_{32} = \frac{M_1P_{30}}{N_1} + \frac{\gamma_{e1}\sinh(\gamma_{e1}d_1)}{N_1\varepsilon_{12}}. \tag{C.83}$$

Substituting (C.80) into (C.25) gives

$$B_1(\alpha,\beta) = \frac{-\gamma_{e2}P_{31}}{M_1}\frac{\alpha\widetilde{J}_{x2}+\beta\widetilde{J}_{z2}}{\omega\varepsilon_0(\alpha^2+\beta^2)} - \frac{\gamma_{e2}}{M_1}\left[P_{32}-\sinh(\gamma_{e2}d_1)\right]\frac{\alpha\widetilde{J}_{x1}+\beta\widetilde{J}_{z1}}{\omega\varepsilon_0(\alpha^2+\beta^2)}, \tag{C.84}$$

Next, substituting (C.81) into (C.56) and (C.58) and factoring, results in the following coefficients

$$B_3(\alpha,\beta) = \left[-\frac{M_6\gamma_{e1}\gamma_{e2}\sinh(\gamma_{e1}d_1)\cosh(\gamma_{e2}d_{12})}{P_{11}N_1N_6\varepsilon_{12}\varepsilon_{22}}\right.$$

$$\left.+\frac{M_6P_{12}(P_{15}P_{16}+P_{17})}{N_6P_{11}(P_{18}+P_{19})}\right]\frac{\alpha\widetilde{J}_{x1}+\beta\widetilde{J}_{z1}}{\omega\varepsilon_0(\alpha^2+\beta^2)}$$

$$-\left[\frac{M_6P_{12}}{N_6P_{11}(P_{18}+P_{19})}\right]\frac{\alpha\widetilde{J}_{x2}+\beta\widetilde{J}_{z2}}{\omega\varepsilon_0(\alpha^2+\beta^2)}, \tag{C.85}$$

$$B_4(\alpha,\beta) = \left[-\frac{\gamma_{e1}\gamma_{e2}\gamma_{e3}\sinh(\gamma_{e1}d_1)\cosh(\gamma_{e2}d_{12})}{P_{11}N_1N_6\varepsilon_{12}\varepsilon_{22}\varepsilon_{32}}\right.$$

$$\left.+\frac{\gamma_{e3}P_{12}(P_{15}P_{16}+P_{17})}{\varepsilon_{32}N_6P_{11}(P_{18}+P_{19})}\right]\frac{\alpha\widetilde{J}_{x1}+\beta\widetilde{J}_{z1}}{\omega\varepsilon_0(\alpha^2+\beta^2)}$$

$$-\left[\frac{\gamma_{e3}P_{12}}{\varepsilon_{32}N_6P_{11}(P_{18}+P_{19})}\right]\frac{\alpha\widetilde{J}_{x2}+\beta\widetilde{J}_{z2}}{\omega\varepsilon_0(\alpha^2+\beta^2)}. \tag{C.86}$$

Substituting (C.74) into (C.27), (C.30) and (C.63) and factoring results in the following coefficients

$$\begin{aligned} A_1(\alpha,\beta) &= \left[\frac{\cosh(\gamma_{h2}d_1)}{N_4}-\frac{\gamma_{h2}(P_{22}+P_{20}P_{21})}{N_4(P_{23}+P_{24})}\right]\frac{\beta\widetilde{J}_{x1}-\alpha\widetilde{J}_{z1}}{j(\alpha^2+\beta^2)} \\ &\quad +\left[\frac{\gamma_{h2}}{N_4(P_{23}+P_{24})}\right]\frac{\beta\widetilde{J}_{x2}-\alpha\widetilde{J}_{z2}}{-j(\alpha^2+\beta^2)}, \end{aligned} \tag{C.87}$$

$$\begin{aligned} A_2'(\alpha,\beta) &= \left[\frac{\sinh(\gamma_{h1}d_1)}{N_4}-\frac{M_4(P_{22}+P_{20}P_{21})}{N_4(P_{23}+P_{24})}\right]\frac{\beta\widetilde{J}_{x1}-\alpha\widetilde{J}_{z1}}{j(\alpha^2+\beta^2)} \\ &\quad +\left[\frac{M_4}{N_4(P_{23}+P_{24})}\right]\frac{\beta\widetilde{J}_{x2}-\alpha\widetilde{J}_{z2}}{-j(\alpha^2+\beta^2)}, \end{aligned} \tag{C.88}$$

$$\begin{aligned} A_3'(\alpha,\beta) &= \left[\frac{\sinh(\gamma_{h1}d_1)\cosh(\gamma_{h2}d_{12})}{N_4P_{13}}-\frac{P_{14}(P_{22}+P_{20}P_{21})}{P_{13}(P_{23}+P_{24})}\right]\frac{\beta\widetilde{J}_{x1}-\alpha\widetilde{J}_{z1}}{j(\alpha^2+\beta^2)} \\ &\quad +\left[\frac{P_{14}}{P_{13}(P_{23}+P_{24})}\right]\frac{\beta\widetilde{J}_{x2}-\alpha\widetilde{J}_{z2}}{-j(\alpha^2+\beta^2)}. \end{aligned} \tag{C.89}$$

Next, substituting (C.89) into (C.57) and (C.59) and factoring results in the following coefficients

$$\begin{aligned} A_3(\alpha,\beta) &= \left[-\frac{M_7\sinh(\gamma_{h1}d_1)\cosh(\gamma_{h2}d_{12})}{P_{13}N_4N_7}\right. \\ &\quad \left.+\frac{M_7P_{14}(P_{22}+P_{20}P_{21})}{N_7P_{13}(P_{23}+P_{24})}\right]\frac{\beta\widetilde{J}_{x1}-\alpha\widetilde{J}_{z1}}{j(\alpha^2+\beta^2)} \end{aligned}$$

$$-\left[\frac{M_7 P_{14}}{N_7 P_{13}(P_{23}+P_{24})}\right]\frac{\beta\widetilde{J}_{x2}-\alpha\widetilde{J}_{z2}}{-j(\alpha^2+\beta^2)}, \tag{C.90}$$

$$\begin{aligned} A_4(\alpha,\beta) \;=\; & \left[\frac{\gamma_{h3}\sinh(\gamma_{h1}d_1)\cosh(\gamma_{h2}d_{12})}{P_{13}N_4N_7}\right. \\ & \left.-\frac{\gamma_{h3}P_{14}(P_{22}+P_{20}P_{21})}{N_7P_{13}(P_{23}+P_{24})}\right]\frac{\beta\widetilde{J}_{x1}-\alpha\widetilde{J}_{z1}}{j(\alpha^2+\beta^2)} \\ & +\left[\frac{\gamma_{h3}P_{14}}{N_7P_{13}(P_{23}+P_{24})}\right]\frac{\beta\widetilde{J}_{x2}-\alpha\widetilde{J}_{z2}}{-j(\alpha^2+\beta^2)}. \end{aligned} \tag{C.91}$$

Next, the previously derived coefficients will be used to write the expression of the electric field in region 2. This expression for the electric field will then be used to solve for the unknown surface currents $\widetilde{J}_1$ and $\widetilde{J}_2$ in Figure 18. Substituting (C.74), (C.88), (C.80) and (C.66) into (3.168) and factoring extensively yields

$$\widetilde{E}_{x2}(\alpha,y,\beta)=\widetilde{J}_{x1}\widetilde{Z}_{xx1}+\widetilde{J}_{z1}\widetilde{Z}_{xz1}+\widetilde{J}_{x2}\widetilde{Z}_{xx2}+\widetilde{J}_{z2}\widetilde{Z}_{xz2} \tag{C.92}$$

where

$$\begin{aligned} \widetilde{Z}_{xx1} \;=\; & \frac{\alpha^2}{\alpha^2+\beta^2}\left[\frac{\gamma_{e2}P_{30}\sinh(\gamma_{e2}y)}{j\omega\varepsilon_0\varepsilon_{22}}+\frac{\gamma_{e2}P_{32}\cosh(\gamma_{e2}y)}{-j\omega\varepsilon_0\varepsilon_{22}}\right]+ \\ & \frac{\beta^2}{\alpha^2+\beta^2}\left[j\omega\mu_0P_{28}\cosh(\gamma_{h2}y)-j\omega\mu_0P_{26}\sinh(\gamma_{h2}y)\right], \end{aligned} \tag{C.93}$$

$$\widetilde{Z}_{xz1} \;=\; \frac{\alpha\beta}{\alpha^2+\beta^2}\left[\frac{\gamma_{e2}P_{32}\cosh(\gamma_{e2}y)}{-j\omega\varepsilon_0\varepsilon_{22}}+\frac{\gamma_{e2}P_{30}\sinh(\gamma_{e2}y)}{j\omega\varepsilon_0\varepsilon_{22}}\right]+$$

$$\frac{\alpha\beta}{\alpha^2+\beta^2}\Big[j\omega\mu_0 P_{26}\sinh(\gamma_{h2}y) - j\omega\mu_0 P_{28}\cosh(\gamma_{h2}y)\Big], \tag{C.94}$$

$$\begin{aligned}\widetilde{Z}_{xx2} &= \frac{\alpha^2}{\alpha^2+\beta^2}\left[\frac{\gamma_{e2}P_{29}\sinh(\gamma_{e2}y)}{-j\omega\varepsilon_0\varepsilon_{22}} + \frac{\gamma_{e2}P_{31}\cosh(\gamma_{e2}y)}{-j\omega\varepsilon_0\varepsilon_{22}}\right] + \\ &\quad \frac{\beta^2}{\alpha^2+\beta^2}\Big[- j\omega\mu_0 P_{25}\sinh(\gamma_{h2}y) - j\omega\mu_0 P_{27}\cosh(\gamma_{h2}y)\Big],\end{aligned} \tag{C.95}$$

$$\begin{aligned}\widetilde{Z}_{xz2} &= \frac{\alpha\beta}{\alpha^2+\beta^2}\left[\frac{\gamma_{e2}P_{29}\sinh(\gamma_{e2}y)}{-j\omega\varepsilon_0\varepsilon_{22}} + \frac{\gamma_{e2}P_{31}\cosh(\gamma_{e2}y)}{-j\omega\varepsilon_0\varepsilon_{22}}\right] + \\ &\quad \frac{\alpha\beta}{\alpha^2+\beta^2}\Big[j\omega\mu_0 P_{25}\sinh(\gamma_{h2}y) + j\omega\mu_0 P_{27}\cosh(\gamma_{h2}y)\Big]\end{aligned} \tag{C.96}$$

where

$$P_{25} = \frac{1}{P_{23}+P_{25}} \tag{C.97}$$

$$P_{26} = \frac{P_{20}P_{21}+P_{22}}{P_{23}+P_{24}} \tag{C.98}$$

$$P_{27} = \frac{M_4}{N_4(P_{23}+P_{24})} \tag{C.99}$$

$$P_{28} = \frac{\sinh(\gamma_{h1}d_1)}{N_4} - \frac{M_4(P_{20}P_{21}+P_{22})}{N_4(P_{23}+P_{24})}. \tag{C.100}$$

Next, substituting (C.74), (C.88), (C.80) and (C.66) into (3.170) and extensive factoring yields

$$\widetilde{E}_{z2}(\alpha,y,\beta) = \widetilde{J}_{x1}\widetilde{Z}_{zx1} + \widetilde{J}_{z1}\widetilde{Z}_{zz1} + \widetilde{J}_{x2}\widetilde{Z}_{zx2} + \widetilde{J}_{z2}\widetilde{Z}_{zz2} \tag{C.101}$$

where

$$\widetilde{Z}_{zx1} = \widetilde{Z}_{xz1}, \tag{C.102}$$

$$\begin{aligned}\widetilde{Z}_{zz1} &= \frac{\alpha^2}{\alpha^2+\beta^2}\Big[j\omega\mu_0 P_{28}\cosh(\gamma_{h2}y) - j\omega\mu_0 P_{26}\sinh(\gamma_{h2}y)\Big] + \\ &\quad \frac{\beta^2}{\alpha^2+\beta^2}\left[\frac{\gamma_{e2}P_{30}\sinh(\gamma_{e2}y)}{j\omega\varepsilon_0\varepsilon_{22}} - \frac{\gamma_{e2}P_{32}\cosh(\gamma_{e2}y)}{j\omega\varepsilon_0\varepsilon_{22}}\right],\end{aligned} \tag{C.103}$$

$$\widetilde{Z}_{zx2} = \widetilde{Z}_{xz2}, \tag{C.104}$$

$$\begin{aligned}\widetilde{Z}_{zz2} &= \frac{\alpha^2}{\alpha^2+\beta^2}\Big[-j\omega\mu_0 P_{25}\sinh(\gamma_{h2}y) - j\omega\mu_0 P_{27}\cosh(\gamma_{h2}y)\Big] + \\ &\quad \frac{\beta^2}{\alpha^2+\beta^2}\left[\frac{\gamma_{e2}P_{29}\sinh(\gamma_{e2}y)}{-j\omega\varepsilon_0\varepsilon_{22}} + \frac{\gamma_{e2}P_{31}\cosh(\gamma_{e2}y)}{-j\omega\varepsilon_0\varepsilon_{22}}\right].\end{aligned} \tag{C.105}$$

APPENDIX D. INFINITE MICROSTRIP EXAMPLE CODE

The following code evaluates the convergence and charge distribution of Davidson's *et.al.* [84] infinite microstrip example.

```
clc
clear all

W=.01;
d=.01;
er=2.2;
e0=8.85418781762e-12;

Vo=1;                                                    %conductor potential
s=0;                                                     %counter reset
for N=5:5:40;                                            %number of spacial points
    s=s+1;                                               %counter
    Bmax=10;                                             %constant defined by Davidson
    Bk=50;                                               %constant defined by Davidson
    delx=W/N;                                            %max spectral value
    kmax=Bmax/delx;                                      %spectral step size
    Nk=Bk*2*kmax*W/pi;                                   %number of spectral points
    delk=kmax/Nk;                                        %spectral step size
    ki=delk/1e300:delk:Nk*delk;                          %spectral points
    xm=-W/2+delx/2:delx:W/2-delx/2;                      %spacial match points
    xn=xm;                                               %spacial expansion points
    PHI=delx*sin(ki*delx/2)./(ki*delx/2);                %sinc function
    G=1./(e0*abs(ki).*(1+er*coth(abs(ki)*d)));           %spectral domain Green's function
    for m=1:N;
        for n=1:N;
            a=(1/pi)*G.*PHI.^2.*cos(ki.*(xm(m)-xn(n)));  %evaluates amn (eq. 28) in Davidson's paper
            amn(m,n)=sum(a)*delk;
        end
        V(m)=Vo;                                         %voltage matrix
    end

    phi=V*inv(amn)*delx;                                 %calculates the line charge
    Q=sum(phi)*delx;                                     %total charge for capacitance calculations
    C(s)=Q/Vo                                            %total capacitance

end

figure
plot(xm*1e3,phi*1e9,'o-')                                %plots line charge
xlabel('x (mm)');
ylabel('Charge per unit length (nC/m)')
legend('\epsilon_r = 2.2')
title('Charge distribution for N=40,B_{max}=10 and B_k=50')

figure plot(5:5:40,C*1e12,'o-')
xlabel('Number of segments N')
ylabel('Capacitance (pF/m)')
title('Convergence of the spectral-domain solution for B_{max}=10 and B_k=50')
legend('\epsilon_r = 2.2')
```

APPENDIX E. INPUT IMPEDANCE CODE FOR A SINGLE DIPOLE ON A SINGLE ANISOTROPIC LAYER

```
%*************************************************************************
% Author:       Ben Braaten
% Date:         11/23/08
% Description:  This code calculates the input impedance of a single
%               printed dipole on a single anisotropic dielectric substrate.
%               The dipole can have length L and width W.
%*************************************************************************
%                         FFFFF   IIIII   N     N      A       L
%                         F         I     N N   N     A A      L
%                         FFF       I     N  N  N    AAAAA     L
%                         F         I     N   N N   A     A    L
%                         F       IIIII   N     N  A       A   LLLLL

% DDDD    IIIII      SSS     SSS    EEEE    RRRR    TTTTT       A       TTTTT  IIIII    OOOO    N     N
% D   D     I       S       S       E       R   R     T        A A        T      I     O    O   N N   N
% D   D     I         S       S     EEE     RRRR      T       AAAAA       T      I     O    O   N  N  N
% D   D     I           S       S   E       R  R      T      A     A      T      I     O    O   N   N N
% DDDD    IIIII      SSS     SSS    EEEE    R   R     T     A       A     T    IIIII    OOOO    N     N

%                              CCC    OOOO    DDDD    EEEE
%                             C      O    O   D   D   E
%                             C      O    O   D   D   EEE
%                             C      O    O   D   D   E
%                              CCC    OOOO    DDDD    EEEE


clc
clear all


s=0;                                                        %resets counter
f=1e9;                                                      %center frequency

w=2*pi*f;                                                   %omega
c=3e8;                                                      %speed of light
lambda0=c/f;                                                %free-space wavelength
a=.0001*lambda0;                                            %radius of the wire
W=4*a;                                                      %width of the strip
M=94;                                                       %number of dipole segments
for L=.49*lambda0:.03*lambda0:.8*lambda0;                   %length of dipole
    d=.1016*lambda0;                                        %depth of substrate
    e0=8.854e-12;                                           %constant
    e11=5.12;                                               %aniso. permittivity
    e12=3.14;                                               %aniso. permittivity
    e21=1;                                                  %permittivity of air
    e22=1;                                                  %permittivity of air
    u0=1.2566e-6;                                           %constant
    k0=w*sqrt(u0*e0)                                        %free-space wave number
    k=w*sqrt(u0*e0*e11)                                     %aniso. wavenumber


    s=s+1;                                                  %counter
    N=M;                                                    %number of expansion fcns.
    Vs=1;                                                   %delta source voltage
    delx=L/N;                                               %x-step size
    delz=W;                                                 %z-step size
    xm=-L/2+delx:delx:L/2-delx;                             %x-dim. match points
    xn=xm;                                                  %x-dim. source points
    zm=zeros(1,length(xm));                                 %z-dim. match points
    zn=zm;                                                  %z-dim. source points
    w=2*pi*f;                                               %omega

    %root finding routine
    %The following routine uses the secant method
    %to find the poles in the spectral domain
    %immittance fuctions.

    iteration=100;
    root1(1)=k;
    root1(2)=k-.1;
    root2(1)=0;
    root2(2)=.9*k0*j;

    p=2;
    while p<iteration;
        if e11==1;
            p=iteration+1;
            root1(p)=k0;
        else
            p=p+1;
```

```
        gamma01=sqrt(root1(p-1)^2-w^2*u0*e0);
        gamma02=sqrt(root1(p-2)^2-w^2*u0*e0);
        gammae1=sqrt((e12)/(e11)*(root1(p-1)^2-w^2*u0*e0*e11));
        gammae2=sqrt((e12)/(e11)*(root1(p-2)^2-w^2*u0*e0*e11));
        gammah1=sqrt(root1(p-1)^2-w^2*u0*e0*e12);
        gammah2=sqrt(root1(p-2)^2-w^2*u0*e0*e12);
        f11=gammae1+gamma01*e12*coth(gammae1*d);
        f12=gammae2+gamma02*e12*coth(gammae2*d);
        root1(p)=root1(p-1)-(f11)*(root1(p-1)-root1(p-2))/((f11)-(f12));

        gamma01=sqrt(root2(p-1)^2-w^2*u0*e0);
        gamma02=sqrt(root2(p-2)^2-w^2*u0*e0);
        gammae1=sqrt((e12)/(e11)*(root1(p-1)^2-w^2*u0*e0*e11));
        gammae2=sqrt((e12)/(e11)*(root1(p-2)^2-w^2*u0*e0*e11));
        gammah1=sqrt(root1(p-1)^2-w^2*u0*e0*e12);
        gammah2=sqrt(root1(p-2)^2-w^2*u0*e0*e12);
        f11=gamma01+gammah1*coth(gammah1*d);
        f12=gamma02+gammah2*coth(gammah2*d);
        root2(p)=root2(p-1)-(f11)*(root2(p-1)-root2(p-2))/((f11)-(f12));

        if abs(root1(p)-root1(p-1))<.0001&p>10
            p=iteration+1;
        else
                %do nothing
        end
    end
end

root=real(root1(length(root1)))                                          %saves root

mult=500+(L-.5*lambda0)*(-500/lambda0);
kmax_alpha=mult*k0;
kmax_beta=mult*k0;
Nalpha=kmax_alpha/k0;
Nbeta=kmax_beta/k0;

%polar points
%The following routines setup the polar integration points.
if root>=k0
    del_r_fine=k0/50;
    del_r_very_fine=(k-k0)*.01;
    r_fine_lower=del_r_fine:del_r_fine:k0-del_r_fine/2;
    r_very_fine=[fliplr([root-del_r_very_fine:-del_r_very_fine:k0+del_r_very_fine+del_r_fine/2]) ...
    root+del_r_very_fine:del_r_very_fine:k-del_r_very_fine];
    r_fine=[r_fine_lower r_very_fine];
    r=r_fine;
    del_r=[del_r_fine*ones(1,length(r_fine_lower)) del_r_very_fine*ones(1,length(r_very_fine))];
else
    del_r_fine=k0/30;
    del_r_very_fine=root/30;
    r_very_fine=[[del_r_very_fine:del_r_very_fine:root-del_r_very_fine] ...
        [root+del_r_very_fine:del_r_very_fine:k-del_r_very_fine]];
    r_fine=[r_very_fine];
    r=r_fine;
    del_r=[del_r_very_fine*ones(1,length(r_very_fine))];
end

del_theta=pi/50;
theta=[del_theta/2:del_theta:pi/2-del_theta/2 pi/2+del_theta/2:del_theta:pi-del_theta/2 ...
    pi+del_theta/2:del_theta:3*pi/2-del_theta/2 3*pi/2+del_theta/2:del_theta:2*pi-del_theta/2];

Kxx_matrix=zeros(length(r),length(theta));
Zxx=zeros(length(r),length(theta));


%rectangular points
%The following routines setup the rectangular integration points.
del_alpha_lower=kmax_alpha/Nalpha;
del_alpha_upper=del_alpha_lower;
del_alpha_middle=k/30;

alpha_lower=-fliplr([k+del_alpha_lower/2:del_alpha_lower:kmax_alpha]);
alpha_middle=-k+del_alpha_middle/2:del_alpha_middle:k-del_alpha_middle/2;
alpha_upper=k+del_alpha_upper/2:del_alpha_upper:kmax_alpha;
alpha=[alpha_lower alpha_middle alpha_upper];
del_alpha=[del_alpha_lower*ones(1,length(alpha_lower)) del_alpha_middle*ones(1,length(alpha_middle)) ...
del_alpha_upper*ones(1,length(alpha_upper))];

del_beta=kmax_beta/Nbeta;


%Polar integration routine
%The following routine integrates in the polar coordinates around and
%near the poles between k0 and k.
for m=1:M-1;
    m
    for n=1:N-1;
        Kxx_matrix_fine=0;
        Kxx_matrix=0;
```

```
        for g=1:length(r);

            ks=k;
            R=1;

            %  2-D PWS
            rxn_PWS=(2./sin(ks*delx)).*(1./(ks-r(g).*sin(theta))+1./(ks+r(g).*sin(theta))).*exp(-j*r(g).* ...
                sin(theta)*xn(n)).*sin((ks*delx+r(g).*sin(theta)*delx)/2).*sin((ks*delx-r(g).*sin(theta)*delx)/2);
            rxm_PWS=(2./sin(ks*delx)).*(1./(ks--r(g).*sin(theta))+1./(ks+-r(g).*sin(theta))).*exp(j*r(g).* ...
                sin(theta)*xm(m)).*sin((ks*delx+-r(g).*sin(theta)*delx)/2).*sin((ks*delx--r(g).*sin(theta)*delx)/2);

            rxn_pulse=exp(-j*r(g).*cos(theta)*zn(n)).*(delz*sin(r(g).*cos(theta)*delz/2)./(delz*r(g).* ...
                cos(theta)/2)).*exp(j*-r(g).*cos(theta)*delz/2);

            rxm_pulse=exp(j*r(g).*cos(theta)*zm(m)).*(delz*sin(r(g).*cos(theta)*delz/2)./(delz*r(g).* ...
                cos(theta)/2)).*exp(j*r(g).*cos(theta)*delz/2);

            rxn=rxn_PWS.*rxn_pulse;
            rxm=rxm_PWS.*rxm_pulse;

            gamma0=sqrt(r(g)^2-w^2*u0*e0);
            gammae1=sqrt((e12/e11)*(r(g)^2-w^2*u0*e0*e11));
            gammah1=sqrt(r(g)^2-w^2*u0*e0*e12);

            Zxx=(cos(theta).^2).*(-j*w*u0./(gamma0+gammah1.*coth(gammah1*d)))+ ...
                   (sin(theta).^2).*(-gammae1.*gamma0./(j*w*e0*(gammae1+gamma0*e12.*coth(gammae1*d))));

            Kxx_matrix=Kxx_matrix+sum(Zxx.*rxm.*rxn.*R.*del_theta.*del_r(g)*r(g));

        end

        matrix_polar(m,n)=(1/(2*pi)^2)*Kxx_matrix;

    end
end



clear Kxx_matrix Zxx

%rectangular integration routine
%The following routine integrates the rectangular region outside of the
%k circle.  This routine avoids the poles associated with +/-k in the
%basis functions
for m=1:M-1;
    m
    for n=1:N-1;
        Kxx_matrix_fine=0;
        Kxx_matrix=0;
        for g=1:length(alpha);

            if abs(alpha(g))<k
                beta_jump=sqrt(k^2-alpha(g)^2)+del_beta/2;
                beta=beta_jump:del_beta:kmax_beta;
                beta=[beta -beta];
            else
                beta=del_beta/2:del_beta:kmax_beta;
                beta=[beta -beta];
            end

            ks=k;

            %  2-D PWS

            rxn_PWS=(2./sin(ks*delx)).*(1./(ks-alpha(g))+1./(ks+alpha(g))).*exp(-j*alpha(g)*xn(n)).* ...
                sin((ks*delx+alpha(g)*delx)/2).*sin((ks*delx-alpha(g)*delx)/2);
            rxm_PWS=(2./sin(ks*delx)).*(1./(ks--alpha(g))+1./(ks+-alpha(g))).*exp(j*alpha(g)*xm(m)).* ...
                sin((ks*delx+-alpha(g)*delx)/2).*sin((ks*delx--alpha(g)*delx)/2);

            rxn_pulse=exp(-j*beta.*zn(n)).*(delz*sin(beta.*delz/2)./(delz*beta./2)).*exp(-j*beta.*delz/2);

            rxm_pulse=exp(j*beta.*zm(m)).*(delz*sin(beta.*delz/2)./(delz*beta./2)).*exp(j*beta.*delz/2);

            rxn=rxn_PWS.*rxn_pulse;
            rxm=rxm_PWS.*rxm_pulse;

            R=1;

            gamma0=sqrt(alpha(g)^2+beta.^2-w^2*u0*e0);
            gammae1=sqrt((e12/e11)*(alpha(g)^2+beta.^2-w^2*u0*e0*e11));
            gammah1=sqrt(alpha(g)^2+beta.^2-w^2*u0*e0*e12);

            Zxx=(beta.^2./(beta.^2+alpha(g)^2)).*(-j*w*u0./(gamma0+gammah1.*coth(gammah1*d)))+ ...
                    (alpha(g).^2./(beta.^2+alpha(g)^2)).*(-gammae1.*gamma0./(j*w*e0*(gammae1+gamma0*e12.*coth(gammae1*d))));

            Kxx_matrix=Kxx_matrix+sum(Zxx.*rxm.*rxn.*R.*del_beta.*del_alpha(g));

        end
```

```
            matrix_rect(m,n)=(1/(2*pi)^2)*Kxx_matrix;

        end
    end

    matrix=matrix_polar+matrix_rect;                                %saves the rectangular
                                                                    %and polar integration results
                                                                    %in the impedance matrix.

    V=zeros(M-1,1);                                                 %fills in voltage matrix
    ws=2*(1-cos(k*delx))/(k*sin(k*delx))*delz;
    V(ceil(M/2))=-Vs*ws/(2*delx);
    V(ceil(M/2)-1)=.5*V(ceil(M/2));
    V(ceil(M/2)+1)=.5*V(ceil(M/2));

    J=inv(matrix)*V                                                 %solves for surface current (A/m)
    I=J*delz;                                                       %solves for total current   (A)
    Z_in(s)=Vs/I(ceil(M/2))                                         %solves for input impedance

end
```

APPENDIX F. MUTUAL COUPLING CODE FOR TWO DIPOLES ON A SINGLE ANISOTROPIC LAYER

```
%**********************************************************************
% Author:       Ben Braaten
% Date:         11/23/08
% Description:  This code calculates the mutual impedance between two
%               printed dipoles on a single anisotropic dielectric layer.
%               The dipoles can have length L and width W.
%**********************************************************************
%                          FFFFF   IIIII   N     N      A       L
%                          F         I     N N   N     A A      L
%                          FFF       I     N  N  N    AAAAA     L
%                          F         I     N   N N   A     A    L
%                          F       IIIII   N     N  A       A   LLLLL

% DDDD    IIIII      SSS     SSS    EEEE    RRRR    TTTTT       A       TTTTT  IIIII    OOOO    N     N
% D   D     I       S       S       E       R   R     T        A A        T      I     O    O   N N   N
% D   D     I         S       S     EEE     RRRR      T       AAAAA       T      I     O    O   N  N  N
% D   D     I           S       S   E       R  R      T      A     A      T      I     O    O   N   N N
% DDDD    IIIII      SSS     SSS    EEEE    R   R     T     A       A     T    IIIII    OOOO    N     N

%                              CCC    OOOO    DDDD    EEEE
%                             C      O    O   D   D   E
%                             C      O    O   D   D   EEE
%                             C      O    O   D   D   E
%                              CCC    OOOO    DDDD    EEEE



clc
clear all


s=0;                                                    %counter reset
f=.5e9;                                                 %frequency
w=2*pi*f;                                               %omega
c=3e8;                                                  %speed of light
lambda0=c/f;                                            %free-space wavelength
a=.4e-3;                                                %dipole radius
W=.5e-3;                                                %dipole width


e11_matrix=[3.25 5.12 3.25 5.12 5.12];                  %aniso. permittivity matrix
e12_matrix=[3.25 3.25 5.12 3.25 3.25];                  %aniso. permittivity matrix
d1_matrix=[1.58e-3 1.58e-3 1.58e-3 5*1.58e-3 10*1.58e-3];   %substrate thickness matrix

for count=1:5;


    for G=0e-3:10e-3:600e-3;                            %steps through values of G
        S=10e-3;                                        %separation distance (Echelon)
        M=14;                                           %number of dipole segments
        L=15e-2+2*W;                                    %length of dipole
        d1=d1_matrix(count);                            %substrate thickness
        e0=8.854e-12;                                   %constant
        e11=e11_matrix(count);                          %aniso. permittivity
        e12=e12_matrix(count);                          %aniso. permittivity
        u0=1.2566e-6;                                   %constant
        k=w*sqrt(u0*e0*e11)                             %wavenumber in the material
        k0=w*sqrt(u0*e0)                                %free-space wavenumber

        s=s+1;                                          %counter
        N=M;                                            %number of source points
        Vs=1;                                           %magnitude of delta-source
        delx=L/N;                                       %x-dim. step size
        delz=W;                                         %z-dim. step size
        y=[d1*ones(1,M-1) d1*ones(1,M-1)];              %both dipole locations
        xm=-L/2+delx:delx:L/2-delx;                     %x-dim. match points
        xm=[xm xm+G];
        xn=xm;                                          %x-dim. source points
        zm=[zeros(1,M-1),S*ones(1,M-1)];                %z-dim. match points
        zn=zm;                                          %z-dim. source points
        w=2*pi*f;                                       %omega

        %root finding routine
        %The following routine uses the secant method
        %to find the poles in the spectral domain
        %immittance fuctions.

        iteration=100;
        root1(1)=k;
        root1(2)=k-.01;
```

```
root2(1)=0;
root2(2)=.9*k0*j;

p=2;
while p<iteration;
    if e11==1;
        p=iteration+1;
        root1(p)=k0;
    else
        p=p+1;
        gamma01=sqrt(root1(p-1)^2-w^2*u0*e0);
        gamma02=sqrt(root1(p-2)^2-w^2*u0*e0);
        gammae1=sqrt((e12)/(e11)*(root1(p-1)^2-w^2*u0*e0*e11));
        gammae2=sqrt((e12)/(e11)*(root1(p-2)^2-w^2*u0*e0*e11));
        gammah1=sqrt(root1(p-1)^2-w^2*u0*e0*e12);
        gammah2=sqrt(root1(p-2)^2-w^2*u0*e0*e12);
        f11=gammae1+gamma01*e12*coth(gammae1*d1);
        f12=gammae2+gamma02*e12*coth(gammae2*d1);
        root1(p)=root1(p-1)-(f11)*(root1(p-1)-root1(p-2))/((f11)-(f12));


        gamma01=sqrt(root2(p-1)^2-w^2*u0*e0);
        gamma02=sqrt(root2(p-2)^2-w^2*u0*e0);
        gammae1=sqrt((e12)/(e11)*(root1(p-1)^2-w^2*u0*e0*e11));
        gammae2=sqrt((e12)/(e11)*(root1(p-2)^2-w^2*u0*e0*e11));
        gammah1=sqrt(root1(p-1)^2-w^2*u0*e0*e12);
        gammah2=sqrt(root1(p-2)^2-w^2*u0*e0*e12);
        f11=gamma01+gammah1*coth(gammah1*d1);
        f12=gamma02+gammah2*coth(gammah2*d1);
        root2(p)=root2(p-1)-(f11)*(root2(p-1)-root2(p-2))/((f11)-(f12));

        if abs(root1(p)-root1(p-1))<.001&p>1
            p=iteration+1;
        else
            % do nothing
        end

    end
end

root=real(root1(length(root1)))                                    %saves root

%polar points
%The following routines setup the polar integration points.
mult=500+(L-.5*lambda0)*(-500/lambda0)+200
kmax_alpha=mult*k0;
kmax_beta=mult*k0;
Nalpha=kmax_alpha/k0;
Nbeta=kmax_beta/k0;

if root>=k0
    del_r_fine=k0/50;
    del_r_very_fine=(k-k0)*.01;
    r_fine_lower=del_r_fine:del_r_fine:k0-del_r_fine/2;
    r_very_fine=[fliplr([root-del_r_very_fine:-del_r_very_fine:k0+del_r_very_fine+del_r_fine/2]) ...
        root+del_r_very_fine:del_r_very_fine:k-del_r_very_fine];
    r_fine=[r_fine_lower r_very_fine];
    r=r_fine;
    del_r=[del_r_fine*ones(1,length(r_fine_lower)) del_r_very_fine*ones(1,length(r_very_fine))];
else
    del_r_fine=k0/30;
    del_r_very_fine=root/30;
    r_very_fine=[[del_r_very_fine:del_r_very_fine:root-del_r_very_fine] ...
        [root+del_r_very_fine:del_r_very_fine:k-del_r_very_fine]];
    r_fine=[r_very_fine];
    r=r_fine;
    del_r=[del_r_very_fine*ones(1,length(r_very_fine))];
end

del_theta=pi/50;
theta=[del_theta/2:del_theta:pi/2-del_theta/2 pi/2+del_theta/2:del_theta:pi-del_theta/2 ...
    pi+del_theta/2:del_theta:3*pi/2-del_theta/2 3*pi/2+del_theta/2:del_theta:2*pi-del_theta/2];

Kxx_matrix=zeros(length(r),length(theta));
Zxx=zeros(length(r),length(theta));


%rectangular points
%The following routines setup the rectangular integration points.
del_alpha_lower=kmax_alpha/Nalpha;
del_alpha_upper=del_alpha_lower;
del_alpha_middle=k/30;

alpha_lower=-fliplr([k+del_alpha_lower/2:del_alpha_lower:kmax_alpha]);
alpha_middle=-k+del_alpha_middle/2:del_alpha_middle:k-del_alpha_middle/2;
alpha_upper=k+del_alpha_upper/2:del_alpha_upper:kmax_alpha;
alpha=[alpha_lower alpha_middle alpha_upper];
del_alpha=[del_alpha_lower*ones(1,length(alpha_lower)) del_alpha_middle*ones(1,length(alpha_middle)) ...
    del_alpha_upper*ones(1,length(alpha_upper))];
```

```
del_beta=kmax_beta/Nbeta;


%Polar integration routine
%The following routine integrates in the polar coordinates around and
%near the poles between k0 and k.
for m=1:2*(M-1);
    m
    for n=1:2*(N-1);
        Kxx_matrix_fine=0;
        Kxx_matrix=0;
        for g=1:length(r);

            ks=k;

            %  2-D PWS
            rxn_PWS=(2./sin(ks*delx)).*(1./(ks-r(g).*sin(theta))+1./(ks+r(g).*sin(theta))).*exp(-j*r(g).* ...
                sin(theta)*xn(n)).*sin((ks*delx+r(g).*sin(theta)*delx)/2).*sin((ks*delx-r(g).*sin(theta)*delx)/2);
            rxm_PWS=(2./sin(ks*delx)).*(1./(ks--r(g).*sin(theta))+1./(ks+-r(g).*sin(theta))).*exp(j*r(g).* ...
                sin(theta)*xm(m)).*sin((ks*delx+-r(g).*sin(theta)*delx)/2).*sin((ks*delx--r(g).*sin(theta)*delx)/2);

            rxn_pulse=exp(j*-r(g).*cos(theta)*zn(n)).*(delz*sin(r(g).*cos(theta)*delz/2)./(delz*r(g).* ...
                cos(theta)/2)).*exp(j*-r(g).*cos(theta)*delz/2);

            rxm_pulse=exp(j*r(g).*cos(theta)*zm(m)).*(delz*sin(r(g).*cos(theta)*delz/2)./(delz*r(g).* ...
                cos(theta)/2)).*exp(j*r(g).*cos(theta)*delz/2);

            rxn=rxn_PWS.*rxn_pulse;
            rxm=rxm_PWS.*rxm_pulse;


            gamma0=sqrt(r(g)^2-w^2*u0*e0);
            gammae1=sqrt((e12/e11)*(r(g)^2-w^2*u0*e0*e11));
            gammah1=sqrt(r(g)^2-w^2*u0*e0*e12);

            R=1;

            Zxx=(cos(theta).^2).*(-j*w*u0./(gamma0+gammah1.*coth(gammah1*d1)))+ ...
                   (sin(theta).^2).*(-gammae1.*gamma0./(j*w*e0*(gammae1+gamma0*e12.*coth(gammae1*d1))));

            Kxx_matrix=Kxx_matrix+sum(Zxx.*rxm.*rxn.*R.*del_theta.*del_r(g)*r(g));
        end
        matrix_polar(m,n)=(1/(2*pi)^2)*Kxx_matrix;
    end
end



clear Kxx_matrix Zxx

%rectangular integration routine
%The following routine integrates the rectangular region outside of the
%k circle.  This routine avoids the poles associated with +/-k in the
%basis functions

for m=1:2*(M-1);
    m
    for n=1:2*(N-1);
        Kxx_matrix_fine=0;
        Kxx_matrix=0;
        for g=1:length(alpha);

            if abs(alpha(g))<k
                beta_jump=sqrt(k^2-alpha(g)^2)+del_beta/2;
                beta=beta_jump:del_beta:kmax_beta;
                beta=[beta -beta];
            else
                beta=del_beta/2:del_beta:kmax_beta;
                beta=[beta -beta];
            end

            ks=k;

            %  2-D PWS

            rxn_PWS=(2./sin(ks*delx)).*(1./(ks-alpha(g))+1./(ks+alpha(g))).*exp(-j*alpha(g)*xn(n)).* ...
                sin((ks*delx+alpha(g)*delx)/2).*sin((ks*delx-alpha(g)*delx)/2);
            rxm_PWS=(2./sin(ks*delx)).*(1./(ks--alpha(g))+1./(ks+-alpha(g))).*exp(j*alpha(g)*xm(m)).* ...
                sin((ks*delx+-alpha(g)*delx)/2).*sin((ks*delx--alpha(g)*delx)/2);

            rxn_pulse=exp(j*-beta.*zn(n)).*(delz*sin(beta.*delz/2)./(delz*beta./2)).*exp(j*-beta.*delz/2);

            rxm_pulse=exp(j*beta.*zm(m)).*(delz*sin(beta.*delz/2)./(delz*beta./2)).*exp(j*beta.*delz/2);


            rxn=rxn_PWS.*rxn_pulse;
            rxm=rxm_PWS.*rxm_pulse;
```

```
                R=1;

                gamma0=sqrt(alpha(g)^2+beta.^2-w^2*u0*e0);
                gammae1=sqrt((e12/e11)*(alpha(g)^2+beta.^2-w^2*u0*e0*e11));
                gammah1=sqrt(alpha(g)^2+beta.^2-w^2*u0*e0*e12);

                Zxx=(beta.^2./(beta.^2+alpha(g)^2)).*(-j*w*u0./(gamma0+gammah1.*coth(gammah1*d1)))+ ...
                        (alpha(g).^2./(beta.^2+alpha(g)^2)).*(-gammae1.*gamma0./(j*w*e0*(gammae1+gamma0*e12.*coth(gammae1*d1))));

                Kxx_matrix=Kxx_matrix+sum(Zxx.*rxm.*rxn.*R.*del_beta.*del_alpha(g));

            end
            matrix_rect(m,n)=(1/(2*pi)^2)*Kxx_matrix;
        end
    end

    matrix=matrix_polar+matrix_rect;                                %saves the rectangular
                                                                    %and polar integration results
                                                                    %in the impedance matrix.
    V=zeros(2*(M-1),1);                                             %fills in voltage matrix
    ws=2*(1-cos(k*delx))/(k*sin(k*delx))*delz;
    V(ceil(M/2))=-Vs*ws/(2*delx);
    V(ceil(M/2)-1)=.5*V(ceil(M/2));
    V(ceil(M/2)+1)=.5*V(ceil(M/2));

    J=inv(matrix)*V                                                 %solves for surface current (A/m)
    I=J*delz;                                                       %solves for total current (A)
    Z_in(s)=Vs/I(ceil(M/2))                                         %calculates short-circuit impedance

    matrix_mutual=matrix(1:M-1,1:M-1);

    V_mutual=zeros(M-1,1);                                          %removes parasitic dipole
    ws=2*(1-cos(k*delx))/(k*sin(k*delx))*delz;
    V_mutual(ceil(M/2))=-Vs*ws/(2*delx);
    V_mutual(ceil(M/2)-1)=.5*V_mutual(ceil(M/2));
    V_mutual(ceil(M/2)+1)=.5*V_mutual(ceil(M/2));
    I_mutual=inv(matrix_mutual)*V_mutual*delz;

    I1p=I_mutual(ceil(M/2));
    Z_oc(s)=Vs/I1p                                                  %solves for open-circuit voltage
    Z_m(s)=sqrt(Z_oc(s)*(Z_oc(s)-Z_in(s)))                          %solves for mutual impedance

end

end
```

APPENDIX G. INPUT IMPEDANCE CODE FOR A SINGLE DIPOLE IN TWO ANISOTROPIC LAYERS

```
%************************************************************************
% Author:       Ben Braaten
% Date:         11/23/08
% Description:  This code calculates the input impedance of a single
%               printed dipole in two anisotropic dielectric layers.
%               The dipole can have length L and width W.
%************************************************************************
%                          FFFFF   IIIII   N     N      A       L
%                          F         I     N N   N     A A      L
%                          FFF       I     N  N  N    AAAAA     L
%                          F         I     N   N N   A     A    L
%                          F       IIIII   N     N  A       A   LLLLL

% DDDD    IIIII      SSS     SSS    EEEE    RRRR    TTTTT       A       TTTTT  IIIII    OOOO    N     N
% D   D     I       S       S       E       R   R     T        A A        T      I     O    O   N N   N
% D   D     I         S       S     EEE     RRRR      T       AAAAA       T      I     O    O   N  N  N
% D   D     I           S       S   E       R  R      T      A     A      T      I     O    O   N   N N
% DDDD    IIIII      SSS     SSS    EEEE    R   R     T     A       A     T    IIIII    OOOO    N     N

%                              CCC    OOOO    DDDD    EEEE
%                             C      O    O   D   D   E
%                             C      O    O   D   D   EEE
%                             C      O    O   D   D   E
%                              CCC    OOOO    DDDD    EEEE



clc
clear all



s=0;                                                    %resets counter
for f=.96e9:.01e9:1.09e9;                               %frequency step (for sweep)
    w=2*pi*f;                                           %omega
    c=3e8;                                              %speed of light
    lambda0=c/f;                                        %free-space wavelength
    a=.4e-3;                                            %dipole radius
    W=.5e-3;                                            %width of dipole
    M=34;                                               %number of segments
    L=15e-2+2*W;                                        %length of dipole
    d1=1.58e-3;                                         %layer 1 thickness
    d2=1.58e-3;                                         %layer 2 thickness
    d12=d1+d2;
    y=d1;                                               %dipole layer
    e0=8.854e-12;                                       %constant
    e11=3.25;                                           %aniso. permittivity
    e12=3.25;                                           %aniso. permittivity
    e21=5.12;                                           %aniso. permittivity
    e22=5.12;                                           %aniso. permittivity
    e31=1;                                              %permittivity of air
    e32=1                                               %permittivity of air;
    u0=1.2566e-6;                                       %constant
    k=w*sqrt(u0*e0*e11)                                 %wavenumber in the substrate
    k0=w*sqrt(u0*e0)                                    %free-space wavenumber


    s=s+1;                                              %counter
    N=M;                                                %number of expansion modes
    Vs=1;                                               %magnitude of the voltage source
    delx=L/N;                                           %x-dim. step size
    delz=W;                                             %z-dim. step size
    xm=-L/2+delx:delx:L/2-delx;                         %x-dim. match points
    xn=xm;                                              %x-dim. source points
    zm=zeros(1,length(xm));                             %z-dim. match points
    zn=zm;                                              %z-dim. source points
    w=2*pi*f;                                           %omega


    %root finding routine
    %The following routine uses the secant method
    %to find the poles in the spectral domain
    %immittance fuctions.
    iteration=100;
    root1(1)=k;
    root1(2)=k-.01;
    root2(1)=0;
    root2(2)=.9*k0*j;

    p=2;
```

```
while p<iteration;
    if e11==1;
        p=iteration+1;
        root1(p)=k0;
    else
        p=p+1;
        gamma01=sqrt(root1(p-1)^2-w^2*u0*e0);
        gamma02=sqrt(root1(p-2)^2-w^2*u0*e0);
        gammae1=sqrt((e12)/(e11)*(root1(p-1)^2-w^2*u0*e0*e11));
        gammae2=sqrt((e12)/(e11)*(root1(p-2)^2-w^2*u0*e0*e11));
        gammah1=sqrt(root1(p-1)^2-w^2*u0*e0*e12);
        gammah2=sqrt(root1(p-2)^2-w^2*u0*e0*e12);
        f11=gammae1+gamma01*e12*coth(gammae1*d1);
        f12=gammae2+gamma02*e12*coth(gammae2*d1);
        root1(p)=root1(p-1)-(f11)*(root1(p-1)-root1(p-2))/((f11)-(f12));


        gamma01=sqrt(root2(p-1)^2-w^2*u0*e0);
        gamma02=sqrt(root2(p-2)^2-w^2*u0*e0);
        gammae1=sqrt((e12)/(e11)*(root1(p-1)^2-w^2*u0*e0*e11));
        gammae2=sqrt((e12)/(e11)*(root1(p-2)^2-w^2*u0*e0*e11));
        gammah1=sqrt(root1(p-1)^2-w^2*u0*e0*e12);
        gammah2=sqrt(root1(p-2)^2-w^2*u0*e0*e12);
        f11=gamma01+gammah1*coth(gammah1*d1);
        f12=gamma02+gammah2*coth(gammah2*d1);
        root2(p)=root2(p-1)-(f11)*(root2(p-1)-root2(p-2))/((f11)-(f12));

        if abs(root1(p)-root1(p-1))<.001&p>1
            p=iteration+1;
        else
            %do nothing
        end
    end
end

root=real(root1(length(root1)))                                          %saves root

%polar points
%The following routines setup the polar integration points.
mult=400-150*(f-.9e9)/(.2e9)
kmax_alpha=mult*k0;
kmax_beta=mult*k0;
Nalpha=kmax_alpha/k0;
Nbeta=kmax_beta/k0;

if root>=k0
    del_r_fine=k0/50;
    del_r_very_fine=(k-k0)*.01;
    r_fine_lower=del_r_fine:del_r_fine:k0-del_r_fine/2;
    r_very_fine=[fliplr([root-del_r_very_fine:-del_r_very_fine:k0+del_r_very_fine+del_r_fine/2]) ...
    root+del_r_very_fine:del_r_very_fine:k-del_r_very_fine];
    r_fine=[r_fine_lower r_very_fine];
    r=r_fine;
    del_r=[del_r_fine*ones(1,length(r_fine_lower)) del_r_very_fine*ones(1,length(r_very_fine))];
else
    del_r_fine=k0/30;
    del_r_very_fine=root/30;
    r_very_fine=[[del_r_very_fine:del_r_very_fine:root-del_r_very_fine] ...
        [root+del_r_very_fine:del_r_very_fine:k-del_r_very_fine]];
    r_fine=[r_very_fine];
    r=r_fine;
    del_r=[del_r_very_fine*ones(1,length(r_very_fine))];
end

del_theta=pi/50;
theta=[del_theta/2:del_theta:pi/2-del_theta/2 pi/2+del_theta/2:del_theta:pi-del_theta/2 ...
    pi+del_theta/2:del_theta:3*pi/2-del_theta/2 3*pi/2+del_theta/2:del_theta:2*pi-del_theta/2];

Kxx_matrix=zeros(length(r),length(theta));
Zxx=zeros(length(r),length(theta));


%rectangular points
%The following routines setup the rectangular integration points.
del_alpha_lower=kmax_alpha/Nalpha;
del_alpha_upper=del_alpha_lower;
del_alpha_middle=k/30;

alpha_lower=-fliplr([k+del_alpha_lower/2:del_alpha_lower:kmax_alpha]);
alpha_middle=-k+del_alpha_middle/2:del_alpha_middle:k-del_alpha_middle/2;
alpha_upper=k+del_alpha_upper/2:del_alpha_upper:kmax_alpha;
alpha=[alpha_lower alpha_middle alpha_upper];
del_alpha=[del_alpha_lower*ones(1,length(alpha_lower)) del_alpha_middle*ones(1,length(alpha_middle)) ...
del_alpha_upper*ones(1,length(alpha_upper))];

del_beta=kmax_beta/Nbeta;
```

```
%Polar integration routine
%The following routine integrates in the polar coordinates around and
%near the poles between k0 and k.
for m=1:M-1;
    m
    for n=1:N-1;
        Kxx_matrix_fine=0;
        Kxx_matrix=0;
        for g=1:length(r);

            ks=k;

            R=1;

            %  2-D PWS
            rxn_PWS=(2./sin(ks*delx)).*(1./(ks-r(g).*sin(theta))+1./(ks+r(g).*sin(theta))).*exp(-j*r(g).* ...
                sin(theta)*xn(n)).*sin((ks*delx+r(g).*sin(theta)*delx)/2).*sin((ks*delx-r(g).*sin(theta)*delx)/2);
            rxm_PWS=(2./sin(ks*delx)).*(1./(ks--r(g).*sin(theta))+1./(ks+-r(g).*sin(theta))).*exp(j*r(g).* ...
                sin(theta)*xm(m)).*sin((ks*delx+-r(g).*sin(theta)*delx)/2).*sin((ks*delx--r(g).*sin(theta)*delx)/2);

            rxn_pulse=exp(j*-r(g).*cos(theta)*zn(n)).*(delz*sin(r(g).*cos(theta)*delz/2)./(delz*r(g).* ...
                cos(theta)/2)).*exp(j*-r(g).*cos(theta)*delz/2);

            rxm_pulse=exp(j*r(g).*cos(theta)*zm(m)).*(delz*sin(r(g).*cos(theta)*delz/2)./(delz*r(g).* ...
                cos(theta)/2)).*exp(j*r(g).*cos(theta)*delz/2);

            rxn=rxn_PWS.*rxn_pulse;
            rxm=rxm_PWS.*rxm_pulse;


            gamma0=sqrt(r(g)^2-w^2*u0*e0);
            gammae1=sqrt((e12/e11)*(r(g)^2-w^2*u0*e0*e11));
            gammah1=sqrt(r(g)^2-w^2*u0*e0*e12);
            gammae2=sqrt((e22/e21)*(r(g)^2-w^2*u0*e0*e21));
            gammah2=sqrt(r(g)^2-w^2*u0*e0*e22);

            N1=(gammae2./e22).*cosh(gammae1*d1).*cosh(gammae2*d1) ...
                -(gammae1./e12).*sinh(gammae1*d1).*sinh(gammae2*d1);

            M1=(gammae2./e22).*cosh(gammae1*d1).*sinh(gammae2*d1) ...
                -(gammae1./e12).*cosh(gammae2*d1).*sinh(gammae1*d1);

            N2=(gamma0/e32).*sinh(gammae2.*d12)+(gammae2/e22).*cosh(gammae2*d12);

            M2=(gamma0/e32).*cosh(gammae2.*d12)+(gammae2/e22).*sinh(gammae2*d12);

            N3=gamma0*cosh(gammah2*d12)+gammah2*sinh(gammah2*d12);

            M3=gamma0*sinh(gammah2*d12)+gammah2*cosh(gammah2*d12);

            N4=-gammah1.*cosh(gammah2*d1).*cosh(gammah1*d1)+ ...
                gammah2.*sinh(gammah2*d1).*sinh(gammah1*d1);

            M4=gammah1.*sinh(gammah2*d1).*cosh(gammah1*d1)- ...
                gammah2.*cosh(gammah2*d1).*sinh(gammah1*d1);

            P1=N1.*M2-N2.*M1;

            P2=N4.*M3+N3.*M4;

            P3=sinh(gammah2*y).*N3./P2;

            P4=cosh(gammah2*y).*M3./P2;

            P5=sinh(gammae2*y).*N2./P1;

            P6=cosh(gammae2*y).*M2./P1;

            P7=sinh(gammah2*y).*N4./P2;

            P8=sinh(gammae2*y).*N1./P1;

            P9=cosh(gammae2*y).*M1./P1;

            P10=cosh(gammah2*y).*M4./P2;

            Zxx1=(cos(theta).^2).*(j*w*u0*sinh(gammah1*d1).*(P4-P3))+ ...
                   (sin(theta).^2).*(gammae1.*gammae2.*sinh(gammae1*d1).*(P6-P5)./(-j*w*e0*e12*e22));

            Kxx_matrix=Kxx_matrix+sum(Zxx1.*rxm.*rxn.*R.*del_theta.*del_r(g)*r(g));

        end
        matrix_polar(m,n)=(1/(2*pi)^2)*Kxx_matrix;
    end
end

clear Kxx_matrix Zxx
```

```
%rectangular integration routine
%The following routine integrates the rectangular region outside of the
%k circle.  This routine avoids the poles associated with +/-k in the
%basis functions
for m=1:M-1;
    m
    for n=1:N-1;
        Kxx_matrix_fine=0;
        Kxx_matrix=0;
        for g=1:length(alpha);

            if abs(alpha(g))<k
                beta_jump=sqrt(k^2-alpha(g)^2)+del_beta/2;
                beta=beta_jump:del_beta:kmax_beta;
                beta=[beta -beta];
            else
                beta=del_beta/2:del_beta:kmax_beta;
                beta=[beta -beta];
            end

            ks=k; %2*pi/delx-root*sin(theta);



            %  2-D PWS

            rxn_PWS=(2./sin(ks*delx)).*(1./(ks-alpha(g))+1./(ks+alpha(g))).*exp(-j*alpha(g)*xn(n)).* ...
                sin((ks*delx+alpha(g)*delx)/2).*sin((ks*delx-alpha(g)*delx)/2);
            rxm_PWS=(2./sin(ks*delx)).*(1./(ks--alpha(g))+1./(ks+-alpha(g))).*exp(j*alpha(g)*xm(m)).* ...
                sin((ks*delx+-alpha(g)*delx)/2).*sin((ks*delx--alpha(g)*delx)/2);

            rxn_pulse=exp(j*-beta.*zn(n)).*(delz*sin(beta.*delz/2)./(delz*beta./2)).*exp(j*-beta.*delz/2);

            rxm_pulse=exp(j*beta.*zm(m)).*(delz*sin(beta.*delz/2)./(delz*beta./2)).*exp(j*beta.*delz/2);


            rxn=rxn_PWS.*rxn_pulse;
            rxm=rxm_PWS.*rxm_pulse;


            R=1;

            gamma0=sqrt(alpha(g)^2+beta.^2-w^2*u0*e0);
            gammae1=sqrt((e12/e11)*(alpha(g)^2+beta.^2-w^2*u0*e0*e11));
            gammah1=sqrt(alpha(g)^2+beta.^2-w^2*u0*e0*e12);
            gammae2=sqrt((e22/e21)*(alpha(g)^2+beta.^2-w^2*u0*e0*e21));
            gammah2=sqrt(alpha(g)^2+beta.^2-w^2*u0*e0*e22);


            N1=(gammae2./e22).*cosh(gammae1*d1).*cosh(gammae2*d1) ...
                -(gammae1./e12).*sinh(gammae1*d1).*sinh(gammae2*d1);

            M1=(gammae2./e22).*cosh(gammae1*d1).*sinh(gammae2*d1) ...
                -(gammae1./e12).*cosh(gammae2*d1).*sinh(gammae1*d1);

            N2=(gamma0/e32).*sinh(gammae2.*d12)+(gammae2/e22).*cosh(gammae2*d12);

            M2=(gamma0/e32).*cosh(gammae2.*d12)+(gammae2/e22).*sinh(gammae2*d12);

            N3=gamma0.*cosh(gammah2*d12)+gammah2.*sinh(gammah2*d12);

            M3=gamma0.*sinh(gammah2*d12)+gammah2.*cosh(gammah2*d12);

            N4=-gammah1.*cosh(gammah2*d1).*cosh(gammah1*d1)+ ...
                gammah2.*sinh(gammah2*d1).*sinh(gammah1*d1);

            M4=gammah1.*sinh(gammah2*d1).*cosh(gammah1*d1)- ...
                gammah2.*cosh(gammah2*d1).*sinh(gammah1*d1);



            P1=N1.*M2-N2.*M1;

            P2=N4.*M3+N3.*M4;

            P3=sinh(gammah2*y).*N3./P2;

            P4=cosh(gammah2*y).*M3./P2;

            P5=sinh(gammae2*y).*N2./P1;

            P6=cosh(gammae2*y).*M2./P1;

            P7=sinh(gammah2*y).*N4./P2;

            P8=sinh(gammae2*y).*N1./P1;

            P9=cosh(gammae2*y).*M1./P1;
```

```
            P10=cosh(gammah2*y).*M4./P2;

            Zxx1=(beta.^2./(beta.^2+alpha(g)^2)).*(j*w*u0*sinh(gammah1*d1).*(P4-P3))+ ...
                    (alpha(g).^2./(beta.^2+alpha(g)^2)).*(gammae1.*gammae2.*sinh(gammae1*d1).*(P6-P5)./(-j*w*e0*e12*e22));


            Kxx_matrix=Kxx_matrix+sum(Zxx1.*rxm.*rxn.*R.*del_beta.*del_alpha(g));

        end

        matrix_rect(m,n)=(1/(2*pi)^2)*Kxx_matrix;

    end
end

matrix=matrix_polar+matrix_rect;                                    %saves the rectangular
                                                                    %and polar integration results
                                                                    %in the impedance matrix.

V=zeros(M-1,1);                                                     %fills in voltage matrix
ws=2*(1-cos(k*delx))/(k*sin(k*delx))*delz;
V(ceil(M/2))=-Vs*ws/(2*delx);
V(ceil(M/2)-1)=.5*V(ceil(M/2));
V(ceil(M/2)+1)=.5*V(ceil(M/2));

J=inv(matrix)*V                                                     %solves for surface current (A/m)
I=J*delz;                                                           %solves for total current (A)
Z_in(s)=Vs/I(ceil(M/2))                                             %solves for input impedance


end
```

APPENDIX H. MUTUAL COUPLING CODE FOR TWO DIPOLES IN TWO ANISOTROPIC LAYERS

```
%*************************************************************************
% Author:       Ben Braaten
% Date:         11/23/08
% Description:  This code calculates the mutual impedance between two
%               printed dipoles in two anisotropic dielectric layers.
%               The dipoles can have length L and width W.
%*************************************************************************
%                         FFFFF   IIIII   N     N      A       L
%                         F         I     N N   N     A A      L
%                         FFF       I     N  N  N    AAAAA     L
%                         F         I     N   N N   A     A    L
%                         F       IIIII   N     N  A       A   LLLLL

% DDDD    IIIII      SSS     SSS    EEEE    RRRR    TTTTT       A       TTTTT  IIIII    OOOO    N     N
% D   D     I       S       S       E       R   R     T        A A        T      I     O    O   N N   N
% D   D     I         S       S     EEE     RRRR      T       AAAAA       T      I     O    O   N  N  N
% D   D     I           S       S   E       R  R      T      A     A      T      I     O    O   N   N N
% DDDD    IIIII      SSS     SSS    EEEE    R   R     T     A       A     T    IIIII    OOOO    N     N

%                              CCC    OOOO    DDDD    EEEE
%                             C      O    O   D   D   E
%                             C      O    O   D   D   EEE
%                             C      O    O   D   D   E
%                              CCC    OOOO    DDDD    EEEE


clc
clear all


s=0;                                                    %counter reset
f=.5e9;                                                 %center frequency
w=2*pi*f;                                               %omega
c=3e8;                                                  %speed of light
lambda0=c/f;                                            %freespace wavelength
a=.4e-3;                                                %dipole radius
W=.5e-3;                                                %width of dipole
for S=2e-3:1e-3:12e-3;                                  %dipole separation S
    M=14;                                               %number of dipole segments
    L=15e-2+2*W;                                        %dipole length
    d1=1.58e-3;                                         %layer 1 thickness
    d2=1.58e-3;                                         %layer 2 thickness
    d12=d1+d2;
    e0=8.854e-12;                                       %constant
    e11=3.25;                                           %aniso. permittivity
    e12=3.25;                                           %aniso. permittivity
    e21=3.25;                                           %aniso. permittivity
    e22=3.25;                                           %aniso. permittivity
    e31=1;                                              %permittivity of air
    e32=1;                                              %permittivity of air

    u0=1.2566e-6;                                       %constant
    k=w*sqrt(u0*e0*e11)                                 %material wavenumber
    k0=w*sqrt(u0*e0)                                    %freespace wavenumber


    s=s+1;                                              %counter
    N=M;                                                %number of expansion functions
    Vs=1;                                               %delta-source magnitude
    delx=L/N;                                           %x-dir. step size
    delz=W;                                             %z-dir. step size
    y=[d1*ones(1,M-1) d12*ones(1,M-1)];                 %dipole layer locations
    xm=-L/2+delx:delx:L/2-delx;                         %x-dir. match points
    xm=[xm xm];
    xn=xm;                                              %x-dir. source points
    zm=[zeros(1,M-1),S*ones(1,M-1)];                    %z-dir. match points
    zn=zm;                                              %z-dir. source points
    w=2*pi*f;                                           %omega

    %root finding routine
    %The following routine uses the secant method
    %to find the poles in the spectral domain
    %immittance fuctions.

    iteration=100;
    root1(1)=k;
    root1(2)=k-.01;
    root2(1)=0;
    root2(2)=.9*k0*j;
```

```
p=2;
while p<iteration;
    if e11==1;
        p=iteration+1;
        root1(p)=k0;
    else
        p=p+1;
        gamma01=sqrt(root1(p-1)^2-w^2*u0*e0);
        gamma02=sqrt(root1(p-2)^2-w^2*u0*e0);
        gammae1=sqrt((e12)/(e11)*(root1(p-1)^2-w^2*u0*e0*e11));
        gammae2=sqrt((e12)/(e11)*(root1(p-2)^2-w^2*u0*e0*e11));
        gammah1=sqrt(root1(p-1)^2-w^2*u0*e0*e12);
        gammah2=sqrt(root1(p-2)^2-w^2*u0*e0*e12);
        f11=gammae1+gamma01*e12*coth(gammae1*d1);
        f12=gammae2+gamma02*e12*coth(gammae2*d1);
        root1(p)=root1(p-1)-(f11)*(root1(p-1)-root1(p-2))/((f11)-(f12));


        gamma01=sqrt(root2(p-1)^2-w^2*u0*e0);
        gamma02=sqrt(root2(p-2)^2-w^2*u0*e0);
        gammae1=sqrt((e12)/(e11)*(root1(p-1)^2-w^2*u0*e0*e11));
        gammae2=sqrt((e12)/(e11)*(root1(p-2)^2-w^2*u0*e0*e11));
        gammah1=sqrt(root1(p-1)^2-w^2*u0*e0*e12);
        gammah2=sqrt(root1(p-2)^2-w^2*u0*e0*e12);
        f11=gamma01+gammah1*coth(gammah1*d1);
        f12=gamma02+gammah2*coth(gammah2*d1);
        root2(p)=root2(p-1)-(f11)*(root2(p-1)-root2(p-2))/((f11)-(f12));

        if abs(root1(p)-root1(p-1))<.001&p>1
            p=iteration+1;
        else
            %do nothing
        end
    end
end

root=real(root1(length(root1)))                                          %saves root

%polar points
%The following routines setup the polar integration points.
mult=500+(L-.5*lambda0)*(-500/lambda0)
kmax_alpha=mult*k0;
kmax_beta=mult*k0;
Nalpha=kmax_alpha/k0;
Nbeta=kmax_beta/k0;


if root>=k0
    del_r_fine=k0/50;
    del_r_very_fine=(k-k0)*.01;
    r_fine_lower=del_r_fine:del_r_fine:k0-del_r_fine/2;
    r_very_fine=[fliplr([root-del_r_very_fine:-del_r_very_fine:k0+del_r_very_fine+del_r_fine/2]) ...
        root+del_r_very_fine:del_r_very_fine:k-del_r_very_fine];
    r_fine=[r_fine_lower r_very_fine];
    r=r_fine;
    del_r=[del_r_fine*ones(1,length(r_fine_lower)) del_r_very_fine*ones(1,length(r_very_fine))];
else
    del_r_fine=k0/30;
    del_r_very_fine=root/30;
    r_very_fine=[[del_r_very_fine:del_r_very_fine:root-del_r_very_fine] ...
        [root+del_r_very_fine:del_r_very_fine:k-del_r_very_fine]];
    r_fine=[r_very_fine];
    r=r_fine;
    del_r=[del_r_very_fine*ones(1,length(r_very_fine))];
end

del_theta=pi/50;
theta=[del_theta/2:del_theta:pi/2-del_theta/2 pi/2+del_theta/2:del_theta:pi-del_theta/2 ...
    pi+del_theta/2:del_theta:3*pi/2-del_theta/2 3*pi/2+del_theta/2:del_theta:2*pi-del_theta/2];

Kxx_matrix=zeros(length(r),length(theta));
Zxx=zeros(length(r),length(theta));


%rectangular points
%The following routines setup the rectangular integration points.
del_alpha_lower=kmax_alpha/Nalpha;
del_alpha_upper=del_alpha_lower;
del_alpha_middle=k/30;

alpha_lower=-fliplr([k+del_alpha_lower/2:del_alpha_lower:kmax_alpha]);
alpha_middle=-k+del_alpha_middle/2:del_alpha_middle:k-del_alpha_middle/2;
alpha_upper=k+del_alpha_upper/2:del_alpha_upper:kmax_alpha;
alpha=[alpha_lower alpha_middle alpha_upper];
del_alpha=[del_alpha_lower*ones(1,length(alpha_lower)) del_alpha_middle*ones(1,length(alpha_middle)) ...
    del_alpha_upper*ones(1,length(alpha_upper))];

del_beta=kmax_beta/Nbeta;
```

```
%Polar integration routine
%The following routine integrates in the polar coordinates around and
%near the poles between k0 and k.
for m=1:2*(M-1);
    m
    for n=1:2*(N-1);
        Kxx_matrix_fine=0;
        Kxx_matrix=0;
        for g=1:length(r);

            ks=k;

            R=1;
            %  2-D PWS
            rxn_PWS=(2./sin(ks*delx)).*(1./(ks-r(g).*sin(theta))+1./(ks+r(g).*sin(theta))).*exp(-j*r(g).* ...
                sin(theta)*xn(n)).*sin((ks*delx+r(g).*sin(theta)*delx)/2).*sin((ks*delx-r(g).*sin(theta)*delx)/2);
            rxm_PWS=(2./sin(ks*delx)).*(1./(ks--r(g).*sin(theta))+1./(ks+-r(g).*sin(theta))).*exp(j*r(g).* ...
                sin(theta)*xm(m)).*sin((ks*delx+-r(g).*sin(theta)*delx)/2).*sin((ks*delx--r(g).*sin(theta)*delx)/2);

            rxn_pulse=exp(j*-r(g).*cos(theta)*zn(n)).*(delz*sin(r(g).*cos(theta)*delz/2)./(delz*r(g).* ...
                cos(theta)/2)).*exp(j*-r(g).*cos(theta)*delz/2);

            rxm_pulse=exp(j*r(g).*cos(theta)*zm(m)).*(delz*sin(r(g).*cos(theta)*delz/2)./(delz*r(g).* ...
                cos(theta)/2)).*exp(j*r(g).*cos(theta)*delz/2);

            rxn=rxn_PWS.*rxn_pulse;
            rxm=rxm_PWS.*rxm_pulse;


            gamma0=sqrt(r(g)^2-w^2*u0*e0);
            gammae1=sqrt((e12/e11)*(r(g)^2-w^2*u0*e0*e11));
            gammah1=sqrt(r(g)^2-w^2*u0*e0*e12);
            gammae2=sqrt((e22/e21)*(r(g)^2-w^2*u0*e0*e21));
            gammah2=sqrt(r(g)^2-w^2*u0*e0*e22);

            N1=(gammae2./e22).*cosh(gammae1*d1).*cosh(gammae2*d1) ...
                -(gammae1./e12).*sinh(gammae1*d1).*sinh(gammae2*d1);

            M1=(gammae2./e22).*cosh(gammae1*d1).*sinh(gammae2*d1) ...
                -(gammae1./e12).*cosh(gammae2*d1).*sinh(gammae1*d1);

            N2=(gamma0/e32).*sinh(gammae2.*d12)+(gammae2/e22).*cosh(gammae2*d12);

            M2=(gamma0/e32).*cosh(gammae2.*d12)+(gammae2/e22).*sinh(gammae2*d12);

            N3=gamma0*cosh(gammah2*d12)+gammah2*sinh(gammah2*d12);

            M3=gamma0*sinh(gammah2*d12)+gammah2*cosh(gammah2*d12);

            N4=-gammah1.*cosh(gammah2*d1).*cosh(gammah1*d1)+ ...
                gammah2.*sinh(gammah2*d1).*sinh(gammah1*d1);

            M4=gammah1.*sinh(gammah2*d1).*cosh(gammah1*d1)- ...
                gammah2.*cosh(gammah2*d1).*sinh(gammah1*d1);

            P1=N1.*M2-N2.*M1;

            P2=N4.*M3+N3.*M4;

            P3=sinh(gammah2*y(m)).*N3./P2;

            P4=cosh(gammah2*y(m)).*M3./P2;

            P5=sinh(gammae2*y(m)).*N2./P1;

            P6=cosh(gammae2*y(m)).*M2./P1;

            P7=sinh(gammah2*y(m)).*N4./P2;

            P8=sinh(gammae2*y(m)).*N1./P1;

            P9=cosh(gammae2*y(m)).*M1./P1;

            P10=cosh(gammah2*y(m)).*M4./P2;

            if y(n)==d1
                Zxx1=(cos(theta).^2).*(j*w*u0*sinh(gammah1*d1).*(P4-P3))+ ...
                    (sin(theta).^2).*(gammae1.*gammae2.*sinh(gammae1*d1).*(P6-P5)./(-j*w*e0*e12*e22));
                Zxx=Zxx1;
            else
                Zxx2=(sin(theta).^2).*(gamma0.*gammae2.*(P8-P9)./(-j*w*e0*e22*e32))+ ...
                    (cos(theta).^2).*(-j*w*u0*(P7+P10));
                Zxx=Zxx2;
            end
            Kxx_matrix=Kxx_matrix+sum(Zxx.*rxm.*rxn.*R.*del_theta.*del_r(g)*r(g));
        end
        matrix_polar(m,n)=(1/(2*pi)^2)*Kxx_matrix;
    end
```

```
end

clear Kxx_matrix Zxx

%rectangular integration routine
%The following routine integrates the rectangular region outside of the
%k circle.  This routine avoids the poles associated with +/-k in the
%basis functions
for m=1:2*(M-1);
    m
    for n=1:2*(N-1);
        Kxx_matrix_fine=0;
        Kxx_matrix=0;
        for g=1:length(alpha);

            if abs(alpha(g))<k
                beta_jump=sqrt(k^2-alpha(g)^2)+del_beta/2;
                beta=beta_jump:del_beta:kmax_beta;
                beta=[beta -beta];
            else
                beta=del_beta/2:del_beta:kmax_beta;
                beta=[beta -beta];
            end

            ks=k;

            %  2-D PWS

            rxn_PWS=(2./sin(ks*delx)).*(1./(ks-alpha(g))+1./(ks+alpha(g))).*exp(-j*alpha(g)*xn(n)).* ...
                sin((ks*delx+alpha(g)*delx)/2).*sin((ks*delx-alpha(g)*delx)/2);
            rxm_PWS=(2./sin(ks*delx)).*(1./(ks--alpha(g))+1./(ks+-alpha(g))).*exp(j*alpha(g)*xm(m)).* ...
                sin((ks*delx+-alpha(g)*delx)/2).*sin((ks*delx--alpha(g)*delx)/2);

            rxn_pulse=exp(j*-beta.*zn(n)).*(delz*sin(beta.*delz/2)./(delz*beta./2)).*exp(j*-beta.*delz/2);

            rxm_pulse=exp(j*beta.*zm(m)).*(delz*sin(beta.*delz/2)./(delz*beta./2)).*exp(j*beta.*delz/2);


            rxn=rxn_PWS.*rxn_pulse;
            rxm=rxm_PWS.*rxm_pulse;


            R=1;

            gamma0=sqrt(alpha(g)^2+beta.^2-w^2*u0*e0);
            gammae1=sqrt((e12/e11)*(alpha(g)^2+beta.^2-w^2*u0*e0*e11));
            gammah1=sqrt(alpha(g)^2+beta.^2-w^2*u0*e0*e12);
            gammae2=sqrt((e22/e21)*(alpha(g)^2+beta.^2-w^2*u0*e0*e21));
            gammah2=sqrt(alpha(g)^2+beta.^2-w^2*u0*e0*e22);


            N1=(gammae2./e22).*cosh(gammae1*d1).*cosh(gammae2*d1) ...
                -(gammae1./e12).*sinh(gammae1*d1).*sinh(gammae2*d1);

            M1=(gammae2./e22).*cosh(gammae1*d1).*sinh(gammae2*d1) ...
                -(gammae1./e12).*cosh(gammae2*d1).*sinh(gammae1*d1);

            N2=(gamma0/e32).*sinh(gammae2.*d12)+(gammae2/e22).*cosh(gammae2*d12);

            M2=(gamma0/e32).*cosh(gammae2.*d12)+(gammae2/e22).*sinh(gammae2*d12);

            N3=gamma0.*cosh(gammah2*d12)+gammah2.*sinh(gammah2*d12);

            M3=gamma0.*sinh(gammah2*d12)+gammah2.*cosh(gammah2*d12);

            N4=-gammah1.*cosh(gammah2*d1).*cosh(gammah1*d1)+ ...
                gammah2.*sinh(gammah2*d1).*sinh(gammah1*d1);

            M4=gammah1.*sinh(gammah2*d1).*cosh(gammah1*d1)- ...
                gammah2.*cosh(gammah2*d1).*sinh(gammah1*d1);



            P1=N1.*M2-N2.*M1;

            P2=N4.*M3+N3.*M4;

            P3=sinh(gammah2*y(m)).*N3./P2;

            P4=cosh(gammah2*y(m)).*M3./P2;

            P5=sinh(gammae2*y(m)).*N2./P1;

            P6=cosh(gammae2*y(m)).*M2./P1;

            P7=sinh(gammah2*y(m)).*N4./P2;

            P8=sinh(gammae2*y(m)).*N1./P1;
```

```
            P9=cosh(gammae2*y(m)).*M1./P1;

            P10=cosh(gammah2*y(m)).*M4./P2;


            if y(n)==d1
                Zxx1=(beta.^2./(beta.^2+alpha(g)^2)).*(j*w*u0*sinh(gammah1*d1).*(P4-P3))+ ...
                    (alpha(g).^2./(beta.^2+alpha(g)^2)).*(gammae1.*gammae2.*sinh(gammae1*d1).*(P6-P5)./(-j*w*e0*e12*e22));
                Zxx=Zxx1;
            else
                Zxx2=(alpha(g).^2./(beta.^2+alpha(g)^2)).*(gamma0.*gammae2.*(P8-P9)./(-j*w*e0*e22*e32))+ ...
                    (beta.^2./(beta.^2+alpha(g)^2)).*(-j*w*u0*(P7+P10));
                Zxx=Zxx2;
            end


            Kxx_matrix=Kxx_matrix+sum(Zxx.*rxm.*rxn.*R.*del_beta.*del_alpha(g));

        end
        matrix_rect(m,n)=(1/(2*pi)^2)*Kxx_matrix;
    end
end

matrix=matrix_polar+matrix_rect;                                    %saves the rectangular
                                                                    %and polar integration results
                                                                    %in the impedance matrix.
V=zeros(2*(M-1),1);                                                 %fills in voltage matrix


ws=2*(1-cos(k*delx))/(k*sin(k*delx))*delz;
V(ceil(M/2))=-Vs*ws/(2*delx);
V(ceil(M/2)-1)=.5*V(ceil(M/2));
V(ceil(M/2)+1)=.5*V(ceil(M/2));
J=inv(matrix)*V                                                     %solves for surface current (A/m)
I=J*delz;                                                           %solves for total current (A)
Z_in(s)=Vs/I(ceil(M/2))                                             %solves for short-circuit impedance


matrix_mutual=matrix(1:M-1,1:M-1);                                  %removes parasitic dipole
V_mutual=zeros(M-1,1);
ws=2*(1-cos(k*delx))/(k*sin(k*delx))*delz;
V_mutual(ceil(M/2))=-Vs*ws/(2*delx);
V_mutual(ceil(M/2)-1)=.5*V_mutual(ceil(M/2));
V_mutual(ceil(M/2)+1)=.5*V_mutual(ceil(M/2));
I_mutual=inv(matrix_mutual)*V_mutual*delz;

I1p=I_mutual(ceil(M/2));
Z_oc(s)=Vs/I1p                                                      %solves for open-circuit voltage

Z_m(s)=sqrt(Z_oc(s)*(Z_oc(s)-Z_in(s)))                              %solves for mutual impedance


end
```

APPENDIX I. INPUT IMPEDANCE CODE FOR A SINGLE DIPOLE IN THREE ANISOTROPIC LAYERS

```
%*********************************************************************
% Author:       Ben Braaten
% Date:         11/23/08
% Description:  This code calculates the input impedance of a single
%               printed dipole in three anisotropic dielectric layers.
%               The dipole can have length L and width W.
%*********************************************************************
%                          FFFFF   IIIII   N     N      A       L
%                          F         I     N N   N     A A      L
%                          FFF       I     N  N  N    AAAAA     L
%                          F         I     N   N N   A     A    L
%                          F       IIIII   N     N  A       A   LLLLL

% DDDD    IIIII      SSS     SSS    EEEE    RRRR    TTTTT       A       TTTTT  IIIII    OOOO    N     N
% D   D     I       S       S       E       R   R     T        A A        T      I     O    O   N N   N
% D   D     I         S       S     EEE     RRRR      T       AAAAA       T      I     O    O   N  N  N
% D   D     I           S       S   E       R  R      T      A     A      T      I     O    O   N   N N
% DDDD    IIIII      SSS     SSS    EEEE    R   R     T     A       A     T    IIIII    OOOO    N     N

%                              CCC    OOOO    DDDD    EEEE
%                             C      O    O   D   D   E
%                             C      O    O   D   D   EEE
%                             C      O    O   D   D   E
%                              CCC    OOOO    DDDD    EEEE


clc
clear all



s=0;
for f=.2e9:.1e9:.8e9;                                          %source frequency
    w=2*pi*f;                                                  %omega
    c=3e8;                                                     %speed of light
    lambda0=c/f;                                               %free-space wavelength
    a=.4e-3;                                                   %dipole radius
    W=.5e-3;                                                   %dipole width
    M=54;                                                      %number of dipole segments
    L=150e-3+2*W;                                              %dipole length
    d1=1.58e-3;                                                %layer 1 thickness
    d2=1.58e-3;                                                %layer 2 thickness
    d3=1.58e-3;                                                %layer 3 thickness
    d12=d1+d2;
    d13=d12+d3;
    y=d12;                                                     %dipole's y-position (layer)
    e0=8.854e-12;                                              %constant
    e11=3.25;                                                  %aniso. permittivity
    e12=3.25;                                                  %aniso. permittivity
    e21=5.12;                                                  %aniso. permittivity
    e22=5.12;                                                  %aniso. permittivity
    e31=5.12;                                                  %aniso. permittivity
    e32=5.12;                                                  %aniso. permittivity
    e41=1;                                                     %permittivity of air
    e42=1;                                                     %permittivity of air

    u0=1.2566e-6;                                              %constant
    k0=w*sqrt(u0*e0)                                           %free-space wave number
    k=w*sqrt(u0*e0*e11)                                        %aniso. wavenumber


    s=s+1;                                                     %counter
    N=M;                                                       %number of expansion fcns.
    Vs=1;                                                      %delta source voltage
    delx=L/N;                                                  %x-step size
    delz=W;                                                    %z-step size
    xm=-L/2+delx:delx:L/2-delx;                                %x-dim. match points
    xn=xm;                                                     %x-dim. source points
    zm=zeros(1,length(xm));                                    %z-dim. match points
    zn=zm;                                                     %z-dim. source points
    w=2*pi*f;                                                  %omega


    %root finding routine
    %The following routine uses the secant method
    %to find the poles in the spectral domain
    %immittance fuctions.

    iteration=100;
    root1(1)=k-1;
    root1(2)=k-.01;
```

```
root2(1)=0;
root2(2)=.9*k0*j;

p=2;
while p<iteration;
    if e11==1;
        p=iteration+1;
        root1(p)=k0;
    else
        p=p+1;
        gamma01=sqrt(root1(p-1)^2-w^2*u0*e0);
        gamma02=sqrt(root1(p-2)^2-w^2*u0*e0);
        gammae1=sqrt((e12)/(e11)*(root1(p-1)^2-w^2*u0*e0*e11));
        gammae2=sqrt((e12)/(e11)*(root1(p-2)^2-w^2*u0*e0*e11));
        gammah1=sqrt(root1(p-1)^2-w^2*u0*e0*e12);
        gammah2=sqrt(root1(p-2)^2-w^2*u0*e0*e12);
        f11=gammae1+gamma01*e12*coth(gammae1*d1);
        f12=gammae2+gamma02*e12*coth(gammae2*d1);
        root1(p)=root1(p-1)-(f11)*(root1(p-1)-root1(p-2))/((f11)-(f12));


        gamma01=sqrt(root2(p-1)^2-w^2*u0*e0);
        gamma02=sqrt(root2(p-2)^2-w^2*u0*e0);
        gammae1=sqrt((e12)/(e11)*(root1(p-1)^2-w^2*u0*e0*e11));
        gammae2=sqrt((e12)/(e11)*(root1(p-2)^2-w^2*u0*e0*e11));
        gammah1=sqrt(root1(p-1)^2-w^2*u0*e0*e12);
        gammah2=sqrt(root1(p-2)^2-w^2*u0*e0*e12);
        f11=gamma01+gammah1*coth(gammah1*d1);
        f12=gamma02+gammah2*coth(gammah2*d1);
        root2(p)=root2(p-1)-(f11)*(root2(p-1)-root2(p-2))/((f11)-(f12));

    end
end

root=real(root1(length(root1)))                                          %saves roots

slope=(925-640)/(.2e9-.3e9);
mult=640+slope*(f-.3e9)
if mult<200
    mult=250
else
    %do nothing
end

kmax_alpha=mult*k0;                                                      %integration limits
kmax_beta=mult*k0;
Nalpha=kmax_alpha/k0;
Nbeta=kmax_beta/k0;

%polar points
%The following routines setup the polar integration points.
if root>=k0
    del_r_fine=k0/50;
    del_r_very_fine=(k-k0)*.01;
    r_fine_lower=del_r_fine:del_r_fine:k0-del_r_fine/2;
    r_very_fine=[fliplr([root-del_r_very_fine:-del_r_very_fine:k0+del_r_very_fine+del_r_fine/2]) ...
        root+del_r_very_fine:del_r_very_fine:k-del_r_very_fine];
    r_fine=[r_fine_lower r_very_fine];
    r=r_fine;
    del_r=[del_r_fine*ones(1,length(r_fine_lower)) del_r_very_fine*ones(1,length(r_very_fine))];
else
    del_r_fine=k0/30;
    del_r_very_fine=root/30;
    r_very_fine=[[del_r_very_fine:del_r_very_fine:root-del_r_very_fine] ...
        [root+del_r_very_fine:del_r_very_fine:k-del_r_very_fine]];
    r_fine=[r_very_fine];
    r=r_fine;
    del_r=[del_r_very_fine*ones(1,length(r_very_fine))];
end

del_theta=pi/50;
theta=[del_theta/2:del_theta:pi/2-del_theta/2 pi/2+del_theta/2:del_theta:pi-del_theta/2 ...
    pi+del_theta/2:del_theta:3*pi/2-del_theta/2 3*pi/2+del_theta/2:del_theta:2*pi-del_theta/2];

Kxx_matrix=zeros(length(r),length(theta));
Zxx=zeros(length(r),length(theta));


%rectangular points
%The following routines setup the rectangular integration points.
del_alpha_lower=kmax_alpha/Nalpha;
del_alpha_upper=del_alpha_lower;
del_alpha_middle=k/30;

alpha_lower=-fliplr([k+del_alpha_lower/2:del_alpha_lower:kmax_alpha]);
alpha_middle=-k+del_alpha_middle/2:del_alpha_middle:k-del_alpha_middle/2;
alpha_upper=k+del_alpha_upper/2:del_alpha_upper:kmax_alpha;
alpha=[alpha_lower alpha_middle alpha_upper];
del_alpha=[del_alpha_lower*ones(1,length(alpha_lower)) del_alpha_middle*ones(1,length(alpha_middle)) ...
```

```
    del_alpha_upper*ones(1,length(alpha_upper))];

del_beta=kmax_beta/Nbeta;

%Polar integration routine
%The following routine integrates in the polar coordinates around and
%near the poles between k0 and k.
for m=1:M-1;
    m
    for n=1:N-1;
        Kxx_matrix_fine=0;
        Kxx_matrix=0;
        for g=1:length(r);

            ks=k;
            R=1;
            %  2-D PWS
            rxn_PWS=(2./sin(ks*delx)).*(1./(ks-r(g).*sin(theta))+1./(ks+r(g).*sin(theta))).*exp(-j*r(g).* ...
                sin(theta)*xn(n)).*sin((ks*delx+r(g).*sin(theta)*delx)/2).*sin((ks*delx-r(g).*sin(theta)*delx)/2);
            rxm_PWS=(2./sin(ks*delx)).*(1./(ks--r(g).*sin(theta))+1./(ks+-r(g).*sin(theta))).*exp(j*r(g).* ...
                sin(theta)*xm(m)).*sin((ks*delx+-r(g).*sin(theta)*delx)/2).*sin((ks*delx--r(g).*sin(theta)*delx)/2);

            rxn_pulse=exp(j*-r(g).*cos(theta)*zn(n)).*(delz*sin(r(g).*cos(theta)*delz/2)./(delz*r(g).* ...
                cos(theta)/2)).*exp(j*-r(g).*cos(theta)*delz/2);

            rxm_pulse=exp(j*r(g).*cos(theta)*zm(m)).*(delz*sin(r(g).*cos(theta)*delz/2)./(delz*r(g).* ...
                cos(theta)/2)).*exp(j*r(g).*cos(theta)*delz/2);

            rxn=rxn_PWS.*rxn_pulse;
            rxm=rxm_PWS.*rxm_pulse;


            gamma0=sqrt(r(g)^2-w^2*u0*e0);
            gammae1=sqrt((e12/e11)*(r(g)^2-w^2*u0*e0*e11));
            gammah1=sqrt(r(g)^2-w^2*u0*e0*e12);
            gammae2=sqrt((e22/e21)*(r(g)^2-w^2*u0*e0*e21));
            gammah2=sqrt(r(g)^2-w^2*u0*e0*e22);
            gammae3=sqrt((e32/e31)*(r(g)^2-w^2*u0*e0*e31));
            gammah3=sqrt(r(g)^2-w^2*u0*e0*e32);


            N1=(gammae2./e22).*cosh(gammae1*d1).*cosh(gammae2*d1) ...
                -(gammae1./e12).*sinh(gammae1*d1).*sinh(gammae2*d1);

            M1=(gammae2./e22).*cosh(gammae1*d1).*sinh(gammae2*d1) ...
                -(gammae1./e12).*cosh(gammae2*d1).*sinh(gammae1*d1);


            N4=-gammah1.*cosh(gammah2*d1).*cosh(gammah1*d1)+ ...
                gammah2.*sinh(gammah2*d1).*sinh(gammah1*d1);

            M4=gammah1.*sinh(gammah2*d1).*cosh(gammah1*d1)- ...
                gammah2.*cosh(gammah2*d1).*sinh(gammah1*d1);

            M6=(gamma0./e42).*sinh(gammae3*d13)+(gammae3./e32).*cosh(gammae3*d13);

            N6=(gamma0./e42).*cosh(gammae3*d13)+(gammae3./e32).*sinh(gammae3*d13);

            M7=gamma0.*cosh(gammah3*d13)+gammah3.*sinh(gammah3*d13);

            N7=gamma0.*sinh(gammah3*d13)+gammah3.*cosh(gammah3*d13);


            P11=(gammae3./e32).*cosh(gammae3*d12)-(M6./N6).*(gammae3./e32).*sinh(gammae3*d12);

            P12=(gammae2./e22).*sinh(gammae2*d12)-(M1./N1).*(gammae2./e22).*cosh(gammae2*d12);

            P13=cosh(gammah3*d12)-(M7./N7).*sinh(gammah3*d12);

            P14=sinh(gammah2*d12)+(M4./N4).*cosh(gammah2*d12);

            P15=(gammae1.*gammae2./(P11.*N1*e12*e22)).*sinh(gammae1*d1).*cosh(gammae2*d12);

            P16=(M6./N6).*cosh(gammae3*d12)-sinh(gammae3*d12);

            P17=(gammae1./(N1*e12)).*sinh(gammae1*d1).*sinh(gammae2*d12);

            P18=((M6.*P12)./(N6.*P11)).*cosh(gammae3*d12)-(P12./P11).*sinh(gammae3*d12);

            P19=-(M1./N1).*sinh(gammae2*d12)+cosh(gammae2*d12);

            P20=sinh(gammah1*d1).*cosh(gammah2*d12)./(N4.*P13);

            P21=(M7./N7).*gammah3.*cosh(gammah3*d12)-gammah3.*sinh(gammah3*d12);

            P22=gammah2.*sinh(gammah1*d1).*sinh(gammah2*d12)./N4;

            P23=((M7.*P14)./(N7.*P13)).*gammah3.*cosh(gammah3*d12)-(P14./P13).*gammah3.*sinh(gammah3*d12);
```

```
            P24=(M4./N4).*gammah2.*sinh(gammah2*d12)+gammah2.*cosh(gammah2*d12);

            P25=1./(P23+P24);

            P26=(P20.*P21+P22)./(P23+P24);

            P27=M4./(N4.*(P23+P24));

            P28=sinh(gammah1*d1)./N4-M4.*(P20.*P21+P22)./(N4.*(P23+P24));

            P29=1./(P18+P19);

            P30=(P15.*P16+P17)./(P18+P19);

            P31=-M1.*P29./N1;

            P32=M1.*P30./N1+gammae1.*sinh(gammae1*d1)./(N1.*e12);

            if y==d1
                Zxx1=(sin(theta).^2).*(gammae2.*P30.*sinh(gammae2*y)./(j*w*e0*e22) + ...
                    gammae2.*P32.*cosh(gammae2*y)./(-j*w*e0*e22))+ ...
                    (cos(theta).^2).*(j*w*u0*P28.*cosh(gammah2*y)-j*w*u0*P26.*sinh(gammah2*y));
                Zxx=Zxx1;
            else

                Zxx2=(sin(theta).^2).*(gammae2.*P29.*sinh(gammae2*y)./(-j*w*e0*e22)+ ...
                    gammae2.*P31.*cosh(gammae2*y)./(-j*w*e0*e22))+ ...
                    (cos(theta).^2).*(-j*w*u0*P25.*sinh(gammah2*y)-j*w*u0*P27.*cosh(gammah2*y));
                Zxx=Zxx2;
            end
            Kxx_matrix=Kxx_matrix+sum(Zxx.*rxm.*rxn.*R.*del_theta.*del_r(g)*r(g));
        end
        matrix_polar(m,n)=(1/(2*pi)^2)*Kxx_matrix;
    end
end



clear Kxx_matrix Zxx

%rectangular integration routine
%The following routine integrates the rectangular region outside of the
%k circle.  This routine avoids the poles associated with +/-k in the
%basis functions
for m=1:M-1;
    m
    for n=1:N-1;
        Kxx_matrix_fine=0;
        Kxx_matrix=0;
        for g=1:length(alpha);

            if abs(alpha(g))<k
                beta_jump=sqrt(k^2-alpha(g)^2)+del_beta/2;
                beta=beta_jump:del_beta:kmax_beta;
                beta=[beta -beta];
            else
                beta=del_beta/2:del_beta:kmax_beta;
                beta=[beta -beta];
            end

            ks=k;

            %  2-D PWS

            rxn_PWS=(2./sin(ks*delx)).*(1./(ks-alpha(g))+1./(ks+alpha(g))).*exp(-j*alpha(g)*xn(n)).* ...
                sin((ks*delx+alpha(g)*delx)/2).*sin((ks*delx-alpha(g)*delx)/2);
            rxm_PWS=(2./sin(ks*delx)).*(1./(ks--alpha(g))+1./(ks+-alpha(g))).*exp(j*alpha(g)*xm(m)).* ...
                sin((ks*delx+-alpha(g)*delx)/2).*sin((ks*delx--alpha(g)*delx)/2);

            rxn_pulse=exp(j*-beta.*zn(n)).*(delz*sin(beta.*delz/2)./(delz*beta./2)).*exp(j*-beta.*delz/2);

            rxm_pulse=exp(j*beta.*zm(m)).*(delz*sin(beta.*delz/2)./(delz*beta./2)).*exp(j*beta.*delz/2);


            rxn=rxn_PWS.*rxn_pulse;
            rxm=rxm_PWS.*rxm_pulse;

            R=1;

            gamma0=sqrt(alpha(g)^2+beta.^2-w^2*u0*e0);
            gammae1=sqrt((e12/e11)*(alpha(g)^2+beta.^2-w^2*u0*e0*e11));
            gammah1=sqrt(alpha(g)^2+beta.^2-w^2*u0*e0*e12);
            gammae2=sqrt((e22/e21)*(alpha(g)^2+beta.^2-w^2*u0*e0*e21));
            gammah2=sqrt(alpha(g)^2+beta.^2-w^2*u0*e0*e22);
            gammae3=sqrt((e32/e31)*(alpha(g)^2+beta.^2-w^2*u0*e0*e31));
            gammah3=sqrt(alpha(g)^2+beta.^2-w^2*u0*e0*e32);


            N1=(gammae2./e22).*cosh(gammae1*d1).*cosh(gammae2*d1) ...
```

```
            -(gammae1./e12).*sinh(gammae1*d1).*sinh(gammae2*d1);

        M1=(gammae2./e22).*cosh(gammae1*d1).*sinh(gammae2*d1) ...
            -(gammae1./e12).*cosh(gammae2*d1).*sinh(gammae1*d1);


        N4=-gammah1.*cosh(gammah2*d1).*cosh(gammah1*d1)+ ...
            gammah2.*sinh(gammah2*d1).*sinh(gammah1*d1);

        M4=gammah1.*sinh(gammah2*d1).*cosh(gammah1*d1)- ...
            gammah2.*cosh(gammah2*d1).*sinh(gammah1*d1);

        M6=(gamma0./e42).*sinh(gammae3*d13)+(gammae3./e32).*cosh(gammae3*d13);

        N6=(gamma0./e42).*cosh(gammae3*d13)+(gammae3./e32).*sinh(gammae3*d13);

        M7=gamma0.*cosh(gammah3*d13)+gammah3.*sinh(gammah3*d13);

        N7=gamma0.*sinh(gammah3*d13)+gammah3.*cosh(gammah3*d13);


        P11=(gammae3./e32).*cosh(gammae3*d12)-(M6./N6).*(gammae3./e32).*sinh(gammae3*d12);

        P12=(gammae2./e22).*sinh(gammae2*d12)-(M1./N1).*(gammae2./e22).*cosh(gammae2*d12);

        P13=cosh(gammah3*d12)-(M7./N7).*sinh(gammah3*d12);

        P14=sinh(gammah2*d12)+(M4./N4).*cosh(gammah2*d12);

        P15=(gammae1.*gammae2./(P11.*N1*e12*e22)).*sinh(gammae1*d1).*cosh(gammae2*d12);

        P16=(M6./N6).*cosh(gammae3*d12)-sinh(gammae3*d12);

        P17=(gammae1./(N1*e12)).*sinh(gammae1*d1).*sinh(gammae2*d12);

        P18=((M6.*P12)./(N6.*P11)).*cosh(gammae3*d12)-(P12./P11).*sinh(gammae3*d12);

        P19=-(M1./N1).*sinh(gammae2*d12)+cosh(gammae2*d12);

        P20=sinh(gammah1*d1).*cosh(gammah2*d12)./(N4.*P13);

        P21=(M7./N7).*gammah3.*cosh(gammah3*d12)-gammah3.*sinh(gammah3*d12);

        P22=gammah2.*sinh(gammah1*d1).*sinh(gammah2*d12)./N4;

        P23=((M7.*P14)./(N7.*P13)).*gammah3.*cosh(gammah3*d12)-(P14./P13).*gammah3.*sinh(gammah3*d12);

        P24=(M4./N4).*gammah2.*sinh(gammah2*d12)+gammah2.*cosh(gammah2*d12);

        P25=1./(P23+P24);

        P26=(P20.*P21+P22)./(P23+P24);

        P27=M4./(N4.*(P23+P24));

        P28=sinh(gammah1*d1)./N4-M4.*(P20.*P21+P22)./(N4.*(P23+P24));

        P29=1./(P18+P19);

        P30=(P15.*P16+P17)./(P18+P19);

        P31=-M1.*P29./N1;

        P32=M1.*P30./N1+gammae1.*sinh(gammae1*d1)./(N1.*e12);

        if y==d1
            Zxx1=(alpha(g).^2./(beta.^2+alpha(g)^2)).*(gammae2.*P30.*sinh(gammae2*y)./(j*w*e0*e22) + ...
                gammae2.*P32.*cosh(gammae2*y)./(-j*w*e0*e22))+ ...
                (beta.^2./(beta.^2+alpha(g)^2)).*(j*w*u0*P28.*cosh(gammah2*y)-j*w*u0*P26.*sinh(gammah2*y));
            Zxx=Zxx1;

        else
            Zxx2=(alpha(g).^2./(beta.^2+alpha(g)^2)).*(gammae2.*P29.*sinh(gammae2*y)./(-j*w*e0*e22)+ ...
                gammae2.*P31.*cosh(gammae2*y)./(-j*w*e0*e22))+ ...
                (beta.^2./(beta.^2+alpha(g)^2)).*(-j*w*u0*P25.*sinh(gammah2*y)-j*w*u0*P27.*cosh(gammah2*y));
            Zxx=Zxx2;
        end
        Kxx_matrix=Kxx_matrix+sum(Zxx.*rxm.*rxn.*R.*del_beta.*del_alpha(g));
    end
    matrix_rect(m,n)=(1/(2*pi)^2)*Kxx_matrix;
  end
end



matrix=matrix_polar+matrix_rect;                                %saves the rectangular
                                                                %and polar integration results
                                                                %in the impedance matrix.
```

```
    V=zeros(M-1,1);                                          %fills in voltage matrix
    ws=2*(1-cos(k*delx))/(k*sin(k*delx))*delz;
    V(ceil(M/2))=-Vs*ws/(2*delx);
    V(ceil(M/2)-1)=.5*V(ceil(M/2));
    V(ceil(M/2)+1)=.5*V(ceil(M/2));

    J=inv(matrix)*V                                          %solves for surface current (A/m)
    I=J*delz;                                                %solves for total current   (A)
    Z_in(s)=Vs/I(ceil(M/2))                                  %solves for input impedance


end
```

APPENDIX J. MUTUAL COUPLING CODE FOR TWO DIPOLES IN THREE ANISOTROPIC LAYERS

```
%*********************************************************************
% Author:       Ben Braaten
% Date:         11/23/08
% Description:  This code calculates the mutual impedance between two
%               printed dipoles in three anisotropic dielectric layers.
%               The dipoles can have length L and width W.
%*********************************************************************
%                          FFFFF   IIIII   N     N      A       L
%                          F         I     N N   N     A A      L
%                          FFF       I     N  N  N    AAAAA     L
%                          F         I     N   N N   A     A    L
%                          F       IIIII   N     N  A       A   LLLLL

% DDDD    IIIII      SSS     SSS    EEEE    RRRR    TTTTT       A       TTTTT  IIIII    OOOO    N     N
% D   D     I       S       S       E       R   R     T        A A        T      I     O    O   N N   N
% D   D     I         S       S     EEE     RRRR      T       AAAAA       T      I     O    O   N  N  N
% D   D     I           S       S   E       R  R      T      A     A      T      I     O    O   N   N N
% DDDD    IIIII      SSS     SSS    EEEE    R   R     T     A       A     T    IIIII    OOOO    N     N

%                              CCC    OOOO    DDDD    EEEE
%                             C      O    O   D   D   E
%                             C      O    O   D   D   EEE
%                             C      O    O   D   D   E
%                              CCC    OOOO    DDDD    EEEE


clc
clear all


s=0;                                                    %counter reset
f=.5e9;                                                 %center frequency
w=2*pi*f;                                               %omega
c=3e8;                                                  %speed of light
lambda0=c/f;                                            %freespace wavelength
a=.4e-3;                                                %dipole radius
W=.5e-3;                                                %width of dipole
for S=0e-3;


    M=14;                                               %number of dipole segments
    L=15e-2+2*W;                                        %dipole length
    d1=1.58e-3;                                         %layer 1 thickness
    d2=1.58e-3;                                         %layer 2 thickness
    d3=1.58e-3;                                         %layer 3 thickness
    d12=d1+d2;
    d13=d12+d3;
    e0=8.854e-12;                                       %constant
    e11=3.25;                                           %aniso. permittivity
    e12=3.25;                                           %aniso. permittivity
    e21=3.25;                                           %aniso. permittivity
    e22=3.25;                                           %aniso. permittivity
    e31=3.25;                                           %aniso. permittivity
    e32=3.25;                                           %aniso. permittivity
    e41=1;                                              %permittivity of air
    e42=1;                                              %permittivity of air

    u0=1.2566e-6;
    k=w*sqrt(u0*e0*e11)
    k0=w*sqrt(u0*e0)


u0=1.2566e-6;                                           %constant
    k=w*sqrt(u0*e0*e11)                                 %material wavenumber
    k0=w*sqrt(u0*e0)                                    %freespace wavenumber


    s=s+1;                                              %counter
    N=M;                                                %number of expansion functions
    Vs=1;                                               %delta-source magnitude
    delx=L/N;                                           %x-dir. step size
    delz=W;                                             %z-dir. step size
    y=[d1*ones(1,M-1) d12*ones(1,M-1)];                 %dipole layer locations
    xm=-L/2+delx:delx:L/2-delx;                         %x-dir. match points
    xm=[xm xm];
    xn=xm;                                              %x-dir. source points
    zm=[zeros(1,M-1),S*ones(1,M-1)];                    %z-dir. match points
    zn=zm;                                              %z-dir. source points
    w=2*pi*f;                                           %omega


    %root finding routine
```

```
%The following routine uses the secant method
%to find the poles in the spectral domain
%immittance fuctions.
iteration=100;
root1(1)=k;
root1(2)=k-.01;
root2(1)=0;
root2(2)=.9*k0*j;

p=2;
while p<iteration;
    if e11==1;
        p=iteration+1;
        root1(p)=k0;
    else
        p=p+1;
        gamma01=sqrt(root1(p-1)^2-w^2*u0*e0);
        gamma02=sqrt(root1(p-2)^2-w^2*u0*e0);
        gammae1=sqrt((e12)/(e11)*(root1(p-1)^2-w^2*u0*e0*e11));
        gammae2=sqrt((e12)/(e11)*(root1(p-2)^2-w^2*u0*e0*e11));
        gammah1=sqrt(root1(p-1)^2-w^2*u0*e0*e12);
        gammah2=sqrt(root1(p-2)^2-w^2*u0*e0*e12);
        f11=gammae1+gamma01*e12*coth(gammae1*d1);
        f12=gammae2+gamma02*e12*coth(gammae2*d1);
        root1(p)=root1(p-1)-(f11)*(root1(p-1)-root1(p-2))/((f11)-(f12));


        gamma01=sqrt(root2(p-1)^2-w^2*u0*e0);
        gamma02=sqrt(root2(p-2)^2-w^2*u0*e0);
        gammae1=sqrt((e12)/(e11)*(root1(p-1)^2-w^2*u0*e0*e11));
        gammae2=sqrt((e12)/(e11)*(root1(p-2)^2-w^2*u0*e0*e11));
        gammah1=sqrt(root1(p-1)^2-w^2*u0*e0*e12);
        gammah2=sqrt(root1(p-2)^2-w^2*u0*e0*e12);
        f11=gamma01+gammah1*coth(gammah1*d1);
        f12=gamma02+gammah2*coth(gammah2*d1);
        root2(p)=root2(p-1)-(f11)*(root2(p-1)-root2(p-2))/((f11)-(f12));

    if abs(root1(p)-root1(p-1))<.001&p>1
        p=iteration+1;
    else
        %do nothing
    end




    end
end

root=real(root1(length(root1)))                                          %saves root

%polar points
%The following routines setup the polar integration points.
mult=500+(L-.5*lambda0)*(-500/lambda0)-300
kmax_alpha=mult*k0;
kmax_beta=mult*k0;
Nalpha=kmax_alpha/k0;
Nbeta=kmax_beta/k0;

if root>=k0
    del_r_fine=k0/50;
    del_r_very_fine=(k-k0)*.01;
    r_fine_lower=del_r_fine:del_r_fine:k0-del_r_fine/2;
    r_very_fine=[fliplr([root-del_r_very_fine:-del_r_very_fine:k0+del_r_very_fine+del_r_fine/2]) ...
        root+del_r_very_fine:del_r_very_fine:k-del_r_very_fine];
    r_fine=[r_fine_lower r_very_fine];
    r=r_fine;
    del_r=[del_r_fine*ones(1,length(r_fine_lower)) del_r_very_fine*ones(1,length(r_very_fine))];
else
    del_r_fine=k0/30;
    del_r_very_fine=root/30;
    r_very_fine=[[del_r_very_fine:del_r_very_fine:root-del_r_very_fine] ...
        [root+del_r_very_fine:del_r_very_fine:k-del_r_very_fine]];
    r_fine=[r_very_fine];
    r=r_fine;
    del_r=[del_r_very_fine*ones(1,length(r_very_fine))];
end

del_theta=pi/50;
theta=[del_theta/2:del_theta:pi/2-del_theta/2 pi/2+del_theta/2:del_theta:pi-del_theta/2 ...
    pi+del_theta/2:del_theta:3*pi/2-del_theta/2 3*pi/2+del_theta/2:del_theta:2*pi-del_theta/2];

Kxx_matrix=zeros(length(r),length(theta));
Zxx=zeros(length(r),length(theta));


%rectangular points
%The following routines setup the rectangular integration points.
del_alpha_lower=kmax_alpha/Nalpha;
```

```
del_alpha_upper=del_alpha_lower;
del_alpha_middle=k/30;

alpha_lower=-fliplr([k+del_alpha_lower/2:del_alpha_lower:kmax_alpha]);
alpha_middle=-k+del_alpha_middle/2:del_alpha_middle:k-del_alpha_middle/2;
alpha_upper=k+del_alpha_upper/2:del_alpha_upper:kmax_alpha;
alpha=[alpha_lower alpha_middle alpha_upper];
del_alpha=[del_alpha_lower*ones(1,length(alpha_lower)) del_alpha_middle*ones(1,length(alpha_middle)) ...
    del_alpha_upper*ones(1,length(alpha_upper))];

del_beta=kmax_beta/Nbeta;


%Polar integration routine
%The following routine integrates in the polar coordinates around and
%near the poles between k0 and k.
for m=1:2*(M-1);
    m
    for n=1:2*(N-1);
        Kxx_matrix_fine=0;
        Kxx_matrix=0;
        for g=1:length(r);

            ks=k;
            R=1;

            %  2-D PWS
            rxn_PWS=(2./sin(ks*delx)).*(1./(ks-r(g).*sin(theta))+1./(ks+r(g).*sin(theta))).*exp(-j*r(g).* ...
                sin(theta)*xn(n)).*sin((ks*delx+r(g).*sin(theta)*delx)/2).*sin((ks*delx-r(g).*sin(theta)*delx)/2);
            rxm_PWS=(2./sin(ks*delx)).*(1./(ks--r(g).*sin(theta))+1./(ks+-r(g).*sin(theta))).*exp(j*r(g).* ...
                sin(theta)*xm(m)).*sin((ks*delx+-r(g).*sin(theta)*delx)/2).*sin((ks*delx--r(g).*sin(theta)*delx)/2);

            rxn_pulse=exp(j*-r(g).*cos(theta)*zn(n)).*(delz*sin(r(g).*cos(theta)*delz/2)./(delz*r(g).* ...
                cos(theta)/2)).*exp(j*-r(g).*cos(theta)*delz/2);

            rxm_pulse=exp(j*r(g).*cos(theta)*zm(m)).*(delz*sin(r(g).*cos(theta)*delz/2)./(delz*r(g).* ...
                cos(theta)/2)).*exp(j*r(g).*cos(theta)*delz/2);

            rxn=rxn_PWS.*rxn_pulse;
            rxm=rxm_PWS.*rxm_pulse;


            gamma0=sqrt(r(g)^2-w^2*u0*e0);
            gammae1=sqrt((e12/e11)*(r(g)^2-w^2*u0*e0*e11));
            gammah1=sqrt(r(g)^2-w^2*u0*e0*e12);
            gammae2=sqrt((e22/e21)*(r(g)^2-w^2*u0*e0*e21));
            gammah2=sqrt(r(g)^2-w^2*u0*e0*e22);
            gammae3=sqrt((e32/e31)*(r(g)^2-w^2*u0*e0*e31));
            gammah3=sqrt(r(g)^2-w^2*u0*e0*e32);


            N1=(gammae2./e22).*cosh(gammae1*d1).*cosh(gammae2*d1) ...
                -(gammae1./e12).*sinh(gammae1*d1).*sinh(gammae2*d1);

            M1=(gammae2./e22).*cosh(gammae1*d1).*sinh(gammae2*d1) ...
                -(gammae1./e12).*cosh(gammae2*d1).*sinh(gammae1*d1);


            N4=-gammah1.*cosh(gammah2*d1).*cosh(gammah1*d1)+ ...
                gammah2.*sinh(gammah2*d1).*sinh(gammah1*d1);

            M4=gammah1.*sinh(gammah2*d1).*cosh(gammah1*d1)- ...
                gammah2.*cosh(gammah2*d1).*sinh(gammah1*d1);

            M6=(gamma0./e42).*sinh(gammae3*d13)+(gammae3./e32).*cosh(gammae3*d13);

            N6=(gamma0./e42).*cosh(gammae3*d13)+(gammae3./e32).*sinh(gammae3*d13);

            M7=gamma0.*cosh(gammah3*d13)+gammah3.*sinh(gammah3*d13);

            N7=gamma0.*sinh(gammah3*d13)+gammah3.*cosh(gammah3*d13);


            P11=(gammae3./e32).*cosh(gammae3*d12)-(M6./N6).*(gammae3./e32).*sinh(gammae3*d12);

            P12=(gammae2./e22).*sinh(gammae2*d12)-(M1./N1).*(gammae2./e22).*cosh(gammae2*d12);

            P13=cosh(gammah3*d12)-(M7./N7).*sinh(gammah3*d12);

            P14=sinh(gammah2*d12)+(M4./N4).*cosh(gammah2*d12);

            P15=(gammae1.*gammae2./(P11.*N1*e12*e22)).*sinh(gammae1*d1).*cosh(gammae2*d12);

            P16=(M6./N6).*cosh(gammae3*d12)-sinh(gammae3*d12);

            P17=(gammae1./(N1*e12)).*sinh(gammae1*d1).*sinh(gammae2*d12);

            P18=((M6.*P12)./(N6.*P11)).*cosh(gammae3*d12)-(P12./P11).*sinh(gammae3*d12);
```

```
            P19=-(M1./N1).*sinh(gammae2*d12)+cosh(gammae2*d12);

            P20=sinh(gammah1*d1).*cosh(gammah2*d12)./(N4.*P13);

            P21=(M7./N7).*gammah3.*cosh(gammah3*d12)-gammah3.*sinh(gammah3*d12);

            P22=gammah2.*sinh(gammah1*d1).*sinh(gammah2*d12)./N4;

            P23=((M7.*P14)./(N7.*P13)).*gammah3.*cosh(gammah3*d12)-(P14./P13).*gammah3.*sinh(gammah3*d12);

            P24=(M4./N4).*gammah2.*sinh(gammah2*d12)+gammah2.*cosh(gammah2*d12);

            P25=1./(P23+P24);

            P26=(P20.*P21+P22)./(P23+P24);

            P27=M4./(N4.*(P23+P24));

            P28=sinh(gammah1*d1)./N4-M4.*(P20.*P21+P22)./(N4.*(P23+P24));

            P29=1./(P18+P19);

            P30=(P15.*P16+P17)./(P18+P19);

            P31=-M1.*P29./N1;

            P32=M1.*P30./N1+gammae1.*sinh(gammae1*d1)./(N1.*e12);

            if y(n)==d1;
                Zxx1=(sin(theta).^2).*(gammae2.*P30.*sinh(gammae2*y(m))./(j*w*e0*e22) + ...
                    gammae2.*P32.*cosh(gammae2*y(m))./(-j*w*e0*e22))+ ...
                    (cos(theta).^2).*(j*w*u0*P28.*cosh(gammah2*y(m))-j*w*u0*P26.*sinh(gammah2*y(m)));
                Zxx=Zxx1;
            else

                Zxx2=(sin(theta).^2).*(gammae2.*P29.*sinh(gammae2*y(m))./(-j*w*e0*e22)+ ...
                    gammae2.*P31.*cosh(gammae2*y(m))./(-j*w*e0*e22))+ ...
                    (cos(theta).^2).*(-j*w*u0*P25.*sinh(gammah2*y(m))-j*w*u0*P27.*cosh(gammah2*y(m)));
                Zxx=Zxx2;
            end

            Kxx_matrix=Kxx_matrix+sum(Zxx.*rxm.*rxn.*R.*del_theta.*del_r(g)*r(g));
        end
        matrix_polar(m,n)=(1/(2*pi)^2)*Kxx_matrix;
    end
end


clear Kxx_matrix Zxx


%rectangular integration routine
%The following routine integrates the rectangular region outside of the
%k circle.  This routine avoids the poles associated with +/-k in the
%basis functions.
for m=1:2*(M-1);
    m
    for n=1:2*(N-1);
        Kxx_matrix_fine=0;
        Kxx_matrix=0;
        for g=1:length(alpha);

            if abs(alpha(g))<k
                beta_jump=sqrt(k^2-alpha(g)^2)+del_beta/2;
                beta=beta_jump:del_beta:kmax_beta;
                beta=[beta -beta];
            else
                beta=del_beta/2:del_beta:kmax_beta;
                beta=[beta -beta];
            end

            ks=k;

            %  2-D PWS

            rxn_PWS=(2./sin(ks*delx)).*(1./(ks-alpha(g))+1./(ks+alpha(g))).*exp(-j*alpha(g)*xn(n)).* ...
                sin((ks*delx+alpha(g)*delx)/2).*sin((ks*delx-alpha(g)*delx)/2);
            rxm_PWS=(2./sin(ks*delx)).*(1./(ks--alpha(g))+1./(ks+-alpha(g))).*exp(j*alpha(g)*xm(m)).* ...
                sin((ks*delx+-alpha(g)*delx)/2).*sin((ks*delx--alpha(g)*delx)/2);

            rxn_pulse=exp(j*-beta.*zn(n)).*(delz*sin(beta.*delz/2)./(delz*beta./2)).*exp(j*-beta.*delz/2);

            rxm_pulse=exp(j*beta.*zm(m)).*(delz*sin(beta.*delz/2)./(delz*beta./2)).*exp(j*beta.*delz/2);


            rxn=rxn_PWS.*rxn_pulse;
            rxm=rxm_PWS.*rxm_pulse;
```

```
R=1;


gamma0=sqrt(alpha(g)^2+beta.^2-w^2*u0*e0);
gammae1=sqrt((e12/e11)*(alpha(g)^2+beta.^2-w^2*u0*e0*e11));
gammah1=sqrt(alpha(g)^2+beta.^2-w^2*u0*e0*e12);
gammae2=sqrt((e22/e21)*(alpha(g)^2+beta.^2-w^2*u0*e0*e21));
gammah2=sqrt(alpha(g)^2+beta.^2-w^2*u0*e0*e22);
gammae3=sqrt((e32/e31)*(alpha(g)^2+beta.^2-w^2*u0*e0*e31));
gammah3=sqrt(alpha(g)^2+beta.^2-w^2*u0*e0*e32);


N1=(gammae2./e22).*cosh(gammae1*d1).*cosh(gammae2*d1) ...
    -(gammae1./e12).*sinh(gammae1*d1).*sinh(gammae2*d1);

M1=(gammae2./e22).*cosh(gammae1*d1).*sinh(gammae2*d1) ...
    -(gammae1./e12).*cosh(gammae2*d1).*sinh(gammae1*d1);


N4=-gammah1.*cosh(gammah2*d1).*cosh(gammah1*d1)+ ...
    gammah2.*sinh(gammah2*d1).*sinh(gammah1*d1);

M4=gammah1.*sinh(gammah2*d1).*cosh(gammah1*d1)- ...
    gammah2.*cosh(gammah2*d1).*sinh(gammah1*d1);

M6=(gamma0./e42).*sinh(gammae3*d13)+(gammae3./e32).*cosh(gammae3*d13);

N6=(gamma0./e42).*cosh(gammae3*d13)+(gammae3./e32).*sinh(gammae3*d13);

M7=gamma0.*cosh(gammah3*d13)+gammah3.*sinh(gammah3*d13);

N7=gamma0.*sinh(gammah3*d13)+gammah3.*cosh(gammah3*d13);


P11=(gammae3./e32).*cosh(gammae3*d12)-(M6./N6).*(gammae3./e32).*sinh(gammae3*d12);

P12=(gammae2./e22).*sinh(gammae2*d12)-(M1./N1).*(gammae2./e22).*cosh(gammae2*d12);

P13=cosh(gammah3*d12)-(M7./N7).*sinh(gammah3*d12);

P14=sinh(gammah2*d12)+(M4./N4).*cosh(gammah2*d12);

P15=(gammae1.*gammae2./(P11.*N1*e12*e22)).*sinh(gammae1*d1).*cosh(gammae2*d12);

P16=(M6./N6).*cosh(gammae3*d12)-sinh(gammae3*d12);

P17=(gammae1./(N1*e12)).*sinh(gammae1*d1).*sinh(gammae2*d12);

P18=((M6.*P12)./(N6.*P11)).*cosh(gammae3*d12)-(P12./P11).*sinh(gammae3*d12);

P19=-(M1./N1).*sinh(gammae2*d12)+cosh(gammae2*d12);

P20=sinh(gammah1*d1).*cosh(gammah2*d12)./(N4.*P13);

P21=(M7./N7).*gammah3.*cosh(gammah3*d12)-gammah3.*sinh(gammah3*d12);

P22=gammah2.*sinh(gammah1*d1).*sinh(gammah2*d12)./N4;

P23=((M7.*P14)./(N7.*P13)).*gammah3.*cosh(gammah3*d12)-(P14./P13).*gammah3.*sinh(gammah3*d12);

P24=(M4./N4).*gammah2.*sinh(gammah2*d12)+gammah2.*cosh(gammah2*d12);

P25=1./(P23+P24);

P26=(P20.*P21+P22)./(P23+P24);

P27=M4./(N4.*(P23+P24));

P28=sinh(gammah1*d1)./N4-M4.*(P20.*P21+P22)./(N4.*(P23+P24));

P29=1./(P18+P19);

P30=(P15.*P16+P17)./(P18+P19);

P31=-M1.*P29./N1;

P32=M1.*P30./N1+gammae1.*sinh(gammae1*d1)./(N1.*e12);


if y(n)==d1;
    Zxx1=(alpha(g).^2./(beta.^2+alpha(g)^2)).*(gammae2.*P30.*sinh(gammae2*y(m))./(j*w*e0*e22) + ...
        gammae2.*P32.*cosh(gammae2*y(m))./(-j*w*e0*e22))+ ...
        (beta.^2./(beta.^2+alpha(g)^2)).*(j*w*u0*P28.*cosh(gammah2*y(m))-j*w*u0*P26.*sinh(gammah2*y(m)));
    Zxx=Zxx1;

else
    Zxx2=(alpha(g).^2./(beta.^2+alpha(g)^2)).*(gammae2.*P29.*sinh(gammae2*y(m))./(-j*w*e0*e22)+ ...
        gammae2.*P31.*cosh(gammae2*y(m))./(-j*w*e0*e22))+ ...
        (beta.^2./(beta.^2+alpha(g)^2)).*(-j*w*u0*P25.*sinh(gammah2*y(m))-j*w*u0*P27.*cosh(gammah2*y(m)));
```

```
                Zxx=Zxx2;
            end
            Kxx_matrix=Kxx_matrix+sum(Zxx.*rxm.*rxn.*R.*del_beta.*del_alpha(g));
        end
        matrix_rect(m,n)=(1/(2*pi)^2)*Kxx_matrix;
    end
end

matrix=matrix_polar+matrix_rect;                                    %saves the rectangular
                                                                    %and polar integration results
                                                                    %in the impedance matrix.
V=zeros(2*(M-1),1);                                                 %fills in voltage matrix


ws=2*(1-cos(k*delx))/(k*sin(k*delx))*delz;
V(ceil(M/2))=-Vs*ws/(2*delx);
V(ceil(M/2)-1)=.5*V(ceil(M/2));
V(ceil(M/2)+1)=.5*V(ceil(M/2));
J=inv(matrix)*V                                                     %solves for surface current (A/m)
I=J*delz;                                                           %solves for total current (A)
Z_in(s)=Vs/I(ceil(M/2))                                             %solves for short-circuit impedance


matrix_mutual=matrix(1:M-1,1:M-1);                                  %removes parasitic dipole
V_mutual=zeros(M-1,1);
ws=2*(1-cos(k*delx))/(k*sin(k*delx))*delz;
V_mutual(ceil(M/2))=-Vs*ws/(2*delx);
V_mutual(ceil(M/2)-1)=.5*V_mutual(ceil(M/2));
V_mutual(ceil(M/2)+1)=.5*V_mutual(ceil(M/2));
I_mutual=inv(matrix_mutual)*V_mutual*delz;

I1p=I_mutual(ceil(M/2));
Z_oc(s)=Vs/I1p                                                      %solves for open-circuit voltage

Z_m(s)=sqrt(Z_oc(s)*(Z_oc(s)-Z_in(s)))                              %solves for mutual impedance


end
```